2016

Understanding The Activity Of Model Catalyst Surfaces: Ultrahigh Vacuum And Atmospheric Pressure Studies

Kangmin Xie
University of South Carolina

UNDERSTANDING THE ACTIVITY OF MODEL CATALYST SURFACES: ULTRAHIGH VACUUM AND ATMOSPHERIC PRESSURE STUDIES

by

Kangmin Xie

Bachelor of Science
University of Science and Technology of China, 2011

Submitted in Partial Fulfillment of the Requirements

For the Degree of Doctor of Philosophy in

Chemistry

College of Arts and Sciences

University of South Carolina

2016

Accepted by:

Donna A. Chen, Major Professor

Andrew B. Greytak, Committee Member

Brian C. Benicewicz, Committee Member

John R. Monnier, Committee Member

Cheryl L. Addy, Vice Provost and Dean of the Graduate School

DEDICATION

This dissertation dedicates to my parents and my wife, for their love and support all the time.

ACKNOWLEDGEMENT

First, I would like to express my greatest gratitude to my advisor Dr. Donna Chen. In the past five years, benefit from her careful instruction and insightful guidance, I acquired a lot of knowledge in the field of surface science and catalysis, got well-trained in operating multiple powerful surface analysis techniques, and most importantly I learned how to analyze problems in a scientific way. Second, I want to give my thanks to Dr. John Monnier, whose expertise in heterogeneous catalysis is so impressive. I would also like to acknowledge my committee members Dr. Andrew Greytak and Dr. Brian Benicewicz, for taking precious time to teach me and make my work better.

Thanks to all my previous and current group members: Dr. Samuel Tenney who taught me the operating of micro-reactor system; Dr. Hui Yan who instructed me about the TPD chamber; Dr. Randima Galhanage who did most of characterization work for Pt-Ru on HOPG and Pt-Re on TiO_2; Dr. Audrey Duke (Dr. Phillips now) who was the primary contributor in surface preparation and XPS analysis of the model catalysts for kinetics evaluation before April 2016; Amy Brandt and Thathsara Maddumapatabandi, for their valuable supports in surface preparation, XPS and IR experiments for all under-going projects; Grant Seuser for all the discussions we had for catalysis and all the help he offered; Deependra Shakya, Lauren Hensley, Mara Levine, Dr.Ali Ahsen, Tyler Hernandez and Nhat Nguyen for being nice members to me. Thanks so much to Arthur Illingworth and Allen Frye for their immeasurable support and help from machine shop. Also thanks to the service teams from Omicron, Hiden and Duniway companies.

Thanks to all professors who had taught me and helped me: Dr. Mark Berg, Dr. Hui Wang, Dr. Michael Myrick, Dr. Sophya Garashchuk, Dr. Vitaly Rassolov, Dr. Chuanbing Tang and Dr. Harry Ploehn. Thanks to all the department staffs for their wonderful assistant in providing a friendly and nice environment. Also thanks a lot to the collaborators in Chemical Engineering: Dr. Weijian Diao, Dr. Yunya Zhang, Dr. John Tengco for immense help in ED projects; Dr. Abraham Rodriguez for reactor setup, GC's calibration; Dr. Yating Mao for the AFM work; Carol Stock for helps in CO cylinders.

Thanks for the financial support from the National Science Foundation, the Department of Energy, and the University of South Carolina's Office of Research.

Thanks to my friends at USC and Chinese Soccer Team, appreciate the time we spent together in our golden age: Dr. Haorui Wu, Li Wang, Qingfeng Zhang, Lichao Sun, Dr. Bing Gu, Yinyan He, Dr. Hong Guan, Dr. Shengnan Meng, Guangfang Li, Qiuli Liu, Dr. Rui Tan, Dr. Yi Shen, Dr. Jiuyang Zhang, Dr. Mingwei Chen, Dr. Sheng Feng, Dr. Shuai Tan, Dr. Siwei Wang, Dr. Xiaoguang Ma, Dr. Chao Li, Dr. Kejian Yao, Dr. Lei Wang, Dr.Wei Zhao, Dr. Jiayu Wang, Bo Zhao, Yong Li, Wanze Xie, Yuleng Zeng, Dr. Wuzhao Yan, Huidong Zhou, Dr. Yongqiang Chu, Dr. Diansheng Guo, Dr. Xiaofeng Wang, Xin Liu, Zhongwen Luo, Qun Fang, Yichao Lin, Hongbo Liu, Yan Zhang, Dr. Meng Guo, Dr. Yu Chen, Dr. Longfei Ye, Jianguo Yu, Jie Cai, Zhihao Zhang and so on.

Thanks to my family members, my father Guangping Xie, my mother Tujiao Zhu and my wife Mengxuan Liu. Without their love and support, I could never make it.

ABSTRACT

Heterogeneous Catalysis plays an extremely important role in the world. Metal particles supported on oxide supports are the most widely employed heterogeneous catalysts. In order to provide insight into the development of new catalytic materials, a fundamental understanding of surface reactions is required. Vapor-deposited metal clusters on single-crystal surfaces are well-defined systems that can be used to understand the structure-relationships in commercial catalysts. The pressure gap between fundamental surface analysis under ultra-high vacuum (UHV, P~10^{-10} Torr) conditions and kinetic evaluation of catalysts under realistic pressures has been bridged by constructing a micro-reactor interfaced with UHV chamber: pre- and post-reaction surfaces can be examined by X-ray photoelectron spectroscopy (XPS) without exposing the sample to air. The performance of this micro-reactor has been verified by reproducing kinetic parameters for CO oxidation on Pt/TiO_2 (110).

Pt-Re systems were studied in order to understand the nature of the enhanced bimetallic activity for oxidation reactions and the water gas shift (WGS) reaction. Model Pt-Re catalysts were prepared by sequential deposition of Pt and Re on a rutile TiO_2 (110) support. Active sites on the Pt-Re bimetallic clusters were investigated by temperature programmed desorption (TPD) using CO and methanol as probe molecules. At room temperature, Re on top of Pt can diffuse into Pt clusters in a kinetically limited process, and the surface composition of Re can be controlled by varying the Re coverage. Lattice oxygen participates in the recombination of dissociated CO and promotes CO_2

formation on bimetallic surfaces. In methanol oxidation reactions on Pt-Re surface alloys, higher long-term activity is observed for Pt-Re compared to Pt because less carbonaceous deposits are formed on the alloy surface. However, surface Re is unstable due to formation and subsequent sublimation of Re_2O_7. For the WGS reaction, bimetallic surfaces consisting of Pt on Re have higher activity than pure Pt, while Re alone has no activity. Furthermore, XPS studies show that the active species for WGS is metallic Re rather than Re oxides.

TABLE OF CONTENTS

LIST OF TABLES

LIST OF FIGURES

LIST OF ABBREVIATIONS

AES ..... Auger electron spectroscopy

AFM ..... atomic-force microscopy

CW ..... clockwise

CCW ..... count-clockwise

DFT ..... density functional theory

FID ..... flame ionization detector

GC ..... gas chromatography

LEED ..... low energy electron diffraction

LEIS ..... low energy ion scattering spectroscopy

QCM ..... quartz crystal microbalance

SCCM ..... standard cubic centimeters per minutes

STM ..... scanning tunneling microscopy

TCD ..... thermal conductivity detector

TPD ..... temperature programmed desorption

VLE ..... vapor-liquid equilibrator

XPS ..... X-ray photoelectron spectroscopy

CHAPTER 1 INTRODUCTION

1.1 CATALYSIS AND HETEROGENEOUS CATALYSIS

Catalysis usually refers to the acceleration of a chemical reaction by the action of a catalyst. It is a kinetic concept: the catalyst does not change the thermodynamics of the reaction; it changes the reaction pathway, through which a less activation energy is required[1]. Catalysis is of great important in our modern society. It has been estimated that 90% of chemical products involve catalytic processes[2]. From an economic perspective, catalysis potentially contributes to over 30% of GDP in the whole world[3], and the global demand on catalysts was approximately 29.5 billion USD in 2010[4].

Usually catalysis is divided into three categories[5]: (i) homogeneous catalysis, typically reactions in liquid phase solutions (eg, Suzuki reaction catalyzed by ligand-free palladium catalyst[6, 7]); (ii) heterogeneous catalysis, which deals with the catalytic reactions on gas-solid surface or liquid-solid phase (eg, CO oxidation by transition metals such as Pt[8, 9] or Au/TiO_2[10-12]) and (iii) bio-catalysis in biological systems that using natural catalysts such as protein enzymes (eg, hydrolysis of proteins[13, 14]). Among them heterogeneous catalysis plays the most crucial role in industrial processes. For example, the refining of petroleum[15-17], energy conversions steps like gas reforming, water-gas shift reaction and preferential oxidation of CO in proton exchange membrane fuel cells (PEMFC)[18, 19] and environmentally, the emission control of automobile exhaust[20-22].

Supported catalysts consisting of metal particles dispersed on the internal surface of porous oxides or carbon are the most important materials in heterogeneous catalysis [23, 24]. Catalysts with higher activity, better selectivity and longer life time are always desired. In order to provide effective guidance to design better catalysts for industrial processes, it is crucial to know about the chemical nature behind the high activity and selectivity.

Despite the extensive use of solid supported catalysts, it is hard to fully understand the exact mechanism of improving factors and deactivation reasons, since traditional solid catalysts are too complicated systems for fundamental studies. For example, catalyst support can be amorphous or microcrystalline materials, and could contain different crystal phases and due to the fact that most of synthesis and treatment recipe are based on empirical studies, it is challenging to maintain dispersion and control for impurities[25]. In many cases only bulk information can be extracted by conventional characterizations methods in solid catalysts, while surface is the location where most reactions take place. Hence, it is extremely difficult to grasp the structure-activity relationship there because a complete analysis of the surface is difficult to establish.

1.2 Importance of Surface Science in Catalysis

Surface science is the study of physical and chemical phenomena that occur at the interface of two phases, which has a major influence on the understanding of processes relevant to heterogeneous catalysis in nature[26]. As emphasized by Campbell, the goal of surface science is to fundamentally understand the relationship between atomic level structure of a catalyst surface and its catalytic performance[27], for example, extracting the connection between the surface structure of a certain gas-solid surface and its macro kinetic behaviors such as activity, selectivity and stability.

In order to gain fundamental understanding of real world catalysts, it is necessary to get started with a system where the complexities of those catalysts are reduced. The ultimate goal is to systematically study the key structural and electronic factors for the function of the real catalytic material[28]. To achieve this end, the model catalyst approach had been put forward[29-31].

The basic concept of model catalyst approach is simplifying the complexities of real catalyst, so that surface composition, morphology as well as surface active sites can be identified and accurately controlled. In a starting point, a planar metal single crystal which is highly uniform in surface structure serves as the model catalyst[32]. Later on, the supported model catalyst, which consists of metal clusters deposited on oxide substrate, has been widely employed. For our fundamental studies, ultra high vacuum (UHV) condition (pressure<10^{-10} Torr), which can guarantee a contamination-free surface in atomic scale to keep adsorption of residual gases below 10^{-3} monolayer/second[33], is required to minimized impurities and maintain a clean environment, so that the surface chemistry can be well understood.

Impressive progresses have been made in the surface science and catalysis with the powerful characterization techniques under UHV conditions. Those important electronic and ion based techniques in this work including scanning tunneling microscope (STM), low energy ion scattering (LEIS), X-ray photoelectron spectroscopy (XPS), Auger electron spectroscopy(AES) and temperature programmed desorption (TPD). Most surface analysis techniques must be carried out in high vacuum, since electrons and ions are scattered by molecules in the gas phase. Though photon based techniques can be operated in the ambient pressure in principle, sometimes gas phase absorption of photons can occur and as a consequence their operation also require vacuum operation[33]. Benefit those surface science techniques, our model catalyst can be prepared and controlled precisely in an atomic clean environment, comprehensively characterized, followed by carefully chemical activity study under UHV conditions.

1.3 Motivation of This Thesis Work

The combination of powerful surface analysis techniques in UHV chamber enables us to gain comprehensive knowledge of the surface information (morphology, composition and structure). Assuming the fundamental studies for a certain industrial catalyst is provided, the question is: do the behaviors observed in the model system truly reflect or represent those in the real reactions? This is a difficult question to answer. It is generally accepted that there are mainly two gaps between real catalytic reaction studies and surface science studies: the materials gap and pressure gap.

The pressure gap is usually the main concern between the surface science study and conventional heterogeneous catalysis, since the majority of surface analysis techniques must be undertaken in UHV condition (P ~10^{-9} Torr), the adsorption and desorption behavior for reactants or probe molecules in vacuum could be totally different from that in real case, since most of industrial reactions run at higher pressure condition (P~10^{+2} Torr or higher). A micro-reactor coupled to the UHV system can bridge the pressure gap for catalytic kinetic evaluation and surface analysis techniques [34]. By this design the kinetic part on a given surface can be measured using the elevated pressure reactor, while the analysis of the structure and composition of the surface can be achieved both before and after reaction without exposure to air, a suitable gate valve could hold the pressure difference in standby state. When opening the gate valve, a transfer arm can be used to move the sample or "catalyst" between the higher pressure reactor and UHV chamber. The detail of reactor design is included in chapter 2.

The primary objective of this work is to understand the activity of model catalysts under both UHV conditions and realistic catalytic conditions. Pt and Pt-Re clusters

supported on TiO_2 (110) are the main model surfaces employed in this work. The CO oxidation (chapter 2), methanol oxidation (chapter 3 and chapter 6) and water-gas shift reaction (chapter 4) are the typical probe reactions investigated, within the capability of current reactor system's configurations. The chemical activity studies of those surfaces under UHV conditions (TPD) were also examined (chapter 5 and appendix A).

To summarize, compared with complicated conventional catalysts, the supported model catalyst is a much simplified system which can be fully characterized and extensively studied under UHV condition. Meanwhile, the chemical activity and kinetics of model catalysts can also be measured in simulated real reaction conditions without exposure to air between pre- and post-reaction surface analysis. With atomic-level clean surface, well-defined surface structure and composition, precise control of background, simulated real reaction study, the model catalyst system is believed to provide a more fundamental understanding of surface structure-function relationship, for the guidance of design of better catalysts.

1.4 Experimental Techniques

The supported model catalysts in this thesis were prepared in UHV chambers by physical vapor deposition (PVD) if no further mentioned. The characterizations of model surfaces were achieved by a set of surface techniques explained one by one below. The activity tests under realistic catalytic conditions were performed in a higher pressure micro-reactor which will be illustrated in Chapter 2 in detail.

1.4.1 Temperature Programmed Desorption (TPD)

TPD is also called temperature-programmed reaction spectroscopy (TPRS), or thermal desorption spectroscopy (TDS)[35]. It is a powerful surface science technique

which studies the chemical activity of model surface under UHV condition. It helps to determine surface coverages as well as provides information on the strength of the bond between adsorbate and substrate[36]. For example, H_2-TPD helps to understand the active sites of model Pt and Pd surface[37, 38]. Figure 1.1 shows a schematic set-up for TPD in vacuum chamber. The sample surface which usually mounted on a manipulator is heated resistively via thin tantalum or tungsten wires. A thermocouple which is spot-welded to the crystal is used to monitor the temperature. This type of sample responds much more rapidly to heating than a catalyst in a reactor. The concentration of desorbing species is usually measured by a quadrupole mass spectrometer. Pumping capacity is an important consideration in TPD. The pumping speed should be sufficiently high to prevent re-adsorption of the desorbed species back onto the surface.

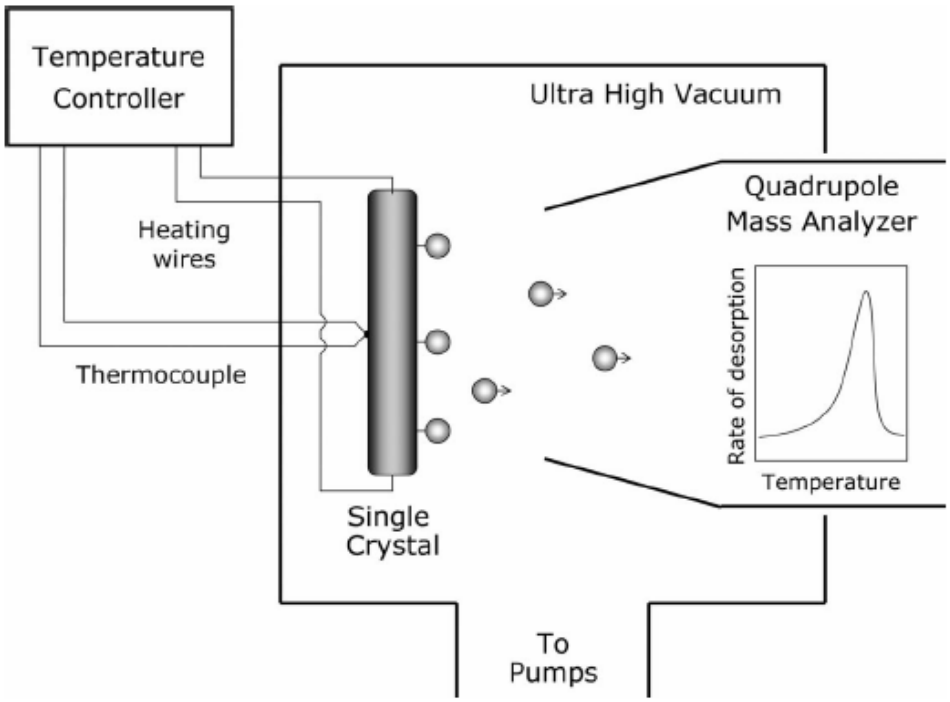

Figure 1.1: Schematic of temperature programmed desorption in vacuum chamber[36]

Figure 1.2 shows the TPD setup in this work. The Hiden mass spectrometer is shielded with gold-covered flag that has a 2mm diameter hole in the center of the flag. The sample is placed approximately 3 mm from the aperture in the flag, which helps to eliminate any contribution from molecules that desorb from the rest of the sample holder or manipulator. Before preparing any surface for a standard TPD experiment, the surface must be free of adsorbates, and the cool-flash-cool procedure is applied. For example, after being sputtering and annealing, the sample is cooled by liquid nitrogen to ~80 K to adsorb weakly bound species. After that a flash step is applied to remove those adsorbates right before dosing metal clusters.

The flag of mass spectrometer here is to prevent detection of species desorption from the sample holder. The performance has been verified by excellent baseline in successful control experiments. During the temperature programmed linear ramping, the sample is also biased at -100 V to avoid any electron-induced chemistry on the surface.

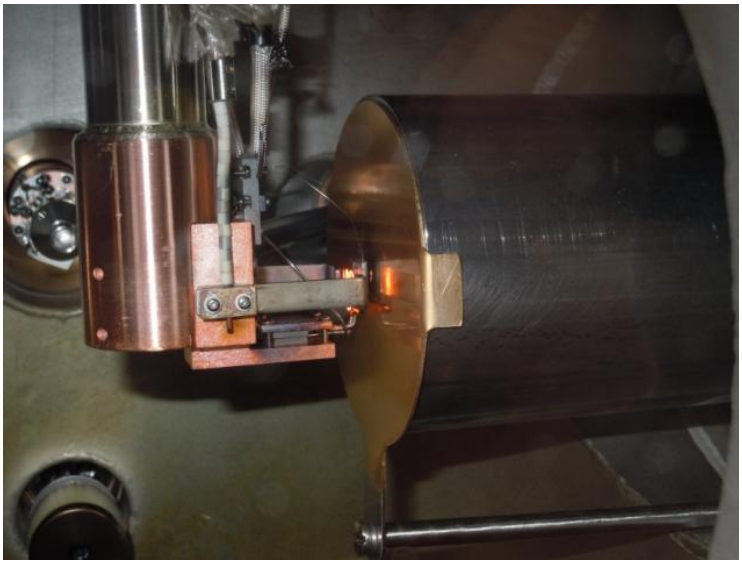

Figure 1.2: TPD setup in this work, showing clean TiO_2 sample is in front of the mass spectrometer flag[39]

1.4.2 X-RAY PHOTOELECTRON SPECTROSCOPY (XPS)

XPS, also named Electron Spectroscopy for Chemical Analysis (ESCA), is among the most frequently used surface sensitive techniques in heterogeneous catalysis [40]. XPS can determine elemental compositions of the surface (top 0-10 nm usually), obtain oxidation state information of certain elements as well as the valence band structure. It is the core analysis method for the characterization of model catalysts in this work.

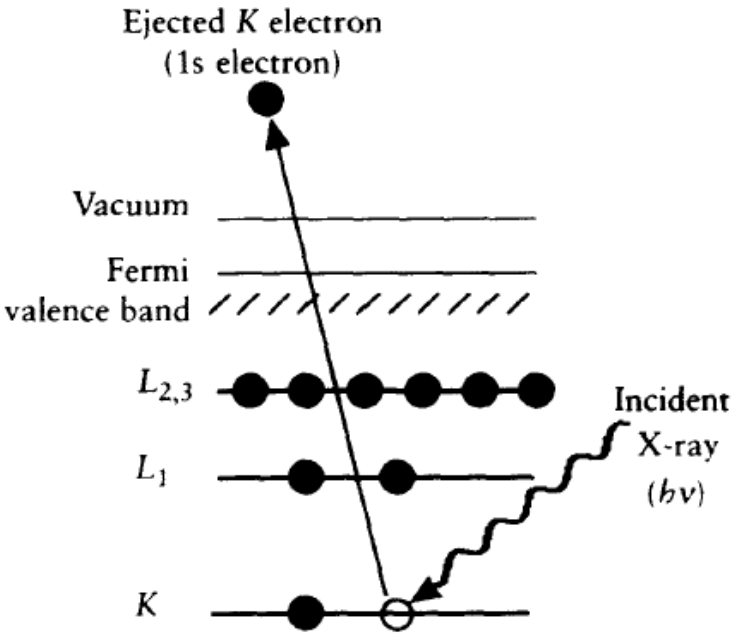

Figure 1.3: Schematic diagram of the XPS process, showing photoionization of an atom by the ejection of a 1s electron[41]

In principle, XPS is based on the photoelectric effect as outlined by Einstein in 1905, which can be expressed by equation $E_k=h\nu-E_b-\varphi$. In the equation, ν is defined as the frequency of exciting radiation of X-ray, and the energy of the incident light would be $h\nu$ (h is Planck's constant); E_b is the binding energy of the electron which is the parameter identifies the electron specifically, and φ is the work function of the spectrometer, which denotes the minimum energy necessary to eject an electron from the valence band into

vacuum, and can be measured by a standard reference. Theoretically if the energy transfer is sufficient, that is, hν is larger than (E_b+φ), a core or valence electron with binding energy E_b will be ejected with kinetic energy E_k. By using an X-ray source, routinely Al-Kα (1486.6 eV) or Mg-Kα line (1253.6 eV), photons are created which have the ability to transfer their entire energy to electrons within atoms by striking them. The process of photoemission is shown schematically in Figure 1.3, where a 1s electron from the K shell is ejected.

XPS works by sending X-rays of a known energy toward the sample to produce photoelectrons and comparing the E_k with the initial energy of the photon. As described, this part of energy difference is the summation of E_b and work function φ, while φ can be calculated from a standard reference. Therefore by collecting the E_k we will be able to calculate the E_b, which is dependent on the type of atom the electron came from as well as the environment it came from. Hence the photoelectron spectrum will reproduce the electronic structure of an element quite accurately since all electrons with a binding energy less than the photon energy will be featured in the spectrum[42].

As illustrated in Figure 1.4, the XPS spectrum is superimposed on a representation of the electron orbital. The electrons which are excited and escape without energy loss contribute to the characteristic peaks in the spectrum; while those that undergo inelastic scattering and suffer energy loss contribute to the background of the spectrum. A change of the oxidation state of a certain element will result in a shift of the binding energy. Therefore, a “chemical shift” can be detected in XPS and based on chemical shift the oxidation state information can be exacted.

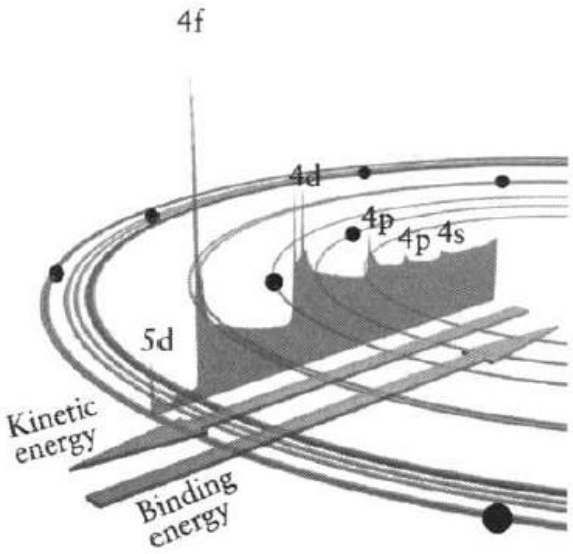

Figure 1.4: Photo electron spectrum of lead showing the manner in which electrons escaping from the solid can contribute to discrete peaks or suffer energy loss and contribute to the background[41]

It should be noted that regular XPS experiment must be conducted under a pressure lower than 10^{-9} Torr, since the emitted photoelectrons must be able to travel from the sample through the analyzer to the detector without colliding with gas phase molecules, meanwhile the surface composition of the sample under investigation must not change during experiment[40]. For studies in UHV chambers, the pressure is not a problem. Technically XPS can also be used to probe surface at ~10^{+1} Torr range if differential pump stages can be achieved, this is also ambient-pressure XPS. AP-XPS has been well-developed in past years[43, 44] for *in situ*.

1.4.3 AUGER ELECTRON SPECTROSCOPY (AES)

Auger Electron Spectroscopy (AES) is also one of the most important chemical surface analysis tools for conducting samples, which could provide information essentially on the elemental composition of the first 2–10 atomic layers[45]. Unlike XPS, AES is a three-electron process. When the surface is irradiated with electrons, core

electrons are ejected in the same way as that in XPS. The other possibility is that the core hole (for example K shell vacancy as shown in Figure 1.3) may be filled by an electron from a higher level, thus another electron must be ejected from the atom conforming with the principle of the conservation of energy. For instance, for the $L_{2,3}$ level in Figure 1.5, this electron is termed the $KL_{2,3}L_{2,3}$ Auger electron.

The energy of an Auger transition (KLM) can be approximately given by $E_{KLM} = E_K - E_L - E_M - \delta E - \varphi$. In this equation: E_{KLM} is the kinetic energy of the Auger electron; E_K, E_L and E_M is the binding energy of an electron in the K-, L- and M-shell; φ is the work function; δE is the energy shift caused by relaxation effects.

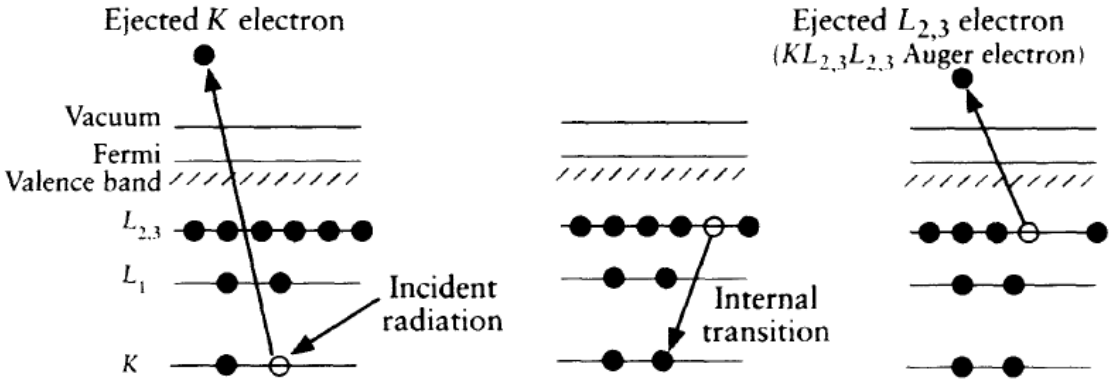

Figure 1.5: Relaxation of ionized atom by emission of a $KL_{2,3}$ $L_{2,3}$ Auger electron[41]

AES provides element-specific information on the surface region. Compared with XPS, Auger spectra has a better spatial resolution, which can be obtained from spots with diameters as small as a few nanometers[36, 45].For many catalytically relevant elements (C, Cl, S, Pt, Ir, Rh), the main Auger electrons have energies in the range of 100 to 300 eV, where the mean free path of the electrons is at its minimum. Thus, for those elements, AES is considerably more surface sensitive than XPS[42].

1.4.4 Low Energy Electron Diffraction (LEED)

LEED is use d to determine the surface structure of single crystal surfaces and the structure of ordered adsorbate layers[46]. The principle of LEED is illustrated in Figure 1.6: a beam of mono energetic low-energy electrons (50–200 eV) minimum mean free path) falls on a surface, whereupon electrons are scattered elastically in all directions[36].

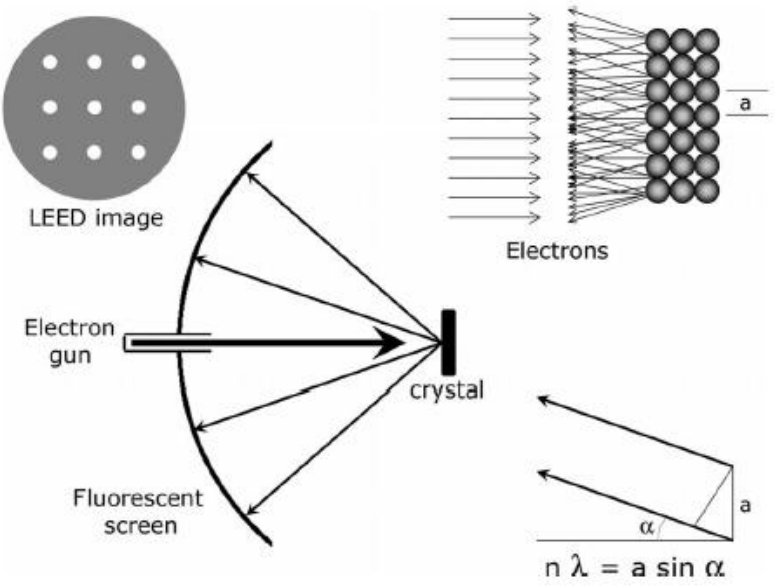

Figure 1.6: The principle of low-energy electron diffraction (LEED)[36]

The electrons can be considered as a wave with wavelength $\lambda = h \cdot (2 \cdot m_e \cdot E_{kin})^{-1/2}$, where h is Planck's constant; m_e is the mass of the electron; E_{kin} is the kinetic energy of the electron. Hence, scattered electrons will exhibit an interference pattern with constructive interference in directions with and the other symbols as defined. Hence, if the scattered electrons are collected with a fluorescent screen, one observes a pattern of spots, each of which corresponds to a direction in which constructive interference takes

place. The set-up is shown schematically in Figure 1.6. For work in this thesis, LEED was used to verify there is no reconstruction of TiO_2 (110) surface.

1.4.5 Low Energy Ion Scattering Spectroscopy (LEIS)

Low-energy ion scattering, also referred to as ion scattering spectroscopy (ISS), is exclusively sensitive for the top-first surface layer, which makes this technique an extremely powerful tool for the characterization of catalysts. It is the surface-sensitive counterpart of the Rutherford backscattering technique. The principle of LEIS is shown in Figure 1.7. The primary ion with certain energy will be ejected to surface, by collecting the energy of scattered ions, information of surface atoms can be extracted. Because of its extreme surface sensitivity, LEIS requires vacuum conditions which allow the sample to be prepared and maintained in a defined state for a sufficiently long period. Therefore the scattering chamber must be a UHV system with a base pressure below 10^{-9} Torr[46]. LEIS experiments were carried out with a beam of helium ions in this work.

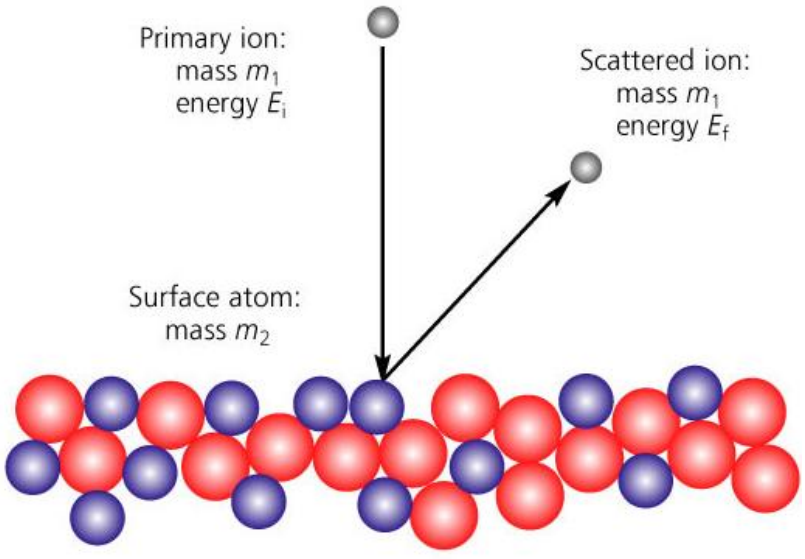

Figure 1.7: Principle of low energy ion scattering (LEIS)[47]

1.4.6 SCANNING TUNNELING MICROSCOPY (STM)

The STM is an example of the practical application of quantum mechanical phenomenon: quantum tunneling[48]. Based on quantum theory, the cloud of electrons at the surface is not entirely confined to the surface atoms, electrons have probability that extend into the vacuum. As can be illustrated from Figure 1.8, when a fine STM tip approaches the surface (~a few Angstroms), the electron clouds of the tip and surface begin to overlap. A small positive potential on the tip is sufficient to cause a measurable tunneling current over the gap between the tip and the surface, therefore a certain relationship can be built between the tunneling current and the distance. Using a constant current mode, STM experiments were conducted to image the surface, to obtain the surface morphology and cluster size information.

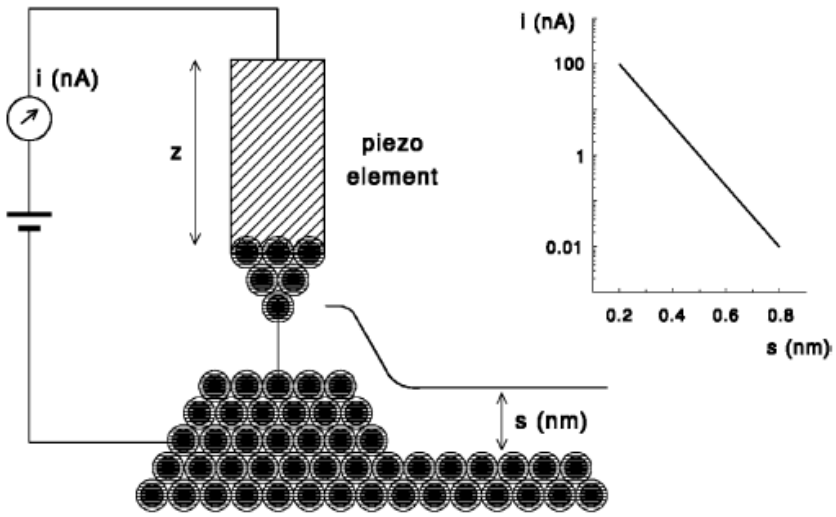

Figure 1.8: Principle of scanning tunneling microscope (STM)[36]

Since STM relies on the tunneling current between a tip and the surface, its operation must limit to conducting substrates, usually metals and semiconductors, while it is still possible for us to image oxides using STM, for example, the TiO_2 (110) support,

which is the primary single crystal support in this work. The structure of rutile TiO_2 is shown in Figure 1.9. Even though TiO_2 itself is an insulator, after heating to high temperature in vacuum condition or bombardment by ions, the oxygen atoms on the surface can be removed, leaving oxygen vacancies there. Those oxygen vacancies could provide sufficient conductivity for the application of STM. Many high quality images of the TiO_2 (110) surface have been reported[49-51], and due to its outstanding chemical and physical properties, in the past decades, TiO_2 surfaces have been used as a model support for metal particles[12, 52, 53].

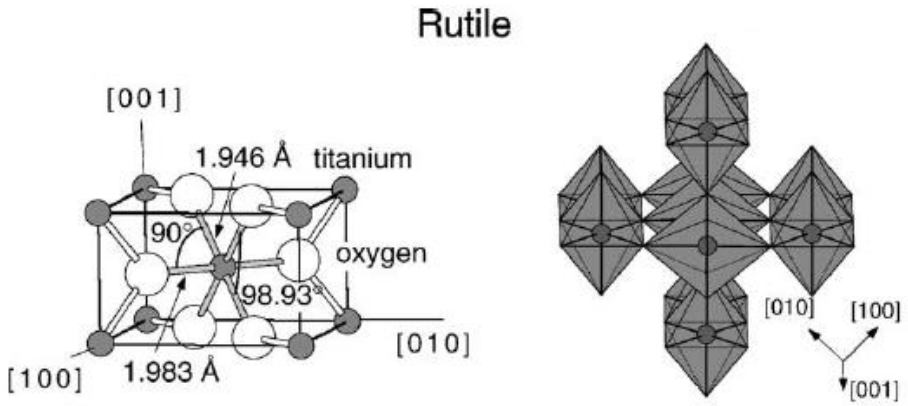

Figure 1.9: Structure of Rutile TiO_2 [54]

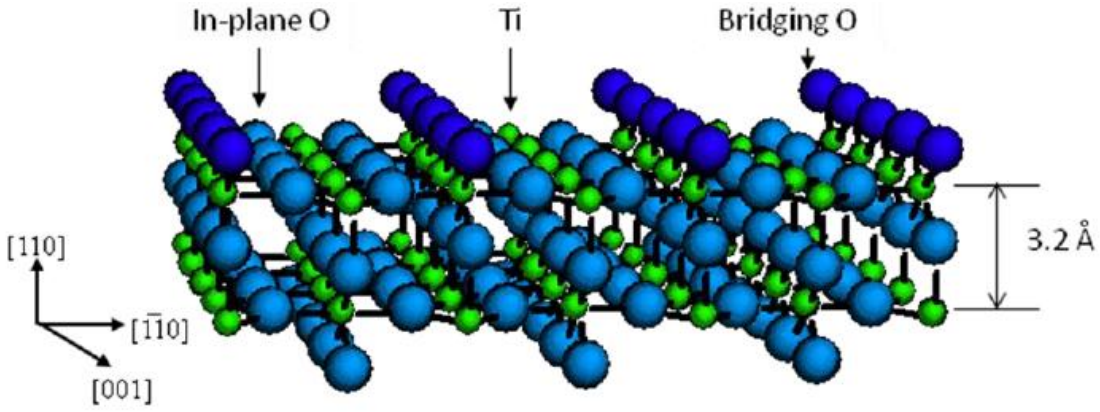

Figure 1.10: Crystal structure of the rutile TiO_2 surface cut along the [110] plane[39]

1.5 REFERENCES

(1) Webb, S. J.; Thomson, G., *Heterogeneous Catalysis*. **1969;** p 1-200.

(2) Chorkendorff, I.; Niemantsverdriet, J. W., *Introduction to Catalysis. In Concepts of Modern Catalysis and Kinetics*, Wiley-VCH Verlag GmbH & Co. KGaA: 2005; pp 1-21.

(3) Recognizing the Best in Innovation: Breakthrough Catalyst. *R&D Magazine* September 2005, p 20.

(4) https://en.wikipedia.org/wiki/Catalysis#cite_note-33.

(5) Rothenberg, G., *Catalyis*. Wiley: **2008**.

(6) Leadbeater, N. E.; Marco, M., Ligand-Free Palladium Catalysis of the Suzuki Reaction in Water Using Microwave Heating. *Organic Letters* **2002,** 4 (17), 2973-2976.

(7) Durap, F.; Baysal, A.; Elma, D.; Aydemir, M.; Ok, Ö.; Baysal, Z., p(HEMA)-Pd(II) and p(HEMA-MAH)-Pd(II) Microspheres: Efficient, Recyclable and Ligand-Free Catalyst for Suzuki-Miyaura Cross-Coupling Reaction in Water. *Synthesis and Reactivity in Inorganic, Metal-Organic, and Nano-Metal Chemistry* **2016,** 46 (9), 1402-1409.

(8) Langmuir, I., The mechanism of the catalytic action of platinum in the reactions $2CO+O_2= 2CO_2$ and $2H_2+O_2= 2H_2O$. *Transactions of the Faraday Society* **1922,** 17, 621-654.

(9) Goodman, D. W.; Kelley, R. D.; Madey, T. E.; Yates Jr, J. T., Kinetics of the hydrogenation of CO over a single crystal nickel catalyst. *Journal of Catalysis* **1980,** 63 (1), 226-234.

(10) Haruta, M.; Kobayashi, T.; Sano, H.; Yamada, N., Novel Gold Catalysts for the Oxidation of Carbon Monoxide at a Temperature far Below 0 deg C. *Chemistry Letters* **1987,** 16 (2), 405-408.

(11) Lin, S. D.; Bollinger, M.; Vannice, M. A., Low temperature CO oxidation over Au/TiO_2 and Au/SiO_2 catalysts. *Catalysis Letters* **1993,** 17 (3), 245-262.

(12) Valden, M.; Lai, X.; Goodman, D. W., Onset of Catalytic Activity of Gold Clusters on Titania with the Appearance of Nonmetallic Properties. *Science* **1998,** 281 (5383), 1647-1650.

(13) Hill, R. L., *Hydrolysis of Proteins. In Advances in Protein Chemistry*, C.B. Anfinsen, M. L. A. J. T. E.; Frederic, M. R., Eds. Academic Press: 1965; Vol. Volume 20, pp 37-107.

(14) Silveira, S. T.; Martínez-Maqueda, D.; Recio, I.; Hernández-Ledesma, B., Dipeptidyl peptidase-IV inhibitory peptides generated by tryptic hydrolysis of a whey protein concentrate rich in β-lactoglobulin. *Food Chemistry* **2013,** 141 (2), 1072-1077.

(15) Gates, B. C.; Topsøe, H., Reactivities in deep catalytic hydrodesulfurization: challenges, opportunities, and the importance of 4-methyldibenzothiophene and 4,6-dimethyldibenzothiophene. *Polyhedron* **1997,** 16 (18), 3213-3217.

(16) Miller, J. T.; Reagan, W. J.; Kaduk, J. A.; Marshall, C. L.; Kropf, A. J., Selective Hydrodesulfurization of FCC Naphtha with Supported MoS_2 Catalysts: The Role of Cobalt. *Journal of Catalysis* **2000,** 193 (1), 123-131.

(17) Estrada-Villagrana, A. D.; Quiroz-Sosa, G. B.; Jiménez-Alarcón, M. L.; Alemán-Vázquez, L. O.; Cano-Domínguez, J. L., Comparison between a conventional process and reactive distillation for naphtha hydrodesulfurization. *Chemical Engineering and Processing: Process Intensification* **2006,** 45 (12), 1036-1040.

(18) Park, E. D.; Lee, D.; Lee, H. C., Recent progress in selective CO removal in a H-2-rich stream. *Catalysis Today* **2009,** 139 (4), 280-290.

(19) Liu, Y.; Fu, Q.; Stephanopoulos, M. F., Preferential oxidation of CO in H_2 over CuO-CeO_2 catalysts. *Catalysis Today* **2004,** 93-95, 241-246.

(20) Hodjati, S.; Vaezzadeh, K.; Petit, C.; Pitchon, V.; Kiennemann, A., Absorption/desorption of NO_x process on perovskites: performances to remove NO_x from a lean exhaust gas. *Applied Catalysis B: Environmental* **2000,** 26 (1), 5-16.

(21) Wang, Y.; Li, X.; Zhan, L.; Li, C.; Qiao, W.; Ling, L., Effect of SO_2 on Activated Carbon Honeycomb Supported CeO_2–MnO_x Catalyst for NO Removal at Low Temperature. *Industrial & Engineering Chemistry Research* **2015,** 54 (8), 2274-2278.

(22) Castoldi, L.; Aneggi, E.; Matarrese, R.; Bonzi, R.; Llorca, J.; Trovarelli, A.; Lietti, L., Silver-based catalytic materials for the simultaneous removal of soot and NO_x. *Catalysis Today* **2015,** 258, Part 2, 405-415.

(23) Tauster, S. J.; Fung, S. C.; Baker, R. T. K.; Horsley, J. A., Strong Interactions in Supported-Metal Catalysts. *Science* **1981,** 211 (4487), 1121-1125.

(24) Henry, C. R., Surface studies of supported model catalysts. *Surface Science Reports* **1998,** 31 (7–8), 231-325.

(25) Chusuei, C. C.; Lai, X.; Luo, K.; Goodman, D. W., Modeling heterogeneous catalysts: metal clusters on planar oxide supports. *Topics in Catalysis* **2000,** 14 (1), 71-83.

(26) Somorjai, G. A., Surface Science and Catalysis. *Science* **1985,** 227 (4689), 902-908.

(27) Charles T, C., *Studies of Model Catalysts with Well-Defined Surfaces Combining Ultrahigh Vacuum Surface Characterization with Medium- and High-Pressure Kinetics. In Advances in Catalysis*, D.D. Eley, H. P.; Paul, B. W., Eds. Academic Press: 1989; Vol. Volume 36, pp 1-54.

(28) Freund, H.-J., The Surface Science of Catalysis and More, Using Ultrathin Oxide Films as Templates: A Perspective. *Journal of the American Chemical Society* **2016,** 138 (29), 8985-8996.

(29) Campbell, C. T., *Studies of Model Catalysts with Well-Defined Surfaces Combining Ultrahigh Vacuum Surface Characterization with Medium- and High-Pressure Kinetics. In Advances in Catalysis*, D.D. Eley, H. P.; Paul, B. W., Eds. Academic Press: 1989; Vol. Volume 36, pp 1-54.

(30) Freund, H. J.; Bäumer, M.; Libuda, J.; Risse, T.; Rupprechter, G.; Shaikhutdinov, S., Preparation and characterization of model catalysts: from ultrahigh vacuum to in situ conditions at the atomic dimension. *Journal of Catalysis* **2003,** 216 (1–2), 223-235.

(31) Boudart, M., Model catalysts: reductionism for understanding. *Topics in Catalysis* **2000,** 13 (1), 147.

(32) Somorjai, G. A.; Mujumdar, A. S., Introduction to Surface Chemistry and Catalysis. *Drying Technology* **1995,** 13 (1-2), 507-508.

(33) Vickerman, J. C., *Introduction. In Surface Analysis – The Principal Techniques*, John Wiley & Sons, Ltd: 2009; pp 1-8.

(34) Goodman, D. W., Correlations between Surface Science Models and "Real-World" Catalysts. *The Journal of Physical Chemistry* **1996,** 100 (31), 13090-13102.

(35) Vickerman, J. C., *Molecular Surface Mass Spectrometry by SIMS. In Surface Analysis – The Principal Techniques*, John Wiley & Sons, Ltd: 2009; pp 113-205.

(36) Niemantsverdriet, J. W., Spectroscopy in Catalysis. **2007**.

(37) Greenlief, C. M.; Akhter, S.; White, J. M., Temperature-programmed desorption study of hydrogen-deuterium exchange on platinum(111) and the role of subsurface sites. *The Journal of Physical Chemistry* **1986,** 90 (17), 4080-4083.

(38) Miller, J. T.; Meyers, B. L.; Modica, F. S.; Lane, G. S.; Vaarkamp, M.; Koningsberger, D. C., Hydrogen Temperature-Programmed Desorption (H_2 TPD) of Supported Platinum Catalysts. *Journal of Catalysis* **1993,** 143 (2), 395-408.

(39) Tenney, S. A. *Characterization and Chemical Activity of Titania-Supported AU-Based Bimetallic Clusters (Ph.D. Dissertation).* University of South Carolina, **2012**.

(40) Ratner, B. D.; Castner, D. G., *Electron Spectroscopy for Chemical Analysis. In Surface Analysis – The Principal Techniques*, John Wiley & Sons, Ltd: 2009; pp 47-112.

(41) Watts, J. F.; Wolstenholme, J., *Electron Spectroscopy: Some Basic Concepts. In An Introduction to Surface Analysis by XPS and AES*, John Wiley & Sons, Ltd: 2005; pp 1-15.

(42) Surface Science: An Introduction. *Materials Today* **2003,** 6 (9), 40.

(43) Tao, F., Operando Studies of Catalyst Surfaces during Catalysis and under Reaction Conditions: Ambient Pressure X-Ray Photoelectron Spectroscopy with a Flow-Cell Reactor. *ChemCatChem* **2012,** 4 (5), 583-590.

(44) Tao, F., Design of an in-house ambient pressure AP-XPS using a bench-top X-ray source and the surface chemistry of ceria under reaction conditions. *Chemical Communications* **2012,** 48 (32), 3812-3814.

(45) Mathieu, H. J., *Auger Electron Spectroscopy. In Surface Analysis – The Principal Techniques*, John Wiley & Sons, Ltd: 2009; pp 9-45.

(46) Taglauer, E., *Low-Energy Ion Scattering and Rutherford Backscattering. In Surface Analysis – The Principal Techniques*, John Wiley & Sons, Ltd: 2009; pp 269-331.

(47) Galhenage, R. P. *Metals on Titania/HOPG as Models for Heterogeneous Catalysts (Ph.D. Dissertation).* University of South Carolina, **2015**.

(48) Leggett, G. J., *Scanning Probe Microscopy. In Surface Analysis – The Principal Techniques*, John Wiley & Sons, Ltd: 2009; pp 479-562.

(49) Suzuki, S.; Onishi, H.; Sasaki, T.; Fukui, K.-i.; Iwasawa, Y., Identification of individual 4-methylpyridine molecules physisorbed and chemisorbed on TiO_2(110)-(1 x 1) surface by STM. *Catalysis Letters* **1998,** 54 (4), 177-180.

(50) Bennett, R. A.; Stone, P.; Price, N. J.; Bowker, M., Two (1x2) Reconstructions of TiO_2(110): Surface Rearrangement and Reactivity Studied Using Elevated Temperature Scanning Tunneling Microscopy. *Physical Review Letters* **1999,** 82 (19), 3831-3834.

(51) Iwasawa, Y.; Onishi, H.; Fukui, K.-i., In situ STM study of surface catalytic reactions on TiO_2(110) relevant to catalyst design. *Topics in Catalysis* **2000,** 14 (1), 163-172.

(52) Xu, C.; Lai, X.; Zajac, G. W.; Goodman, D. W., Scanning tunneling microscopy studies of the TiO_2(110) surface: Structure and the nucleation growth of Pd. *Physical Review B* **1997,** 56 (20), 13464-13482.

(53) Starr, D. E.; Shaikhutdinov, S. K.; Freund, H.-J., Gold Supported on Oxide Surfaces: Environmental Effects as Studied by STM. *Topics in Catalysis* **2005,** 36 (1), 33-41.

(54) Diebold, U., The surface science of titanium dioxide. *Surface Science Reports* **2003,** 48 (5–8), 53-229.

CHAPTER 2 NOVEL RECIRCULATING LOOP REACTOR FOR STUDIES ON MODEL CATALYSTS: CO OXIDATION ON PT/TiO_2 (110)[1]

[1]Reprinted from Samuel A. Tenney, Kangmin Xie, John R. Monnier, Abraham Rodriguez, Randima P. Galhenage, Audrey S. Duke and Donna A. Chen, "Novel recirculating loop reactor for studies on model catalysts: CO oxidation on Pt/TiO_2(110)", *Review of Scientific Instruments* **2013**, 84 (10), 104101.,with the permission of AIP Publishing, Copyright 2013 American Institute of Physics.

2.1 INTRODUCTION

The ability to couple basic surface science with more practical catalyst evaluation methods provides detailed surface characterization that is critical for guiding the development of new catalytic materials. Studies of model catalysts in ultrahigh vacuum (UHV, $P<1x10^{-10}$ Torr) are desirable due to the precisely controlled environment and the ability to use electron and ion based spectroscopies for characterization of atomic composition and structure. Furthermore, the uses of model catalysts that consist of metal particles deposited on single-crystal surfaces provide surface structures that are known and well-defined on the atomic level. A number of studies in the literature have illustrated the importance and utility of combining UHV surface analysis with studies of reaction rates[1-4]. However, one of the most critical concerns regarding kinetic studies on atomically flat, single-crystal surfaces is the low concentration of catalytic sites. Therefore, the bridge between model surfaces and real catalysts is difficult to establish, and significant effort has been devoted to the construction of reactor systems that can couple kinetic evaluation of model surfaces with UHV analysis; these designs have been summarized in a review article by Campbell[1] and in subsequent papers[5-8].

The various reactor designs each have their strengths and weaknesses, and in general they can be divided into two categories: the reactor cup design and the transfer rod design. In all cases the reaction products are analyzed either by gas chromatography (GC) with flame ionization or thermal conductivity detectors, or by mass spectrometry. The internal reactor cup design was pioneered by Somorjai and coworkers and represents the first study that couples UHV analysis on single crystals with high pressure reaction conditions[9].Subsequent modifications of this reactor cup design have been used by a

number of research groups[6, 7, 10-17]. The main advantage of the reactor cup design is that high pressures of 100 atm can be achieved; the reactor cup is sealed against the sample holder by using a hydraulic piston to apply 2000 lb/in^2 to the metal gasket seal[12]. A disadvantage is that the reactor cannot be isolated from the UHV chamber after the cup is removed from the sample holder, and therefore outgassing from the walls of the reactor limits the pressure in the UHV chamber. Although the reactor cup itself often has a small volume (~30 cm^3)[10, 11], the entire reactor system typically has a volume of 100 cm^3 [10, 11, 14] since the position of the reactor within the UHV chamber limits the proximity to the GC system. Consequently, the gas mixture is recirculated to avoid concentration gradients. In the transfer rod design, the sample holder is introduced into separate chamber or reaction cell, and the sample transfer rod supporting the sample holder is isolated from the main chamber by sliding seals consisting of differentially-pumped O-rings[8, 18-22]. In some cases, a relative large reaction cell is used (500 cm^3)[21], and the reaction cell is physically isolated from the UHV chamber by a gate valve when the reactor is not in operation. However, mass transfer limitations can be an issue at high pressures in the absence of recirculation in the larger volume reactors[23, 24]. While in other cases, a much smaller volume of the reaction cell (~30 cm^3) is used to avoid issues of mass transfer even without recirculation[18]; however, the small volume precludes regular sampling of the reaction mixture over long reaction times because the pressure in the reaction cell cannot be maintained. The second disadvantage of the transfer rod design is that the differential pumping removes gas from the reaction cell at rates of 0.05-0.3 cm^3/min [1, 8, 18]. Because the pressure of the reactant gases decrease either by gas sampling or differential pumping, it is not possible to measure steady-state reaction

kinetics. A maximum reactor pressure of 10 atm has been achieved with transfer rod design[18],and although higher pressures are possible, additional stages of differential pumping would be required[1].

In this study, we report the design and operation of a novel recirculating loop microreactor that allows frequent sampling of reaction mixtures over extended time periods and is directly coupled to a UHV chamber. This reactor combines several desirable features that distinguish it from the existing reactors previously reported in the literature. First, the reactor is completely isolated from the UHV chamber except during sample transfer, and therefore the chamber pressure is never limited by outgassing from the reactor walls during normal operation. Second, the small reactor volume (32 cm^3) and ability to recirculate the gas mixture allow high sensitivity for detection and preclude mass transfer limitations. Third, the ability to replenish the reaction mixture with fresh feed gas after every injection into the GC permits extensive sampling over long reaction times despite the small reactor volume. However, a drawback of this design is that sample heating in the reactor does not share the heating stage used for the UHV sample holder, as in many of the reactor cup and transfer rod designs. Also, the maximum pressure in the reactor is limited to 1 atm in the current configuration although valves and fitting designed for higher pressures could be used to increase the range of operating pressures. Recirculating loop reactors have the potential to contaminate the model surfaces since the reactant gases have increased contact time with surfaces other than the catalyst[1], but recirculation also eliminates concentration gradients and stagnant regions present in batch reactors, as well as enhances sensitivity over single-pass flow reactors.

CO oxidation over titania-supported Pt clusters was chosen as a system to establish a proof of concept for the reactor because CO oxidation on Pt has been well studied in the literature[25-28]. Furthermore, the investigation of catalytic activity on metal clusters deposited on single crystal oxide supports is even more challenging than on single crystal metal surfaces due to the smaller number of active sites, and consequently there have been comparatively few such studies in the literature[29-31]. Our experiments for CO oxidation on 2 ML Pt clusters on TiO_2(110) with an estimated $1.2x10^{15}$ active sites show that the CO_2 product can easily be detected after only 15 minutes of recirculation and reaction. During these experiments, automated GC sampling of the reaction mixture occurred every 15 minutes over the course of 24 hours for reaction temperatures between 145 and 165 ℃. Our reactor experiments successfully reproduced kinetic parameters from the literature for CO oxidation on Pt, such as activation energy, turnover frequencies and reaction order in O_2 and CO[28, 32].

2.2 BUILD-UP OF NOVEL MICRO-REACTOR SYSTEM

The housing for the reactor is a cylindrically shaped stainless steel piece (diameter 1.5", and height 0.875"), which can be separated into two halves and attaches to a 2 3/4" outer diameter ConFlat flange (Figure 2.1a). The two VCR fittings welded onto the atmospheric side of this flange serve as the gas inlet and outlet, and a type K thermocouple is fed through the gas outlet so that the temperature of the reactant gas can be measured directly. A slot is cut in the body of the reactor to house the single-crystal sample (1 cm ×1 cm ×1 mm) mounted on a Ta plate, which can be transferred directly from the reactor to the sample holder in the attached UHV chamber; the two holes positioned directly under the sample slot and the beveled edges at the top and bottom of

the slot accommodate the gripping mechanism of the sample transfer system. Figure 2.1b shows the reactor flange with only the bottom half of the housing attached so that the gas inlet port behind the top half of the housing is visible, as well as the details of the sample holder inside the housing.

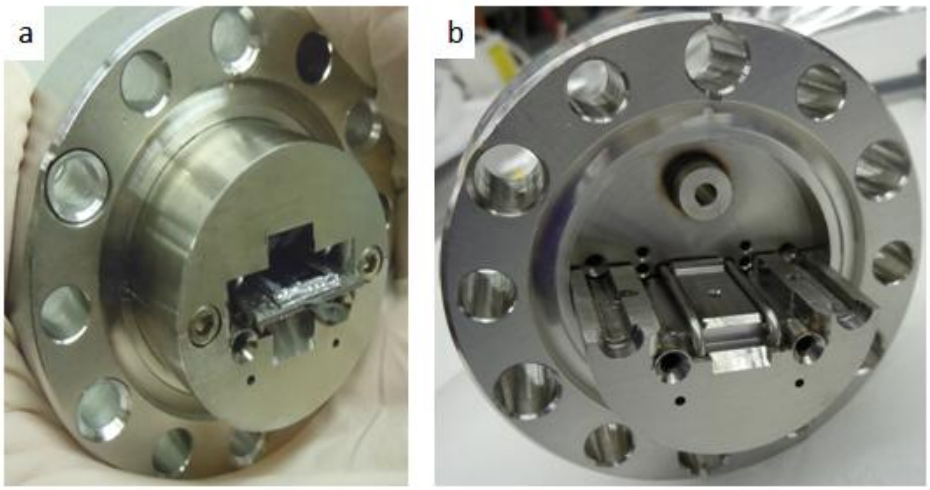

Figure 2.1: Photographs of: a) the reactor housing showing the Ta plate with the TiO_2(110) crystal partially inserted into the sample holder; and b) the reactor housing with the top half removed to show the sample holder and the gas inlet

The reactor housing sits inside of an all-metal gate valve (VAT 481) that isolates the reactor from the UHV chamber, and the gap between reactor housing and inside wall of the gate valve is 1-2 mm (Figure 2.2). The flanges of the gate valve and reactor are sealed with Ag or Au-plated Cu gaskets to eliminate CO oxidation activity from the Cu surface[33].

A differentially pumped glass nipple and another gate valve separate the VAT valve from the UHV chamber to prevent heat transfer and diffusion of He from the reactor to the UHV chamber. Before opening the reactor to UHV chamber, the reactor is isolated from the remainder of the recirculation loop by closing two Swagelok bellows-sealed

valves and then opening a third valve to a 150 l/s turbomolecular pump (Leybold Turbovac) to evacuate the reactor. The resulting chamber pressure during sample transfer is $1x10^{-7}$ Torr, and the chamber pressure dropped to ~$2x10^{-10}$ Torr within 5 minutes of closing the gate valve to the reactor. Operation of the reactor had no effect on the chamber pressure, which remained below $2x10^{-10}$ Torr, and no He diffusion into the chamber was detected by the quadrupole mass spectrometer.

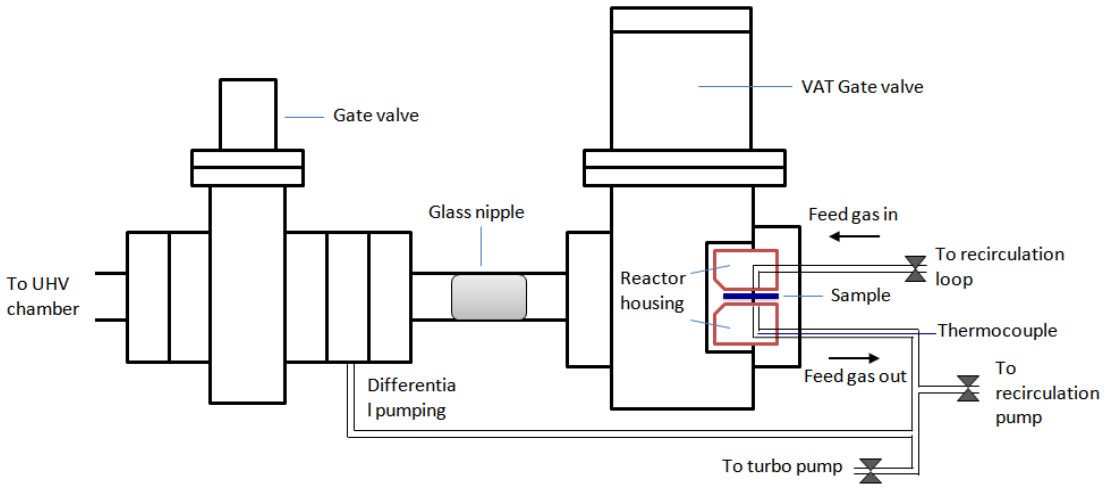

Figure 2.2: Diagram of the entire reactor setup coupled to the UHV chamber.

One of the key features of this recirculation loop reactor is the use of four VICI switching valves, which allow operation of the reactor to be switched between single-pass, recirculation, sampling and feed gas makeup mode. The VICI valves and the reactor are coupled by 0.0625" outer diameter and 0.040” inner diameter stainless steel tubing. By turning valve 4 (V4) from clockwise (CW) to counterclockwise (CCW) and closing the vent valve , the system is switched from the single-pass, catalyst pretreatment mode in which the effluent goes to vent, to a closed-loop recirculation mode (Figure 2.3, Table 2.1). The feed manifold consists of an array of mass flow controllers (Brooks 5850e and 5850i) for O_2, He, and CO, and each flow controller is calibrated with a digital flowmeter

(Agilent Technologies ADM2000) over the appropriate range. A low dead volume absolute capacitance manometer (MKS Instruments Baratron 722A) records the pressure of the gas in the system.

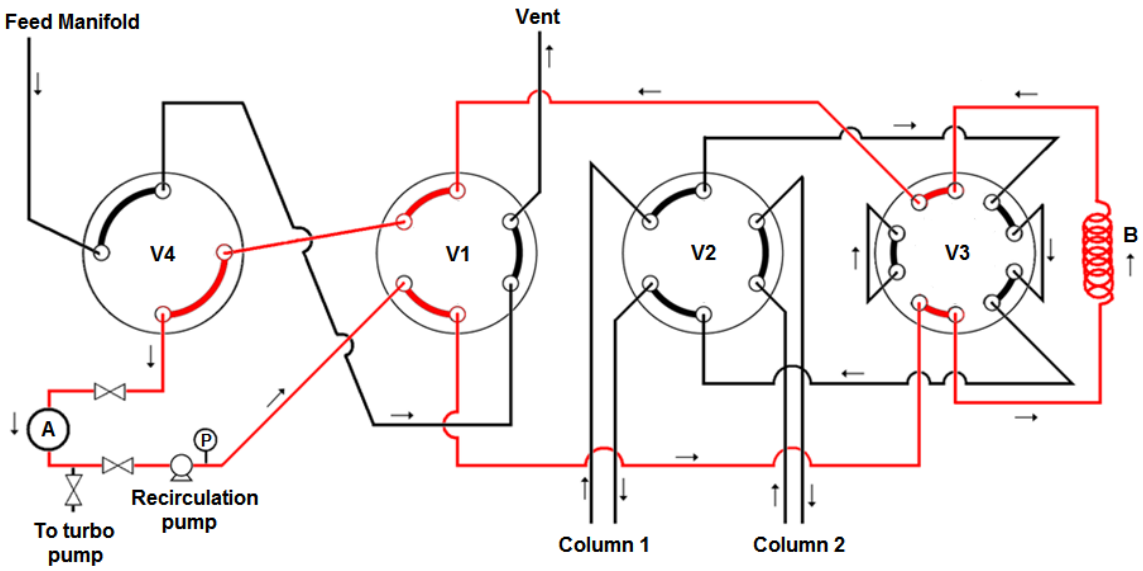

Figure 2.3: Schematic of the reactor system shown in recirculation mode with the following valve positions: V1:CW, V2:CW, V3:CW, V4:CCW. The positions of the valves for the other modes of operation are described in Table I

In the recirculation mode of operation, the gas stream is passed through the reactor that houses the 1 cm^2 sample (A) before being recirculated by a stainless steel bellows pump (Metal Bellows Corp. MB-21). This recirculation pump is throttled by a metering valve (Swagelok SS-SS2-VH) set to allow 15 standard cubic centimeters per minute (sccm) of gas flow through the system in order to minimize pressure differentials generated by the high capacity of the recirculation pump. For V1and V2, the valves are rotated through a 60 °arc to connect alternating pairs of ports, whereas for V3 and V4 the valves are rotated 36 °and 90 °, respectively, to connect alternating ports. In the position shown in Figure 2.3, the gas flow passes through the sample loop (B) and then back into

the recirculation loop reactor, where it undergoes another recirculation cycle. The contents of the sample loop are injected into the GC by turning V3 through a 36 °arc from the CW to CCW position, using the He carrier gas from the GC to sweep the contents of the sample loop into the column inlet (sampling mode). Note that when this occurs, the reactor gas and the He carrier gas flows are only momentarily halted (< 0.2 sec) while V2 is being switched to essentially maintain continuous flow conditions.

Table 2.1: Positions of the switching valves for the reactor system for the four different modes of operation.

Mode	V1	V2 (TCD column)	V3	V4
Singe-pass	CW	CW	CW	CW
Recirculation	CW	CW	CW	CCW
Sampling	CW	CW	CCW	CCW
Make-up	CCW	CW	CW	CCW

In the sampling mode, the contents of the gas sample loop (B) are directed to a gas chromatograph (HP 5890A) employing both a thermal conductivity detector (TCD) and a flame ionization detector (FID), with V2 allowing column selection. The TCD is connected to a PLOT molecular sieve 5A or PoraPLOT Q capillary GC column to allow accurate analysis of non-organic gases such as CO, CO_2, O_2, H_2, and H_2O, while the FID is linked to a second PoraPLOT Q capillary GC column for more sensitive analysis of organic compounds. Following sample injection, V1 is turned CCW to shorten the recirculation pathway between V4 and V1. V3 is then turned back from CCW to CW (the normal recirculation position), which permits the sample loop to be filled with fresh feed gas (makeup mode) in order to compensate for the loss of gas during injection and to maintain constant pressure in the system. After V1 is switched back from the CCW to the CW position, the recirculation loop pathway is restored, and the feed gas contents in the

sample loop are added into the recirculation loop. An in-house LabVIEW program controls the operation of V1, V3 and V4 for automated switching between the various modes of operation. The positions of the switching valves in Figure 3 for the different modes are described Table 2.1.

The following high purity gases were used for all experiments: 5% CO balance He (Praxair), O_2 (Airgas 99.5%) and He (Praxair 99.999%). The CO was passed through an alumina trap heated to 150 ℃ in order to remove any metal carbonyls from the feed. The temperature of the reactor was controlled externally by heating tapes, which were regulated by a Chromalox 2104 series temperature controller and achieved reactor gas temperatures up to 200 ℃; the gas lines and gas sampling loop were always maintained at 60 ºC using a Valco Instruments temperature controller. Based on the volume of the reactor and the measured 15 sccm recirculation rate, the reactant gases recirculate over the catalyst once every 2 minutes.

The model catalysts consisted of 2 ML of Pt vapor deposited onto a rutile TiO_2(110) single crystal. The TiO2 support was cleaned by multiple cycles of Ar^+ sputtering followed by annealing to ~1000 K, and Pt was evaporated using a commercial electron beam evaporator (Oxford Applied Research, EGC04) from a high purity Pt rod (99.95%). The Pt coverage was measured by an independently calibrated quartz crystal microbalance[34], and one monolayer is defined according to the packing density of Pt(111) ($1.50x10^{15}$ atoms/cm^2). Detailed descriptions of the UHV chamber and the surface preparation procedures have been previously reported[35-40]. For the studies reported here, the Pt/TiO_2 catalysts were prepared in a separate UHV chamber and then transferred in air to the load lock of the UHV chamber attached to the reactor[41];exposure

time to air was approximately 30 min. A vacuum transfer system allows samples to be moved directly from the UHV analysis chamber to the reactor using a gripper mechanism that holds the key on the end of the Ta plate on which the TiO_2 crystal is mounted (Figure 2.1a). The UHV chamber attached to the reactor is now set up for sample cleaning, metal deposition and surface analysis so that model surfaces can be prepared in situ in the future. After delivery into the reactor, the catalyst was heated to the desired temperature in a flow of He (35 sccm) at 760 Torr. The samples were held at the desired temperature for five hours, and then the reactant gases were introduced into the reactor loop in the single-pass mode before switching to recirculation mode. The measured pressure in the reactor during recirculation was approximately 850 torr for all of the experiments.

Dead volumes for the various sections of the reactor system were measured by first evacuating the entire reactor system with the turbomolecular pump and then allowing He from a cylinder with a known pressure and volume to expand into reactor system; the volumes of the various sections were calculated using the ideal gas law and measured pressures after filling with He from the calibration cylinder. The following volumes of the reactor system were measured: the reactor only (18.04 cm^3), the total recirculation loop (30.49 cm^3), sample injection loop for the GC (1.10 cm^3) and the section of the recirculation loop plus sample loop filled with fresh feed gas during makeup mode (1.15 cm^3).

2.3 Result and Discussion

CO oxidation on 2 ML Pt deposited on TiO_2(110) was carried out at the following temperatures: 145, 152, 156, 160 and 165 ℃ using a feed gas mixture of 0.83% CO, 17.4 % O_2, balance helium. Experiments at each temperature were conducted over 24

hours, and the reaction gas mixture was sampled by the GC every 15 minutes using the TCD to measure the CO_2 concentration. The number of moles of CO_2 in the entire recirculation loop was determined from the number of moles of CO_2 detected in the GC analysis, the ratio of the volumes of the sample injection loop and recirculation loop, and the ideal gas law for the measured temperatures and pressures of the recirculation and sample injection loops. Furthermore, the total amount of CO_2 produced as function of time on-line included the corrections for the gas lost due to injection into the GC and the gas replaced by fresh feed gas after each injection. The partial pressures of O_2 and CO in the recirculation loop after each injection were calculated from the known CO_2 concentration and the reaction stoichiometry to determine how much of the reactant gases were consumed in the CO oxidation reaction. The conversion of CO and O_2 is defined as the moles of gas consumed by reaction divided by the moles of gas consumed by reaction plus the moles of gas currently in the recirculation loop. Thus, conversion is decreased by more frequent sampling of the reaction mixture because fresh feed gas (~1 cm^3) replaces the gas lost to GC injection, and this represents 3% of the total volume of the system (32 cm^3). The activity of the empty reactor and the clean TiO_2(110) crystal without Pt constituted only ~3% of the activity for CO oxidation on 2 ML Pt at 160 ℃.

Figure 2.4 shows the CO2 produced, integral rate of CO_2 formation and % CO conversion as a function of time on-line for CO oxidation over the 2 ML Pt clusters at various temperatures. For each temperature, the amount of CO_2 produced increases linearly with time up to 24 hours, illustrating the effectiveness of the recirculation of the reactant gases over the catalyst for enhancement of product concentrations. The CO_2 concentration at the lowest temperature after the first 15 min online is already sufficiently

high to be detected by the GC, and the system is capable of detecting concentrations in the recirculation loop as low as 1 nmol/cm^3.

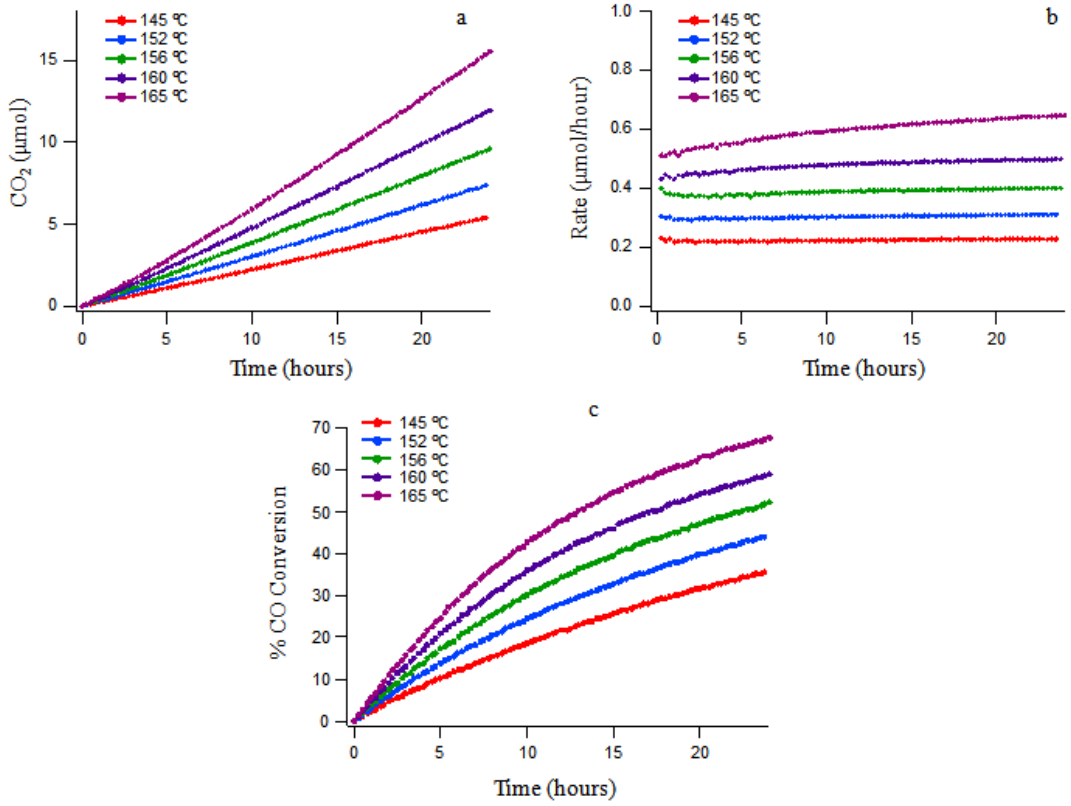

Figure 2.4: CO oxidation data for 2 ML Pt on TiO_2(110) as a function of time on-line at various temperatures: a) CO_2 production in mol; b) integral rate in mol of CO_2/hour; and c) % CO conversion. The feed gas composition was 0.83% CO/17.4% O_2/balance He

For reaction temperatures of 145 to 156 ℃, the integral rate of reaction was constant over the entire 24 hour reaction period, implying that pseudo-steady state reaction conditions are reached. At a 15 minute interval between injections, the concentrations of reactants are kept constant because the rate of consumption for the limiting reagent CO is equal to rate at which the feed gas is replaced in makeup mode after each injection. Therefore, by adjusting the injection time, it is possible to achieve pseudo state-steady conditions in which the concentration of the reactants are not changing. This assumes that

a reaction temperature is chosen such that the reaction rate can be matched by the rate at which feed gas can be restored in makeup mode. For longer injection intervals like 60 min, the rate is no longer constant because the reactants are consumed more quickly than they are replenished. Similarly, at 160 and 165 ℃, the changes in reactant concentrations are greater, and the rate increases slightly over time rather than remaining constant. Furthermore, since the reaction order in CO is known to be negative for CO oxidation on Pt[25, 28], the reaction rate is expected to increase as more CO is consumed at the longer reaction times; this effect should be more pronounced at the higher temperatures, as observed in the 160 and 165 ℃ experiments. Figure 4c illustrates that the CO conversion reaches 68% after 24 hours at 165 ℃ and decreases as a function of temperature, with only 36% conversion after 24 hours at 145 ℃.

An activation energy of 16.4 kcal/mol was calculated from the Arrhenius plot for CO oxidation over the 145-165 ℃ range (Figure 2.5, Table 2.2). The reaction rates were determined from the differential rates, and these values were averaged over the time range in which the CO conversion was less than 10% at each temperature. This reaction time was 0.5-4.5 hours for the 145 ℃ data and 0.5-1.75 hours at the highest temperature of 165 ℃, where changes in concentrations occurred most rapidly. Experiments were conducted on the same 2 ML Pt/TiO_2 surface by successively increasing the temperature from 145 to 165 ℃. The experiment at 160 ℃ then was repeated, and the reaction rate for the second experiment was nearly identical (within 4%) to that of the first, indicating that the surface was not poisoned by sequential experiments. The high degree of linearity for the Arrhenius plot demonstrates that the activation energy for CO oxidation is constant over this temperature range.

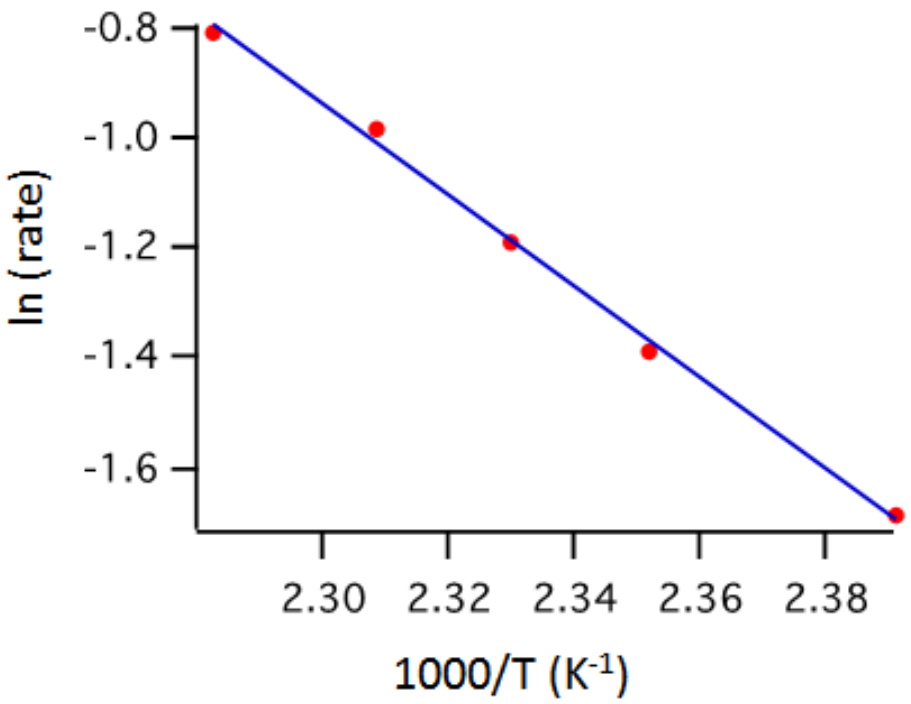

Figure 2.5: Arrhenius plot for CO oxidation on 2 ML Pt on TiO_2(110) at various temperatures. The feed gas composition was 0.83% CO/17.4% O2/balance He

Table 2.2: Comparison of kinetic parameters from this work with those on Pt(100) and Pt clusters supported on powdered oxides.

	2 ML Pt on TiO_2(110)	Pt(100)	Pt/SiO_2[31]	Pt/SiO_2[42]	Pt/TiO_2[43]
E_a (kcal/mol)	16.4	13.0[28]	17-19	13.4	12.2
Order in O_2	0.9 (160 ℃) 0.9 (145 ℃)	1.0 (150-230 ℃) [28]	----	0.9 (177 ℃)	----
Order in CO	-0.8 (160 ℃) -0.5 (145 ℃)	0 to -0.6 (150-230 ℃)[28]	----	-0.2 (177 ℃)	----
TOF (molec)/(site s)	0.03 (152 ℃) 0.06 (165 ℃)	0.01-0.02 (152 ℃) [44]	0.01-0.02 177 ℃	0.04 (177 ℃)	0.009 (27 ℃)

The reaction order in O_2 for CO oxidation at 160 ℃ was determined to be 0.9, based on the slope of the plot of ln(rate) vs. ln(P_{O2}) (Figure 2.6). For these experiments, the CO concentration was fixed at 0.83%, the O_2 concentrations were 5%, 8%, 12% and 17.4%, and the reaction mixture was sampled every 15 min. Reaction rates were calculated by

averaging the differential rates between 0.5 and 1.25 hours so that the CO conversion was always less than 5%, with the maximum conversion occurring for the highest oxygen concentration. A single Pt/TiO_2 sample was used for this set of experiments, and the experiments were conducted by varying the O_2 concentration from high to low values. The order in O_2 at 145 ℃ was also determined to be 0.9 from a similar set of experiments for O_2 concentrations of 5%, 8% and 17.4% and a fixed CO concentration of 0.83% (Figure 2.10). The differential rates were averaged over the entire experiment, which ranged from 4-10 hours, keeping the maximum conversion less than 10%.

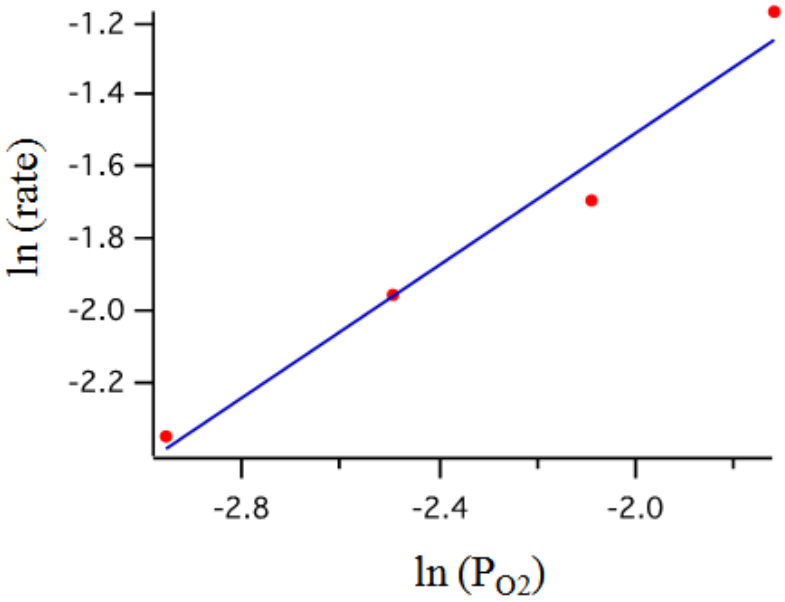

Figure 2.6: Plot of ln(rate) vs. ln(P_{O2}) for CO oxidation on 2 ML Pt clusters on TiO_2(110) at 160 °C with feed gas compositions of 0.83% CO and 5, 8, 12 and 17.4% O_2/balance He. From the slope of the plot, the order in O_2 was 0.9.

The reaction order in CO was determined to be -0.8 at 160 ℃ from the data in Figure 2.7. It was not possible to determine CO reaction order by varying the initial concentrations of CO while keeping the O_2 concentration fixed because the surface deactivated rapidly at CO concentrations greater than 0.83%; at lower CO concentrations,

differential conversion conditions (<10% conversion) could not be achieved at 160 ℃ due to the accelerated reaction rates. Instead, the data in Figure 2.7 were extracted from a single experiment in which the initial concentration was 0.83% CO/17.4% O_2, and the time interval between injections was 1 hour. In this manner, the CO partial pressure decreased from 0.00741 to 0.00215 atm as it was consumed during the 14 hour reaction period reaction, whereas the relatively high concentration of O_2 diminished by less than 2% over the same period. For longer reaction times, the plot of ln(rate) vs. ln(P_{CO}) became nonlinear as the O_2 concentration began to change more significantly. The differential rates in Figure 2.7 were calculated from a 3 point moving average in order to reduce the scatter, but the slope of the plot was unchanged by the smoothing process. The CO concentration corresponding to each differential rate was determined by averaging the initial and final concentrations.

At 145 ℃, the order in CO was determined to be -0.5, based on a series of experiments with initial CO concentrations of 0.2%, 0.4% and 0.8% and an O_2 concentration fixed at 17.4% O_2 (Figure 2.11). Data were collected over a 1-5.6 hour time period when the conversion of CO was less than 10%. Furthermore, the order in CO at 145 ℃ was also calculated as -0.5 from a single experiment for 0.21%CO/17.4% O_2, in which the gas mixture was sampled every 15 min; under these conditions, the O_2 concentration was unchanged (<0.3%) and the CO concentration varied from 0.00168 atm to 0.00117 atm (Figure 2.12). In general, reaction orders at 145 ℃ were more difficult to calculate because the surface was easily poisoned at the lower temperatures, particularly for high CO and low O_2 concentrations. For example, a repeat of the 0.2% CO/17.4% O_2 experiment at 145 ℃ resulted in a ~15% decrease in activity.

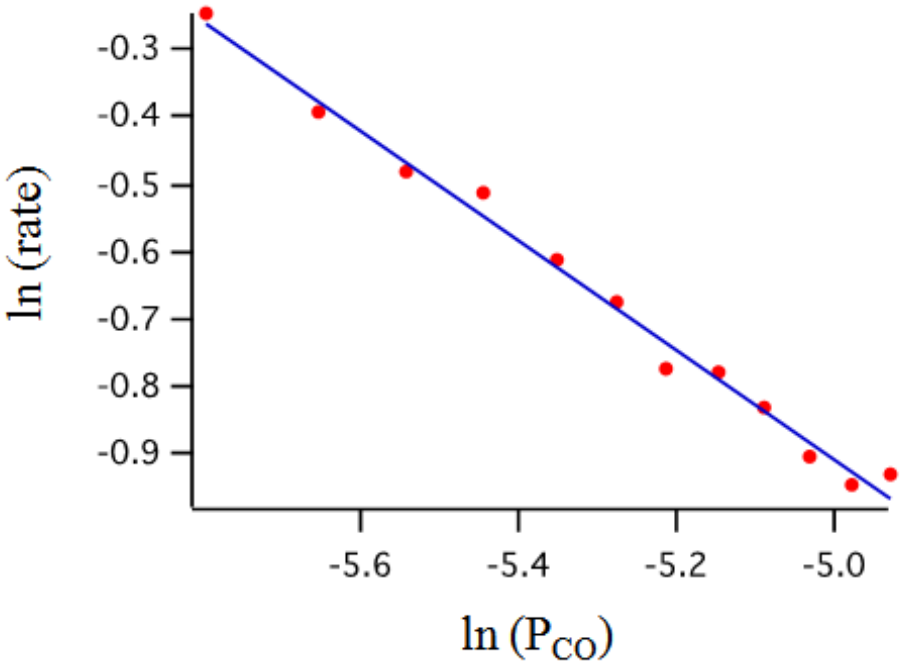

Figure 2.7: Plot of ln(rate) vs. ln(P_{CO}) for CO oxidation on 2 ML Pt clusters on TiO_2(110) at 160 °C with an initial feed gas composition of 0.83% CO/17.4% O_2/balance He. Data was collected at 60 minute intervals, over which the CO partial pressure varied from 0.00741 to 0.00215 atm. From the slope of the plot, the order in CO was -0.8

The kinetic parameters for CO oxidation determined from these experiments are compared with values from the literature in Table 2.2 for CO oxidation on Pt(100) as well as Pt clusters supported on powdered oxide supports. The activation energy of 16.4 kcal/mol calculated for the Pt clusters on TiO_2 (110) is in general agreement with the literature values for similar reaction temperatures. For example, activation energies of 17-19 kcal/mol were reported for high surface area Pt/SiO_2 catalysts that were evaluated in a flow reactor[32].A slightly lower value of 13 kcal/mol was reported on Pt(100) for a batch reactor study[28] and 12-13 kcal/mol was also reported for CO oxidation on Pt/SiO_2[42] and Pt/TiO_2[43] in flow reactors. CO oxidation on Pt is a well-studied system, and it is believed that the reaction occurs via a Langmuir-Hinshelwood mechanism in which

adsorbed CO reacts with absorbed oxygen atoms produced from dissociation of O_2[27, 28, 45]. The surface is predominantly covered with CO, and the reaction rate is controlled by the rate of CO desorption from the surface. Under these conditions, CO desorption must occur for in order for Pt sites to be available for oxygen adsorption, and the reaction is first order in oxygen and negative order in CO[25]. However, CO oxidation on Pt is believed have two distinctly different reaction mechanisms with different activation energies. The change between the mechanisms occurs around 200 ℃, which is the temperature range corresponding to CO desorption. Above 230 ℃, the activation energy on Pt(100) increases to 33 kcal/mol, which is a value similar to the binding energy of CO on Pt[28].Since the transition between the two mechanisms occurs around the high temperature range for our experiments, it is not surprising that there are differences between the activation energy reported here and the literature values, given that the activation energy is temperature dependent below 230 ℃[28].

For CO oxidation on Pt clusters on TiO_2(110), the calculated order in O_2 was 0.9 at both 145 and 160 ℃, and this value agrees well with orders in O_2 of 0.9-1 on Pt(100) [28] and Pt/SiO_2[42]. The order in CO is -0.8 at 160 ℃ and -0.5 at 145 ℃ for Pt/TiO_2(110) compared to 0.9-1 on Pt(100) [28] and Pt/SiO_2 [42]. Furthermore, the order in CO is known to change with reaction temperature, ranging from 0 to -0.6 on Pt(100) below 230 ℃, with larger negative orders observed at the higher temperatures [28]. On Pt/SiO_2, the order for CO is -0.2 at 177 ℃ [42]. Our reaction orders in CO are consistent with the negative values reported in the literature, indicating that CO has an inhibiting effect on the reaction since the high concentrations of CO block sites on Pt for O_2 adsorption and dissociation.

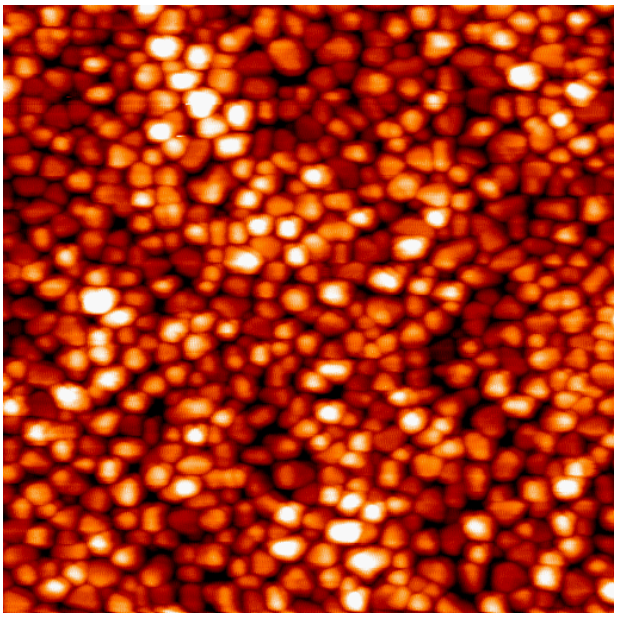

Figure 2.8: STM image of 2 ML Pt supported on TiO_2 (110). The image size is 1000 Ax1000A, and the image was acquired at a +2.3 V bias to the sample and 0.1 nA tunneling current.

Turnover frequencies (TOF) for the 2 ML Pt /TiO_2(110) catalyst at 152 and 165 ℃ were calculated from the average differential rate and the concentration of active sites ($1.5x10^{15}$ cm^{-2}). The active sites were estimated from the total Pt surface area, which was calculated from a numerical integration of a STM image for 2 ML Pt on TiO_2 (Figure 2.8)[35]; it was also assumed that the packing density of the atoms on the surface of the Pt clusters is the same as Pt(111) and that one Pt atom constitutes an active site. The calculated TOFs of 0.03-0.06 molecules/(site s) are slightly higher than those reported in the literature for reaction on Pt(100) (0.01-0.02 at 152 ℃)[44] and Pt/SiO_2 (0.01[32]-0.04[42] at 177 ℃). However, TOF values are extremely sensitive changes in reaction temperature and also dependent on an accurate estimation of the number of active sites. Therefore, the

minor differences between our TOF and those reported in the literature are not outside the range of expected experimental error.

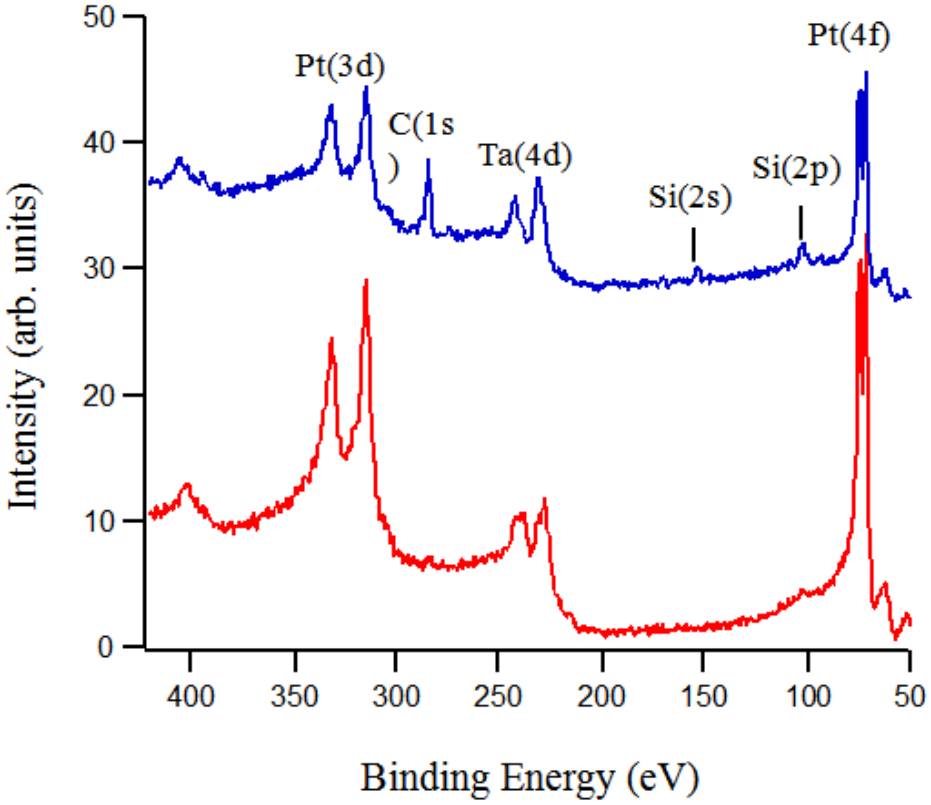

Figure 2.9: XPS data for 2 ML Pt on TiO_2(110) before (red) and after (blue) CO oxidation experiments in the reactor.

XPS experiments were conducted on the 2 ML Pt clusters on TiO_2(110) before and after CO oxidation in the catalytic reactor. A comparison of survey scans show that carbon is the major surface contaminant based on the C(1s) feature that appears at 284.5 eV; note that the Ta(4d) features are from the Ta foil straps that hold the crystal to the back plate (Figure 2.8). Trace amounts of Si are also detected, with the Si(2p) and Si(2s) features appearing at 102.5 and 153.0 eV, respectively. The Si(2p) binding energy for the Si contaminant corresponds more closely with SiO_2 (103.4 eV) than with unoxidized Si (99.2 eV)[44]. Low energy ion scattering experiments confirmed that Si was a contaminant

present in the top monolayer of the surface (data not shown). The silica contaminant does not have any activity for CO oxidation under these experimental conditions since accumulation of silica on TiO_2(110) did not contribute to CO oxidation activity. The exact origin of the silica contamination is not known, but it is possible that a flake of fiberglass insulation from the external heating tapes was accidentally introduced into the reactor system.

XPS spectra were collected over the 0-1200 eV energy range, but only the 50-450 eV range is shown in Figure 2.9 for the sake of clarity. After reaction in the recirculating reactor for 24 hours, the Pt/TiO_2 surfaces showed no evidence of fluorine contamination (F(2p) at 685 eV) associated with the fluorine-containing Kalrez and PTFE seals for the switching valves.

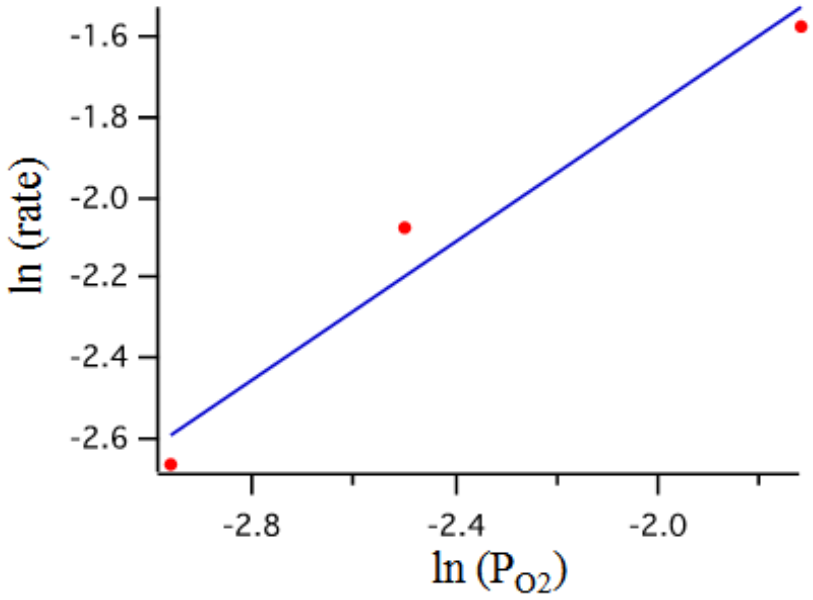

Figure 2.10: Plot of ln(rate) vs. ln(P_{O2}) for CO oxidation on 2 ML Pt clusters on TiO_2(110) at 145 °C with feed gas compositions of 0.83% CO and 5, 8, and 17.4% O_2/balance He. From the slope of the plot, the order in O_2 was 0.9

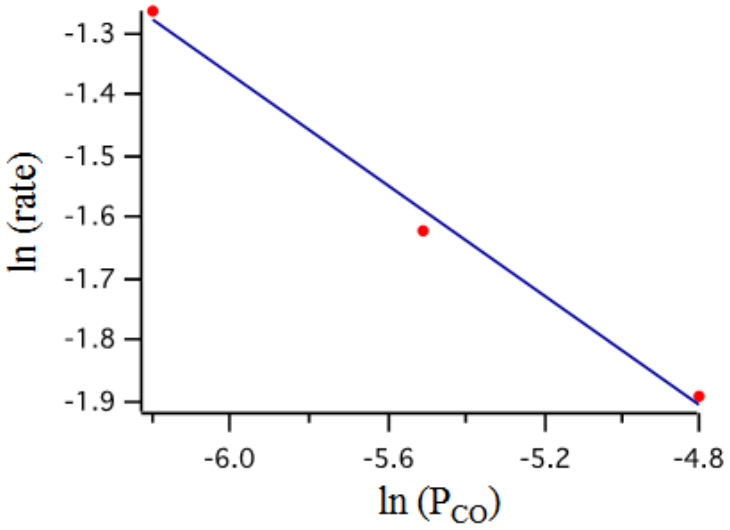

Figure 2.11: Plot of ln(rate) vs. ln(PCO) for CO oxidation on 2 ML Pt clusters on TiO_2(110) at 145 °C with feed gas compositions of 17.4% O_2 and 0.2, 0.4 and 0.8% O_2/balance He. From the slope of the plot, the order in CO was -0.5.

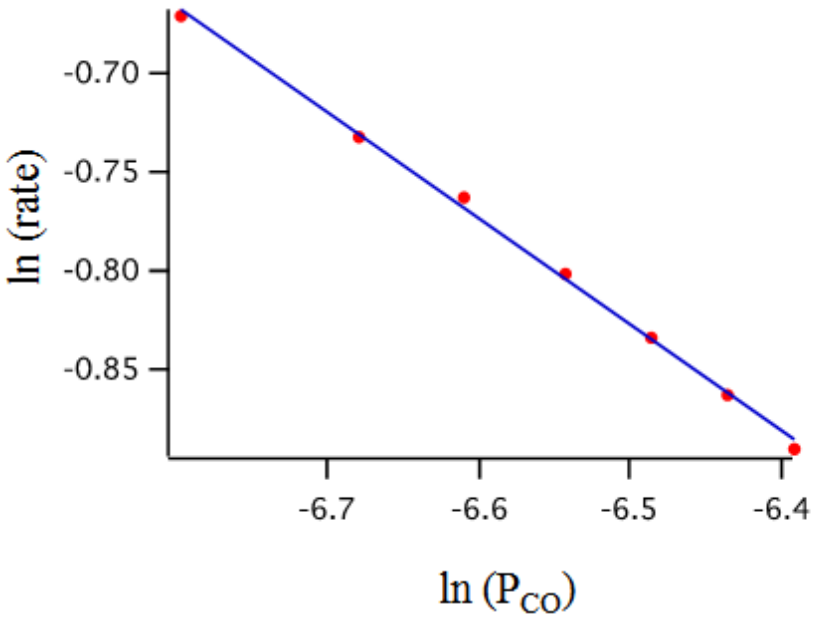

Figure 2.12: Plot of ln(rate) vs. ln(P_{CO}) for CO oxidation on 2 ML Pt clusters on TiO_2(110) at 145 °C with an initial feed gas composition of 0.21% CO/17.4% O_2/balance He. Data was collected at 15 minute intervals, over which the CO partial pressure varied from 0.00168 to 0.00117 atm. From the slope of the plot, the order in CO was -0.5

2.4 CONCLUSIONS

A novel recirculation loop reactor has been constructed for catalytic evaluation of model catalysts with low concentrations of active sites. This reactor is directly attached to a UHV chamber so that surface analysis can be conducted before and after reaction without exposure of the catalyst to air. The volume of the entire reaction system has been kept to a minimum (32 cm^3) for faster build-up of concentrations of reaction products, and the recirculation capability eliminates heat and mass transfer issues often associated with batch reactors. Furthermore, the gas removed for injection into the GC is automatically replaced with fresh feed gas so that there is no pressure decrease in the reactor due to sampling. Consequently, catalytic activity can be studied at frequent sampling intervals (15 min) over extended periods of time on-line (24 hours), despite the small volume of the reaction cell. One of the main advantages of this reactor design is that kinetics can be investigated under near steady-state conditions by adjusting the time interval between injections such that the concentrations of the reactants are unchanged even over extended times on-line. The fact that the reactor is completely isolated from the UHV chamber except during sample transfer means that samples can be analyzed by the various surface science techniques immediately after introduction into the UHV chamber. Catalytic evaluation of 2 ML Pt clusters on vapor-deposited on TiO_2 (110) for CO oxidation were conducted in this reactor as a proof of concept study. Kinetic parameters such as activation energy, order in CO and O_2 and TOFs were in good agreement with those reported in the literature for Pt(100) and Pt clusters supported on conventional, powdered oxide supports.

ACKNOWLEDGEMENTS

Thanks to Dr. John Monnier, Dr. Donna Chen, Dr. Samuel Tenney and Dr. Abraham Rodriguez for the original construction of micro-reactor, also thanks to Dr. Tenney for instruction in operating the automated system and data processing; also thanks to Dr. Randima Galhenage and Dr. Audrey Duke for the preparation and characterizations (STM and XPS) of 2 ML Pt-TiO_2 catalyst.

2.5 REFERENCES

(1) Campbell, C. T., *Studies of Model Catalysts with Well-Defined Surfaces Combining Ultrahigh Vacuum Surface Characterization with Medium- and High-Pressure Kinetics. In Advances in Catalysis*, D.D. Eley, H. P.; Paul, B. W., Eds. Academic Press: 1989; Vol. Volume 36, pp 1-54.

(2) McClure, S. M.; Goodman, D. W., New insights into catalytic CO oxidation on Pt-group metals at elevated pressures. *Chemical Physics Letters* **2009,** 469 (1–3), 1-13.

(3) Sun, Y. N.; Qin, Z. H.; Lewandowski, M.; Carrasco, E.; Sterrer, M.; Shaikhutdinov, S.; Freund, H. J., Monolayer iron oxide film on platinum promotes low temperature CO oxidation. *Journal of Catalysis* **2009,** 266 (2), 359-368.

(4) McClure, S. M.; Goodman, D. W., Simulating the Complexities of Heterogeneous Catalysis with Model Systems: Case studies of SiO_2 Supported Pt-Group Metals. *Topics in Catalysis* **2011,** 54 (5), 349-362.

(5) Wang, L.; Tysoe, W. T., An investigation of ethylene hydrogenation catalyzed by metallic molybdenum using an isolatable high-pressure reactor: Identification of the reaction site and the role of carbonaceous deposits. *Journal of Catalysis* **1991,** 128 (2), 320-336.

(6) Wang, Y.-N.; McAllister, R.; Herman, R. G.; Simmons, G. W.; Klier, K., Design and construction of a simple UHV-compatible high-pressure reaction cell. *Review of Scientific Instruments* **1992,** 63 (12), 5767-5770.

(7) Kuhrs, C.; Swoboda, M.; Weiss, W., Single crystal flow reactor for studying reactivities on metal oxide model catalysts at atmospheric pressure to bridge the pressure gap to the adsorption properties determined under UHV conditions. *Topics in Catalysis* **2001,** 15 (1), 13-18.

(8) Zhao, Z.; Diemant, T.; Haring, T.; Rauscher, H.; Behm, R. J., Small-volume, ultrahigh-vacuum-compatible high-pressure reaction cell for combined kinetic and in situ IR spectroscopic measurements on planar model catalysts. *Review of Scientific Instruments* **2005,** 76 (12), 123903-8.

(9) Kahn, D. R.; Petersen, E. E.; Somorjai, G. A., The hydrogenolysis of cyclopropane on a platinum stepped single crystal at atmospheric pressure. *Journal of Catalysis* **1974,** 34 (2), 294-306.

(10) Blakely, D. W.; Kozak, E. I.; Sexton, B. A.; Somorjai, G. A., New instrumentation and techniques to monitor chemical surface reactions on single crystals over a wide pressure range (10^{-8}-10^{+5} Torr) in the same apparatus. *Journal of Vacuum Science and Technology* **1976,** 13 (5), 1091-1096.

(11) Sexton, B. A.; Somorjai, G. A., The hydrogenation of CO and CO_2 over polycrystalline rhodium: Correlation of surface composition, kinetics and product distributions. *Journal of Catalysis* **1977,** 46 (2), 167-189.

(12) Cabrera, A. L.; Spencer, N. D.; Kozak, E.; Davies, P. W.; Somorjai, G. A., Improved instrumentation to carry out surface analysis and to monitor chemical surface reactions in situ on small area catalysts over a wide pressure range (10^{-8}--10^{+5} Torr). *Review of Scientific Instruments* **1982,** 53 (12), 1888-1893.

(13) Henry, R. M.; Walker, B. W.; Stair, P. C., Adsorption selectivity of Lewis acids and bases on an oxidized Mo(100) surface studied by LEED, Auger, and XPS. *Surface Science* **1985,** 155 (2–3), 732-750.

(14) Rucker, T. G.; Franck, K.; Colomb, D.; Logan, M. A.; Somorjai, G. A., Novel high-pressure isolation cell capable of reaching 120 atm mounted in an ultrahigh-vacuum chamber. *Review of Scientific Instruments* **1987,** 58 (12), 2292-2294.

(15) Kellogg, D. S.; Touvelle, M. S.; Stair, P. C., Cyclopropane hydrogenolysis on clean and chemically modified Mo(100) surfaces. *Journal of Catalysis* **1989,** 120 (1), 192-205.

(16) Taylor, P. A.; Rasmussen, P. B.; Ovesen, C. V.; Stoltze, P.; Chorkendorff, I., Formate synthesis on Cu(100). *Surface Science* **1992,** 261 (1–3), 191-206.

(17) Ludviksson, A.; Yoshihara, J.; Campbell, C. T., A high pressure cell and transfer rod for ultrahigh vacuum chambers. *Review of Scientific Instruments* **1995,** 66 (8), 4370-4374.

(18) Campbell, C. T.; Paffett, M. T., Model studies of ethylene epoxidation catalyzed by the Ag(110) surface. *Surface Science* **1984,** 139 (2–3), 396-416.

(19) Vajo, J. J.; Tsai, W.; Weinberg, W. H., Versatile microreactor for studies of gas--surface catalytic reactions between 10^{-7} and 1000 Torr. *Review of Scientific Instruments* **1985,** 56 (7), 1439-1442.

(20) Ichikawa, S.; Wilson, M. S., Sample transfer system for surface studies in wide pressure range (10^{-7}-10^{6} Pa). *Review of Scientific Instruments* **1987,** 58 (2), 317-319.

(21) Campbell, R. A.; Goodman, D. W., A new design for a multitechnique ultrahigh vacuum surface analysis chamber with high pressure capabilities. *Review of Scientific Instruments* **1992,** 63 (1), 172-174.

(22) Szanyi, J.; Goodman, D. W., Combined elevated pressure reactor and ultrahigh vacuum surface analysis system. *Review of Scientific Instruments* **1993,** 64 (8), 2350-2352.

(23) Gao, F.; Cai, Y.; Gath, K. K.; Wang, Y.; Chen, M. S.; Guo, Q. L.; Goodman, D. W., CO Oxidation on Pt-Group Metals from Ultrahigh Vacuum to Near Atmospheric Pressures. 1. Rhodium. *The Journal of Physical Chemistry C* **2008,** 113 (1), 182-192.

(24) Gao, F.; McClure, S. M.; Cai, Y.; Gath, K. K.; Wang, Y.; Chen, M. S.; Guo, Q. L.; Goodman, D. W., CO oxidation trends on Pt-group metals from ultrahigh vacuum to near atmospheric pressures: A combined in situ PM-IRAS and reaction kinetics study. *Surface Science* **2009,** 603 (1), 65-70.

(25) Langmuir, I., The mechanism of the catalytic action of platinum in the reactions $2CO+O_2= 2CO_2$ and $2H_2+O_2= 2H_2O$. *Transactions of the Faraday Society* **1922,** 17, 621-654.

(26) Engel, T.; Ertl, G., *Elementary Steps in the Catalytic Oxidation of Carbon Monoxide on Platinum Metals. In Advances in Catalysis,* D.D. Eley, H. P.; Paul, B. W., Eds. Academic Press: 1979; Vol. Volume 28, pp 1-78.

(27) Campbell, C. T.; Ertl, G.; Kuipers, H.; Segner, J., A molecular beam study of the catalytic oxidation of CO on a Pt(111) surface. *The Journal of Chemical Physics* **1980,** 73 (11), 5862-5873.

(28) Berlowitz, P. J.; Peden, C. H. F.; Goodman, D. W., Kinetics of carbon monoxide oxidation on single-crystal palladium, platinum, and iridium. *The Journal of Physical Chemistry* **1988,** 92 (18), 5213-5221.

(29) Valden, M.; Lai, X.; Goodman, D. W., Onset of Catalytic Activity of Gold Clusters on Titania with the Appearance of Nonmetallic Properties. *Science* **1998,** 281 (5383), 1647-1650.

(30) Diemant, T.; Hartmann, H.; Bansmann, J.; Behm, R. J., CO adsorption energy on planar Au/TiO_2 model catalysts under catalytically relevant conditions. *Journal of Catalysis* **2007,** 252 (2), 171-177.

(31) Leppelt, R.; Hansgen, D.; Widmann, D.; Haring, T.; Brath, G.; Behm, R. J., Design and characterization of a temporal analysis of products reactor. *Review of Scientific Instruments* **2007,** 78 (10), 104103-9.

(32) Cant, N. W., Metal crystallite size effects and low-temperature deactivation in carbon monoxide oxidation over platinum. *Journal of Catalysis* **1980,** 62 (1), 173-175.

(33) Jernigan, G. G.; Somorjai, G. A., Carbon Monoxide Oxidation over Three Different Oxidation States of Copper: Metallic Copper, Copper (I) Oxide, and Copper (II) Oxide - A Surface Science and Kinetic Study. *Journal of Catalysis* **1994,** 147 (2), 567-577.

(34) Galhenage, R. P.; Ammal, S. C.; Yan, H.; Duke, A. S.; Tenney, S. A.; Heyden, A.; Chen, D. A., Nucleation, Growth, and Adsorbate-Induced Changes in Composition for Co–Au Bimetallic Clusters on TiO_2. *The Journal of Physical Chemistry C* **2012,** 116 (46), 24616-24629.

(35) Zhou, J.; Ma, S.; Kang, Y. C.; Chen, D. A., Dimethyl Methylphosphonate Decomposition on Titania-Supported Ni Clusters and Films: A Comparison of Chemical Activity on Different Ni Surfaces. *The Journal of Physical Chemistry B* **2004,** 108 (31), 11633-11644.

(36) Park, J. B.; Ratliff, J. S.; Ma, S.; Chen, D. A., Understanding the Reactivity of Oxide-Supported Bimetallic Clusters: Reaction of NO with CO on TiO_2(110)-Supported Pt−Rh Clusters. *The Journal of Physical Chemistry C* **2007,** 111 (5), 2165-2176.

(37) Tenney, S. A.; Ratliff, J. S.; Roberts, C. C.; He, W.; Ammal, S. C.; Heyden, A.; Chen, D. A., Adsorbate-Induced Changes in the Surface Composition of Bimetallic Clusters: Pt−Au on TiO_2(110). *The Journal of Physical Chemistry C* **2010,** 114 (49), 21652-21663.

(38) Tenney, S. A.; He, W.; Roberts, C. C.; Ratliff, J. S.; Shah, S. I.; Shafai, G. S.; Turkowski, V.; Rahman, T. S.; Chen, D. A., CO-Induced Diffusion of Ni Atoms to the Surface of Ni–Au Clusters on TiO_2(110). *The Journal of Physical Chemistry C* **2011,** 115 (22), 11112-11123.

(39) Park, J. B.; Conner, S. F.; Chen, D. A., Bimetallic Pt−Au Clusters on TiO_2(110): Growth, Surface Composition, and Metal−Support Interactions. *The Journal of Physical Chemistry C* **2008,** 112 (14), 5490-5500.

(40) Tenney, S. A.; Cagg, B. A.; Levine, M. S.; He, W.; Manandhar, K.; Chen, D. A., Enhanced activity for supported Au clusters: Methanol oxidation on Au/TiO_2(110). *Surface Science* **2012,** 606 (15–16), 1233-1243.

(41) Ozturk, O.; Black, T. J.; Perrine, K.; Pizzolato, K.; Williams, C. T.; Parsons, F. W.; Ratliff, J. S.; Gao, J.; Murphy, C. J.; Xie, H.; Ploehn, H. J.; Chen, D. A.,

Thermal Decomposition of Generation-4 Polyamidoamine Dendrimer Films: Decomposition Catalyzed by Dendrimer-Encapsulated Pt Particles. *Langmuir* **2005,** 21 (9), 3998-4006.

(42) Cant, N. W.; Hicks, P. C.; Lennon, B. S., Steady-state oxidation of carbon monoxide over supported noble metals with particular reference to platinum. *Journal of Catalysis* **1978,** 54 (3), 372-383.

(43) Bamwenda, G. R.; Tsubota, S.; Nakamura, T.; Haruta, M., The influence of the preparation methods on the catalytic activity of platinum and gold supported on TiO_2 for CO oxidation. *Catalysis Letters* **1997,** 44 (1), 83-87.

(44) Peden Charles, H. F., *Carbon Monoxide Oxidation on Model Single-Crystal Catalysts. In Surface Science of Catalysis,* American Chemical Society: 1992; Vol. 482, pp 143-159.

(45) Nilekar, A. U.; Ye, X.; Junliang, Z.; Vukmirovic, M. B.; Sasaki, K.; Adzic, R. R.; Mavrikakis, M., Bimetallic and Ternary Alloys for Improved Oxygen Reduction Catalysis. *Topics in Catalysis* **2007,** 46 (3/4), 276-284.

CHAPTER 3 SUPERIOR LONG-TERM ACTIVITY FOR A PT-RE ALLOY COMPARED TO PT IN METHANOL OXIDATION REACTIONS[1]

[1]Adapted from Audrey S. Duke, Kangmin Xie, J.R. Monnier, D.A. Chen, "Superior Long-Term Activity for a Pt-Re Alloy Compared to Pt in Methanol Oxidation Reactions," submitted to Surface Science, 2016

3.1 INTRODUCTION

Bimetallic surfaces are often highly desirable catalysts due to superior activity, selectivity and stability compared to their monometallic counterparts[1-3]. Bimetallic Pt-Re systems have been used in hydrocarbon reforming since the 1960s[4, 5], and Pt-Re catalysts are reported to have increased activities and longer lifetimes than pure Pt catalysts[6, 7]. This sustained activity on the Pt-Re alloy has been attributed to increased resistance to the accumulation of carbonaceous species, which block active Pt sites[6-10]. Studies have also suggested that the improved activity might be due to Pt-Re electronic interactions in the bimetallic alloy catalysts[10-12]. Pt-Re systems have more recently garnered attention as catalysts for the reforming of biomass-derived products to hydrogen, which is used in hydrogen fuel cells as well as other catalytic applications[13-16]. For example, greater activity is observed for Pt-Re catalysts compared to pure Pt in the aqueous phase reforming (APR) of glycerol and other polyols used as models for understanding chemistry of biomass-derived carbohydrates[15, 17-22]. Higher activity for Pt-Re was attributed to weaker binding of CO and decreased poisoning of active sites by CO on the Pt-Re alloy[12, 18, 23-25]; however, it was also proposed that increased activity for the water gas shift reaction on Pt-Re was responsible for removing CO from the surface during the APR reaction[20, 22, 26]. In addition, Pt-Re catalysts have exhibited higher activity than Pt for the water gas shift reaction itself[26-31], as well as for glycerol hydrogenolysis[32, 33] and electrochemical oxygen reduction reactions[34]. For the water gas shift reaction, ReO_x has been proposed as the active site that promotes dissociation of water [29-31].

The oxidation of alcohols such as methanol is industrially relevant given that these reactions provide the basis for the production of many fine commodity chemicals[35]. For example, selective oxidation of methanol yields products such as formaldehyde and formic acid, which have a variety of applications; while formaldehyde is an important feedstock for the polymer, adhesive and paint industries[36], formic acid is used as a starting reagent for other organic synthesis reactions[37] and in alternative energy[38, 39]. Furthermore, methanol reaction on Pt surfaces has been well-studied in the literature both in reactor systems[40-45] and in ultrahigh vacuum experiments on single crystals[46-54] Methanol is one of the world's large volume commodity chemicals and has a total production of more than 25 million tons[55]. In addition to serving as a feedstock for the production of other chemicals, methanol is particularly relevant in the fuel industry since it can be used in both internal combustion engines and in direct methanol fuel cells[56-60]. Furthermore, methanol oxidation serves as a simple model system for understanding reactions of polyols in oxidation processes like aqueous phase reforming.

In the work reported here, methanol oxidation is studied on Pt and Pt-Re bimetallic surfaces in order to investigate the effect of Re on Pt-Re catalysts in oxidizing environments. Model catalysts consist of a polycrystalline Pt foil and a Pt-Re alloy surface prepared by annealing a Re film deposited on the Pt foil. Activity is investigated in a home-built microreactor coupled to the UHV chamber so that preparation of the surfaces as well as pre- and post-reaction XPS studies can be conducted without exposing the surface to air. The long-term activity of Pt-Re is superior to pure Pt in methanol oxidation at 60 ℃, where formic acid is the main product. The loss of Pt activity after 10-12 hours is attributed to the accumulation of carbon on the surface, whereas almost no

carbon is detected on Pt-Re. Oxygen-induced diffusion of Re to the surface is believed to occur during reaction, and the presence of oxygen on Re species appears to be more efficient at removing carbon from the surface than oxygen on Pt. Since surface carbon is readily oxidized on the Pt surface at higher reaction temperatures, a loss in activity from carbon accumulation is not observed. Furthermore, methanol oxidation does not occur in the absence of surface oxygen, and consequently there is a reaction onset time for activity to reach its maximum value as the oxygen coverage increases. Kinetic parameters such as activation energy (27.9 ±0.2 kJ/mol) and turnover frequency (90 s^{-1} at 100 ℃) determined for the Pt foil in this home-built reactor system agree with the values reported in the literature for methanol oxidation on Pt.

3.2 EXPERIMENTAL

Experiments were performed in an ultrahigh vacuum (UHV) chamber ($P < 3 \times 10^{-10}$ Torr) attached to a custom designed microreactor that has been described in detail elsewhere[61]. The chamber is equipped with an X-ray source (Leybold Heraeus, RQ 20/63) and hemispherical analyzer (SPECS, EA10) for X-ray photoelectron spectroscopy (XPS) experiments, as well as a quadrupole mass spectrometer (Stanford Research Systems, RGA 300). A homemade gripping device was used to remove the Ta sample plate from the sample holder and transfer it to the reactor while the pressure in the chamber remained below 1×10^{-7} Torr[61].

A polycrystalline Pt foil (ESPI Metals, 99.95%, 10 mm × 10 mm × 0.5 mm) was mounted to a Ta sample plate and cleaned by multiple cycles of Ar^+ sputtering (20 minutes, 1 kV) and annealing (3 minutes, 727 ℃); the cleanliness of the foil was confirmed by XPS. The foil was heated via electron bombardment of the Ta back plate,

and the temperature of the foil was measured by an infrared pyrometer (Heitronics, CT18.04). A 2.4 ML Re film was deposited on the Pt foil at room temperature from a 2 mm diameter Re rod (ESPI, 99.99%) in a four-pocket electron-beam evaporator (Oxford Applied Research, EGC04), and a Pt-Re surface alloy was formed by annealing the Re film to 727 ℃ for 5 minutes. Re coverages were determined by a UHV bakeable quartz crystal microbalance (Inficon). One monolayer of Re is defined according to the packing density of Re(0001) (1.52×10^{15} atoms/cm^2). Fresh surfaces were prepared for every experiment unless otherwise specified.

In the reactor, the sample was heated and cooled in a continuous flow of He (Airgas, 99.999%) at 50 sccm to temperatures between 60 ℃ to 150 ℃ at a rate of ~1.5-2 ℃ /min by heating tapes (Briskheat, BWHD) wrapped around the exterior of the reactor housing. Heating was regulated by a feedback loop on a temperature controller (Auber, SYL-4342P) to ensure controlled heating rates. The reactor temperature was measured by a type K thermocouple (Omega, KMQSS-040G-6) welded into the feed gas outlet in close proximity to the surface of the sample. The gas lines were maintained at 60 ℃ using two Valco Instruments temperature controllers. After the sample reached the desired temperature, the reaction mixture of 2% methanol (Fisher Chemical, 99.9%)/ 4% O_2 (Airgas, 99.5%)/ 94% He was mixed and introduced. Both O_2 and He were introduced via independently calibrated mass flow controllers (Brooks, 5850e and 5850i) with the total flow rate of all feed gas maintained at 58 sccm as determined by a digital flow meter (Agilent Technologies, ADM2000). Methanol vapor was introduced into the feed gas line by a homemade vapor-liquid equilibrator (VLE) filled with liquid methanol, where helium served as the sweep gas and was introduced via a mass flow controller. The

temperature of the VLE was controlled by a refrigerating/heating circulating bath (VWR), and the concentration of methanol in the vapor outlet was calculated using the Antoine equation for pure methanol. Pressure was monitored by two capacitance manometers (MKS Instruments, Baratron 722A) located upstream of the reactor in the feed gas line (790-800 Torr) and downstream of the reactor (770 Torr-780 Torr).

The reactor was operated in single-pass mode in which the reactant gas mixture makes one pass over the model catalyst and is then vented from the reactor system. For the activity tests performed over extended periods of time at a single temperature, the automated system was switched to sampling mode every 20 min; a sample of the gas (~1 cm^3) was injected to a gas chromatograph (HP 5890A) which is equipped with a PoraPLOT Q capillary GC column leading to a thermal conductivity detector (TCD). Methanol oxidation was observed for 10 and 24 hour periods over a temperature range of 60-150 ℃. To determine the activation energy of the reaction, a freshly prepared sample was first stabilized in the reaction mixture at 60 ℃ for 10 hours and then stabilized at 80 ℃, 100 ℃, 130 ℃, and 150 ℃ for 80 min each while four sampling injections were taken at each temperature. Response factors for each product were determined as described in the Supporting Information. The reaction rate and % selectivity calculations are based on the formation rate of the three detected carbon-containing products (CO_2, formaldehyde and formic acid). The background activity of the empty reactor and sample support was verified to be zero before and after all experiments.

XPS spectra were collected before and after reactor experiments with an Al Kα anode at a 30 °off normal detection angle. Peak fitting for the C(1s) and O(1s) spectra was

carried out with the shareware program XPSPeak using a Shirley background and Gaussian-Lorentzian peak shapes. The FHWM for the peaks was set at 2.0 eV.

3.3 RESULT

The Pt-Re alloy surfaces were prepared by depositing 2.4 ML Re on the clean Pt foil and annealing to 727 ℃ for 5 minutes. Previous studies of similar coverages of Re deposited on Pt(111) and annealed at 727 ℃ demonstrate that Re diffuses subsurface[53, 62, 63]. Specifically, STM experiments have shown an atomically flat surface with no Re islands after annealing, and the surface appears to be pure Pt based on low energy ion scattering data[63]. For Re deposited on the Pt foil, the integrated Re signal decreases by 30% after annealing (Figure 3.1a). Furthermore, after Re deposition at room temperature, the Pt signal is attenuated to 60% of the intensity for clean Pt, and the Pt signal increases back to 80% of clean Pt value after the Re film is annealed to 727 ℃ (Figure 3.1b). These changes in both the Pt and Re signals are consistent with the diffusion of Re into the Pt surface, and similar changes in the Pt and Re XPS signals were observed for the alloying of Re into Pt(111) (Figure 3.9).

Based on grazing angle XPS experiments, the attenuation of the Pt signal is consistent with Re being in the second and third subsurface layers[53]. In high resolution XPS experiments at the synchrotron, the formation of the Pt-Re alloy was confirmed by a small shift in the Pt(4f) and Re(4f) peaks to higher binding energy compared to the bulk surfaces. For these experiments with a conventional X-ray source, the Pt($4f_{7/2}$) shifts from 70.7 to 70.8 eV after alloying whereas the Re($4f_{7/2}$) of 40.3 eV is close to what is reported on Re single crystal surfaces[64, 65].

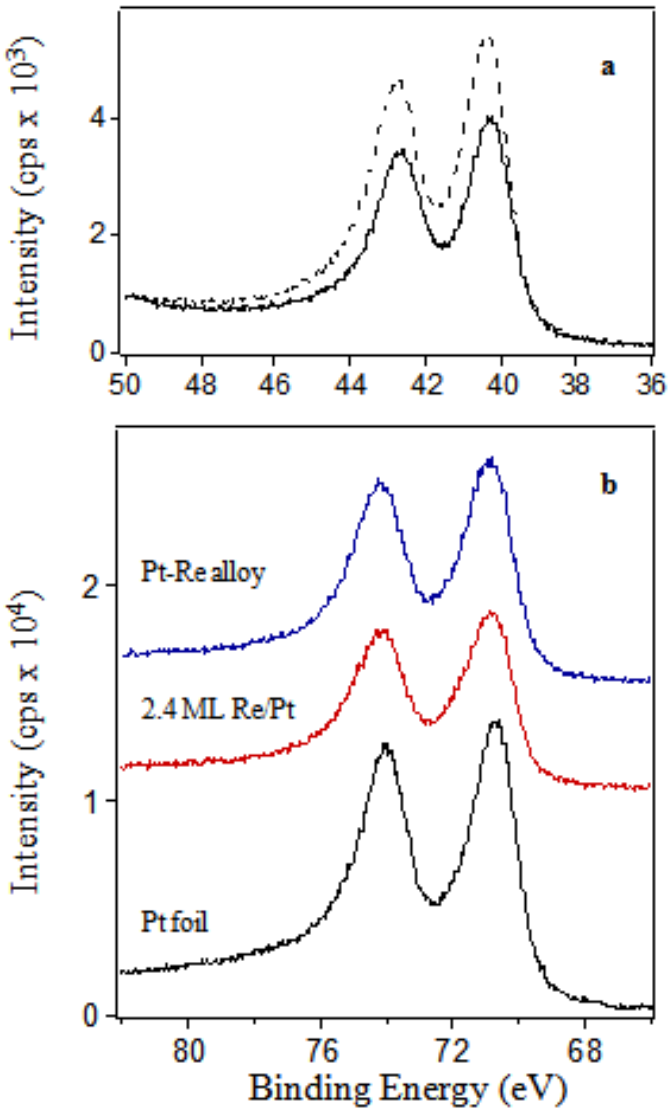

Figure 3.1: X-ray photoelectron spectroscopy data of the: a) Re(4f); and b) Pt(4f) regions for the 2.4 ML Re film annealed at 727 ℃ for 5 min to prepare the Pt-Re alloy. The dotted trace in (a) shows 2.4 ML of Re deposited on the Pt foil before annealing to prepare the alloy

Methanol oxidation studies on the clean Pt foil and Pt-Re alloy surface were carried out in a microreactor coupled to the UHV chamber over the temperature range of 60-150 ℃. All feed gas compositions are 2% methanol/4% O_2/94% He. On both surfaces,

the detected products are CO_2, formaldehyde, formic acid and water; the selectivities of the carbon-containing products as a function of temperature are very similar for Pt and Pt-Re (Figures 3.2 a,b). The selectivity for formic acid is greatest at 60 ℃ but decreases sharply with increasing temperature such that the selectivity is nearly zero at 130 ℃. In contrast, no formaldehyde is observed at 60 ℃, but formaldehyde production increases with temperature. The formaldehyde selectivity is close to its maximum value at 80 ℃ and remains relatively constant at the higher temperatures. The CO_2 yield is also low at 60 ℃ but increases steadily with temperature, and the selectivity to CO_2 reaches its maximum value of ~50% at 150 ℃. Methanol conversion on the Pt foil ranges from 2% at 60 ℃ to 16% at 150 ℃ (Figure 3.10). Data is not reported for temperatures greater than 150 ℃ because the increased product yields at temperatures >170 ℃, resulted in mass transfer limitations even at higher flow rates of 126 sccm.

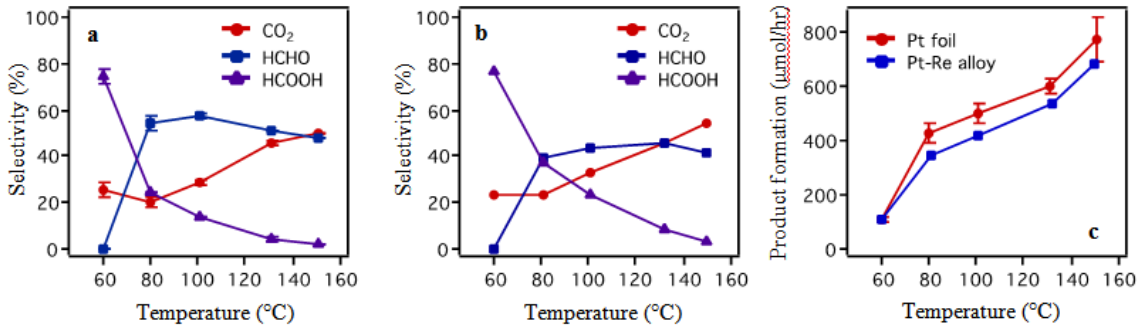

Figure 3.2: Product selectivities as a function of temperature for methanol oxidation on: a) the Pt foil; and b) the Pt-Re alloy. The total product formation as a function of temperature for these two surfaces is shown in (c). Error bars for the Pt data are the standard deviations from two experiments.

Total product formation for methanol oxidation on the Pt-Re alloy is shown in Figure 3.2c as a function of temperature and compared to activity on the Pt foil. At 60 ℃, the two surfaces have identical activities, but at higher temperatures, the product yields on the Pt-Re alloy are 10-20% lower than on the Pt foil. Rates of product formation in

μmol/hour for both surfaces as a function of temperature are shown in Figure 3S3. While the rates of CO_2 and formic acid production are comparable on both surfaces, the lower formaldehyde production on Pt-Re between 80 and 150 ℃ accounts for the lower overall activity of the alloy.

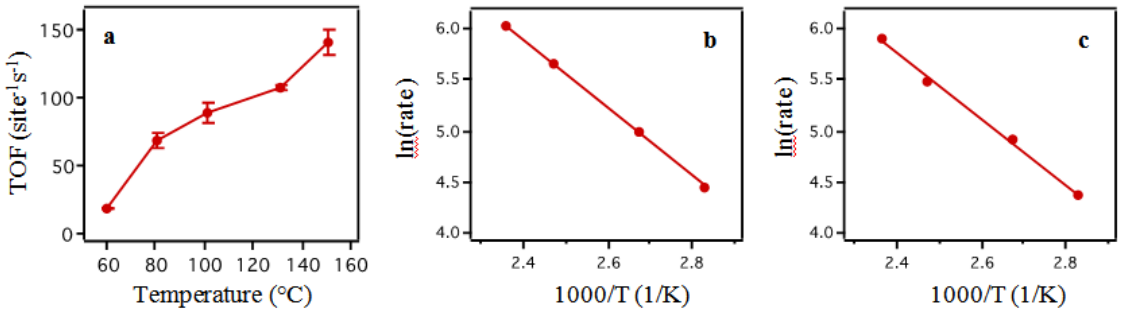

Figure 3.3: Turnover frequency as a function of temperature for methanol oxidation on the Pt foil (a); and Arrhenius plots for CO_2 formation during methanol oxidation on: b) the Pt foil; and c) the Pt-Re alloy. Error bars in (a) are the standard deviations from two experiments

Kinetic parameters such as the turnover frequency (TOF) and activation energy for methanol oxidation were also determined. The Pt foil is estimated to have a total of 1.0×10^{15} active sites; this calculation is based on the total exposed surface area of the foil (0.684 cm^2), and the assumption that the polycrystalline foil has the same number of atoms/cm^2 as the Pt(111) surface. The measured TOF is 88 ± 7 s^{-1} at 100 ℃, which agrees reasonably well with the value of 50 s^{-1} reported in the literature for methanol oxidation on Pt gauzes (Figure 3.3a), again assuming a Pt(111) packing density for Pt[41]. An Arrhenius plot for CO_2 production over the temperature range of 80-150 ℃ yields an activation energy of 27.9 ± 0.2 kJ/mol for reaction on the Pt foil (Figure 3.3b). The fact that the rate at 60 ℃ does not fit the linear trend for the rest of the data suggests that there may be a change in the reaction mechanism between 60 and 80 ℃, especially since product selectivities change significantly in this temperature range. For the Pt-Re alloy

surface, the measured activation energy for CO_2 formation is 27 ±1 kJ/mol (Figure 3.3c). The nearly identical activation energies for the Pt foil and Pt-Re alloy imply that the mechanism for CO_2 formation from methanol oxidation is the same on both surfaces.

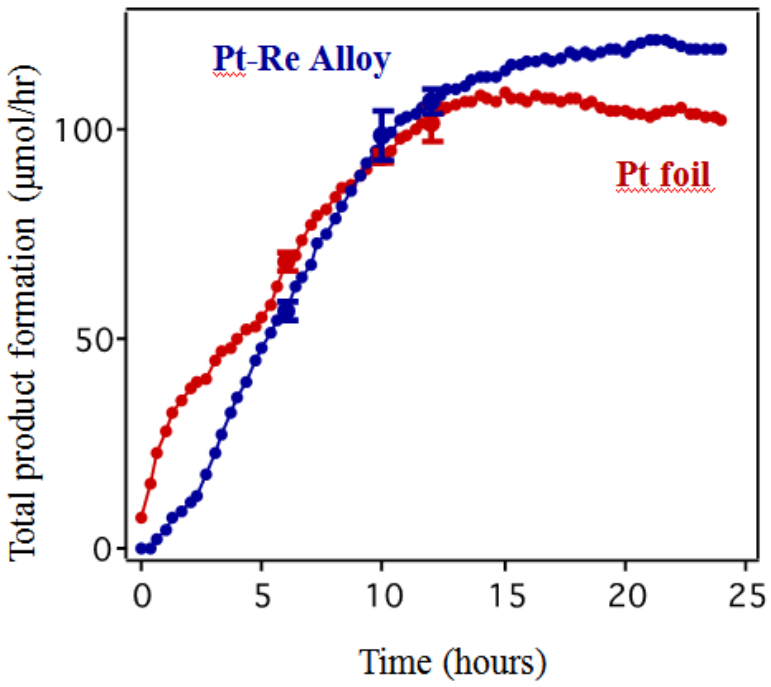

Figure 3.4: Activity data for Pt foil and Pt-Re alloy for methanol oxidation at 60 ℃ over 24 hours. Error bars shown at 6, 10 and 12 hours are the standard deviations from three different experiments on each surface.

Despite the slightly lower activity for Pt-Re compared to pure Pt over a two hour time period, the Pt-Re alloy exhibits greater long-term activity at 60 ℃ (Figure 3.4). In both cases, the initial activity is near zero, and the activity steadily increases over the first 10-15 hours. The activity of the Pt foil is initially higher than that of the Pt-Re alloy, but after roughly 10 hours, the activity of the Pt-Re alloy continues to increase over time whereas the activity of the Pt foil is diminished over the 10-24 hour time period. After 24 hours, the activity of the Pt-Re alloy is 15% higher than for Pt.

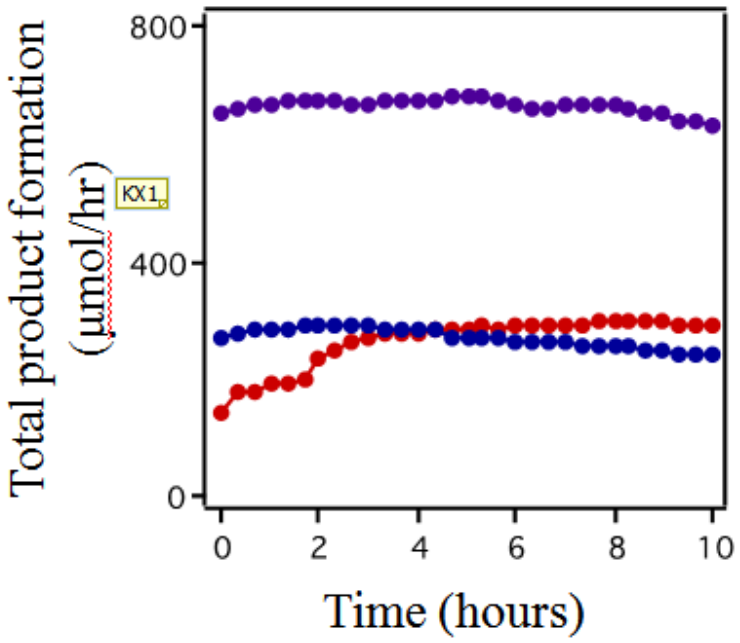

Figure 3.5: Activity for methanol oxidation on the pre-oxidized (blue) and unoxidized (red) Pt foil at 100 ℃, and on the unoxidized Pt foil at 150 ℃ (purple). The pre-oxidized Pt foil was exposed to 100% O_2 at 100 ℃ for 1 hour.

The induction time observed before activity reaches its maximum value is attributed to a lack of surface oxygen, which appears to be necessary to facilitate methanol oxidation. For a Pt foil pre-oxidized at 100 ℃ before exposure to methanol oxidation conditions, the activity for methanol oxidation at 100 ℃ is initially 270 μmol/hour and remains relatively constant over a 10 hour reaction period (Figure 3.5). XPS analysis shows that this oxidation treatment (100% O_2 at 100 ℃ for 1 hour) results in atomic oxygen on the surface, but the Pt remains metallic. In contrast, the activity of the Pt foil subjected to the usual sputtering/annealing treatments without pre-oxidation has an initial activity that is half of what is observed on the pre-oxidized surface; however, the activity on the unoxidized Pt foil increases with reaction time and reaches the same value as on the pre-oxidized surface after approximately 10 hours. At 100 ℃,

the initial activity of the unoxidized surface is significantly higher than at 60 ℃, where the activity is almost zero. Furthermore, at 150 ℃, no induction time for reaction is observed, and the activity is relatively constant over the entire 10 hour reaction period (Figure 3.5). These results are consistent with higher initial activities at 100 and 150 ℃ compared to 60 ℃ due to the greater coverages of surface oxygen initially formed at the elevated temperatures.

Post-reaction XPS data were acquired in order to understand the nature of the decrease in activity at 60 ℃ for reaction on the Pt foil (Figure 3.6). The C(1s) regions show that there is 40% more carbon on the surface of the Pt foil compared to the Pt-Re alloy after 24 hours under reaction conditions. On the Pt surface, the main C(1s) peak appears at 284.8 eV and is attributed to atomic carbon[54, 66, 67], but there is also a smaller feature at 286.0 eV assigned to CO based on the C(1s) spectrum for CO itself on the Pt foil (Figure 3.12), as well as previously reported CO on Pt(111) binding energies[53, 54, 67, 68]. On the Pt-Re alloy surface, both peaks are also observed, but the atomic carbon peak is significantly smaller than on Pt while the CO feature is of comparable intensity. Thus, it appears that the Pt surface is poisoned by atomic carbon whereas the Pt-Re alloy accumulates less carbon and maintains higher activity. C(1s) data for both surfaces after only 10 hours at 60 ℃ show equal coverages of both forms of carbon on the surface, and the subsequent loss of activity on Pt after 10 hours is consistent with the greater carbon buildup on Pt vs. Pt-Re during this time period. When the 10 hour-post reaction surfaces are heated to 427 ℃, the 286 eV peak disappears as expected since CO should desorb from the surface below this temperature. Furthermore, at higher methanol oxidation

temperatures of 100 and 150 ℃, almost no carbon is observed on Pt or Pt-Re after a 10 hour reaction period.

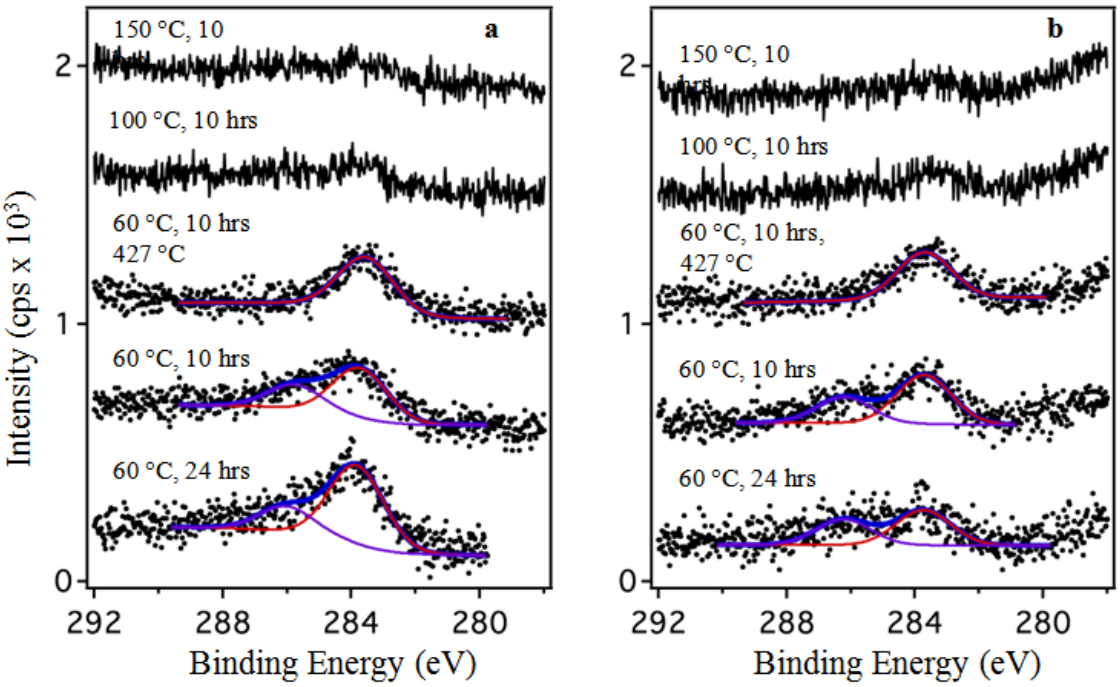

Figure 3.6: X-ray photoelectron spectroscopy data of the C(1s) region for: a) the Pt foil and b) Pt-Re alloy after exposure to methanol oxidation conditions at the designated temperatures and reaction times. The surface after 10 hrs at 60 ℃ was heated to 427 ℃ to desorb the weakly adsorbing surface species. The rising baseline below 280 eV for the Pt-Re alloy is from the Re($4d_{3/2}$) peak.

Post-reaction XPS experiments also show that significant surface oxygen is present on both Pt and the Pt-Re alloy (Figure 3.7). The total oxygen signal is 15% lower on the Pt-Re alloy than on the Pt foil after methanol oxidation at 60 ℃ for 24 hours. The O(1s) spectra for both surfaces can be fit with two peaks, indicating that at least two types of surface oxygen are present. For the Pt surface, the O(1s) region is fit with a peak at 531.0 eV attributed to atomic oxygen or hydroxyls, and at 532.5 eV assigned to water and CO. The 531 eV binding energy is slightly higher than the ~530 eV typically reported for atomic oxygen on Pt(111) surfaces[63, 69-75] but is the same as the binding

energy observed when the Pt foil is exposed to 4% O_2/He at room temperature (Figure 3.13).

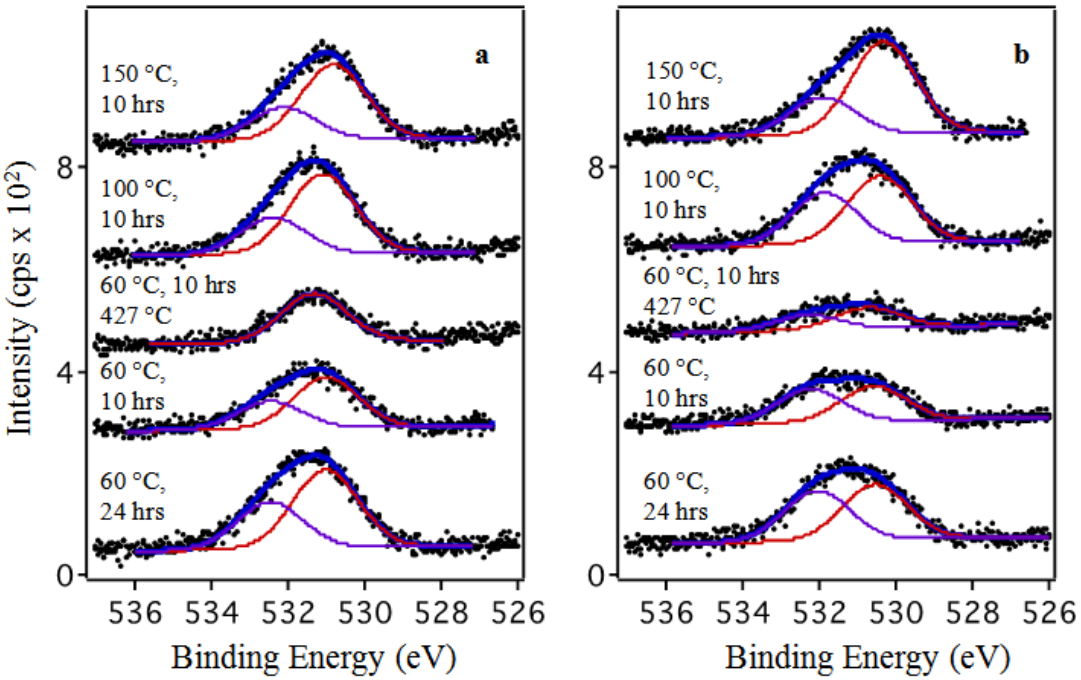

Figure 3.7: X-ray photoelectron spectroscopy data of the O(1s) region for: a) the Pt foil and b) Pt-Re alloy after exposure to methanol oxidation conditions at the designated temperatures and reaction times. The surface after 10 hrs at 60 C was heated to 427 ℃ to desorb the weakly adsorbing surface species.

In many cases, the binding energy of hydroxyl groups on Pt(111) appears at a slightly higher value (530.5-531.5 eV) [69, 73, 76], and this suggests that the observed 531 eV peak has contributions from both atomic oxygen and surface hydroxyls. The 532.5 eV value is consistent with reports of water on Pt(111)[69, 71, 75, 76].In addition, the C(1s) data indicate that CO exists on the surface as a minority carbon species, and therefore CO also contributes to the 532.5 eV peak at 60 ℃, given its similar O(1s) binding energy of ~532.7 eV[53, 68, 77].On the Pt-Re alloy, the species attributed to O/OH appears at 530.5 eV, which is slightly lower than for the O/OH on Pt; this is in agreement with the lower binding energies observed after exposing a 2.4 ML Re film on the Pt foil to O_2 at 100 ℃

(Figure 3.13). Similarly, the oxygen species assigned to water has a lower binding energy (532.1 eV) on the Pt-Re alloy, and this indicates that there is a difference in the adsorption of oxygen-containing species on the Pt-Re alloy compared to the Pt foil. On the Pt foil, the contribution of O/OH is larger than that of water, but on the Pt-Re alloy surface, the two oxygen species have roughly the same concentrations, suggesting that water is more stable on the Pt-Re alloy surface. The spectra collected on both surfaces after a shorter 10 hour reaction time at 60 ℃ demonstrate that 40-45% of the oxygen observed after 24 hours accumulates over the last 14 hours. The loss of the 532.5 eV peak after heating the post reaction Pt foil surface to 427 ℃ confirms the assignment of this feature to a weakly adsorbing species such as water or CO. On the post reaction Pt-Re alloy surface, heating to 427 ℃ removes the majority of oxygen at both binding energies; the loss of the higher binding energy species is due to water desorption, while the decrease in 530.5 eV intensity could be explained by diffusion of oxygen into the subsurface region. The surfaces after reaction at 100 ℃ for 10 hours show that 50-70% more oxygen accumulates at this higher reaction temperature compared to at 60 ℃, but the O(1s) intensities do not increase significantly for reaction at 150 ℃. There should be no contribution of CO to the 532.5 eV peaks at these higher temperatures since the C(1s) region indicates that CO is not present on the surface. At temperatures below 150 ℃, the concentration of O/OH on the Pt-Re alloy is lower than on pure Pt; moreover, the concentrations of water and O/OH are roughly equivalent on the Pt-Re alloy whereas the O/OH concentration is always higher on the Pt foil. At 150 ℃, O/OH becomes the dominant species on the Pt-Re alloy, presumably because water is less stable on the surface at higher temperature.

The Re(4f) and Pt(4f) regions were also collected for the Pt-Re alloy after reaction at various temperatures. Reaction at 60 ℃ results in only metallic Re on the surface since the Re(4f) peak shape is identical to that of metallic Re in the Pt-Re alloy before reaction (Figure 3.8a). There is a small shift in binding energy from 40.3 eV to 40.4 eV after reaction. Because the adsorption of oxygen on the Re surface is known to shift the binding energy by 0.2-0.7 eV[64, 65, 78], the +0.1 eV shift is attributed to the diffusion of a small fraction of Re atoms to the surface and the interaction of oxygen with this surface Re. The Re:Pt ratio decreases to 60% of its initial value before reaction after 10 hours under reaction conditions, and to 45% after 24 hours. The Re:Pt ratio is a better indicator of changes in the surface Re concentration than the absolute Re signal since adsorbate species that accumulate on the surface during reaction attenuate both the Pt and Re intensities. The loss of Re signal is attributed to the formation of Re_2O_7 under methanol oxidation conditions, given that Re_2O_7 is volatile and known to sublime at relatively low temperatures[79, 80]. This behavior has been previously observed by our group for Pt-Re surface alloys formed by Re deposition on Pt(111) in ambient pressure XPS studies for in situ CO and methanol oxidation with O_2[53, 63].

Notably, heating the Pt-Re alloy surface in helium or ultrahigh vacuum did not result in the same attenuation of the Re signal, which is only observed when heating in the presence of oxygen. For the Pt-Re alloy, most of the subsurface Re remains metallic, but O_2 induces diffusion of some fraction of Re to the surface; this surface Re is quickly oxidized to Re_2O_7 which then sublimes from the surface[53, 63]. For methanol oxidation at 100 ℃, metallic Re at 40.4 eV is still present on the surface, but the appearance of a small shoulder at 46 eV indicates that Re is oxidized. The 46 eV feature from ReO_x

becomes more pronounced at the higher reaction temperature of 150 ℃. For these surfaces, the Re:Pt ratio decreases to 46-48% of the value before reaction. For comparison, a 2.4 ML Re film exposed to methanol oxidation at 100 ℃ for 10 hours was also studied. The Re(4f) spectrum shows that Re at the surface is more easily oxidized than subsurface Re in the Pt-Re alloy, given that no metallic Re is present, and the Re:Pt ratio was only 15% of the initial value. The Pt(4f) spectra in Figure 3.8b demonstrate that Pt remains metallic under methanol oxidation conditions at all temperatures.

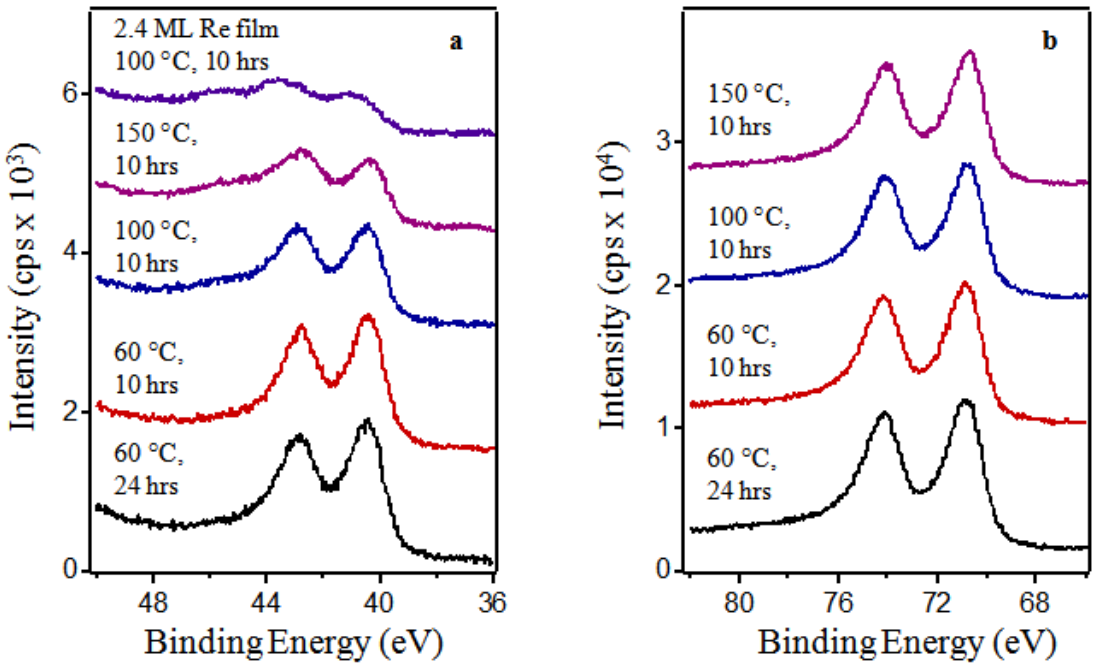

Figure 3.8: X-ray photoelectron spectroscopy data of the: a) Re(4f); and b) Pt(4f) regions for the Pt-Re alloy after exposure to methanol oxidation conditions for the designated reaction times and temperatures. A 2.4 ML Re film exposed to methanol oxidation conditions at 100 ℃ for 10 hrs is also shown in (a).

3.4 Discussion

The Pt-Re alloy surfaces exhibit superior long-term activity compared to pure Pt due to greater carbon buildup on Pt at 60 ℃. At this temperature, there is high selectivity

(~75%) for formic acid production on both Pt and Pt-Re. Other studies of methanol oxidation on Pt have also reported that carbon buildup on the Pt surface leads to eventual deactivation [42, 43]. Pt does not efficiently remove carbon species by oxidation at 60 ℃, but at higher temperatures of 100 and 150 ℃, carbon accumulation and deactivation on Pt were not observed. On the Pt-Re alloy surface, carbonaceous residues are more effectively removed at low temperature than on pure Pt. A possible explanation for this behavior is that some fraction of Re atoms diffuse to the surface under reaction conditions and contribute to oxidation activity. Before exposure to the reactant gases, the Pt-Re alloy consists of pure Pt at the surface[63], and the shift in the Re($4f_{7/2}$) binding energy after exposure of the Pt-Re surface to methanol oxidation conditions implies that Re diffuses to the surface, where it binds with oxygen. Oxygen-induced diffusion of Re to the surface of the Pt-Re surface alloys during methanol and CO oxidation has been previously reported by our group[53, 63]. The initial activity of Pt is greater than that of Pt-Re at all temperatures studied, and we propose that diffusion of Re to the surface of the alloy blocks active sites since Pt is active for methanol oxidation while Re is not[64]. Notably, the decreased activity on Pt-Re is specifically due to diminished production of formaldehyde.

Methanol oxidation on the atomically clean Pt foil produces CO_2, H_2O, formic acid and formaldehyde in the 60-150 ℃ temperature range under oxygen-rich conditions. Previous studies of methanol oxidation on Pt catalysts have also reported that CO_2 and H_2O are the most commonly observed products. The formation of partial oxidation products like formaldehyde and formic acid depend heavily on the specific reaction conditions, including concentration of O_2 in the feed gas mixture and reaction

temperature [42, 43]; the following comparisons with the literature are for feed gas mixtures rich in O_2, as also used in this study. For example, on Pt wire catalysts, CO_2 and formaldehyde are the only carbon-containing products observed [41, 42]. However, activity was not investigated at the low temperatures (<150 ℃) corresponding to high selectivity for formic acid[42].On Pt foil[43] and gauze[40] catalysts, CO_2 and H_2O were observed as the main products. On Pt(111) surfaces, CO_2 and H_2O are produced at low temperatures (<177 ℃), and in one case formaldehyde was also observed[51, 53]. Formic acid was reported as a product from methanol oxidation on catalysts at low temperature[44]. At higher temperatures, it is believed that the surface formate intermediate decomposes too quickly for formic acid desorption to occur, and this may explain the decrease in formic acid production with increasing temperature observed in our study on the Pt foil. Ambient pressure infrared spectroscopy experiments for methanol oxidation on Pt(111) have also detected a surface formate intermediate although no formic acid production was observed[51].

Methanol oxidation activity is extremely sensitive to the coverage of surface oxygen. Specifically, a minimum concentration of surface oxygen is required to promote methanol oxidation, and the atomically clean Pt foil has no initial activity in the absence of surface oxygen. At 60 ℃, a temperature at which dissociation of O_2 is not facile on Pt, there is an onset time of ~10 hours when the activity gradually increases from near zero to its maximum value. At higher methanol oxidation temperatures, O_2 dissociation occurs more readily; consequently, the onset time is shorter at 100 ℃ and is nonexistent at 150 ℃. In addition, methanol oxidation studies on Pt wires have shown that the selectivity to formaldehyde is sensitive to the O_2:methanol feed gas ratio, with higher values resulting

in greater formaldehyde production.40 In our studies we have also found that selectivity for formaldehyde changes depending on the exact preparation of the foil surface. Sputtering and annealing for 12 cycles led to the most consistent activity, whereas exposure to highly oxidizing conditions coupled with only 6 sputter/anneal cycles often resulted in higher selectivities for formaldehyde. Since the two surfaces were indistinguishable by XPS, the higher formaldehyde selectivity could be related to the presence of subsurface oxygen, which is known to exist on other polycrystalline Pt surfaces[81], but could be difficult to detect by XPS if it exists deep in the bulk. Given that formaldehyde production is highly sensitive to adsorbates like oxygen, it is not surprising that the presence of surface Re would also change the formaldehyde yield.

Kinetic parameters such as activation energy (E_a) and turnover frequency (TOF) for methanol oxidation on the Pt foil are in general agreement with values reported in the literature for methanol oxidation on bulk Pt surfaces, and these results confirm that the correct kinetic parameters can be measured in our novel reactor system[61]. On the Pt foil, the calculated Ea was 27.9±0.2 kJ/mol over a temperature range of 80-150 ℃. This value is consistent with the 33 kJ/mol reported on Pt wires[41] and is also close to the 22 kJ/mol observed on Pt(111)[51]. A higher value of 42 kJ/mol was measured for reaction on Pt wire, but these surfaces were oxidized at high temperature (1325-1375 ℃) which may affect activity[42].The TOF of 90 s^{-1} measured for the Pt foil at 100 ℃ is in reasonable agreement with the value of 50 s^{-1} reported on Pt wires at the same temperature[41], given that in both cases the number of active surface sites was roughly estimated from the exposed surface area and an assumed Pt(111) packing density. The similarity in the

activation energies on Pt and the Pt-Re alloy (27.0 ±1.0 kJ/mol) implies that CO_2 production occurs via the same mechanism.

A comparison between in situ ambient pressure XPS (AP-XPS) investigations of methanol oxidation on the Pt and Pt-Re surfaces[53] with the reactor studies reported here provides insight into the differences in activity for the two pressure regimes. For the AP-XPS work, the Pt(111) crystal and the Pt-Re alloy prepared on Pt(111) were exposed to 200 mTorr of O_2 and 100 mTorr of methanol (reactant pressure 0.300 Torr) under reaction conditions. In the reactor experiments, experiments were conducted in a feed gas mixture of 2% methanol/4% O_2/94% He at total pressure of ~760 Torr and reactant partial pressure of 46 Torr. Thus, the O2:methanol ratio was 2:1 in both studies, but the pressure of the reactant gases was ~150 times lower for the AP-XPS experiments. At the higher pressures of the reactor experiments, O_2 dissociation occurs readily, resulting in a significant coverage of surface oxygen detected in post-reaction XPS and attributed to O/OH species; the oxygen coverage increases with reaction temperature. In contrast, almost no surface oxygen was detected in the AP-XPS experiments, and the surface oxygen coverage decreased between 77 ℃ and 127 ℃. Furthermore, in the reactor experiments, almost no carbon was observed at reaction temperatures >100 ℃, whereas the deposition of atomic carbon on Pt(111) in the AP-XPS experiments was significant at 127 ℃ and continued to increase at higher reaction temperatures. Therefore, at higher pressures, it appears that oxygen easily dissociates on the Pt and allows for carbon to be removed above 100 ℃ via oxidation to CO_2. At lower pressures, the rate of oxygen dissociation is slow enough that decomposition of methanol causes accumulation of

atomic carbon faster than it can be removed by oxidation, and this effect becomes more pronounced at the higher temperatures.

Although there are differences in the adsorbed species for methanol oxidation in the higher and lower pressure regimes, alloying Re into Pt enhances surface oxidation processes in both cases. For the AP-XPS studies at lower pressure, the oxygen-induced diffusion of Re to the surface is believed to facilitate O_2 dissociation and provide a source of surface oxygen for the removal of carbonaceous species[53]. As a result, there is less atomic carbon on the Pt-Re alloy surface, and the selectivity for the fully oxidized reaction products like CO_2 and H_2O does not decrease at temperatures of 277 ℃ and higher. However, diffusion of Re to the surface is limited below 177 ℃, and consequently the activities of Pt and Pt-Re are almost identical below this temperature. For the reactor studies at higher pressures, there is evidence for oxygen-induced diffusion of Re to the surface at the much lower temperature of 60 ℃. Deposition of atomic carbon causes the Pt surface to lose activity after 24 hours at 60 ℃, whereas the Pt-Re alloy surface does not become deactivated by surface carbon. Both Pt and Pt-Re dissociate O_2 even at 60 ℃, but the Pt-Re alloy surface is apparently more effective at removing the carbon from the surface through oxidation to CO_2. At higher temperatures, oxidation of surface carbon occurs readily on Pt, and therefore there is no pronounced difference in activity for Pt-Re and Pt.

Although ReO_x has been proposed to be the active site in WGS reactions on Pt-Re catalysts, there is no evidence that ReO_x promotes methanol oxidation on the Pt-Re alloy. Pt-Re shows better long-term activity at 60 ℃, but at these reaction temperatures, Re is not substantially oxidized, presumably because diffusion of Re to the surface is limited.

Although greater Re oxidation occurs at 100 ℃ and 150 ℃, metallic Re still constitutes the majority of surface Re. Under reaction conditions where ReO_x is detected on the surface, the Pt-Re alloy does not show superior activity to Pt itself. Moreover, the extensive oxidation of Re in the alloy is not desirable because Re_2O_7 is volatile and sublimes under reaction conditions. Similar results were reported in the AP-XPS study of methanol oxidation on Pt-Re in which ReO_x also did not promote the reaction[53].

3.5 Conclusions

Pt-Re alloy surfaces exhibit greater long-term activity at low temperatures for methanol oxidation compared to pure Pt because the Pt-Re alloy surface is more effective at removing carbonaceous residues that poison Pt active sites. At 60 ℃, more carbon is deposited on the Pt surface than on Pt-Re over a 24 hour reaction period. The decreased carbon coverage on the Pt-Re alloy surface is attributed to more facile O_2 dissociation and removal of carbon species by oxidation. Diffusion of Re atoms to the surface under reaction conditions may promote O_2 dissociation. Studies of Pt-Re catalysts for other reactions like hydrocarbon reforming also report decreased carbon accumulation and longer lifetimes for Pt-Re compared to Pt catalysts[6, 7, 9-11].On atomically clean Pt and Pt-Re alloy surfaces, there is no activity for methanol oxidation until sufficient oxygen has dissociated on the surface. Re oxide does not enhance activity for methanol oxidation, and diffusion of Re to the surface followed by Re oxidation results in loss of Re due to sublimation of Re_2O_7. Activation energies for methanol oxidation to CO_2 are similar on Pt and Pt-Re (27.9 ± 0.2 and 27 ± 1 kJ/mol respectively), indicating that reaction occurs by the same mechanism, and these values are also consistent with other methanol oxidation studies on bulk Pt surfaces reported in the literature. A comparison of these reactor

studies with AP-XPS experiments carried out at reactant pressures ~150 times lower show that at higher pressures, the surface coverage of oxygen is higher while the carbon coverage is lower. This behavior is attributed to greater oxygen dissociation and oxidation of surface carbon at the higher pressures.

3.6 SUPPORT INFORMATION

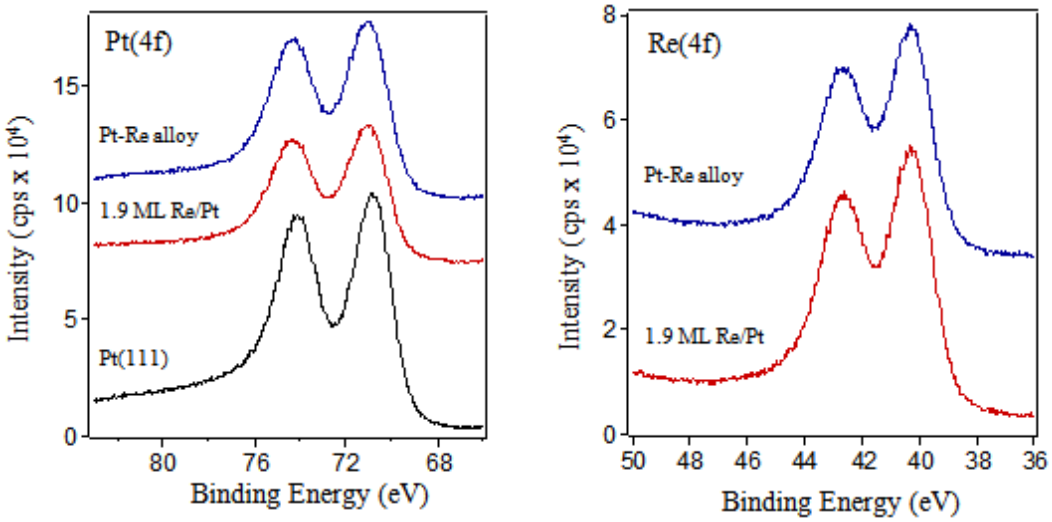

Figure 3.9: XPS data collected with an AlKα source for the Pt(4f) and Re(4f) regions: before deposition; after deposition of 1.9 ML of Re on Pt(111), and after annealing to 1000 K for 5 min to form the Pt-Re surface alloy.

Figure 3.9 shows X-ray photoelectron spectroscopy data collected with an AlKα source for the Pt(4f) and Re(4f) regions: before deposition; after deposition of 1.9 ML of Re on Pt(111), and after annealing to 1000 K for 5 min to form the Pt-Re surface alloy. LEIS and STM data collected for these same surfaces indicate that the surface is pure Pt and that all Re islands diffuse subsurface. The integrated Pt signal is attenuated to 57% of initial value after Re deposition and 76% of the initial value after annealing to 1000 K, as observed for Re on the Pt foil; the Re signal is also attenuated by 80% after annealing, as on the Pt foil.

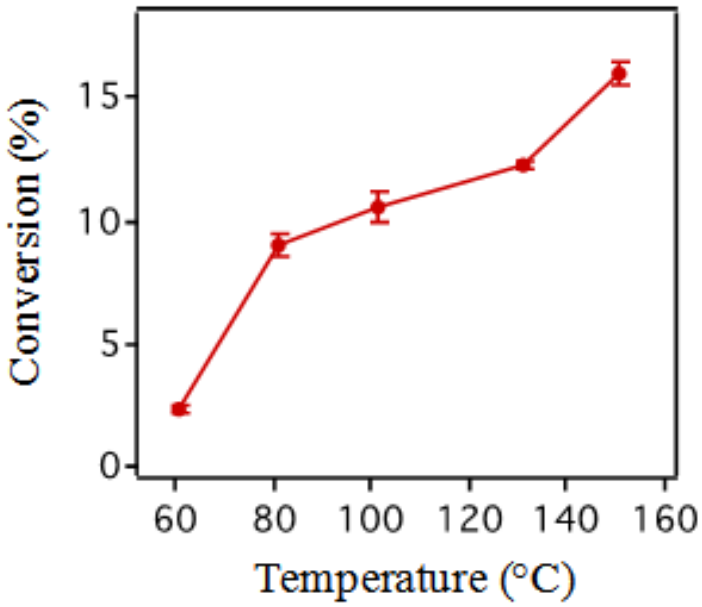

Figure 3.10: Methanol conversion as a function of temperature for methanol oxidation on the Pt foil.

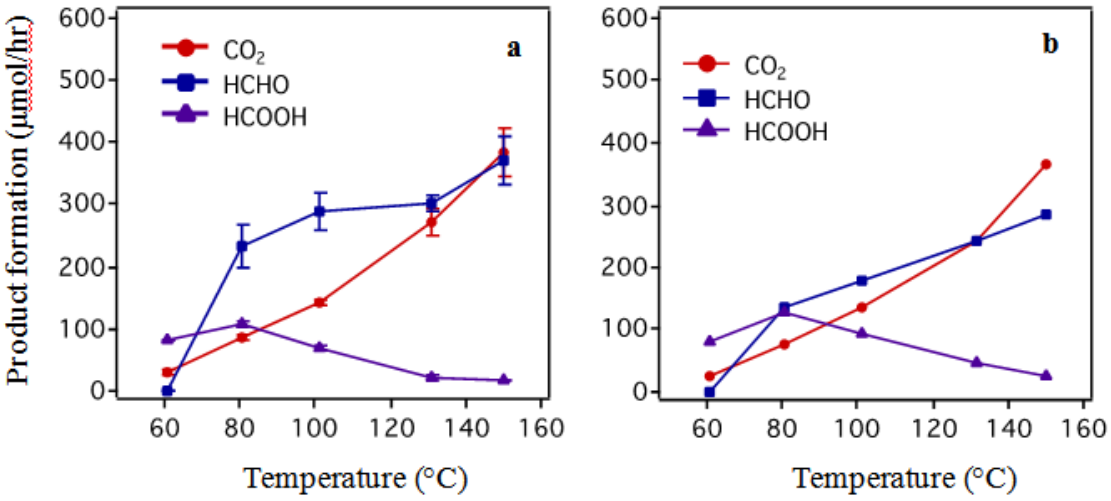

Figure 3.11: Product formation in µmol/hr as a function of temperature for methanol oxidation on the: a) Pt foil and b) Pt-Re alloy. Error bars for the data on the Pt foil are standard deviations from two experiments.

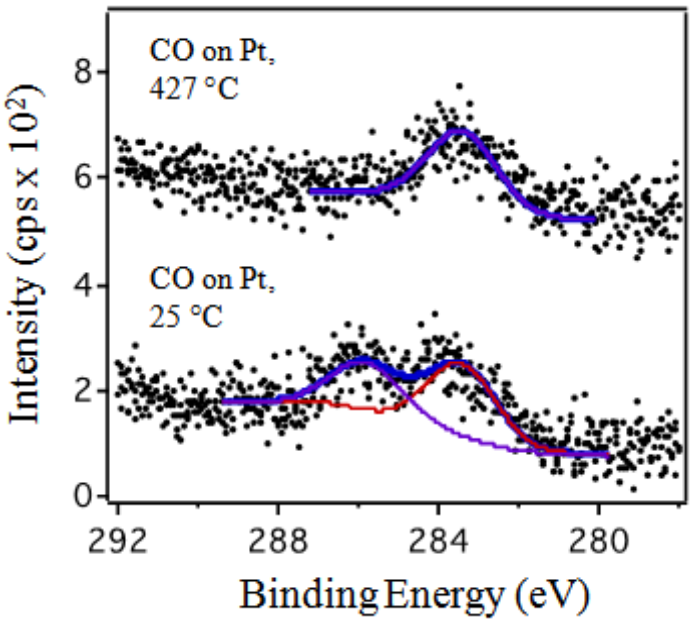

Figure 3.12: X-ray photoelectron spectroscopy data of the C(1s) region for the Pt foil exposed to 5% CO/He at room temperature for 1 hour and the same surface heated to 427 ℃

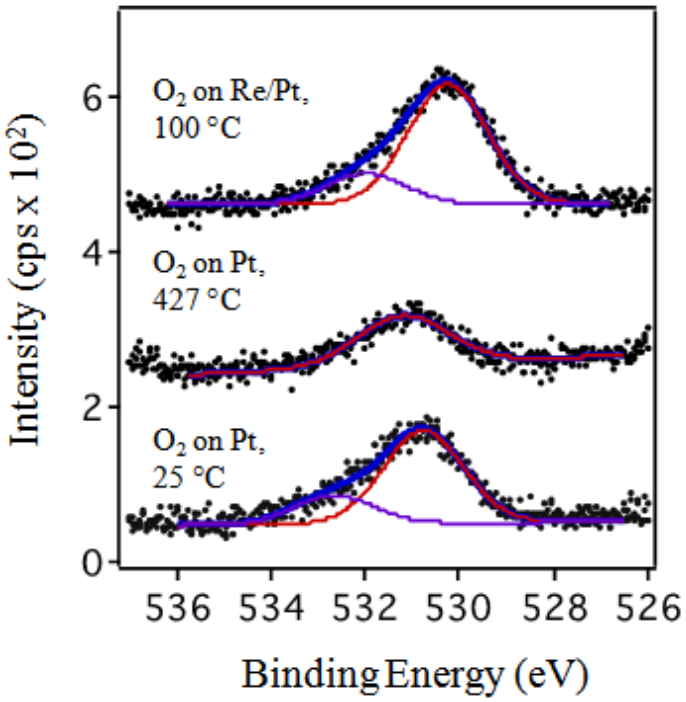

Figure 3.13: X-ray photoelectron spectroscopy data of the O(1s) region for the Pt foil exposed to 4% O2/He at 25 ℃ for 10 hours; the same surface flashed to 427 ℃; and a 2.4 ML Re film on the Pt foil exposed to 100% O_2 for 1 hour at 100 ℃.

Description of response factor calibration:

The response factors for CO_2 and methanol were determined from calibration experiments using different concentrations (1.5-10%) of CO_2 in He and methanol (0.6-2%) in He. The response factor for formaldehyde was determined by direct injection of various concentrations of formaldehyde in ethanol (55-130 nmol). No direct calibration for formic acid was possible since formic acid interacts strongly with itself and solvent molecules in solution and exists in a variety of chemical states. Instead, the rate of formaldehyde production and associated response factor were determined from the difference between the methanol conversion and CO_2 formation at 60 ℃, where the only detectable products were CO_2 and formic acid. The assumption is that no other carbon-containing products are formed; note that a study of methanol oxidation on a Pt foil showed that no CO was formed below 400 ℃ under oxygen-rich reaction conditions. Although we cannot definitively rule out the production of CO, which has an identical retention time to that of the reactant O_2, methanol reaction on Pt should not produce CO in an oxygen-rich feed gas mixture.

ACKNOWLEDGEMENTS

Thanks to Dr. Audrey Duke for the preparation and XPS characterizations of Pt and Pt-Re catalysts in ultrahigh vacuum.

3.7 REFERENCES

(1) Sinfelt, J. H., Catalysis by alloys and bimetallic clusters. *Accounts of Chemical Research* **1977,** 10 (1), 15-20.

(2) Campbell, C. T., Bimetallic Surface Chemistry. *Annual Review of Physical Chemistry* **1990,** 41 (1), 775-837.

(3) Chen, J. G.; Menning, C. A.; Zellner, M. B., Monolayer bimetallic surfaces: Experimental and theoretical studies of trends in electronic and chemical properties. *Surface Science Reports* **2008,** 63 (5), 201-254.

(4) Kluksdahl, H. E., Reforming a sulfur-free naphtha with a platinum-rhenium catalyst. Google Patents: 1968.

(5) Somorjai, G. A., *Introduction to Surface Chemistry and Catalysis*. John Wiley and Sons, Inc: New York, **1994**.

(6) Carter, J. L.; McVinker, G. B.; Weissman, W.; Kmak, M. S.; Sinfelt, J. H., Bimetallic catalysts; application in catalytic reforming. *Applied Catalysis* **1982,** 3 (4), 327-346.

(7) Barbier, J., Deactivation of reforming catalysts by coking - a review. *Applied Catalysis* **1986,** 23 (2), 225-243.

(8) Johnson, M. F. L.; LeRoy, V. M., The state of rhenium in Pt/Re/alumina catalysts. *Journal of Catalysis* **1974,** 35 (3), 434-440.

(9) Parera, J. M.; Beltramini, J. N., Stability of bimetallic reforming catalysts. *Journal of Catalysis* **1988,** 112 (2), 357-365.

(10) Godbey, D. J.; Garin, F.; Somorjai, G. A., The hydrogenolysis of ethane over Re-Pt(111) and Pt-Re(0001) bimetallic crystal surfaces. *Journal of Catalysis* **1989,** 117 (1), 144-154.

(11) Godbey, D. J.; Somorjai, G. A., The adsorption and desorption of hydrogen and carbon monoxide on bimetallic Re-Pt(111) surfaces. *Surface Science* **1988,** 204 (3), 301-318.

(12) Ramstad, A.; Strisland, F.; Raaen, S.; Borg, A.; Berg, C., CO and O_2 adsorption on the Re/Pt(111) surface studied by photoemission and thermal desorption. *Surface Science* **1999,** 440 (1–2), 290-300.

(13) Cortright, R. D.; Davda, R. R.; Dumesic, J. A., Hydrogen from catalytic reforming of biomass-derived hydrocarbons in liquid water. *Nature* **2002,** 418 (6901), 964-967.

(14) Soares, R. R.; Simonetti, D. A.; Dumesic, J. A., Glycerol as a Source for Fuels and Chemicals by Low-Temperature Catalytic Processing. *Angewandte Chemie International Edition* **2006,** 45 (24), 3982-3985.

(15) King, D. L.; Zhang, L.; Xia, G.; Karim, A. M.; Heldebrant, D. J.; Wang, X.; Peterson, T.; Wang, Y., Aqueous phase reforming of glycerol for hydrogen production over Pt–Re supported on carbon. *Applied Catalysis B: Environmental* **2010,** 99 (1–2), 206-213.

(16) Wei, Z.; Karim, A. M.; Li, Y.; King, D. L.; Wang, Y., Elucidation of the roles of Re in steam reforming of glycerol over Pt–Re/C catalysts. *Journal of Catalysis* **2015,** 322, 49-59.

(17) Simonetti, D. A.; Kunkes, E. L.; Dumesic, J. A., Gas-phase conversion of glycerol to synthesis gas over carbon-supported platinum and platinum–rhenium catalysts. *Journal of Catalysis* **2007,** 247 (2), 298-306.

(18) Kunkes, E. L.; Simonetti, D. A.; Dumesic, J. A.; Pyrz, W. D.; Murillo, L. E.; Chen, J. G.; Buttrey, D. J., The role of rhenium in the conversion of glycerol to synthesis gas over carbon supported platinum–rhenium catalysts. *Journal of Catalysis* **2008,** 260 (1), 164-177.

(19) Zhang, L.; Karim, A. M.; Engelhard, M. H.; Wei, Z.; King, D. L.; Wang, Y., Correlation of Pt–Re surface properties with reaction pathways for the aqueous-phase reforming of glycerol. *Journal of Catalysis* **2012,** 287, 37-43.

(20) Ciftci, A.; Ligthart, D. A. J. M.; Hensen, E. J. M., Aqueous phase reforming of glycerol over Re-promoted Pt and Rh catalysts. *Green Chemistry* **2014,** 16 (2), 853-863.

(21) Kirilin, A. V.; Tokarev, A. V.; Manyar, H.; Hardacre, C.; Salmi, T.; Mikkola, J. P.; Murzin, D. Y., Aqueous phase reforming of xylitol over Pt-Re bimetallic catalyst: Effect of the Re addition. *Catalysis Today* **2014,** 223, 97-107.

(22) Ciftci, A.; Ligthart, D. A. J. M.; Hensen, E. J. M., Influence of Pt particle size and Re addition by catalytic reduction on aqueous phase reforming of glycerol for carbon-supported Pt(Re) catalysts. *Applied Catalysis B: Environmental* **2015,** 174–175, 126-135.

(23) Ishikawa, Y.; Liao, M.-S.; Cabrera, C. R., Energetics of H_2O dissociation and COads+OHads reaction on a series of Pt–M mixed metal clusters: a relativistic density-functional study. *Surface Science* **2002,** 513 (1), 98-110.

(24) Greeley, J.; Mavrikakis, M., Near-surface alloys for hydrogen fuel cell applications. *Catalysis Today* **2006,** 111 (1–2), 52-58.

(25) Detwiler, M. D.; Majumdar, P.; Gu, X.-K.; Delgass, W. N.; Ribeiro, F. H.; Greeley, J.; Zemlyanov, D. Y., Characterization and theory of Re films on Pt(111) grown by UHV-CVD. *Surface Science* **2015,** 640, 2-9.

(26) Ciftci, A.; Eren, S.; Ligthart, D. A. J. M.; Hensen, E. J. M., Platinum–Rhenium Synergy on Reducible Oxide Supports in Aqueous-Phase Glycerol Reforming. *ChemCatChem* **2014,** 6 (5), 1260-1269.

(27) Sato, Y.; Terada, K.; Hasegawa, S.; Miyao, T.; Naito, S., Mechanistic study of water–gas-shift reaction over TiO_2 supported Pt–Re and Pd–Re catalysts. *Applied Catalysis A: General* **2005,** 296 (1), 80-89.

(28) Iida, H.; Igarashi, A., Difference in the reaction behavior between Pt–Re/TiO_2 (Rutile) and Pt–Re/ZrO_2 catalysts for low-temperature water gas shift reactions. *Applied Catalysis A: General* **2006,** 303 (1), 48-55.

(29) Azzam, K. G.; Babich, I. V.; Seshan, K.; Lefferts, L., A bifunctional catalyst for the single-stage water–gas shift reaction in fuel cell applications. Part 2. Roles of the support and promoter on catalyst activity and stability. *Journal of Catalysis* **2007,** 251 (1), 163-171.

(30) Azzam, K. G.; Babich, I. V.; Seshan, K.; Lefferts, L., Role of Re in Pt–Re/TiO_2 catalyst for water gas shift reaction: A mechanistic and kinetic study. *Applied Catalysis B: Environmental* **2008,** 80 (1–2), 129-140.

(31) Azzam, K. G.; Babich, I. V.; Seshan, K.; Mojet, B. L.; Lefferts, L., Stable and Efficient Pt–Re/TiO_2 catalysts for Water-Gas-Shift: On the Effect of Rhenium. *ChemCatChem* **2013,** 5 (2), 557-564.

(32) Falcone, D. D.; Hack, J. H.; Klyushin, A. Y.; Knop-Gericke, A.; Schlögl, R.; Davis, R. J., Evidence for the Bifunctional Nature of Pt–Re Catalysts for Selective Glycerol Hydrogenolysis. *ACS Catalysis* **2015,** 5 (10), 5679-5695.

(33) Daniel, O. M.; DeLaRiva, A.; Kunkes, E. L.; Datye, A. K.; Dumesic, J. A.; Davis, R. J., X-ray Absorption Spectroscopy of Bimetallic Pt–Re Catalysts for Hydrogenolysis of Glycerol to Propanediols. *ChemCatChem* **2010,** 2 (9), 1107-1114.

(34) Raciti, D.; Kubal, J.; Ma, C.; Barclay, M.; Gonzalez, M.; Chi, M.; Greeley, J.; More, K. L.; Wang, C., Pt3Re alloy nanoparticles as electrocatalysts for the oxygen reduction reaction. *Nano Energy* **2016,** 20, 202-211.

(35) Liu, X.; Madix, R. J.; Friend, C. M., Unraveling molecular transformations on surfaces: a critical comparison of oxidation reactions on coinage metals. *Chemical Society Reviews* **2008,** 37 (10), 2243-2261.

(36) Bahmanpour Ali, M.; Hoadley, A.; Tanksale, A., Critical review and exergy analysis of formaldehyde production processes. In *Reviews in Chemical Engineering*, 2014; Vol. 30, p 583.

(37) Gibson, H. W., Chemistry of formic acid and its simple derivatives. *Chemical Reviews* **1969,** 69 (5), 673-692.

(38) Rees, N. V.; Compton, R. G., Sustainable energy: a review of formic acid electrochemical fuel cells. *Journal of Solid State Electrochemistry* **2011,** 15 (10), 2095-2100.

(39) Grasemann, M.; Laurenczy, G., Formic acid as a hydrogen source - recent developments and future trends. *Energy & Environmental Science* **2012,** 5 (8), 8171-8181.

(40) Firth, J. G., Catalytic oxidation of methanol over platinum. *Transactions of the Faraday Society* **1971,** 67 (0), 212-215.

(41) Gentry, S. J.; Jones, A.; Walsh, P. T., Kinetics of methanol oxidation over platinum wire catalysts. *Journal of the Chemical Society, Faraday Transactions 1: Physical Chemistry in Condensed Phases* **1980,** 76 (0), 2084-2095.

(42) McCabe, R. W.; McCready, D. F., Kinetics and reaction pathways of methanol oxidation on platinum. *The Journal of Physical Chemistry* **1986,** 90 (7), 1428-1435.

(43) Zum Mallen, M. P.; Schmidt, L. D., Oxidation of Methanol over Polycrystalline Rh and Pt: Rates, OH Desorption, and Model. *Journal of Catalysis* **1996,** 161 (1), 230-246.

(44) Cao, C.; Hohn, K. L., Study of reaction intermediates of methanol decomposition and catalytic partial oxidation on Pt/Al_2O_3. *Applied Catalysis A: General* **2009,** 354 (1–2), 26-32.

(45) Merte, L. R.; Ahmadi, M.; Behafarid, F.; Ono, L. K.; Lira, E.; Matos, J.; Li, L.; Yang, J. C.; Roldan Cuenya, B., Correlating Catalytic Methanol Oxidation with the Structure and Oxidation State of Size-Selected Pt Nanoparticles. *ACS Catalysis* **2013,** 3 (7), 1460-1468.

(46) Sexton, B. A., Methanol decomposition on platinum (111). *Surface Science* **1981,** 102 (1), 271-281.

(47) Levis, R. J.; Zhicheng, J.; Winograd, N.; Akhter, S.; White, J. M., Methyl formation from methanol decomposition on Pd{111} and Pt{111}. *Catalysis Letters* **1988,** 1 (11), 385-389.

(48) Wang, J.; Masel, R. I., Methanol adsorption and decomposition on (2 × 1)Pt(110): enhanced stability of the methoxy intermediate on a stepped surface. *Surface Science* **1991,** 243 (1), 199-209.

(49) Wang, J.; Masel, R. I., Carbon-oxygen bond scission during methanol decomposition on (1.times.1)platinum(110). *Journal of the American Chemical Society* **1991,** 113 (15), 5850-5856.

(50) Endo, M.; Matsumoto, T.; Kubota, J.; Domen, K.; Hirose, C., Oxidation of methanol by molecularly adsorbed oxygen on Pt(111) under vacuum and ambient pressure conditions studied by infrared reflection absorption spectroscopy: identification of formate intermediate. *Surface Science* **1999,** 441 (2–3), L931-L937.

(51) Endo, M.; Matsumoto, T.; Kubota, J.; Domen, K.; Hirose, C., In Situ IRAS Observation of Catalytic Deep Oxidation of Methanol on Pt(111) under Ambient Pressure Conditions. *The Journal of Physical Chemistry B* **2001,** 105 (8), 1573-1577.

(52) Liu, Z. X.; Sawada, T.; Takagi, N.; Watanabe, K.; Matsumoto, Y., Reaction intermediates in the oxidation of methanol on a Pt(111)-(2x2)O surface. *Journal of Chemical Physics* **2003,** 119 (9), 4879-4886.

(53) Duke, A. S.; Galhenage, R. P.; Tenney, S. A.; Ammal, S. C.; Heyden, A.; Sutter, P.; Chen, D. A., In Situ Ambient Pressure X-ray Photoelectron Spectroscopy Studies of Methanol Oxidation on Pt(111) and Pt–Re Alloys. *The Journal of Physical Chemistry C* **2015,** 119 (40), 23082-23093.

(54) Miller, A. V.; Kaichev, V. V.; Prosvirin, I. P.; Bukhtiyarov, V. I., Mechanistic Study of Methanol Decomposition and Oxidation on Pt(111). *The Journal of Physical Chemistry C* **2013,** 117 (16), 8189-8197.

(55) Wu-Hsun CHeng, H. H. K., *Methanol Production and Use*. Dekker: New York, **1994**.

(56) McNicol, B.; Rand, D.; Williams, K., Direct methanol–air fuel cells for road transportation. *Journal of Power Sources* **1999,** 83 (1), 15-31.

(57) Nichols, R. J., The methanol story: a sustainable fuel for the future. *Journal of scientific and industrial research* **2003,** 62 (1/2), 97-105.

(58) McGrath, K. M.; Prakash, G. S.; Olah, G. A., Direct methanol fuel cells. *Journal of Industrial and Engineering Chemistry* **2004,** 10 (7), 1063-1080.

(59) Olah, G. A., Beyond oil and gas: the methanol economy. *Angewandte Chemie International Edition* **2005,** 44 (18), 2636-2639.

(60) Zhen, X.; Wang, Y., An overview of methanol as an internal combustion engine fuel. *Renewable and Sustainable Energy Reviews* **2015,** 52, 477-493.

(61) Tenney, S. A.; Xie, K.; Monnier, J. R.; Rodriguez, A.; Galhenage, R. P.; Duke, A. S.; Chen, D. A., Novel recirculating loop reactor for studies on model catalysts: CO oxidation on Pt/TiO_2(110). *Review of Scientific Instruments* **2013,** 84 (10), 104101.

(62) Ramstad, A.; Strisland, F.; Raaen, S.; Worren, T.; Borg, A.; Berg, C., Growth and alloy formation studied by photoelectron spectroscopy and STM. *Surface Science* **1999,** 425 (1), 57-67.

(63) Duke, A. S.; Galhenage, R. P.; Tenney, S. A.; Sutter, P.; Chen, D. A., In Situ Studies of Carbon Monoxide Oxidation on Platinum and Platinum–Rhenium Alloy Surfaces. *The Journal of Physical Chemistry C* **2015,** 119 (1), 381-391.

(64) Chan, A. S. Y.; Chen, W.; Wang, H.; Rowe, J. E.; Madey, T. E., Methanol Reactions over Oxygen-Modified Re Surfaces: Influence of Surface Structure and Oxidation. *The Journal of Physical Chemistry B* **2004,** 108 (38), 14643-14651.

(65) Chan, A.; Wertheim, G.; Wang, H.; Ulrich, M.; Rowe, J.; Madey, T., Surface atom core-level shifts of clean and oxygen-covered Re (12 3^{-}1). *Physical Review B* **2005,** 72 (3), 035442.

(66) Freyer, N.; Pirug, G.; Bonzel, H. P., C(1s) spectroscopy of hydrocarbons adsorbed on Pt(111). *Surface Science* **1983,** 126 (1–3), 487-494.

(67) Nørskov, J. K.; Rossmeisl, J.; Logadottir, A.; Lindqvist, L.; Kitchin, J. R.; Bligaard, T.; Jonsson, H., Origin of the overpotential for oxygen reduction at a fuel-cell cathode. *The Journal of Physical Chemistry B* **2004,** 108 (46), 17886-17892.

(68) Kiskinova, M.; Pirug, G.; Bonzel, H. P., Coadsorption of potassium and CO on Pt(111). *Surface Science* **1983,** 133 (2–3), 321-343.

(69) Peuckert, M.; Bonzel, H. P., Characterization of oxidized platinum surfaces by X-ray photoelectron spectroscopy. *Surface Science* **1984,** 145 (1), 239-259.

(70) Puglia, C.; Nilsson, A.; Hernnäs, B.; Karis, O.; Bennich, P.; Mårtensson, N., Physisorbed, chemisorbed and dissociated O_2 on Pt(111) studied by different core level spectroscopy methods. *Surface Science* **1995,** 342 (1–3), 119-133.

(71) Schiros, T.; Näslund, L.-Å.; Andersson, K.; Gyllenpalm, J.; Karlberg, G.; Odelius, M.; Ogasawara, H.; Pettersson, L. G.; Nilsson, A., Structure and bonding of the water-hydroxyl mixed phase on Pt (111). *The Journal of Physical Chemistry C* **2007,** 111 (41), 15003-15012.

(72) Miller, D.; Öberg, H.; Kaya, S.; Casalongue, H. S.; Friebel, D.; Anniyev, T.; Ogasawara, H.; Bluhm, H.; Pettersson, L. G.; Nilsson, A., Oxidation of Pt (111) under near-ambient conditions. *Physical Review Letters* **2011,** 107 (19), 195502.

(73) Wakisaka, M.; Udagawa, Y.; Suzuki, H.; Uchida, H.; Watanabe, M., Structural effects on the surface oxidation processes at Pt single-crystal electrodes studied by X-ray photoelectron spectroscopy. *Energy & Environmental Science* **2011,** 4 (5), 1662-1666.

(74) St Petkov, P.; Vayssilov, G. N.; Liu, J.; Shekhah, O.; Wang, Y.; Wöll, C.; Heine, T., Defects in MOFs: A thorough characterization. *ChemPhysChem* **2012,** 13 (8), 2025-2029.

(75) Näslund, L.-Å., Reaction kinetics for the oxygen hydrogenation process on Pt(111) derived from temperature-programmed XPS. *Surface Science* **2013,** 618, 42-48.

(76) Ogasawara, H.; Brena, B.; Nordlund, D.; Nyberg, M.; Pelmenschikov, A.; Pettersson, L.; Nilsson, A., Structure and bonding of water on Pt (111). *Physical Review Letters* **2002,** 89 (27), 276102.

(77) Björneholm, O.; Nilsson, A.; Tillborg, H.; Bennich, P.; Sandell, A.; Hernnäs, B.; Puglia, C.; Mårtensson, N., Overlayer structure from adsorbate and substrate core level binding energy shifts: CO, CCH_3 and O on Pt (111). *Surface Science* **1994,** 315 (1-2), L983-L989.

(78) Ducros, R.; Fusy, J., Core level binding energy shifts of rhenium surface atoms for a clean and oxygenated surface. *Journal of Electron Spectroscopy and Related Phenomena* **1987,** 42 (4), 305-312.

(79) Okal, J.; Kępiński, L.; Krajczyk, L.; Tylus, W., Oxidation and redispersion of a low-loaded Re/γ-Al_2O_3 catalyst. *Journal of Catalysis* **2003,** 219 (2), 362-371.

(80) Shcheglov, P.; Drobot, D., Heterogeneous equilibria in the rhenium-oxygen system. *Russian journal of physical chemistry* **2006,** 80 (11), 1819-1825.

(81) Légaré, P.; Hilaire, L.; Maire, G., Interaction of polycrystalline platinum and a platinum-silicon alloy with oxygen: An XPS study. *Surface Science* **1984,** 141 (2–3), 604-616.

CHAPTER 4 ACTIVITIES OF PT AND PT-RE SUPPORTED CLUSTERS IN THE WATER-GAS SHIFT REACTION[1]

[1]Adapted from Audrey S. Duke*, Kangmin Xie*, A. J. Brandt, T. Maddumapatabandi, John R. Monnier, Donna A. Chen, "Activities of Pt and Pt-Re Supported Clusters in the Water-Gas Shift Reaction", in preparation.
(*these authors contributed equally to this work.)

4.1 INTRODUCTION

Many studies have shown that bimetallic catalysts often have superior activity, stability and selectively compared to either of the pure metals by themselves[1, 2]. These enhanced properties have been attributed to electronic effects from metal-metal interactions, changes in surface structure, or the creation of new bifunctional active sites[2-7].The Pt-Re system represents one of the most successful industrial catalysts since it has been used since the 1960s for the reforming of hydrocarbons[8-10]. The Pt-Re bimetallic catalysts have better long-term activity than Pt alone, and it is believed that the electronic interactions in the bimetallic system inhibit carbon fouling, which causes the Pt catalysts to lose activity[8, 9, 11-14]. Recently Pt-Re bimetallic catalysts have also been reported to show superior activity for the low temperature water-gas shift (WGS) reaction compared to Pt alone[15-20]. There has been significant interest in the development of a WGS catalyst capable of generating clean H_2 for use in fuel cells, which are limited to lower operating temperatures due to the thermal stability of the polymer membranes[19]. However, the nature of this enhanced WGS activity for Pt-Re activity is not well understood. Given that O-H bond breaking in water is believed to be the rate-limiting step in WGS reaction on Pt, it has been proposed that ReO_x provides the active sites for water dissociation in the Pt-Re catalysts[17, 20, 21]. Alternatively, it has also been proposed that CO poisoning is reduced on Pt-Re surfaces due to the weaker binding of CO to Pt compared to Pt-Re[22-24]. One of main challenges in understanding the behavior of the Pt-Re catalysts is the difficulty in making conventional Pt-Re catalysts with controlled bimetallic compositions or sizes. Furthermore, nothing is known about the oxidation states of Re during WGS reaction on Pt-Re catalysts.

In order to better understand the effects of Pt-Re bimetallic composition and Re oxidation states on WGS activity, investigations have been carried out on model systems consisting of vapor-deposited pure and bimetallic clusters deposited on a rutile TiO_2(110) surface. The surfaces were prepared and characterized in ultrahigh vacuum (UHV) and then introduced into a microreactor coupled to the UHV chamber. WGS activity was studied at pressures of ~ 1 atmosphere, and the surfaces were then transferred back into the UHV chamber for X-ray photoelectron spectroscopy (XPS) and infrared absorption reflection spectroscopy (IRAS) studies without exposure to air. In this manner, well-characterized Pt-Re bimetallic surfaces can be studied under catalytically relevant pressure conditions, and for the first time, Re oxidation states in the Pt-Re clusters have been determined after WGS reaction and without exposure to air, which is known to oxidize metallic Re. The bimetallic clusters that exhibit the highest activity for WGS reaction are those consisting of Pt on Re structures. These clusters are prepared either by depositing 2 ML of Pt on 2 ML Re seed clusters, or by depositing submonolayer (0.5 ML) coverages of Re on 2 ML Pt clusters, where the Re atoms diffuse into the Pt cluster. XPS investigations show that the active surfaces contain metallic Re, which is not oxidized under WGS conditions, and furthermore, the presence of ReO_x does not promote WGS activity in the bimetallic clusters. The enhanced activity of the Pt on Re clusters is instead attributed to reduced CO poisoning on the Pt-Re surfaces.

4.2 EXPERIMENTAL

Experiments were conducted in two ultrahigh vacuum chambers which have been described in detail elsewhere. The first chamber[25] ($P < 3x10^{-10}$ Torr) is coupled to a homemade microreactor [26], and is equipped with a residual gas analyzer (Stanford

Research Systems, RGA 300), a hemispherical analyzer (SPECS, EA10) and Mg/Al Ka X-ray source (Leybold Heraeus, RQ 20/63) for XPS, and an infrared reflection absorption spectroscopy (IRAS) system (Bruker, Tensor 27). The second chamber[27-31] ($P \leq 1 \times 10^{-10}$ Torr) houses a quadrupole mass spectrometer (Hiden HAL 301/3F) for temperature programmed desorption studies, a cylindrical mirror analyzer (Omicron CMA 150) for Auger electron spectroscopy, and a low energy electron diffraction optics (Omicron SPECTALEED).

In the first chamber, Pt and Re clusters were deposited onto a rutile TiO_2(110) crystal (Princeton Scientific Corporation, 10 mm x 10 mm x 1 mm) which was mounted on a Ta back plate using thin Ta foil straps. The sample was heated radiatively by a tungsten filament from behind and by electron bombardment from the filament with a positive bias applied to the sample. The sample temperature was monitored via an infrared pyrometer (Heitronics). The crystal was cleaned by cycles of Ar^+ sputtering (20 minutes, 1 kV) and annealing (3 minutes, 950-1000 K) in vacuum. Pt and Re were deposited sequentially onto the titania surface from a Pt rod (ESPI, 2 mm diameter, 99.95%) and a Re rod (ESPI, 2 mm diameter, 99.99%), respectively, using a four-pocket electron-beam evaporator (Oxford Applied Research, EGC04). The metal flux was calibrated with a UHV bakeable quartz crystal microbalance (QCM, Inficon, XTM-2) before each deposition. Metal deposition rates were approximately 0.08-0.1 ML/min, where one monolayer (ML) is defined as the packing density of Pt(111) (1.50×10^{15} atoms/cm^2) or Re(0001) (1.52×10^{15} atoms/cm^2).

XPS data were collected before and after reactor experiments using Al Kα X-rays, a 0.2 s dwell time, and a 0.025 eV step size. Samples were prepared in the UHV chamber

and then transferred in and out of the microreactor without exposing the sample to air. In the reactor, the sample was heated and cooled in a continuous flow of fresh feed gas, which was a mixture of 3% CO (Praxair)/ 7% H_2O/ 90% He (Airgas, 99.999%) with a flow rate of 60 sccm as determined by a digital flow meter (Agilent Technologies, ADM2000). The CO was passed through an alumina trap heated to 150 °C in order to remove metal carbonyl contaminants. Water vapor was introduced to the feed gas line by a homemade vapor-liquid equilibrator (VLE) filled with ultrapure liquid water (18.2 MΩ resistivity, Barnstead EasyPure II 7138), with He serving as the sweep gas. The temperature of the VLE was controlled by a refrigerating/ heating recirculation bath (VWR), and the concentration of water in the vapor outlet was calculated using the Antoine equation. Both CO and He were introduced via independently calibrated mass flow controllers (Brooks, 5850e and 5850i). The sample was heated to temperatures between 130 °C and 190 °C at a rate of ~1.5-2 °C /min by heating tapes (Briskheat, BWHD) wrapped around the exterior of the reactor housing; the heating tapes were regulated by a feedback loop on a temperature controller (Auber, SYL-4342P) to ensure uniform heating and cooling. The temperature of the sample was measured by a type K thermocouple (Omega, KMQSS-040G-6) welded into the feed gas inlet, close to the surface of the sample. The gas lines were maintained at ~65 °C using two Valco Instruments temperature controllers. Pressure was monitored by two capacitance manometers (MKS Instruments, Baratron 722A) located upstream of the reactor in the feed gas line (790 Torr ~ 800 Torr) and downstream of the reactor (770 Torr ~ 780 Torr).

Activity measurements were performed in recirculation mode [26], in which the reactant gases recirculate over the catalyst surface once every 2 min. A gas

sample(~1.096 cm^3) was injected into the gas chromatograph (HP 5890A) equipped with a PoraPLOT Q capillary column and thermal conductivity detector (TCD). Automatic injections occurred every 20 min and were followed by refilling the gas sampling loop with fresh feed gas so that the pressure in the reactor remained unchanged. WGS activity was recorded after 2 hours of reaction at 130 °C, 145 °C, 160 °C, 175 °C, and 190 °C. The background activity of the empty reactor and sample support were evaluated and found to contribute minor amounts of CO_2 to the overall activity, as described on the supplemental section.

For the TPD experiments in the second chamber, the TiO_2 crystal was cleaned by cycles of Ar sputtering followed by annealing, and the cleanliness of the crystal was checked by AES. Pt was deposited from a homemade evaporator consisting of a Pt wire (ESPI, 0.25 mm diameter, 99.999%) wrapped around a tungsten wire (0.50 mm), and Re was deposited from a Re rod (ESPI, 1.6 mm diameter, 99.99%) installed in an Omicron electron beam evaporator (EFM3). The metal fluxes were measured by a QCM before deposition and were found to be 0.06-0.08 ML/min for Pt and 0.018 ML/min for Re. Surfaces were exposed to CO (National Welders, 99.99%) via a stainless steel directed dosing tube, and a saturation exposure of CO was achieved by leaking in CO at a pressure rise of 3.0×10^{-10} Torr for 3 minutes. CO exposure was carried out at room temperature, and the sample was cooled to 100 K before TPD. During TPD experiments, the sample was heated at a rate of 2 K/s and was positioned directly in front of a 4 mm diameter aperture in the shroud of the mass spectrometer in order to minimize detection of products desorbing from the sample holder. A -100 V bias was applied to the sample

during TPD to prevent damage from the electrons emitted by the mass spectrometer filament.

All IRAS spectra were collected at a grazing angle of 87° using a liquid nitrogen cooled mercury cadmium telluride (LN-MCT) detector. The Pt(111) single crystal (99.999%, Princeton Scientific Corp., 8 mm diameter, 2 mm thickness) used for IRAS experiments was mounted by press-fitting two Ta wires into 1.1 mm deep slots cut into the sides of the crystal. The Ta wires were spot welded onto a standard Omicron sample plate with an 8.9 x 8.9 mm^2 window so that the back of the crystal could be directly heated by electron bombardment from a tungsten filament. The crystal was cleaned by cycles of Ar^+ ion sputtering at 1 kV for 20 minutes at room temperature and subsequent annealing to 1000 K for 3 minutes. The temperature of the crystal was measured by an infrared pyrometer. The Pt-Re surface alloys were prepared by heating the Re films to 1000 K for 5 min. The surfaces were then either introduced directly into the reactor for WGS experiments or exposed to CO (Airgas, 99.99%) by backfilling the chamber to a specific pressure of CO by means of a variable leak valve. For each set of data, 1200 spectrometer scans were obtained with 1 cm^{-1} resolution. Background spectra were collected on the clean Pt(111) crystal prior to introduction into the reactor or CO exposure.

4.3 Results and Discussion

Pt-Re bimetallic clusters with varying surface compositions were prepared by the sequential deposition of Pt on Re and Re on Pt, and surface compositions were evaluated by CO TPD. Activity on Pt and Re can be distinguished since CO dissociates on Re but not on Pt; specifically, only molecular desorption around 500 K is observed on Pt,

whereas a high temperature recombinant peak at 950 K is observed on Re in addition to the molecular desorption peak at 500 K. Previous STM studies of 2 ML Re deposited on 2 ML Pt and 2 ML Pt deposited on 2 ML Re have demonstrated that exclusively bimetallic clusters are formed from both orders of deposition[32]. In both cases, the addition of the second metal does not result in the formation of new clusters, indicating that the atoms of the second metal are incorporated into the existing clusters of the first metal. When Re is deposited on 2 ML Pt clusters (Figure 4.1), the recombinant CO peak is not observed at Re coverages $\leq$0.5 ML; this behavior is consistent with the diffusion of Re into the Pt clusters, given that the higher surface free energy of Re (3.6 J/m^2) compared to Pt (2.5 J/m^2) thermodynamically favors Pt remaining at the surface of the clusters [33]. Furthermore, the appearance of the high temperature desorption peak at ~900 K is first observed at a Re coverage of 0.86 ML, and higher Re coverages result in increasing intensities of the high temperature peak, which becomes a prominent feature at 2 ML. The accumulation of Re at the cluster surface at higher coverages is attributed to kinetic limitations for the complete diffusion of Re atoms into the existing clusters. Thus, both Pt and Re atoms exist at the surface for clusters prepared from the deposition of $\geq$0.5 ML of Re on 2 ML Pt clusters. The cluster surfaces undergo substantial changes during annealing to 950 K due to the encapsulation by the TiO_x support upon heating in vacuum [32-35]; however, since CO dissociation occurs at room temperature[22, 34, 36], the intensity of the recombinant peak should still reflect the concentration of Re atoms at the surface when CO was adsorbed at room temperature.

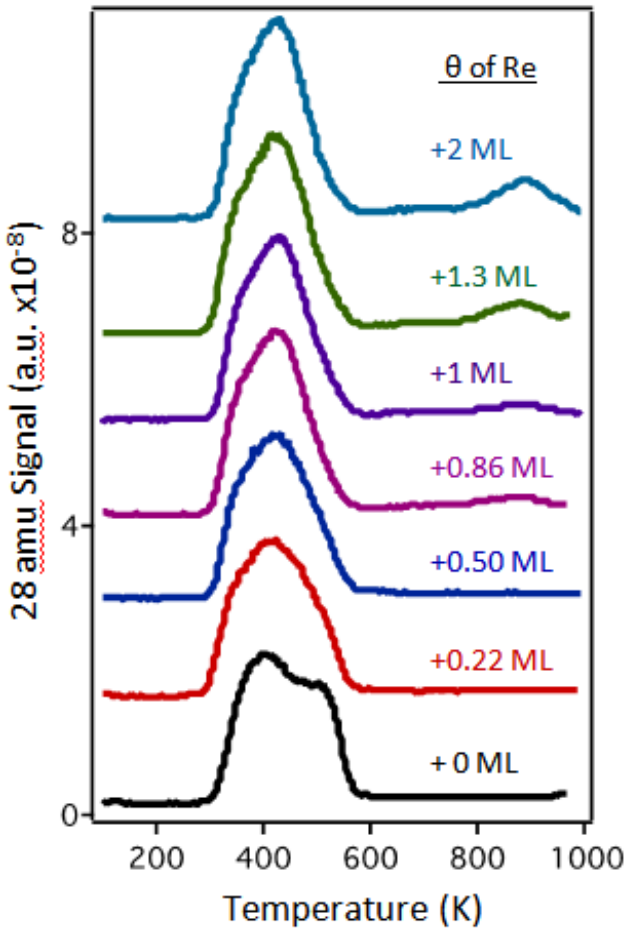

Figure 4.1: Temperature programmed desorption data for saturation exposures of CO at room temperature on 2 ML Pt clusters on TiO_2 after deposition of varying coverages of Re.

For the deposition of Pt on 2 ML Re clusters, almost no CO dissociation is observed at Pt coverages of 0.5 ML and higher (Figure 4.2). After deposition of 0.13 ML Pt, the intensity of the 940 K peak decreases by ~50% as Pt partially covers the Re surface. CO dissociation associated with Re continues to decrease after deposition of 0.25 ML Pt, and at 0.5 ML Pt almost no CO dissociation is detected; although a small feature that is only 15% of the high temperature CO intensity observed on 2 ML of Re is detected, the intensity of this feature continues to gradually decrease to 5% of the intensity on pure 2 ML Re as the Pt coverage is increased from 0.75 ML to 3 ML. The lack of activity

associated with Re for Pt coverages of >0.5 ML on 2 ML Re indicates that the Pt completely covers the Re surface for these coverages. Pt should remain at the cluster surface when deposited on top of Re clusters, based on the lower surface free energy of Pt. Based on the total surface area of the 2 ML Re clusters from a numerical integration of the STM images[32], the minimum coverage of Pt required to completely cover the Re clusters is one monolayer. Therefore, the Pt-Re clusters consist of both Pt and Re atoms at the surface when the Re clusters are partially coverage by Pt at coverage <1 ML. At higher Pt coverages, the bimetallic clusters consist of core-shell structures in which the 2 ML Re core is covered with a Pt shell with thicknesses that increase with Pt coverage.

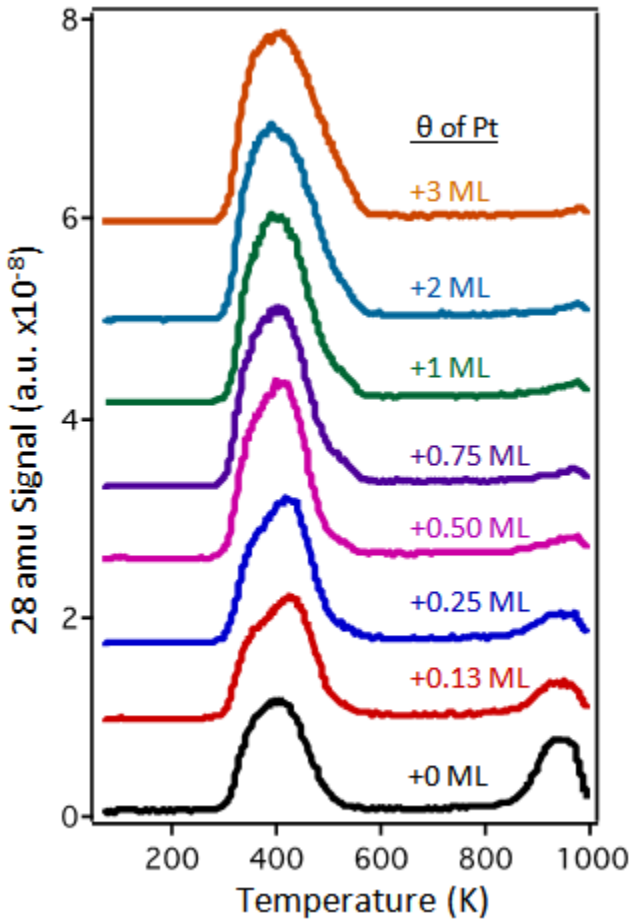

Figure 4.2: Temperature programmed desorption data for saturation exposures of CO at room temperature on 2 ML Re clusters on TiO_2 after deposition of varying coverages of Pt.

XPS for the Re(4f) region for different coverages of Re deposited on 2 ML Pt is consistent with the diffusion of Re into the clusters at coverages below 0.5 ML. Figure 4.3 shows that the binding energy for pure 2 ML Re clusters is at 40.3 eV, which is close to the value on bulk Re surfaces[37-39]. However, the binding energy for 0.13 and 0.25 ML Re deposited on 2 ML Pt is shifted to 40.8 eV and attributed to an electronic interaction between Pt and Re. This same shift to higher binding energy is also observed for Pt-Re surface alloys prepared by annealing Re films on Pt(111) so that the Re atoms diffuse subsurface and the top monolayer consists of pure Pt [40].

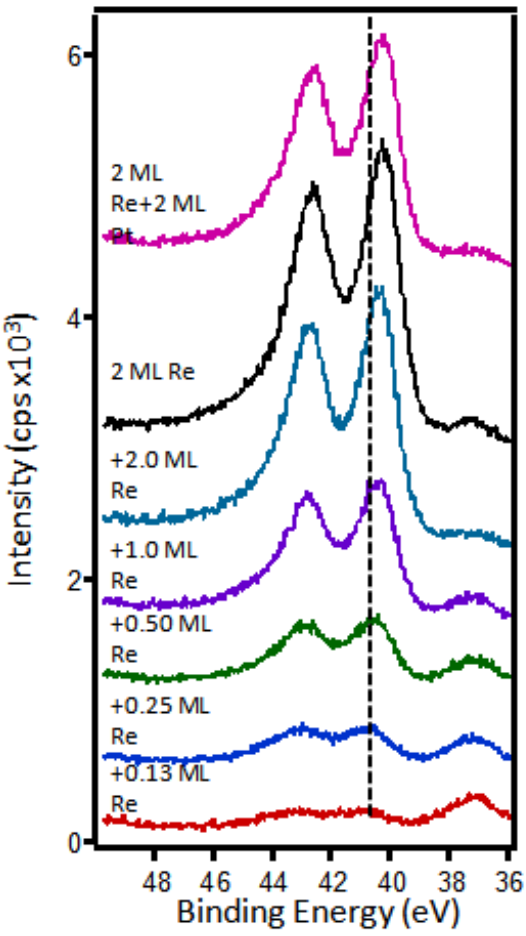

Figure 4.3: Re(4f) XPS data for the following clusters deposited on TiO_2(110): various Re coverages deposited on 2 ML Pt; 2 ML Re; and 2 ML Re+2 ML Pt. The feature at 37 eV is from the Ti($3p_{3/2}$) peak.

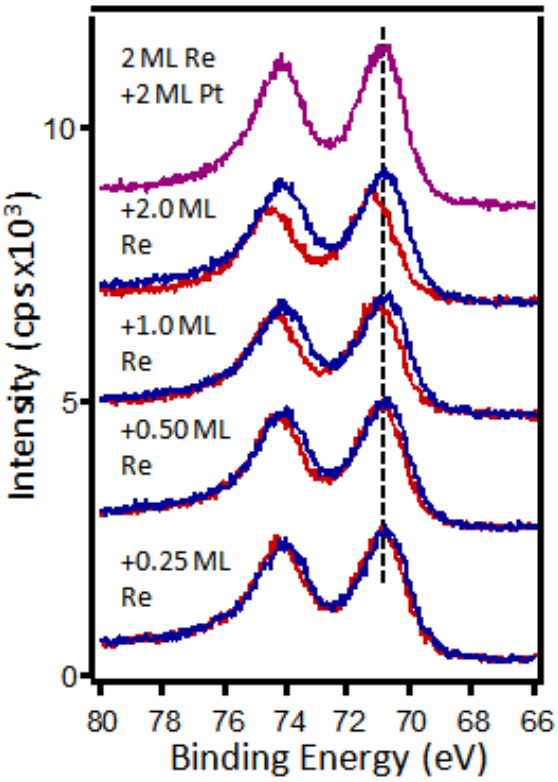

Figure 4.4: Pt(4f) XPS data for various Re coverages deposited on 2 ML Pt. The red traces show the spectrum after Re deposition, and the blue traces for the initial deposition of 2 ML Pt are shown for comparison. The pink trace shows Pt(4f) region for the reverse order of the deposition of 2 ML Re + 2 ML Pt.

As higher coverages of Re are deposited on the 2 ML Pt clusters, the Re($4f_{7/2}$) binding energy gradually shifts from 40.8 eV at 0.13 ML to 40.3 eV at 2.0 ML as the fraction of Re atoms at the surface increases compared to Re atoms intermixing in the cluster. Moreover, the Re($4f_{7/2}$) binding energy for 2 ML Re + 2 ML Pt clusters is the same as for the pure Re clusters (40.3 eV) since all of the Pt remains at the surface and these clusters are not intermixed. XPS data for the Pt($4f_{7/2}$) is also consistent with intermixing of Re into the clusters at lower coverages and accumulation of Re at the surface at higher coverages (Figure 4.4); however, Pt surfaces are known to exhibit a significant shifts in binding energy toward higher values when atoms or adsorbates are deposited on the surface; this effect is known as a surface core level shift (SCLS) and

originates from the lower binding energies (-0.4 eV) for undercoordinated surface Pt atoms compared to Pt atoms in the bulk[41, 42]. As the coverage of Re is increased from 0.25 ML to 2 ML, the Pt($4f_{7/2}$) binding energy shifts from 70.9 to 71.25 eV; for comparison, the spectra before Re deposition are also shown. Thus, the shift in binding energy is consistent with alloying of Re into Pt, as observed for the Pt-Re surface alloys [40], but could also be explained by the SCLS. For 2 ML Re + 2 ML Pt, the Pt($4f_{7/2}$) binding energy appears at 70.9 eV, which is consistent with the fact that Pt atoms reside at the surface as well as lack of Pt-Re intermixing since the deposited Pt remains at the surface rather than diffusing into the clusters.

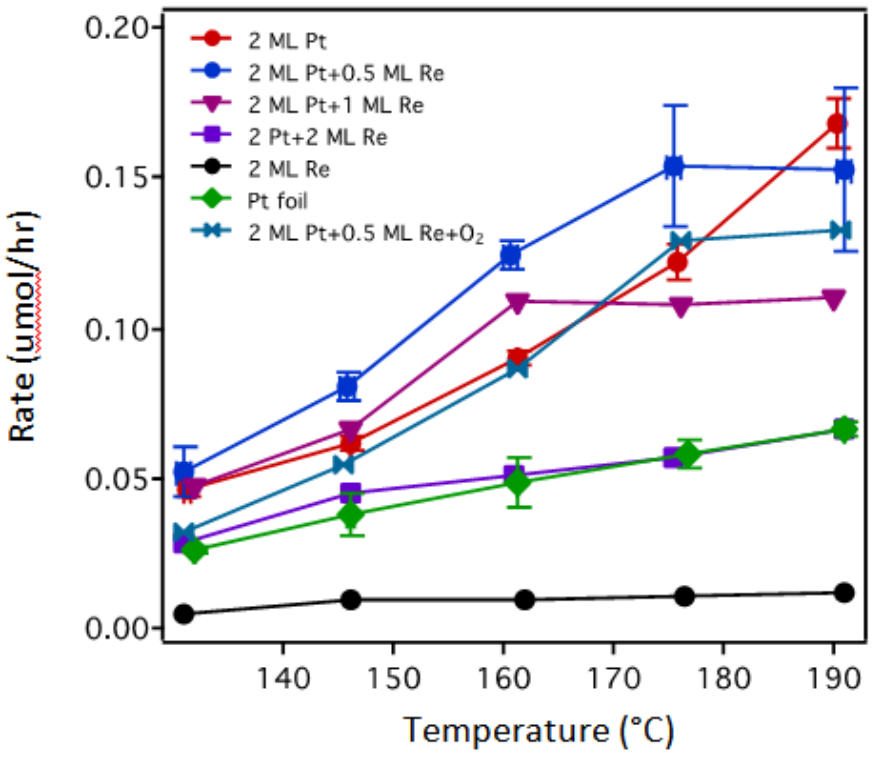

Figure 4.5: Activity data for the rate of CO_2 production in the water gas shift reaction on Pt, Re and Pt-Re clusters on TiO_2 as a function of temperature. The feed gas composition was 3% CO/7% H_2O/balance He, and the feed gas was recirculated over the catalyst for 2 hours before each measurement. Error bars for the 2 ML Pt and 2 ML Pt + 0.5 ML Re are based on standard deviations from three experiments, and error bars for the Pt foil experiment are based on two experiments.

Activity for the water gas shift reaction was studied on pure and bimetallic Pt-Re clusters at temperatures between 130 ºC and 190 ºC. Figure 4.5 shows the rate of CO_2 production as a function of temperature during water gas shift reaction with a feed gas mixture of 3% CO/7% H_2O/ balance He; CO_2 production was measured after a period of two hours at each temperature with the feed gas recirculated over the catalyst in order to increase product concentrations to detectable levels. For the 2 ML Pt clusters, the rate of WGS reaction increases with temperature according to the Arrhenius equation, yielding an activation energy of 44.6 kJ/mol over the temperature range of 145-190 ºC (Supplemental Figure 4.12), which is comparable to the values of 45.7 kJ/mol reported in the literature for WGS reaction on supported Pt clusters in a similar temperature range (50-100 ºC)[15]. Notably, the 2 ML Re clusters have almost no WGS activity, and lack of activity consistent with the dissociative adsorption of CO on Re. Bimetallic clusters consisting of 0.5 ML Re deposited on 2 ML Pt have higher activity than the pure 2 ML Pt clusters except at 190 ºC, where the activity shows a decrease with increasing temperature; for these surfaces, the CO TPD data show that the deposited Re is believed to diffuse into the cluster so that the cluster surface is pure Pt. Furthermore, the standard deviations at 175 and 190 ºC are much higher than at the other temperatures, suggesting that there may be changes in surface composition at the high temperatures such as adsorbate-induced diffusion of Re to the surface of the clusters. For the 2 ML Pt + 1 ML Re clusters, in which some of the deposited Re remains at the surface, the activity is similar to that of pure Pt at 130 and 145 ºC, slightly higher (17%) at 160 ºC but then does not increase at 175 and 190 ºC. For the 2 ML Pt +2 ML Re clusters which have substantial Re at the surface, the activity is lower than that of pure Pt at all temperatures,

and this behavior is consistent with the fact that Re does not provide active sites for WGS. Thus, the bimetallic clusters consisting of pure Pt at the surface and subsurface Re (2 ML Pt+0.5 ML Re) have higher activity than pure Pt clusters, but clusters with significant surface Re concentrations have lower activity, particularly at the higher temperatures. The Pt clusters have the highest activity at 175 and 190 ºC. At this temperature Re diffusion to the surface may occur on the Re on Pt clusters with low Re coverage, given that Re initially diffused into the clusters upon deposition in UHV.

Turnover frequencies (TOF) based on CO_2 production are shown in Figure 4.6 for both Pt on Re and Re on Pt clusters with a 2 ML coverage of the first metal followed by varying coverages of the second metal. The number of sites for each cluster surface was determined from total CO desorption relative to the 2 ML Pt clusters in the TPD experiments (Figure 4.7); furthermore, the absolute number of surface sites for the 2 ML Pt clusters was calculated to be $1.55 \times 10^{+15}$ sites/cm^2 based on a numerical integration of the STM image[43] for this surface and assuming the clusters have the same surface packing density as Pt(111) surface. For Re on 2 ML Pt, the TOF initially increases as the Re coverage is increased to 0.5 ML and then decreases as the Re coverage is further increased to 1.0 and 2.0 ML. Therefore, activity trends in Figure 4.5 for the bimetallic clusters cannot be attributed to differences in surface areas. For the bimetallic clusters prepared by depositing 1-3 ML of Pt on 2 ML Re, the TOFs are higher than for pure 2 ML Pt and increase with Pt coverage; for all of these surfaces, the 2 ML Re clusters should be completely covered by Pt. Specifically, the TOF for the 2 ML Re+2 ML Pt clusters is 1.6 times higher than the pure Pt clusters.

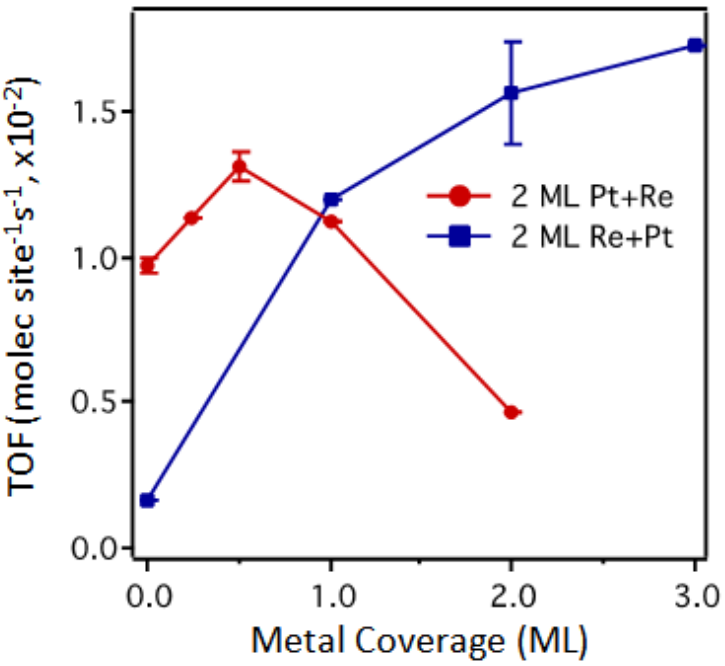

Figure 4.6: Turnover frequencies (TOFs) based on CO_2 production in the water gas shift reaction on Pt, Re and Pt-Re clusters at 160 C. The feed gas composition was 3% CO/7% H_2O/balance He, and the feed gas was recirculated over the catalyst for 2 hours before each measurement. Error bars are based on standard deviations from three experiments.

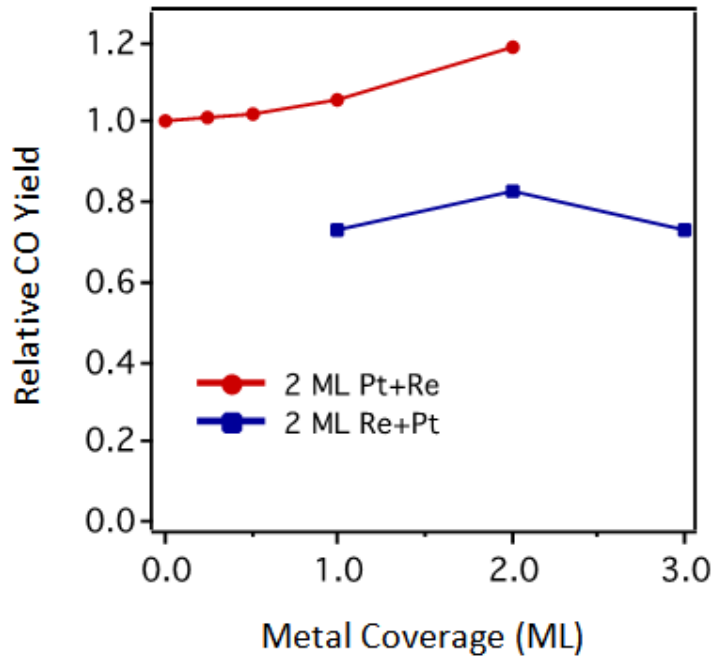

Figure 4.7: CO desorption yields for various coverages of Re on 2 ML Pt and Pt on 2 ML Re. All values relative to the desorption yield for CO on 2 ML of Pt.

In order to understand the Re oxidation states, the Re(4f) spectra before and after WGS reaction were collected (Figure 4.8). The activity of these cluster surfaces for the WGS reaction were investigated at 130-190 ºC (Figure 4.5); the reactor was then evacuated, cooled to room temperature, and the sample of introduced into the UHV chamber for XPS studies. For the pure Re clusters, the Re(4f) spectrum before reaction is fit with a single doublet with a Re($4f_{7/2}$) peak at 40.3 eV, which is a binding energy similar to that observed on single-crystal Re surfaces[37-39].After WGS reaction at 190 ºC, the Re(4f) spectrum is fit with a main peak at 40.6 eV that accounts for 70% of total peak area and is attributed to oxygen coordinated to metallic Re atoms at the surface[39, 44, 45]. There is also 23% contribution from a peak at 41.7 eV that is assigned to Re^{+2} [39] and a small peak (7 %) from Re^{+4} at 43.8 eV[46].Furthermore, the 40% decrease in total Re signal suggests significant sintering of the clusters. It is also possible that Re may leave the surface as volatile Re_2O_7[40, 47], but this seems less likely since the higher oxidation states such as Re^{+6} and Re^{+7} are not observed. For the 2 ML Pt + 2 ML Re clusters, where some Re resides at the surface, there is a much smaller shift of +0.1 eV after reaction which is consistent with the coordination of oxygen to Re surface atoms[39, 44, 45].For the bimetallic clusters that show activity greater than pure Pt (2 ML Pt +0.5 ML Re and 2 ML Re+2 ML Pt), there is no evidence for Re oxidation after WGS reaction. The 2 ML Pt + 0.5 ML Re clusters have a metallic Re($4f_{7/2}$) peak at 40.6 eV before reaction, and this binding energy is consistent with Re intermixed with Pt[48]; after reaction, the peak position and shape are unchanged, and still characteristic of metallic Re. Similarly, the Re($4f_{7/2}$) binding energy is 40.3 eV metallic Re in the 2 ML Re + 2 ML Pt clusters before reaction, and both the peak position and peak shape are unchanged after reaction. Since

these Pt-Re surfaces both consist of pure Pt in the top monolayer, it appears that it is difficult to oxidize subsurface Re under WGS conditions.

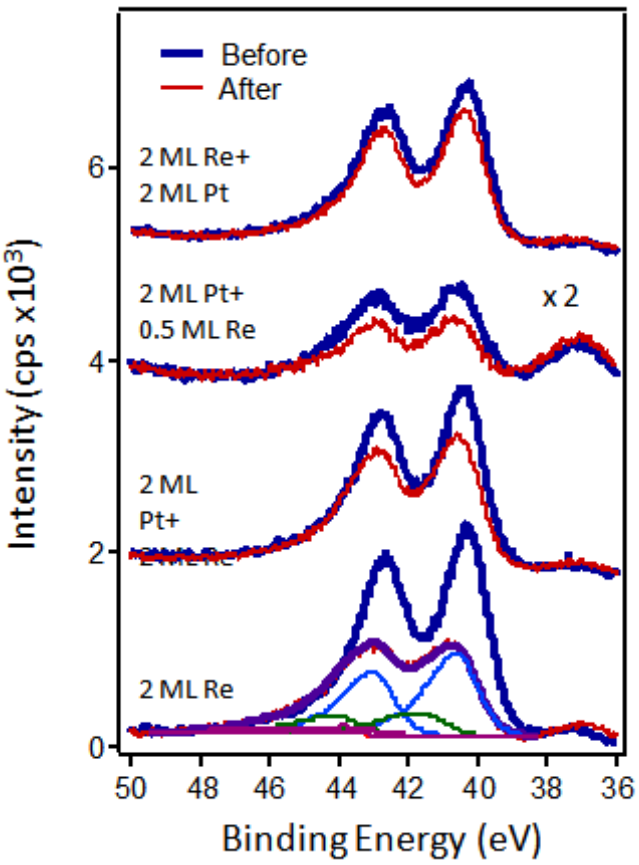

Figure 4.8: XPS data for the Re(4f) region for different cluster surfaces before (blue) and after (red) exposure to WGS reaction conditions. XPS data was collected following the activity measurements at 190 ℃ for the experiments shown in Figure 4.5. Peak fits are shown in purple.

To further investigate the potential role of rhenium oxide in the WGS reaction, the 2 ML Pt+0.5 ML Re clusters were oxidized before exposure to reaction conditions in 4% O_2/He for 1 hour at room temperature. XPS experiments show that a significant fraction of Re becomes highly oxidized with 35% as Re^{+6} (45.0 eV), 20% as Re^{+4} (43.8 eV), 22% as Re^{+2} (42.1 eV)[39, 44, 46, 49], and only 23% as metallic Re (Figure 4.9). After WGS reaction, the oxidized Pt-Re clusters are reduced: Re^{+6} is not observed, and total intensity of the Re^{+4} peak is decrease by approximately a factor of two, whereas the absolute

intensities of the Re^{+2} and Re^{0} peaks are slightly greater than before reaction. The loss of highly oxidized Re^{+6} is attributed to further oxidation to Re^{+7}, followed by the sublimation of volatile Re_2O_7 at the higher reaction temperatures, given that Re_2O_7 is known to sublime at temperatures as low as 177 ºC[40, 47]. A comparison of the activity for CO_2 production on the oxidized Pt-Re clusters with pure Pt and the unoxidized Pt-Re clusters is shown in Figure 4.5. The oxidized clusters have comparable activity to pure 2 ML Pt at all temperatures except 190 ºC, where the activity on pure Pt is significantly higher; this decrease in activity at 190 ºC could be attributed increased diffusion of Re to the cluster surface at elevated temperatures. Furthermore, the unoxidized Pt-Re clusters have higher activity than the oxidized clusters at all temperatures, and therefore there is no evidence that rhenium oxide provides active sites in the WGS reaction.

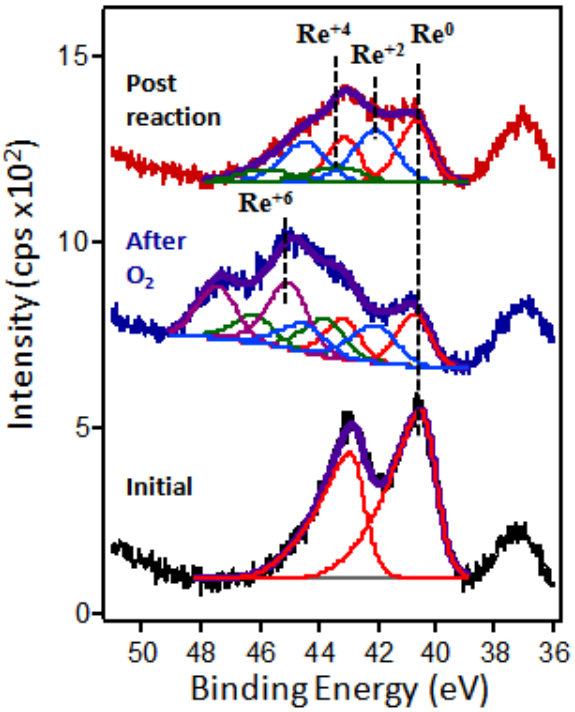

Figure 4.9: XPS data for the Re(4f) region for different cluster surfaces before (blue) and after (red) exposure to WGS reaction conditions. XPS data was collected following the activity measurements at 190 ℃ for the experiments shown in Figure 3. The peak at 37 eV is from the Ti($3p_{3/2}$) peak.

DFT calculations were carried out in order to understand differences in activities for the pure Pt surface compared to the Pt-Re alloy surface. The pure Pt surface was modeled as a 5-layer slab with a (4x3) surface cell, and the second layer of the Pt slab was replaced with Re atoms in the model structure for the Pt-Re alloy surface (Figure 4.13). Since O-H bond scission in water is believed to be the rate limiting step in WGS on Pt catalysts [17, 20, 21], the activation energy barrier for O-H was calculated to determine if more facile O-H bond breaking on Pt-Re contributes to the higher activity. However, the activation energy for O-H bond scission on pure Pt slab (0.77 eV) and was slightly lower than on the Pt-Re alloy surface (0.92 eV). Therefore, E_a for O-H bond breaking cannot explain the higher activity of Pt-Re compared to Pt.

The energies associated with adsorption and dissociation of H_2O, CO and H_2 were also calculated on Pt and Pt-Re, as shown in Table 4.1. For the dissociation of water into $OH_{(ad)}$ and $H_{2(g)}$ or $H_{(ad)}$, the lower reaction energy on Pt-Re demonstrates that dissociation to $OH_{(ad)}$ is more thermodynamically favorable on Pt-Re. In contrast, the adsorption of CO at either top or fcc sites is favored on Pt compared to Pt-Re. Similarly, the dissociation of $H_{2(g)}$ to $H_{(ad)}$ is favored on Pt compared to Pt-Re, whereas the adsorption of gaseous water is equally favored on both surfaces. Based on these results, the stronger bonding of CO to Pt vs. Pt-Re should lead to reduced CO poisoning on the Pt-Re surface and the higher observed activity in the WGS reaction. Active sites on the pure Pt surface are also more likely to be blocked by adsorbed hydrogen than Pt-Re sites, thereby reducing activity for WGS on Pt. Moreover, the higher stability of $OH_{(ad)}$ on the Pt-Re surface provides a greater thermodynamic driving force for water dissociation on Pt-Re vs. Pt.

Table 4.1: Density functional theory calculations for reaction energies on Pt and Pt-Re alloy structures.

Reaction	Reaction Energy (eV)	
	Pt-Pt-Pt-Pt-Pt	Pt-Re-Pt-Pt-Pt
$H_2O_{(g)} \rightarrow OH_{(ad)} + ½ H_{2(g)}$	0.81 (top)	0.55 (top)
$H_2O_{(g)} \rightarrow OH_{(ad)} + H_{(ad)}$	0.32	0.22
$CO_{(g)} \rightarrow CO_{(ad)}$	-1.75/-1.85 (top/fcc)	-1.51/-1.21 (top/fcc)
$H_{2(g)} \rightarrow ½ H_{(ad)}$	-0.49 (fcc)	-0.33 (fcc)
$H_2O_{(g)} \rightarrow H_2O_{(ad)}$	-0.26 (top)	-0.25 (top)

IRAS experiments provide further evidence that the Pt-Re alloy surface is less susceptible to CO poisoning than pure Pt in the WGS reaction. A Pt(111) crystal was exposed to WGS reaction conditions (3%CO/7% H_2O/balance He, 160 ºC, 2 hours), and then IRAS data was collected on the surface after reaction. As shown in Figure 4.10, an intense feature is observed at 2085 cm^{-1} and attributed to CO at top sites[50, 51] and a smaller peak appears at 1848 cm^{-1} and is assigned to CO at bridge sites[50, 51]. The Pt-Re alloy surface is prepared by depositing 2.4 ML of Re on Pt(111) and annealing at 1000 K to form a surface alloy, in which the Re diffuses subsurface and the top surface monolayer consists of pure Pt[40]. After the Pt-Re alloy surface is exposed to identical WGS reaction conditions, the CO stretching peak at 2066 cm^{-1} has an integrated intensity that is 50% of that at 2085 cm^{-1} from CO on Pt(111). The shift toward lower CO stretching frequencies on the Pt-Re alloy cannot be completely accounted for by decreased dipole-dipole coupling at the lower coverages[52, 53]. Specifically, the stretching frequency of CO on Pt(111) decreases from 2090 cm^{-1} at a saturation exposure of 3 L to

2081 cm^{-1} at a 0.01 L exposure, where the peak intensity has decreased by 90%. Thus, the 20 cm^{-1} decrease in C-O stretching frequency is too large to be solely attributed to decreased dipole-dipole coupling at lower coverages on the Pt-Re alloy.

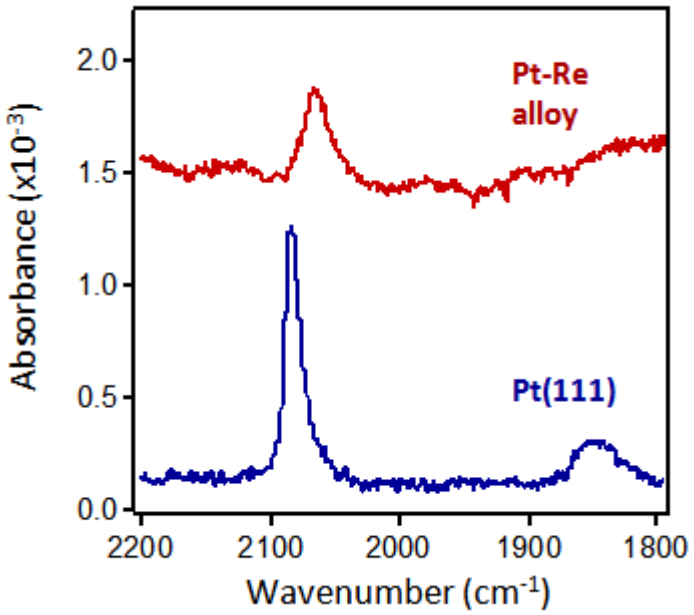

Figure 4.10: Infrared absorption-reflection spectra of the CO stretching region for Pt(111) and the Pt-Re alloy surface (2.4 ML Re on Pt(111) heated to 1000 K for 5 min) after exposure to WGS reaction conditionsfor 2 hours at 160 °C.

Post-reaction XPS data for the O(1s) region was also collected for WGS reaction on various pure and bimetallic clusters following the reactor experiments shown in Figure 4.5. Given that the TiO_2(110) substrate contributes a large O(1s) signal at 530.2 eV, the changes in the O(1s) after reaction are shown in Figure 4.11, where the O(1s) spectrum before reaction has been subtracted from the O(1s) spectra after reaction for each surface. The clean TiO_2 surface, which has no activity for WGS, exhibits a small feature at 531.8 eV and residual signal at ~530 eV, which may be from error in the subtraction of the TiO_2 contribution. The O(1s) difference spectrum for the 2 ML Pt clusters show a peak with a binding energy at 530.7 eV, which is characteristic of oxygen on Pt, given that this same binding energy is observed with a pure Pt foil is exposed to the same WGS reaction

conditions. In contrast, the spectrum for 2 ML Re exhibits a peak at a lower binding energy of 529.5 eV, and therefore oxygen on Re and oxygen on Pt can be distinguished. Intensity also appears at 531.8 eV as a higher binding energy shoulder from oxygen species on TiO_2 for both the 2 ML Pt and 2 ML Re spectra.

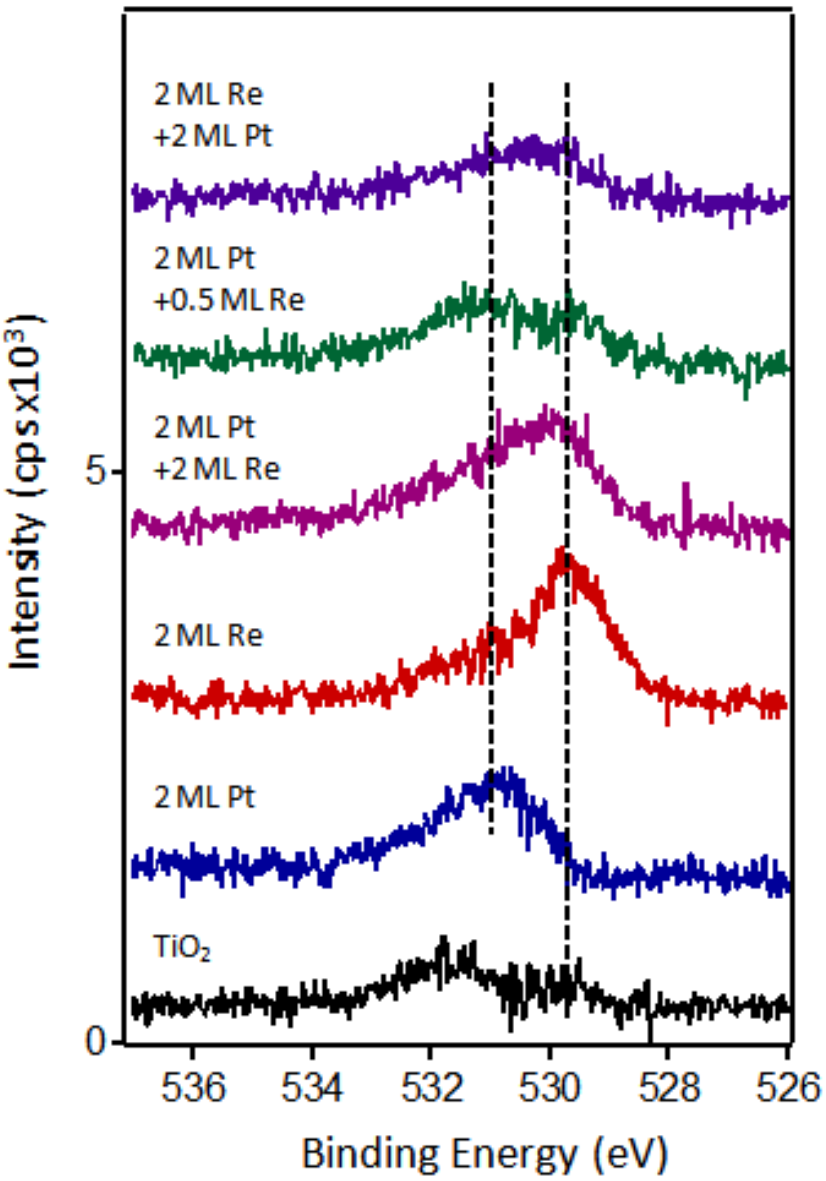

Figure 4.11: XPS data for the O(1s) region after WGS reaction up to 190 ℃ on the various surfaces. For each spectrum, the O(1s) spectrum before reaction was substract from the post-reaction spectrum in order to remove the contribution from TiO_2.

The 2 ML Pt+2 ML Re clusters have both Pt and Re atoms at the surface, and accordingly, the O(1s) difference spectrum shows contribution at both 530.7 and 529.5 eV from oxygen on Pt and Re, respectively. For the 2 ML Pt + 0.5 ML Re clusters, more distinct features are observed at 530.7 and 529.5 eV, with the latter peak suggesting that there is some diffusion of Re to the surface during WGS reaction. The O(1s) difference spectrum after reaction for the 2 ML Re+2 ML Pt clusters has intensity at ~529.5 eV, but this intensity is not greater than what is observed on the post-reaction TiO_2 surface. Consequently, it is not clear that diffusion of Re to the surface occurs for these Re core-Pt shell clusters.

Post-reaction C(1s) data collected on the pure and bimetallic clusters demonstrate that carbon is deposited on all surfaces during reaction, including on the TiO_2 support itself (Figure 4.14). However, for all surfaces, there is no significant difference in the amount of carbon deposited, with the exception of the 2 ML Pt+2 ML Re clusters, which appear to have more carbon than the other surfaces; this is also the only bimetallic surface studied that has a high concentration of Re at the surface. The rising baseline at low binding energies for surfaces containing Re is from the Re($4d_{3/2}$) at 277 eV.

4.4 SUMMARY

Bimetallic Pt on Re clusters were prepared by depositing 2 ML Pt on 2 ML Re to form Re-core-Pt-shell structures, or by depositing 0.5 ML Re on 2 ML Pt clusters, where the Re atoms diffusing into the Pt cluster leaving a monolayer of Pt at the surface. Both of these Pt on Re surfaces exhibited greater activity for WGS than pure Pt clusters; in contrast, bimetallic clusters with a significant fraction of Re atoms at the surface had

lower activity than pure Pt, given that Re is active for the WGS reaction. XPS investigations on the Pt on Re clusters after reaction showed that the Re remained metallic and was not oxidized during reaction. Moroever, Pt-Re clusters that were oxidized before WGS reaction showed lower activity than the unoxidized Pt-Re clusters, and this implies that the active sites for the WGS reaction in Pt-Re catalysts do not involve ReO_x. Both DFT and IRAS studies show that CO binds more strongly to Pt surfaces compared to Pt-Re, and therefore the improved activity on Pt-Re is attributed to reduced CO poisoning.

4.5 Supplemental Information

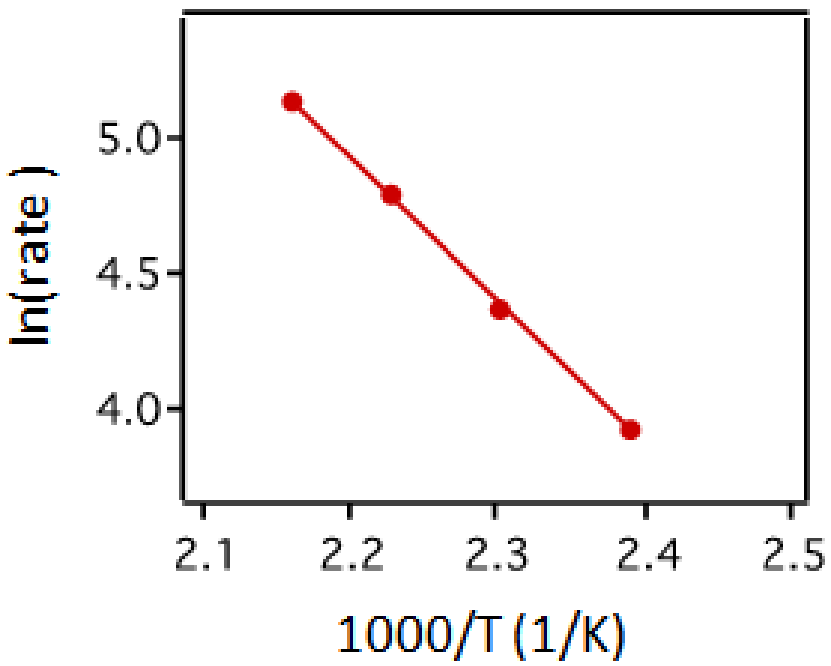

Figure 4.12: Arrhenius plot for WGS reaction on 2 ML Pt clusters on TiO_2(110) over the temperature range of 145-190 °C. Data collected at 130 °C was not included in this plot since it did not fit the linear trend.

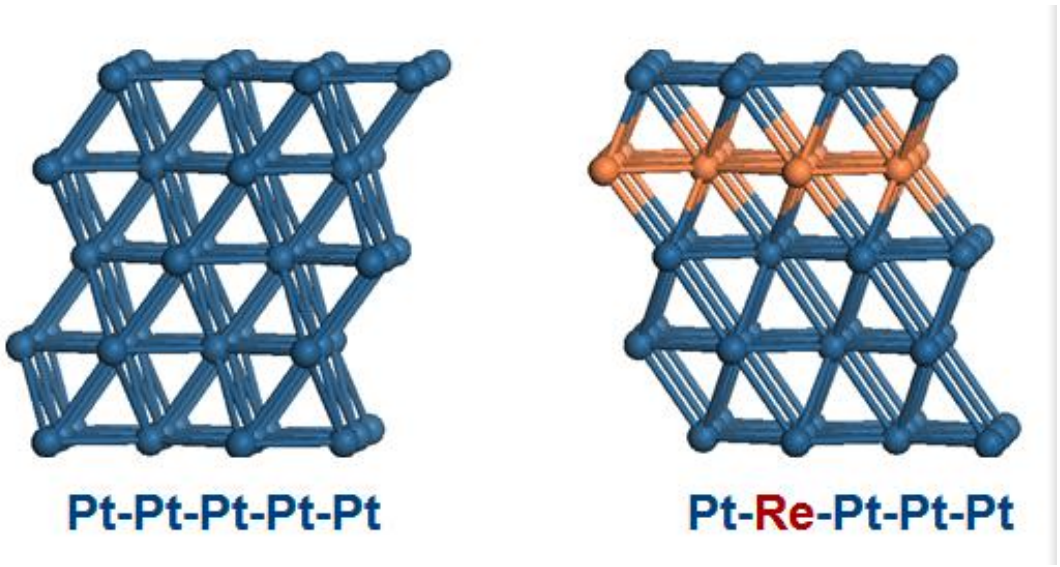

Figure 4.13: Structure for the pure Pt (left) and Pt-Re alloy (right) model surfaces used in the DFT calculations.

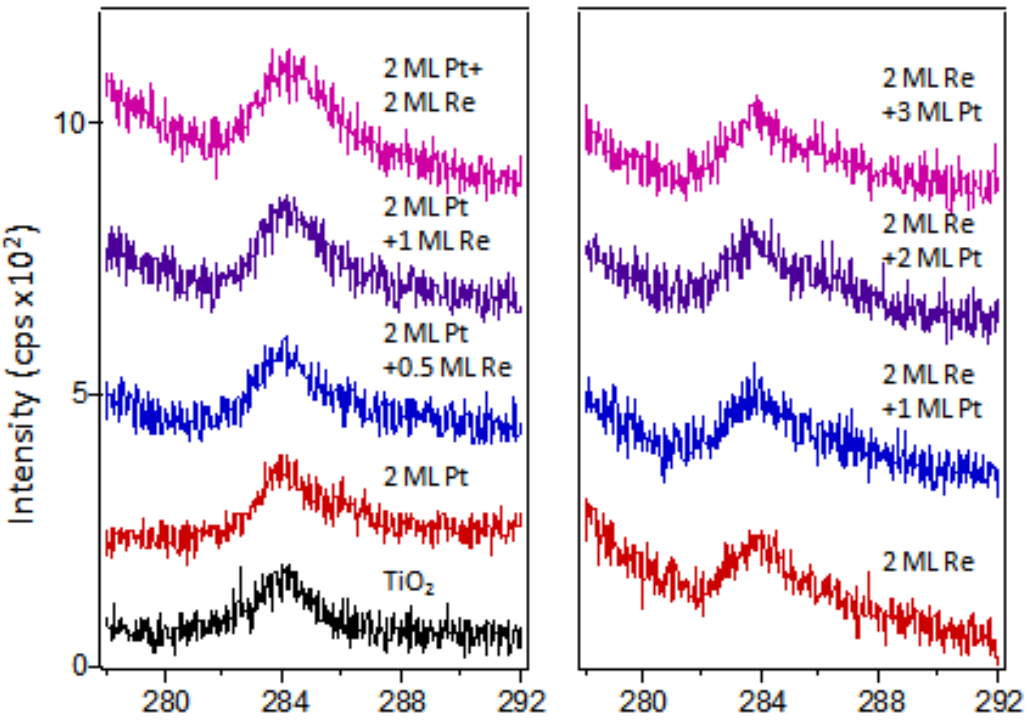

Figure 4.14: XPS data for the C(1s) region after WGS reaction up to 190 ℃ on the various surfaces.

ACKNOWLEDGEMENTS

We gratefully acknowledge financial support from the National Science Foundation (CHE 1300227). AJB also acknowledges funding from the NSF IGERT program. Thanks to Dr. Audrey Duke, Amy Brandt and Thathsara Maddumapatabandi for the preparation and characterizations (XPS and IR) of supported Pt-Re catalysts.

4.6 REFERENCES

(1) Sinfelt, J. H., Catalysis by alloys and bimetallic clusters. *Accounts of Chemical Research* **1977,** 10 (1), 15-20.

(2) Chen, J. G.; Menning, C. A.; Zellner, M. B., Monolayer bimetallic surfaces: Experimental and theoretical studies of trends in electronic and chemical properties. *Surface Science Reports* **2008,** 63 (5), 201-254.

(3) Sinfelt, J. H., *Bimetallic catalysts: discoveries, concepts, and applications*. Wiley: **1983**.

(4) Campbell, C. T., Bimetallic Surface Chemistry. *Annual Review of Physical Chemistry* **1990,** 41 (1), 775-837.

(5) Rodriguez, J., Physical and chemical properties of bimetallic surfaces. *Surface Science Reports* **1996,** 24 (7), 223-287.

(6) Liu, P.; Norskov, J. K., Ligand and ensemble effects in adsorption on alloy surfaces. *Physical Chemistry Chemical Physics* **2001,** 3 (17), 3814-3818.

(7) Yu, W.; Porosoff, M. D.; Chen, J. G., Review of Pt-Based Bimetallic Catalysis: From Model Surfaces to Supported Catalysts. *Chemical Reviews* **2012,** 112 (11), 5780-5817.

(8) Kluksdahl, H. E. Reforming a sulfur-free naphtha with a platinum-rhenium catalyst. US Patent 3415737, 1968.

(9) Carter, J. L.; McVinker, G. B.; Weissman, W.; Kmak, M. S.; Sinfelt, J. H., Bimetallic catalysts; application in catalytic reforming. *Applied Catalysis* **1982,** 3 (4), 327-346.

(10) Somorjai, G. A., *Introduction to surface chemistry and catalysis*. Wiley: **1994**.

(11) Barbier, J., Deactivation of reforming catalysts by coking - a review. *Applied Catalysis* **1986,** 23 (2), 225-243.

(12) Godbey, D. J.; Somorjai, G. A., The adsorption and desorption of hydrogen and carbon monoxide on bimetallic Re-Pt(111) surfaces. *Surface Science* **1988,** 204 (3), 301-318.

(13) Parera, J. M.; Beltramini, J. N., Stability of bimetallic reforming catalysts. *Journal of Catalysis* **1988,** 112 (2), 357-365.

(14) Godbey, D. J.; Garin, F.; Somorjai, G. A., The hydrogenolysis of ethane over Re-Pt(111) and Pt-Re(0001) bimetallic crystal surfaces. *Journal of Catalysis* **1989,** 117 (1), 144-154.

(15) Sato, Y.; Terada, K.; Hasegawa, S.; Miyao, T.; Naito, S., Mechanistic study of water–gas-shift reaction over TiO_2 supported Pt–Re and Pd–Re catalysts. *Applied Catalysis A: General* **2005,** 296 (1), 80-89.

(16) Iida, H.; Igarashi, A., Difference in the reaction behavior between Pt–Re/TiO_2 (Rutile) and Pt–Re/ZrO_2 catalysts for low-temperature water gas shift reactions. *Applied Catalysis A: General* **2006,** 303 (1), 48-55.

(17) Azzam, K. G.; Babich, I. V.; Seshan, K.; Lefferts, L., Role of Re in Pt–Re/TiO_2 catalyst for water gas shift reaction: A mechanistic and kinetic study. *Applied Catalysis B: Environmental* **2008,** 80 (1–2), 129-140.

(18) Iida, H.; Yonezawa, K.; Kosaka, M.; Igarashi, A., Low-temperature water gas shift reaction over Pt–Re/TiO_2 catalysts prepared by a sub-critical drying method. *Catalysis Communications* **2009,** 10 (5), 627-630.

(19) González, I. D.; Navarro, R. M.; Wen, W.; Marinkovic, N.; Rodrigué, J. A.; Rosa, F.; Fierro, J. L. G., A comparative study of the water gas shift reaction over platinum catalysts supported on CeO2, TiO2 and Ce-modified TiO2. *Catalysis Today* **2010,** 149 (3–4), 372-379.

(20) Azzam, K. G.; Babich, I. V.; Seshan, K.; Mojet, B. L.; Lefferts, L., Stable and Efficient Pt–Re/TiO_2 catalysts for Water-Gas-Shift: On the Effect of Rhenium. *ChemCatChem* **2013,** 5 (2), 557-564.

(21) Azzam, K. G.; Babich, I. V.; Seshan, K.; Lefferts, L., A bifunctional catalyst for the single-stage water–gas shift reaction in fuel cell applications. Part 2. Roles of the support and promoter on catalyst activity and stability. *Journal of Catalysis* **2007,** 251 (1), 163-171.

(22) Ramstad, A.; Strisland, F.; Raaen, S.; Borg, A.; Berg, C., CO and O_2 adsorption on the Re/Pt(111) surface studied by photoemission and thermal desorption. *Surface Science* **1999,** 440 (1–2), 290-300.

(23) Ishikawa, Y.; Liao, M.-S.; Cabrera, C. R., Energetics of H_2O dissociation and COads+OHads reaction on a series of Pt–M mixed metal clusters: a relativistic density-functional study. *Surface Science* **2002,** 513 (1), 98-110.

(24) Greeley, J.; Mavrikakis, M., Near-surface alloys for hydrogen fuel cell applications. *Catalysis Today* **2006,** 111 (1–2), 52-58.

(25) Duke, A. S.; Xie, K.; Monnier, J. R.; Chen, D. A., Superior Long-Term Activity for a Pt-Re Alloy Compared to Pt in Methanol Oxidation Reactions. *Submitted to surface science*.

(26) Tenney, S. A.; Xie, K.; Monnier, J. R.; Rodriguez, A.; Galhenage, R. P.; Duke, A. S.; Chen, D. A., Novel recirculating loop reactor for studies on model catalysts: CO oxidation on Pt/TiO_2(110). *Review of Scientific Instruments* **2013,** 84 (10), 104101-104108.

(27) Varazo, K.; Parsons, F. W.; Ma, S.; Chen, D. A., Methanol Chemistry on Cu and Oxygen-Covered Cu Nanoclusters Supported on TiO_2(110). *The Journal of Physical Chemistry B* **2004,** 108 (47), 18274-18283.

(28) Ozturk, O.; Park, J. B.; Black, T. J.; Rodriguez, J. A.; Hrbek, J.; Chen, D. A., Methanethiol chemistry on TiO2-supported Ni clusters. *Surface Science* **2008,** 602 (19), 3077-3088.

(29) Tenney, S. A.; Ratliff, J. S.; Roberts, C. C.; He, W.; Ammal, S. C.; Heyden, A.; Chen, D. A., Adsorbate-Induced Changes in the Surface Composition of Bimetallic Clusters: Pt−Au on TiO_2(110). *The Journal of Physical Chemistry C* **2010,** 114 (49), 21652-21663.

(30) Tenney, S. A.; He, W.; Roberts, C. C.; Ratliff, J. S.; Shah, S. I.; Shafai, G. S.; Turkowski, V.; Rahman, T. S.; Chen, D. A., CO-Induced Diffusion of Ni Atoms to the Surface of Ni–Au Clusters on TiO_2(110). *The Journal of Physical Chemistry C* **2011,** 115 (22), 11112-11123.

(31) Tenney, S. A.; Cagg, B. A.; Levine, M. S.; He, W.; Manandhar, K.; Chen, D. A., Enhanced activity for supported Au clusters: Methanol oxidation on Au/TiO_2(110). *Surface Science* **2012,** 606 (15–16), 1233-1243.

(32) Galhenage, R. P.; Xie, K.; Yan, H.; Seuser, G. S.; Chen, D. A., Understanding the Growth, Chemical Activity, and Cluster–Support Interactions for Pt–Re Bimetallic Clusters on TiO_2(110). *The Journal of Physical Chemistry C* **2016,** 120 (20), 10866-10878.

(33) Boer, F. R. d., *Cohesion in metals : transition metal alloys*. North-Holland ; Sole distributors for the U.S.A. and Canada, Elsevier Scientific Pub. Co.: Amsterdam; New York; New York, N.Y., U.S.A., **1988**.

(34) Ozturk, O.; Park, J. B.; Ma, S.; Ratliff, J. S.; Zhou, J.; Mullins, D. R.; Chen, D. A., Probing the interactions of Pt, Rh and bimetallic Pt–Rh clusters with the TiO2(110) support. *Surface Science* **2007,** 601 (14), 3099-3113.

(35) Tenney, S.; He, W.; Ratliff, J.; Mullins, D.; Chen, D., Characterization of Pt–Au and Ni–Au Clusters on TiO_2 (110). *Topics in Catalysis* **2011,** 54 (1), 42-55.

(36) Ducros, R.; Fusy, J.; Jupille, J.; Pareja, P.; Tatarenko, S., CO adsorption on rhenium single crystal surfaces: Characterization of molecular and dissociated states and influence of structural defects. *Applied Surface Science* **1987,** 29 (2), 179-193.

(37) Ducros, R.; Alnot, M.; Ehrhardt, J. J.; Housley, M.; Piquard, G.; Cassuto, A., A study of the adsorption of several oxygen-containing molecules (O_2, CO, NO, H_2O) on Re(0001) by XPS, UPS and temperature programmed desorption. *Surface Science* **1980,** 94 (1), 154-168.

(38) Mårtensson, N.; Saalfeld, H. B.; Kuhlenbeck, H.; Neumann, M., Structural dependence of the 5 \textit{d} -metal surface energies as deduced from surface core-level shift measurements. *Physical Review B* **1989,** 39 (12), 8181-8186.

(39) Chan, A. S. Y.; Chen, W.; Wang, H.; Rowe, J. E.; Madey, T. E., Methanol Reactions over Oxygen-Modified Re Surfaces: Influence of Surface Structure and Oxidation. *The Journal of Physical Chemistry B* **2004,** 108 (38), 14643-14651.

(40) Duke, A. S.; Galhenage, R. P.; Tenney, S. A.; Sutter, P.; Chen, D. A., In Situ Studies of Carbon Monoxide Oxidation on Platinum and Platinum–Rhenium Alloy Surfaces. *The Journal of Physical Chemistry C* **2015,** 119 (1), 381-391.

(41) Björneholm, O.; Nilsson, A.; Tillborg, H.; Bennich, P.; Sandell, A.; Hernnäs, B.; Puglia, C.; Mårtensson, N., Overlayer structure from adsorbate and substrate core level binding energy shifts: CO, CCH_3 and O on Pt(111). *Surface Science* **1994,** 315 (1–2), L983-L989.

(42) Ramstad, A.; Strisland, F.; Raaen, S.; Worren, T.; Borg, A.; Berg, C., Growth and alloy formation studied by photoelectron spectroscopy and STM. *Surface Science* **1999,** 425 (1), 57-67.

(43) Zhou, J.; Ma, S.; Kang, Y. C.; Chen, D. A., Dimethyl Methylphosphonate Decomposition on Titania-Supported Ni Clusters and Films: A Comparison of Chemical Activity on Different Ni Surfaces. *The Journal of Physical Chemistry B* **2004,** 108 (31), 11633-11644.

(44) Ducros, R.; Fusy, J., Core level binding energy shifts of rhenium surface atoms for a clean and oxygenated surface. *Journal of Electron Spectroscopy and Related Phenomena* **1987,** 42 (4), 305-312.

(45) Liu, P.; Shuh, D. K., Adsorption of O_2 on polycrystalline rhenium metal at room temperature studied by synchrotron X-ray photoemission spectroscopy. *Journal of Electron Spectroscopy and Related Phenomena* **2001,** 114–116, 319-325.

(46) Wagner, C. D.; Muilenberg, G. E., *Handbook of x-ray photoelectron spectroscopy : a reference book of standard data for use in x-ray photoelectron spectroscopy*. Physical Electronics Division, Perkin-Elmer Corp.: Eden Prairie, Minn., **1979**.

(47) Duke, A. S.; Galhenage, R. P.; Tenney, S. A.; Ammal, S. C.; Heyden, A.; Sutter, P.; Chen, D. A., In Situ Ambient Pressure X-ray Photoelectron Spectroscopy Studies of Methanol Oxidation on Pt(111) and Pt–Re Alloys. *The Journal of Physical Chemistry C* **2015,** 119 (40), 23082-23093.

(48) Koso, S.; Watanabe, H.; Okumura, K.; Nakagawa, Y.; Tomishige, K., Comparative study of Rh–MoOx and Rh–ReOx supported on SiO2 for the hydrogenolysis of ethers and polyols. *Applied Catalysis B: Environmental* **2012,** 111–112, 27-37.

(49) Morant, C.; Gal án, L.; Sanz, J. M., X-ray photoelectron spectroscopic study of the oxidation of polycrystalline rhenium by exposure to O2 and low energy O2+ ions. *Analytica Chimica Acta* **1994,** 297 (1–2), 179-186.

(50) Bolivar, C.; Charcosset, H.; Frety, R.; Primet, M.; Tournayan, L.; Betizeau, C.; Leclercq, G.; Maurel, R., Platinum-rhenium-alumina catalysts. *Journal of Catalysis* **1976,** 45 (2), 163-178.

(51) Peri, J. B., Infrared studies of Pt and Pt-Re reforming catalysts. *Journal of Catalysis* **1978,** 52 (1), 144-156.

(52) Scheffler, M., The influence of lateral interactions on the vibrational spectrum of adsorbed CO. *Surface Science* **1979,** 81 (2), 562-570.

(53) Persson, B. N. J.; Ryberg, R., Vibrational interaction between molecules adsorbed on a metal surface: The dipole-dipole interaction. *Physical Review B* **1981,** 24 (12), 6954-6970.

CHAPTER 5 UNDERSTANDING THE GROWTH, CHEMICAL ACTIVITY, AND CLUSTER–SUPPORT INTERACTIONS FOR PT–RE BIMETALLIC CLUSTERS ON TiO_2 (110)[1]

[1]Reprinted (adapted) with permission from Randima P. Galhenage, Kangmin Xie, Hui Yan, Grant S. Seuser and Donna A. Chen, Understanding the Growth, Activity and Cluster-Support Interactions for Pt-Re Bimetallic Clusters on TiO_2(110), *Journal of Physical Chemistry C,* **2016**, *120* (20), pp 10866–10878. Copyright 2016 American Chemical Society.

5.1 INTRODUCTION

The Pt-Re bimetallic system has exhibited unique properties that are different from pure Pt and pure Re for a number of surface reactions and catalytic processes. For example, the Pt-Re on alumina catalysts have been used in industrial naphtha reforming since the 1960s and represent one of the first commercially successful bimetallic catalysts[1, 2].The Pt-Re catalyst has greater selectivity and activity in hydrocarbon reforming reactions[3-5] as well as better long-term activity compare to pure Pt; the presence of Re is believed to inhibit carbon buildup and subsequent deactivation of the Pt sites[3, 5-11]. Furthermore, Pt-Re/TiO_2 catalysts have recently been reported to have higher activity than pure Pt/TiO_2 for the water gas shift (WGS) reaction [12-22]. Recent studies of the aqueous phase reforming (APR) of glycerol and other polyols have demonstrated that Pt-Re/C catalysts have higher turnover frequencies, activities and lifetimes compared to Pt/C [19-27]. The weaker binding of CO to the Pt-Re surface vs. Pt is proposed to be responsible for the APR higher activity due to decreased CO poisoning[23, 28]. Alternatively, it has also been suggested that CO is removed via the enhanced WGS activity at ReO_x sites on the Pt-Re/TiO_2 catalysts [15, 16, 18]. Superior properties for the Pt-Re catalysts have been observed in reactions associated with biomass reforming, such as glycerol hydrogenolysis to propanediols[24, 29] and selective hydrogenation of carboxylic acids[30, 31] and aldehydes[32] to alcohols. In addition, a number of studies report unusual and desirable chemical activity for the bimetallic Pt-Re surfaces. Both the weaker binding of CO [33, 34] and the decreased activation energy for H_2 desorption on Pt-Re compared to Pt(111) have been ascribed to electronic effects[35].Our group's recent investigations show that oxygen dissociates more readily at 500 K on Pt-Re alloy surface compared to Pt(111),

but in this case it is believed that Re diffuses to the alloy surface to facilitate oxygen dissociation[36].

Another effect of the addition of Re to the Pt catalysts is increased Pt dispersion, particularly on oxide supports [4, 13, 29, 37, 38]. Moreover, the Pt-Re particles are more resistant to sintering compared to Pt alone [15, 23, 39]. For example, after 20 hours onstream for WGS at 300 ℃, the Pt/TiO_2 particles lose 36% of their initial dispersion whereas the $Pt\text{-}Re/TiO_2$ particles lose only 8%[15]. However, the increased activity for Pt-Re in the WGS reaction cannot in general be attributed solely to increased dispersion [15, 40].

Despite the many investigations of Pt-Re catalysts, the details of Pt-Re bimetallic interactions, Re oxidation states and interactions of the metal particles with the oxide support are still not completely understood. This is largely because the Re oxidation state and extent of Pt-Re interactions are known to be strongly influenced by exact preparation conditions, including catalyst pretreatment conditions[13, 18, 41-47]. Although it is possible to control the Pt-Re particle size to <2nm, it is not possible to control the Re oxidation state because Re remains partially oxidized even after high temperature reduction in H_2 [3, 24, 29]. Therefore, studies of model surfaces consisting of vapor-deposited Pt, Re and Pt-Re clusters on a single crystal oxide support are important in order to better understand the chemical interactions in the oxide-supported Pt-Re system.

Furthermore, there have been no detailed studies of Re growth and interaction on an oxide support surface like TiO_2. The Re on TiO_2 catalyst itself has attracted attention for selective oxidation of methanol to methylal [48, 49] and selective hydrogenation of steric acid to octadecanol [31]. In both cases, it is believed that rhenium oxide is responsible for the active sites. Thus, it is valuable to investigate the nature of Re

interaction with the TiO_2 support and understand how interactions with the TiO_2 support could affect oxidation states.

In the work reported here, we have deposited Pt, Re and Pt-Re clusters on rutile TiO_2(110) and studied these surfaces by scanning tunneling microscopy (STM) in order to understand the nucleation, growth and formation of bimetallic clusters, as well as the effect of annealing on cluster size. Furthermore, Re oxidation states were investigated by X-ray photoelectron spectroscopy (XPS), and the atomic composition of the cluster surfaces were examined by low energy ion scattering (LEIS) and temperature programmed desorption (TPD) using CO as a probe molecule. We find that Pt-Re bimetallic clusters can be grown via sequential deposition of Pt on Re or Re on Pt, the cluster surfaces are Pt-rich, and there is a strong interaction between Re and the TiO_2 support.

5.2 EXPERIMENTAL

Experiments were carried out in two ultrahigh vacuum chambers ($P<1\times10^{-10}$ Torr), which have been described in detail elsewhere [50-57]. The first chamber is equipped with a variable-temperature scanning tunneling microscope (Omicron VT-25), a hemispherical anayzer (Omicron EA125) for X-ray photoelectron and low energy ion scattering spectroscopies, optics for low energy electron diffraction and Auger electron spectroscopy (Omicron Spec 3) and a quadrupole mass spectrometer (Leybold-Inficon, Transpector 2)[51, 53-57]. The second chamber is equipped with a quadrupole mass spectrometer for temperature programmed desorption studies (Hiden HAL 301/3F), a cylindrical mirror analyzer for Auger electron spectroscopy (Omicron CMA 150), and low energy electron diffraction optics (Omicron SPECTALEED) [50, 52, 55-57].

Rutile TiO_2(110) crystals (Princeton Scientific Corporation, 1cm x 1cm x 0.1 cm) were used as the support surfaces for the growth of the metal clusters. The crystals were mounted on Ta back plates using Ta foil straps; the samples were radiatively heated from a tungsten filament positioned behind the back plate and heated via electron bombardment of the back plate when a positive bias was applied to the sample. The sample temperature was monitored with a type K or type C thermocouple that was spotwelded to the edge of the back plate and independently calibrated using an infrared pyrometer (Heitronics) [53]. The crystals were cleaned by cycles of Ar^+ sputtering at 1 kV for 20 min followed by annealing at 950 K-1000 K for 3 min. This treatment preferentially removes lattice oxygen and results in a n-type semiconductor that is sufficiently conductive for STM, XPS and LEIS experiments. The cleanliness and crystallinity of the TiO_2(110)-(1x1) surface were confirmed by a combination of STM, XPS, low energy electron diffraction and Auger electron spectroscopy studies.

In the first chamber, Re and Pt were deposited from Re (ESPI, 2 mm diameter, 99.99%) and Pt rods (ESPI, 2 mm diameter, 99.95%) using an Oxford electron beam evaporator (EGC04). Metal flux was measured by a quartz crystal microbalance (QCM, Inficon XTM-2), which was independently calibrated by depositing a submonolayer coverage of Au onto a Ru(0001) single crystal[58]. In the second chamber, Re was deposited from a Re rod (ESPI, 1.6 mm diameter, 99.99%) with an Omicron electron beam evaporator (EFM3), while Pt was deposited from a homemade source consisting of Pt wire (ESPI, 0.25 mm diameter, 99.999%) wrapped around a tungsten wire (0.50 mm) through which current was passed. The Pt flux was calibrated with a QCM before each deposition; for Re deposition, the internal flux monitor of the evaporator was used to

control Re flux, and the flux monitor readings were initially calibrated with a QCM. Metal coverages are given in monolayer (ML) equivalents that correspond to packing density of the corresponding metals (Re(0001):1.52×10^{15} atoms/cm^2, Pt(111): 1.50×10^{15} atoms/cm^2). Metal deposition rates were approximately 0.02-0.1 ML/min.

STM experiments were carried out with the sample biased at +2.3 V with respect to the tip, and images were collected at a constant tunneling current of 0.05 nA–0.1 nA. STM tips consisted of 0.38 mm-diameter tungsten wire that was electrochemically etched in NaOH and subjected to Ar^+ sputtering at 3 kV[54]. For the low coverage surfaces (0.11-0.43 ML), cluster heights were determined using an in-house program [56, 59] that measured all clusters in a 500 Åx500 Å region. For the high coverage surfaces (>1.7 ML), average heights were determined from the manual measurement of 30 clusters. Clusters heights are used as a measure of cluster size since the diameters are known to be overestimated due to tip convolution effects, particularly for the smaller clusters [54, 58, 60, 61]. Cluster densities were measured by counting all of the clusters in a 1000 Å×1000 Å image. Numerical integration of the STM images to determine surface area were carried out with a Matlab program[51], and the surface area of uncovered TiO_2 was subtracted to obtain the cluster surface area only.

XPS data were collected with an Al Kα source using a 0.2 s dwell time and 0.02 eV step size. LEIS experiments were conducted with a 600 eV He^+ beam using a 0.2 eV step size and 0.2 s dwell time. The relative sensitivities to Pt and Re were established by LEIS experiments on pure Pt and Re foils (ESPI 99.95% and 99.99% purity, respectively) with identical exposed surface areas. The foils were cleaned by multiple cycles of Ar^+ sputtering at 1 kV for 15 min and annealing at 900 K for 6 min. Curve fitting for the

Ti($2p_{3/2}$) region was carried out with the shareware program XPSPEAK 4.1 using a Shirley background, FWHM of 1.8-2.0 eV and Gaussian-Lorenztian lineshapes. For the deconvoluted LEIS spectra, the data fit using the peak shapes from the spectra of the pure metals at a coverage of ~0.2 ML for the low coverage surfaces and ~2 ML for the high coverage surfaces. The pure Re spectrum was shifted by 0.7-1.0 eV in order to be able to fit the bimetallic spectra. Fitting with Re spectra for different coverages of 0.22-0.43 ML for the low coverage data and 2-10 ML for the high coverage data did not change the calculated compositions by more than 1%; the pure Pt spectra had the same peak shape for all coverages studied.

The surfaces were exposed to CO (National Welders, 99.99%) via a stainless steel directed dosing tube[62]. The sample temperature was held at 300 K during CO dosing, and a saturation exposure of CO was achieved by leaking in CO at a pressure rise of 3.0×10^{-10} Torr for 3 min. After cooling to 100 K, the crystal was heated at a constant rate of 2 K/s in front of the mass spectrometer during TPD experiments. The crystal was positioned ~2 mm in front of a 4 mm diameter hole cut in the shroud of the mass spectrometer in order to minimize sampling of products desorbing from the sample holder. Furthermore, the crystal was biased at −100 V during TPD experiments to avoid damage from the electrons emitted by the mass spectrometer filament. For titania pre-oxidation with ^{18}O2, the crystal was exposed to 1×10^{-7} Torr of $^{18}O_2$ at 800 K for 5 min via directed dosing.

5.3 Result and Discussion

Growth of Pure Re on TiO_2(110)

Submonolayer Re coverages on TiO_2(110) result in the growth of a high density of small clusters that cover most of the surface and have an average height of one to two monolayers. STM images for Re clusters corresponding to different coverages are shown in Figure 5.1a-c. For 0.11 ML of Re, clusters with an average height of 2.9±1.1 Å and cluster density of $31.4\times10^{12}/cm^2$ are observed. Based on the 2.23 Å step height for Re(0001)[63], the majority of the Re clusters are a single layer high. Therefore, nearly the entire surface appears to be covered by a discontinuous two-dimensional layer of Re. For all surfaces, average height and cluster densities are reported in Table 5.1, while histograms of cluster heights are presented in Figure 5.10 for the low coverage clusters. When the Re coverage is doubled (0.22 ML), there is an increase in the average cluster height (3.2±1.1 Å), but the cluster density decreases by ~10% due to cluster coalescence. At 0.43 ML of Re, the average cluster height continues to increase to 4.0±1.3 Å, and the cluster density is reduced by ~20% compared to the value at 0.11 ML. Thus, the density of Re clusters is saturated even at the lowest coverage of 0.11 ML, given that no additional islands are nucleated at the higher coverages. Instead, additional Re deposition causes the clusters to grow in a more three-dimensional manner. This growth behavior is characteristic of metals that interact strongly with the support such that adatom mobility on the surface is low, and therefore relatively small clusters with high cluster densities are formed. Previous studies have shown that the strength of the admetal-titania interaction increases with admetal-oxygen bond strength [64, 65]; given that Re is an oxophilic group 7 element, strong Re-titania interactions are expected and are consistent

with the nearly two-dimensional cluster growth observed here for Re on TiO_2(110). Moreover, our group's previous investigations of different metals on TiO_2 (Au, Ni, Pt, Co) by STM and density function theory calculations reported that the cluster sizes decrease with increasing admetal-TiO_2 and admetal-oxygen bond strengths[64]. Since Re is more oxophilic than later transitions metals like Ni, Cu, Rh, Pt and Au, lower diffusion rates for Re and smaller cluster sizes are observed, as predicted[54, 55, 60, 64, 66, 67].

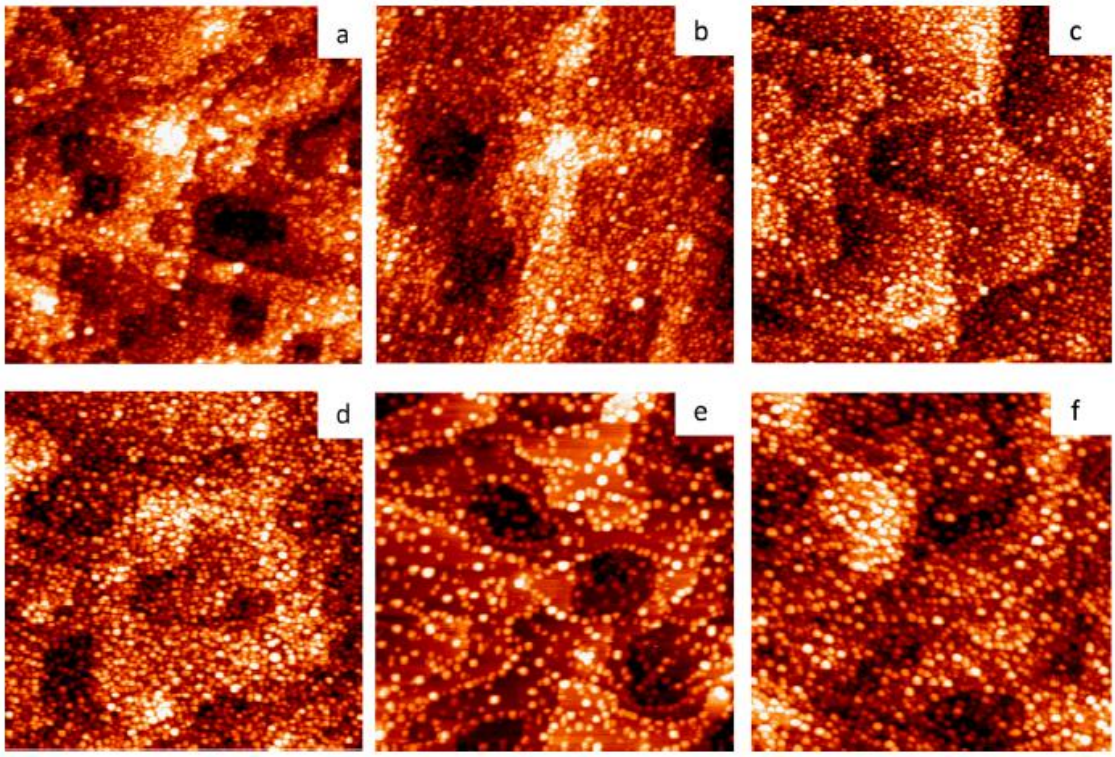

Figure 5.1: Scanning tunneling microscopy images for the following metals deposited at room temperature on TiO_2(110): a) 0.11 ML Re; b) 0.22 ML Re; c) 0.43 ML Re; d) 0.11 ML Re + 0.13 ML Pt; e) 0.13 ML Pt; and f) 0.13 ML Pt + 0.11 ML Re. All images are 1000 Å x1000 Å.

Table 5.1: Average cluster heights and densities for various metals on TiO_2(110)

Surface	Av. cluster height (Å)	Cluster density ($x10^{12}/cm^2$)
0.11 ML Re	2.9±1.1	31.44
0.22 ML Re	3.2±1.1	28.16
0.43 ML Re	4.0±1.3	25.76
0.11 ML Re + 0.13 ML Pt	4.5±1.3	25.58
0.13 ML Pt	4.7±1.7	9.34
0.13 ML Pt + 0.11 ML Re	5.0±1.8	18.60
1.7 ML Re	4.7±1.0	15.49
1.7 ML Re + 2.0 ML Pt	6.3±1.1	10.77
2.0 ML Pt	13.2±2.3	5.66
2.0 ML Pt+1.7 ML Re	17.2±3.1	5.41
0.22 ML Re, annealed at 800 K	4.6±1.4	17.51
0.11 ML Re + 0.13 ML Pt, annealed at 800 K	5.5±2.3	14.61
0.25 ML Pt	6.2±2.1	11.24
0.25 ML Pt, annealed at 800 K	9.1±2.9	5.71
0.13 ML Pt + 0.12 ML Re, annealed at 800 K	5.9±3.1	11.26

LEIS experiments for different coverages of Re deposited on TiO_2(110) demonstrate that titanium and oxygen are still detected in the top monolayer even for the highest Re coverage of 13 ML. The LEIS spectra (Figure 5.2a) indicate that the titanium and oxygen peaks are not completely attenuated at 13 ML, and the decrease in signal intensities for both these peaks is not substantial between 4.3 ML and 13 ML. This behavior suggests that the Re clusters are covered by titania even at room temperature.

Although some diffusion of Re into the titania crystal cannot be ruled out, STM images indicate that Re remains on the surface as clusters. The evolution of the Re LEIS peak is shown in Figure 5.2b as the Re coverage is increased from 0.11 to 8.7 ML, and the spectrum for a Re foil is also presented for comparison. At the submonolayer coverages, the Re peak is broad with significant intensity at a lower kinetic energy of ~505 eV. As more Re is deposited on the surface, the peak shape begins to resemble that of the Re foil with the main intensity at 515 eV, but the broad shoulder around 495 eV remains. The unusual peak shape for submonolayer Re coverages is consistent with TiO_x species partially covering the surface, as also observed in the XPS studies. The peak shape becomes more similar to the metallic Re foil with increasing Re coverage.

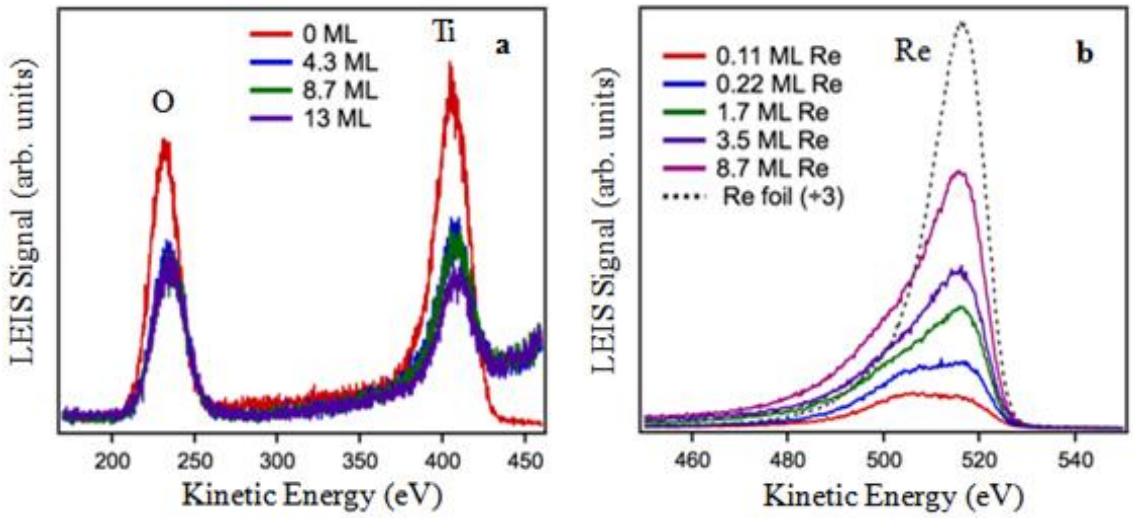

Figure 5.2: Low energy ion scattering spectra for various coverages of Re on TiO_2 (110) for the: a) oxygen and titanium regions; and b) rhenium region. The dotted trace in (b) is for a Re foil.

Growth of Bimetallic Pt-Re Clusters on TiO_2(110)

STM images for similar coverages (0.11-0.13 ML) of Re and Pt on TiO_2(110) are compared in Figures 5.1a and 5.1e. In contrast to Re, the 0.13 ML Pt clusters grow as three-dimensional islands with much larger average heights of 4.7 ±1.7 Å and a lower

cluster density of $9.34 \times 10^{12}/cm^2$. These results are consistent with a stronger Re-TiO_2 interaction compared to Pt-TiO_2, leading to lower diffusion rates for Re on TiO_2.

Bimetallic surfaces were prepared from the sequential deposition of Pt on Re (Re+Pt) or Re on Pt (Pt+Re) for coverages of ~0.1 ML for each metal (Figures 5.1d and 5.1f). For 0.11 ML Re+0.13 ML Pt, the total number of clusters decreases by 19% upon deposition of Pt, whereas the average cluster height increases to 4.5 ± 1.3 Å, indicating that Pt atoms are incorporated into existing Re clusters rather than nucleating new clusters; in this case, exclusively bimetallic clusters are formed. For 0.13 ML Pt+0.11 ML Re, the cluster density increases to 18.60×10^{12} clusters/cm^2, and the average cluster height also increases to 5.0 ± 1.8 Å. This increase in cluster density indicates that roughly 30-40% of the clusters are pure Re clusters while the remaining clusters have Re atoms incorporated into the existing Pt clusters. Thus, exclusively bimetallic Pt-Re clusters can be grown by sequential deposition of the metals when the initial cluster density of the first metal provides sufficient nucleation sites to accommodate the metal atoms from the second deposition. For 0.13 ML Pt+0.11 ML Re, the initial nucleation density of Pt does not provide enough nucleation sites for the less mobile Re atoms, and therefore clusters of pure Re coexist with bimetallic clusters on the surface. In the case of 0.11 ML Re+0.13 ML Pt, only bimetallic clusters are formed since the relatively high cluster density for Re provides sufficient nucleation sites for the more mobile Pt atoms. Similarly, previous studies of other metals grown on TiO_2(110) by sequential deposition, such as Pt-Au[54], Ni-Au[56],Co-Au[58], Co-Pt[67] and Rh-Pt[68], have demonstrated that exclusively bimetallic clusters are prepared from equal metal coverages when the less mobile metal is deposited first, serving as nucleation sites for the more mobile metal. The surface areas of

the various cluster compositions were calculated by a numerical integration of the STM images, followed by subtracting the area of the uncovered TiO_2[51]. These surface areas relative to the 0.25 ML Pt clusters were: 1.4 for Pt+Re, 1.4 for 0.22 ML Re and 1.9 for Re+Pt.

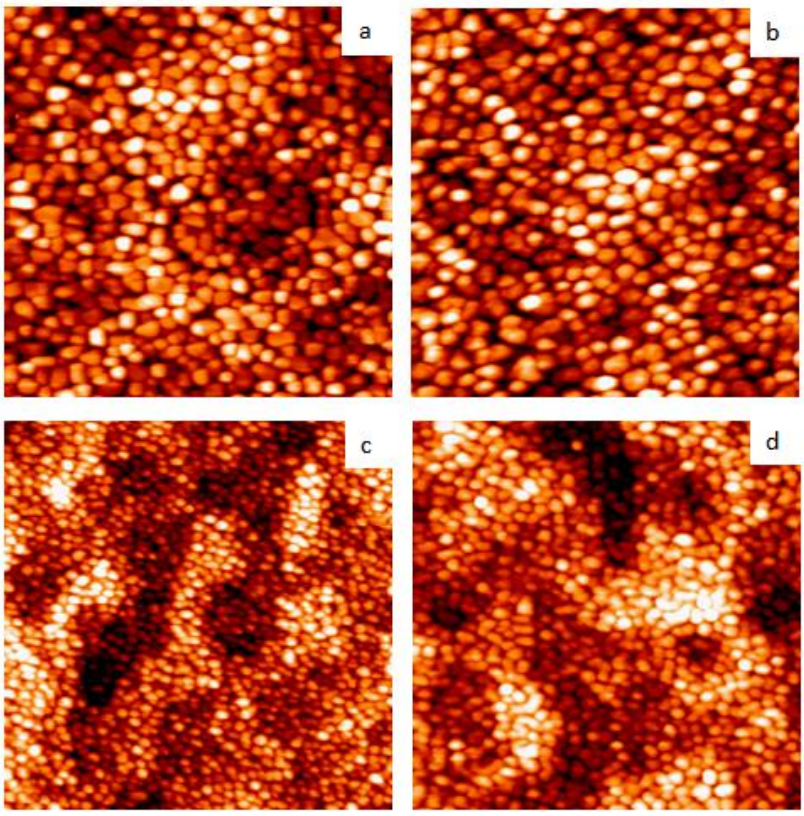

Figure 5.3: Scanning tunneling microscopy images for the following metals deposited at room temperature on TiO_2(110): a) 2.0 ML Pt; b) 2.0 ML Pt+1.7 ML Re; c) 1.7 ML Re; and d) 1.7 ML Re+2.0 ML Pt. All images are 1000 Å x 1000 Å.

It is possible to deposit only bimetallic Pt-Re clusters via either order of deposition at higher metal coverages, where the initial nucleation density is high. When 1.7 ML of Re is deposited on 2.0 ML of Pt (Pt+Re), the cluster density decreases from 5.66 to $5.41 \times 10^{12}/cm^2$ as clusters coalesce. There is no evidence of nucleation of new clusters because the initial cluster density of the Pt seed clusters is sufficient to support

the nucleation of all of the Re atoms (Figure 5.3a,b). The average cluster height increases from 13.2 ±2.3 Å to 17.2 ±3.1 Å, and bimetallic clusters are formed with significantly larger sizes than for the ~0.25 ML total coverage surface. When 2.0 ML Pt is deposited on 1.7 ML Re (Re+Pt), there is a substantial decrease in cluster density from 15.49 to $10.77 \times 10^{12}/cm^2$, and the average cluster height increases from 4.7 ±1.0 Å to 6.3 ±1.1 Å (Figure 5.3c,d). The surface morphologies are different for Pt+Re and Re+Pt surfaces with the lower initial nucleation density for Pt+Re resulting in substantially larger cluster sizes. Notably, the average heights for the 1.7 ML Re and 1.7 ML Re+2.0 ML Pt clusters in Table 5.1 are likely to be underestimated. For these high coverages, clusters appear to be growing on top of an underlying layer of clusters, based on the fraction of the surface covered and the high cluster densities observed at the much lower Re coverages of 0.22 and 0.43 ML. Numerical integration of the STM images yields the following surface areas relative to 2.0 ML Pt: 1.0 for Pt+Re, 0.88 for 1.7 ML Re and 0.88 for Re+Pt. Thus, all of the high coverage surfaces have similar surface areas despite the difference in cluster sizes and densities.

Pt-Re and Metal-TiO_2 Interactions

XPS data for the Ti($2p_{3/2}$) region shows that 1.7 ML of Re induced slight reduction of the titania support upon deposition at room temperature. For comparison, the spectrum for clean TiO_2 is shown in Figure 5.4a, and the spectrum is fit with three peaks corresponding to Ti^{+4} at 459.1 eV, Ti^{+3} at 457.8 eV and Ti^{+2} at 456.2 eV; these assignments are based on binding energies of Ti^{+n} reported in the literature [52, 64, 69-71]. The contributions of the Ti^{+3} and Ti^{+2} species to the total intensities are 16% and 3% respectively. For 1.7 ML Re deposited on TiO_2(110), the contribution from the reduced

species increases to 21% for Ti^{+3} and 11% for Ti^{+2}(Figure 5.4b). However, deposition of 2.0 ML Pt on 1.7 ML Re does not induce further change in the peak shape, suggesting that Pt does not replace Re at the cluster-support interface. For 2.0 ML Pt deposition on TiO_2(110), the contributions of the reduced species are within 2% of those on clean TiO_2, and therefore Pt deposition does not cause significant reduction of TiO2 (Figure 5.4c). No change in the peak shape is observed after deposition of 1.7 ML on top of 2.0 ML Pt, indicating that Re does not substantially replace Pt at the cluster-support interface. The reduction of the TiO_2(110) is not detectable for the low coverage cluster surfaces due to the smaller cluster-support interface. In other oxide-supported Re catalysts, it has also been proposed that Re interacts strongly with an alumina support [3, 4, 72].

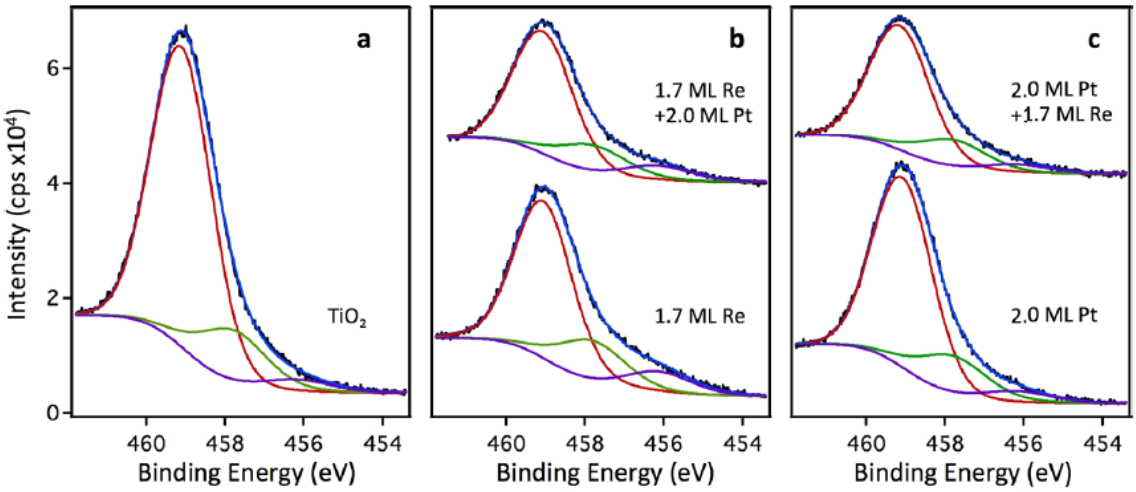

Figure 5.4: X-ray photoelectron spectroscopy data for the Ti($2p_{3/2}$) region for the following cluster surfaces after deposition on TiO_2(110) at room temperature: (a) TiO_2(110) before deposition of any metels; (b) 1.7 ML Re and 1.7 ML Re + 2.0 ML Pt; and (c) 2.0 ML Pt and 2.0 ML Pt + 1.7 ML Re. The vertical axis is the same for all three graphs.

Furthermore, XPS experiments suggest that Pt-Re electronic interactions occur in 1.7 ML Re deposited on 2.0 ML Pt but not for the reverse order of deposition. The Pt($4f_{7/2}$) peak for pure 2 ML Pt clusters appears at 71.1 eV and shifts to 71.5 eV for 1.7

ML Re deposited on 2.0 ML Pt (Figure 5.5a). On bulk Pt surfaces, the Pt($4f_{7/2}$) binding energy is reported to shift by approximately +0.5 eV when adsorbates are present, and this effect is known as a surface core level shift (SCLS)[73, 74]. Undercoordinated Pt atoms at the surface have a lower binding energy than fully coordinated Pt atoms in the bulk; therefore, the presence of surface species diminishes the contribution of the lower binding energy peak from undercoordinated Pt, resulting in an overall shift to higher binding energies. However, the shift in Pt($4f_{7/2}$) observed upon the addition of Re to the 2.0 ML Pt clusters cannot be attributed solely to a SCLS because LEIS data indicate that the majority of the deposited Re atoms have diffused into the bulk of the cluster rather than remaining at the surface. There is no shift in the Pt($4f_{7/2}$) binding energy for 2.0 ML Pt deposited on 1.7 ML Re. This lack of Pt-Re intermixing could be explained by the tendency for Pt atoms to remain at the surface due to the lower surface free energy of Pt compared to Re. In addition, the strong binding of Re to the titania support could inhibit intermixing of the Pt and Re atoms within the clusters. There is also no shift in the Re($4f_{7/2}$) binding energies for the 1.7 ML Re clusters compared to the Pt+Re and Re+Pt bimetallic clusters (Figure 5.5b) since the Re($4f_{7/2}$) peak appears at 40.6 eV for all surfaces. In the case of the lower coverage cluster surfaces, the Pt($4f_{7/2}$) binding energy appears at 71.7 eV for 0.13 ML Pt and is unshifted for the 0.13 ML Pt+0.11 ML Re and 0.11 ML Re+0.13 ML Pt clusters (Figure 5.11a). Likewise, the Re($4f_{7/2}$) binding energy, which is at 41.2 eV for the 0.11 ML Re clusters, is the same for the two bimetallic surfaces (Figure 5.11b). Given that the lower coverage bimetallic clusters are believed to be intermixed, a possible explanation is that strong interactions between Re and the titania support inhibit electronic interactions between Pt and Re. Alternatively, a larger

fraction of Re atoms are at the surface of the smaller clusters, and these Re atoms may be partially oxidized or covered with TiO_x, which would also inhibit Pt-Re interactions.

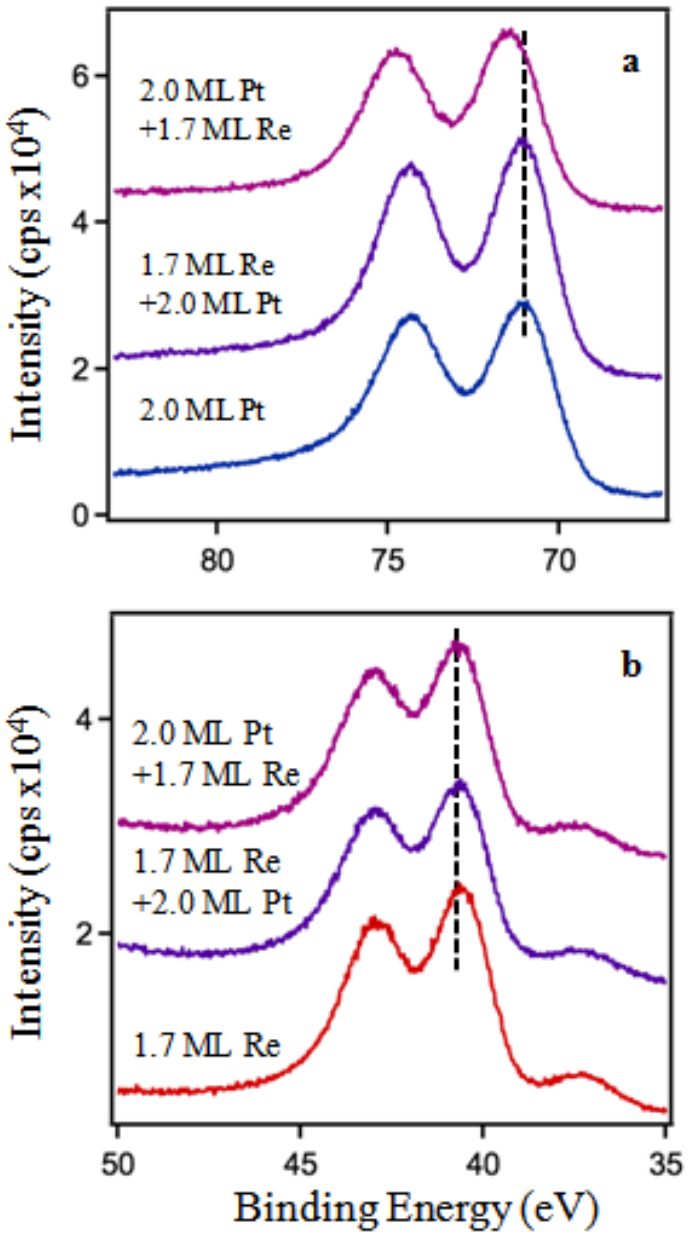

Figure 5.5: X-ray photoelectron spectroscopy data for pure and bimetallic clusters on TiO_2(110) for the: a) Pt(4f) region; and b) Re(4f) region. The peak at 37 eV is from Ti(3p).

For pure Re clusters, the Re($4f_{7/2}$) binding energy shifts from 41.3 eV to 40.6 eV as the Re coverage is increased from 0.11 to 1.7 ML. Cluster size effects can increase the binding energies of clusters to higher values than observed for the bulk metal. Specifically, atoms in small clusters have lower coordination numbers and experience decreased core-hole screening after photoemission; for more highly coordinated atoms, there is a greater number of conduction electrons from neighboring atoms that can shield the core hole, resulting in a lowered energy for the final state[75-80]. However, a comparison with similarly-sized (4-4.6 Å average height) Re clusters on highly oriented pyrolytic graphite suggests the binding energy shift observed for Re on TiO_2 is too large to be explained solely by a cluster size effect[81]. An alternative explanation for the shift in binding energies is that the small clusters are more oxidized or O-covered compared to the large clusters. The large clusters are more metallic, given that their binding energies are closer to that of Re single crystals and polycrystalline Re surfaces (~40.3 eV) [82-86]. On oxygen-covered surfaces, the Re($4f_{7/2}$) binding energy can increase by as much as 0.73 eV when Re is coordinated to three oxygen adatoms [85, 86]. Similar to the shift observed for the Re clusters, the Re($4f_{7/2}$) binding energy for ReO is increased by ~1 eV compared to the bulk value [85, 87, 88]. Re_2O_3 appears at a binding energy ~1.7 eV higher than the bulk value [83, 85], and this is a larger shift than what is observed for the smallest clusters.

The Pt($4f_{7/2}$) binding energy is also higher for the low coverage Pt clusters than for bulk Pt[89] and shifts to lower values with increasing Pt coverage, reaching 71.0 eV for the 2.0 ML Pt clusters. Since Pt is not oxidized on TiO_2, this binding energy shift is attributed to a cluster size effect.

Surface Composition Probed by LEIS

The compositions of the top monolayer of the bimetallic clusters were probed by LEIS experiments (Figure 5.6). Due to the similar masses of Pt and Re, it was not possible to resolve two distinct peaks, but qualitative information regarding the relative compositions of the different cluster surfaces can still be extracted. The spectrum of 0.13 ML Pt exhibits the normal metallic peak shape. In contrast, the 0.11 ML Re spectrum has an unusually broad peak shape with a shoulder extending to 500 eV, and the integrated intensity is less than 20% of that for 0.13 ML Pt despite greater surface area for the smaller Re clusters. This behavior is consistent with the surfaces of the Re clusters being partially covered by TiO_x or oxygen.

For the lower coverage clusters, both bimetallic surfaces have intensities and peak shapes that are similar to that of pure Pt, implying that the cluster surfaces are predominantly Pt (Figure 5.6a). However, both spectra also exhibit a low kinetic energy shoulder assigned to contribution from Re at the surface (Figure 5.11). Thus, when Pt is deposited second to make bimetallic clusters only (Re+Pt), mixing between Pt and Re occurs within the clusters despite the lower surface free energy of Pt (3.6 J/m^2 for Re vs. 2.5 J/m^2 for Pt)[90]. The slightly higher intensity (6%) at 520 eV for Re+Pt compared to pure Pt is attributed to increased dispersion of Pt when nucleated at the Re seed clusters. The Pt+Re spectrum has an intensity at 520 eV from Pt contribution that is 10% lower than the pure 0.13 ML Pt, and this suggests that some of the Re atoms must reside at the surface of the 0.13 ML Pt clusters. The Re LEIS contribution from the pure Re clusters that exist on the Pt+Re surface is relatively low, possibly because the small Re clusters are partially covered by oxygen or titania.

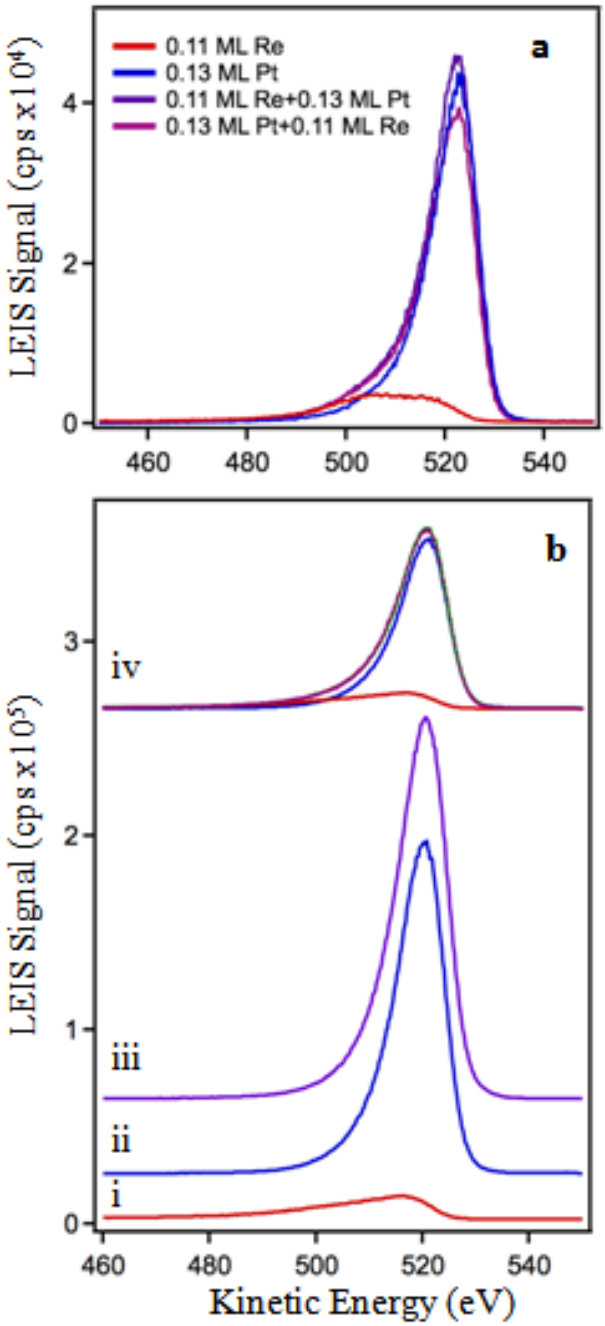

Figure 5.6: Low energy ion scattering spectra for the following metals on TiO_2(110): a) 0.11 ML Re, 0.13 ML Pt, 0.11 ML Re+0.13 ML Pt and 0.13 ML Pt+0.11 ML Re; and b, i) 1.7 ML Re; b ii) 1.7 ML Re+2.0 ML Pt; b, iii) 2.0 ML Pt; and b, iv) 2.0 ML Pt+1.7 ML Re. For the fit data in (b,iv), the blue trace is the Pt contribution, the red trace is the Re contribution, the green trace is the curve fit, and the pink markers represent the raw data.

The two high coverage bimetallic cluster surfaces (2.0 ML Pt, 1.7 ML Re) have different surface compositions based on the different LEIS peak shapes, indicating that there are kinetic limitations for diffusion of metal atoms within the clusters at room temperature (Figure 5.6b). The spectrum of the pure 2.0 ML Pt clusters has an identical peak shape to the 1.7 ML Re+2.0 ML Pt, whereas the 2.0 ML Pt+1.7 ML Re surface exhibits a low kinetic energy shoulder from Re contribution. The absolute intensity of 1.7 ML Re itself is small compared to 2 ML Pt and is again attributed to decoration of the Re clusters by titania. The 1.7 ML Re+2.0 ML Pt clusters have surfaces that are ~100% Pt; based on the lower surface free energy of Pt compared to Re[90], it is expected that Pt remains at the surface when deposited second. For the 2.0 ML Pt+1.7 ML Re clusters, Re deposited on Pt diffuses into the Pt clusters although some fraction of Re atoms remain at the surface. A rough estimate of surface composition was made from the attenuation of the Pt peak in the deconvoluted spectrum of the Pt+Re clusters (Figure 5.6b, top) compared to that of the pure Pt clusters. Since the Pt+Re and pure Pt surfaces have identical surface areas based on the STM images, the 50% attenuation of the Pt peak suggests that the Pt+Re cluster surface is ~50% Pt. Diffusion of metal atoms within the clusters appears to be limited at room temperature since both bimetallic surfaces are richer in the metal that was deposited second. Studies of Pt-Au and Ni-Au bimetallic clusters deposited at room temperature on TiO_2(110) from our group have also reported that the surface compositions are kinetically limited for larger clusters corresponding to ~4 ML total coverage[55, 56, 70].

In order to understand changes in the cluster surfaces upon annealing, the low coverage bimetallic clusters were annealed to 800 K for 1 min. STM images show that

there is some loss of surface area due to cluster sintering for all surfaces, but these changes are not extensive (Figure 5.12, Table 5.1). The decrease in density and increase in height after annealing range from 40-50% for the pure clusters, whereas the changes in cluster density and height range from 20-35% for the bimetallic clusters. If the rate limiting step in cluster sintering is the dissociation of metal-metal bonds, the observed behavior suggests that the reduced sintering for the bimetallic clusters could be attributed to stronger Pt-Re bonds compared to Pt-Pt and Re-Re.

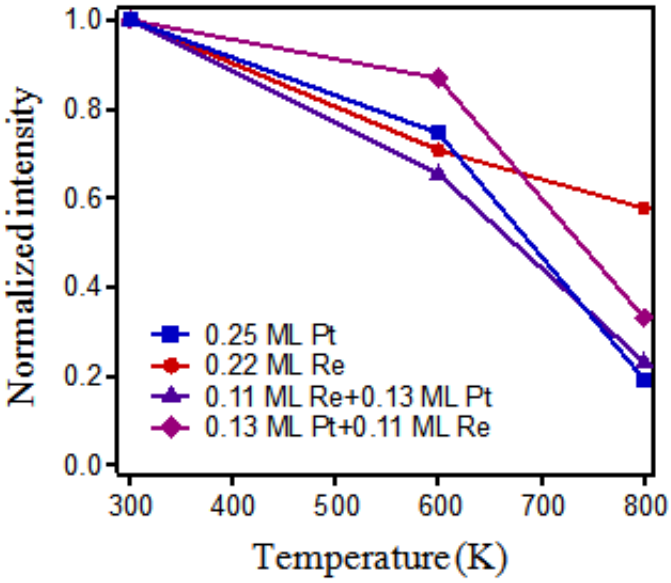

Figure 5.7: Integrated low energy ion scattering spectroscopy intensities for pure and bimetallic clusters as a function of annealing temperature. All of the signals are normalized to the value at room temperature.

Furthermore, the decrease in the integrated Pt-Re LEIS signals as a function of temperature indicates that in addition to sintering, the clusters become encapsulated by the titania support (Figure 5.7). This effect has been well studied in the literature for Pt clusters on TiO_2 heated in a reducing environment (H_2 or UHV) and is known as a strong metal support interaction [91-94]. The pure Pt clusters lose 80% of the integrated LEIS

intensity after heating to 800 K. For each surface, the intensities are normalized to the initial values at room temperature in order to view intensity changes on the same scale. For the 0.22 ML Re clusters, only ~40% of the LEIS signal is lost at 800 K, but the Re clusters are believed to be already covered by titania even at room temperature, thus accounting for the initially low Re contribution to the LEIS intensity. For the bimetallic clusters, the total Pt-Re signal decreases to 25-35% of the room temperature value, which is more comparable to the behavior of pure Pt. These results are consistent with the bimetallic cluster surfaces consisting mainly of Pt or with the surface Re atoms already being partially covered by titania at room temperature.

CO Adsorption

CO TPD experiments on the pure bimetallic clusters were carried out to provide further insight into the surface composition of the clusters (Figure 5.8). Notably, CO does not adsorb on the TiO_2 support at 300 K. On the pure 0.13 ML Pt clusters, the desorption profile is similar to what has been previously reported for Pt clusters on TiO_2 (Figure 5.8a)[55, 67]. The sharp peak at 500 K is attributed to CO adsorption at step sites [95, 96]. As expected, the relative intensity of this feature compared to the peak at 365 K from desorption at terrace sites diminishes with increasing Pt coverage since the larger clusters have a smaller fraction of step sites. For the 0.11 ML Re clusters, the onset of CO desorption is shifted to higher temperature compared to Pt, and the main feature appears at 460 K (Figure 5.8a). There is also a smaller peak at 865 K that is attributed to recombinant CO desorption from the dissociation of CO at lower temperatures; in contrast, there is no evidence for CO dissociation on the pure Pt clusters. CO dissociation on Re but not Pt is in agreement with CO adsorption and reaction in the literature on

single crystal Pt [97-99] and Re [87, 100, 101]surfaces. Given the higher dispersion of Re on the surface due to the smaller cluster size and higher cluster density, it is expected that the total CO desorption yield would be greater on the Re clusters. However, the observed 60% greater desorption yield on the Pt clusters is consistent with the Re clusters being covered by oxygen or TiO_x, which block sites for CO adsorption. In addition, the peak temperature for molecular CO desorption is 70 K greater than on higher coverage Re clusters and bulk Re surfaces [87, 100, 101]. This higher desorption temperature can be explained by the presence of oxygen on the Re clusters since the CO desorption temperature shifts to higher values of ~440 K on oxidized Re(0001) surfaces [100].

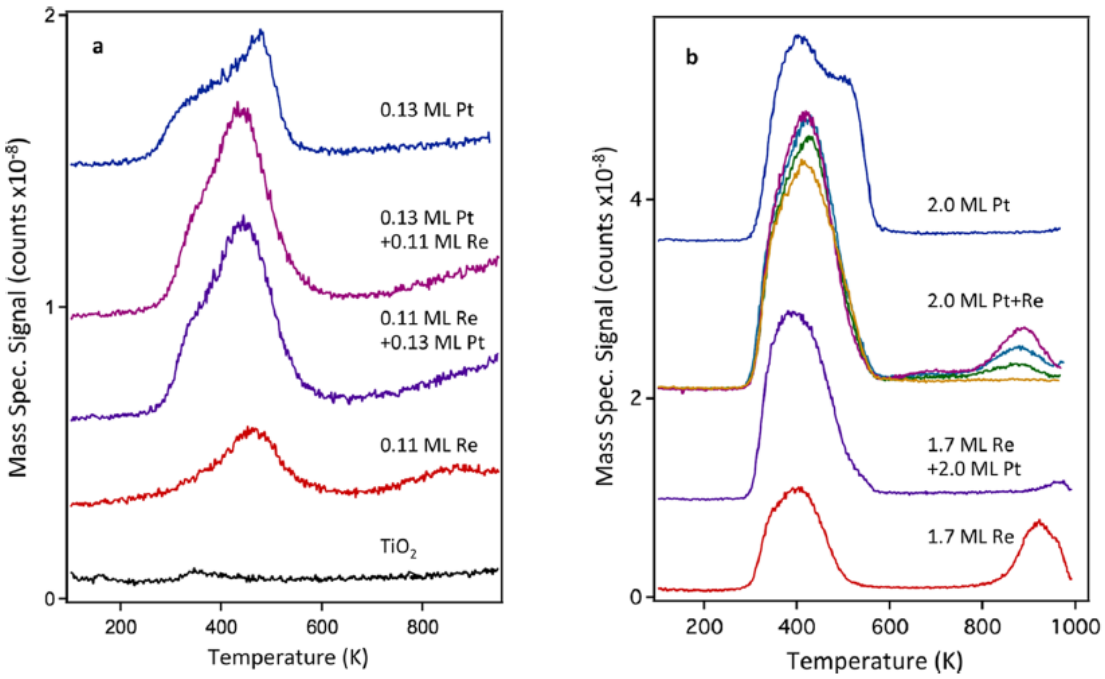

Figure 5.8: Temperature programmed desorption data (28 amu signal) for a saturation exposure of CO at room temperature on the following surfaces: a) low coverage Pt, Pt-Re and Re on TiO_2; and b) high coverage Pt, Pt-Re and Re on TiO_2. In (b), the pink, blue, green and brown traces are for 1.7, 1.3, 0.87, and 0.43 ML of Re, respectively, on 2.0 ML Pt.

CO desorption on the low coverage bimetallic surfaces is presented in Figure 5.8a. The bimetallic clusters formed by depositing 0.11 ML Re on 0.13 ML Pt have a CO desorption yield that is 50% higher than on the pure 0.13 ML Pt clusters, and this behavior is attributed to the greater dispersion of Pt when Pt is deposited on top of high density Re seed clusters. The 0.13 ML Pt+0.11 ML Re clusters have a similar desorption profile to the clusters with the reverse order of deposition even though the pure Re clusters should coexist with Pt-Re bimetallic clusters. This suggests that the small pure Re clusters on the Pt+Re surface do not contribute significantly to CO adsorption since they are likely to be covered by TiO_x or oxygen. Furthermore, the comparable CO desorption intensities for the two bimetallic surfaces implies that Pt dispersion for Pt+Re clusters is also increased compared to pure Pt due to incorporation of Re into the existing Pt clusters and subsequent diffusion of Pt to the surfaces of these higher surface area clusters. The high temperature CO desorption peak associated with pure Re activity is absent for both bimetallic surfaces. Furthermore, there is a shift in the peak maximum toward lower temperature for the Pt-Re bimetallic clusters compared to pure Pt. This ~65 K shift to lower temperature for CO desorption is also observed when Au is deposited on 0.25 ML Pt on $TiO_2(110)$[55], suggesting that the shift is due to blocking of the Pt step sites by the second metal and is not unique to Re on Pt. A similar 65 K shift to lower temperature is observed for CO desorption on 0.13 ML Co deposited on 0.13 ML Pt clusters on TiO_2 compared to desorption on the pure Pt clusters; on the Co-Pt clusters there is also another desorption peak from CO from Co sites below 400 K[67].

CO adsorption on the higher coverage surfaces was also studied by TPD. On the pure 1.7 ML Re clusters, a molecular desorption peak centered at 400 K is observed as

well as a high temperature feature at ~925 K from recombinant CO (Figure 5.8b). In general, the molecular desorption peak shifts to lower temperatures with increasing Re coverage. For CO desorption from the pure 2.0 ML Pt clusters, two distinct features are observed at 410 and 500 K, with the higher temperature peak again ascribed to desorption from step sites. No high temperature desorption peak is detected on the 2.0 ML Pt clusters, demonstrating the lack of CO dissociation on this surface. Unlike the behavior on the lower coverage clusters, the two bimetallic surfaces do not have the same activity for CO adsorption. The 1.7 ML Re+2.0 ML Pt surface, which consists of ~100% Pt at the surface, exhibits a main desorption peak at 500 K with only a very small feature at higher temperature. Furthermore, only a small recombinant CO peak is observed at temperatures significantly higher than that on pure Re (965 K vs. 920 K), and the recombinant CO production is <10% of that on the pure 1.7 ML Re clusters. The 2.0 ML Pt+1.7 ML Re surface exhibits a peak at 420 K that is 45% greater in intensity than for Re+Pt. There is also a high temperature desorption peak, which has a maximum at 890 K and is shifted to lower temperatures compared to the recombinant peak observed on pure Re. The Pt+Re surface shows a small desorption feature at 690 K that is not observed on the Re+Pt surface. This peak is believed to arise from recombinant desorption at step sites on Re since a similar desorption peak at 660 K appears on stepped single-crystal Re surfaces[101]. The 660 K feature is observed for various coverages of Re (>0.43 ML) deposited on 2.0 ML Pt but not for the pure Re clusters, implying that these step sites exist only on the bimetallic clusters. The CO adsorption capacities for both bimetallic cluster surfaces are comparable to that of the 2.0 ML Pt clusters; 2.0 ML Pt + 1.7 ML Re adsorbs 20% more CO than 2.0 ML Pt whereas 1.7 ML Re+2.0 ML Pt adsorbs 18% less. Consequently,

decoration of the bimetallic surfaces by TiO_x does not substantially decrease the number of active metal sites for CO adsorption.

Experiments in which the titania surface is pre-oxidized with $^{18}O_2$ show that the high temperature CO desorption from Re involves oxygen from the TiO_2 lattice. The TiO_2(110) surface was exposed to 1×10^{-7} Torr $^{18}O_2$ at 800 K for 5 min to incorporate ^{18}O into the titania lattice before deposition of 1.7 ML of Re. Results from this experiment indicate that only $C^{18}O$ at 30 amu is observed for the high temperature desorption peak, and only $C^{16}O$ (28 amu) is observed at 400 K. The fact that recombinant $C^{16}O$ is not detected when the titania support is pre-oxidized with $^{18}O_2$ indicates that the ^{16}O from CO decomposition is not available for recombination at elevated temperatures, perhaps due to diffusion of ^{16}O into the titania surface. The 920 K peak temperature for recombinant CO evolution on 1.7 ML Re clusters is significantly higher than the 800-820 K desorption temperature observed on Re(0001) surfaces [87, 100, 101] or Re films on Pt(111)[33, 35, 82]. The rate-limiting step in CO evolution on the titania-supported Re clusters appears to be diffusion of lattice oxygen from the support to the clusters. Consequently CO is evolved at higher temperatures than on pure Re surfaces, where oxygen from CO dissociation is available for recombination with surface carbon at lower temperatures. Moreover, the temperature of the recombinant peak increases with increasing Re coverage, and this behavior is attributed to more facile migration of lattice oxygen to the surfaces of the smaller Re clusters. On the bimetallic 2.0 ML Pt+1.7 ML Re clusters deposited on ^{18}O-labelled TiO_2, only $C^{18}O$ (30 amu) desorbs at 675 and 806 K (Figure 5.14). Thus, lattice oxygen is incorporated into CO for both of these desorption processes.

Since the primary CO desorption peaks for pure Pt and pure Re are both observed at the same temperature of 400 K, it is therefore not possible to distinguish molecular adsorption on Pt vs. Re. This desorption behavior is expected, given that CO on both Re(0001) [87, 100, 101] and Pt(111) [33] exhibit molecular desorption peaks at ~400 K; similar desorption temperatures are also observed for Re films grown on Pt(111)[35, 82]. The main difference in peak shape between desorption on pure Pt and on the Pt-Re clusters is that the pure Pt clusters exhibit a shoulder at 500 K assigned to desorption from Pt step sites, whereas the step sites are blocked by Re in the bimetallic clusters. Furthermore, the 2.0 ML Pt+1.7 ML Re clusters have a slightly higher desorption temperature of 420 K for molecular desorption. This small shift to higher desorption temperatures and appearance of the high temperature recombinant peaks follow the trends observed for Re islands on Pt(111) [33]. On Pt(111), the CO desorption peak is found at 400 K, and the desorption temperature shifts to higher values upon Re deposition, reaching ~420 K at 0.5-1.0 ML. For CO on the Pt-Re alloy surfaces prepared by depositing Re on Pt(111) and annealing at 1100 K[33], the peak temperature shifts to lower values with increasing Re coverage from ~380 K for 0.10 ML Re to ~325 K for 1.10 ML Re [33]. In contrast to these studies on single-crystal alloy surfaces, the gradual shift to lower temperature with increasing Re coverage is not observed for the 2 ML Pt+Re clusters; the loss of the high temperature shoulder peak observed on pure Pt clusters also results in an apparent shift to lower temperature, but this is not the same effect as observed for the Pt-Re alloy surface.

In agreement with LEIS data, the appearance of the high temperature desorption peak in the CO TPD experiments on the 2.0 ML Pt+1.7 ML Re bimetallic clusters indicates the presence of Re at the cluster surface, given that Re dissociates CO while Pt

does not. These results are therefore consistent with the shift in the Pt($4f_{7/2}$) peak for the 2.0 ML Pt+1.7 ML Re cluster attributed to Pt-Re intermixing. Furthermore, the intensity of the high temperature CO desorption peak reflects the concentration of Re at the cluster surface after Re deposition onto pure Pt clusters and subsequent diffusion into the bulk. When different coverages of Re are deposited on 2.0 ML Pt in separate CO TPD experiments, the TPD data show that the concentration of Re atoms that remain at the surface gradually diminishes with decreasing Re coverage from 1.7 ML to 0.43 ML (Figure 8b). For the lower coverages, a greater fraction of Re diffuses into the clusters. At Re coverages < 0.43 ML, the concentration of Re atoms at the surface is not sufficient for CO dissociation to occur, and consequently no high temperature recombinant peak is observed. The 0.43 ML Re on 2.0 ML Pt clusters should have a Re concentration of less than 10%, given that for CO on Re films deposited on Pt(111), the recombinant peak barely detectable at a Re coverage of 0.1 ML[33]. The 500 K observed from desorption from Pt step sites is still apparent at Re coverage of 0.22 ML, demonstrating that the deposited Re diffuses into the cluster rather than remaining at the Pt surface to block step sites. Although the cluster surfaces change during TPD due to the encapsulation effects described in the previous section, information about the surface composition of the bimetallic clusters at room temperature can still be obtained. The total CO adsorption capacity at room temperature still reflects the number of active adsorption sites on the metal surfaces at room temperature regardless of how the surfaces change at elevated temperatures. Also, the CO dissociation on Re occurs below the temperatures at which the clusters encapsulate (400-450 K) [33, 101, 102].

CO_2 production

CO TPD experiments also show significant CO_2 (44 amu) production from CO adsorption on the 1.7 ML Re+2.0 ML Pt clusters (Figure 5.9a) due to oxidation of adsorbed CO by oxygen from the titania support. A smaller amount of CO_2 (40%) is evolved from CO on pure 2 ML Pt clusters on TiO_2 (Figure 5.9b) whereas no CO_2 is observed on the pure 1.7 ML Re clusters (Figure 5.9c). Moreover, no CO_2 is produced on the bimetallic clusters formed from the reverse order of deposition of 2.0 ML Pt+1.7 ML Re (Figure 5.9d). Other Re on Pt bimetallic clusters were prepared by decreasing the Pt coverage (1.7 ML Re+1.0 ML Pt, Figure 5.9e) or decreasing the Re coverage (0.88 ML Re +2.0 ML Pt, Figure 5.9f), but both of these surfaces produced only ~60-70% of the CO_2 formed from 1.7 ML Re + 2.0 ML Pt. When the Pt coverage was increased by 0.5 ML for 1.7 ML Re+2.5 ML Pt (Figure 5.9g), there was no change in CO_2 formation. In order to confirm that lattice oxygen is participating in CO oxidation on the 1.7 ML Re+2.0 ML Pt clusters, experiments were carried out on TiO_2 surfaces that were oxidized at 800 K with $^{18}O_2$ prior to metal deposition (Figure 5.14). Since the majority of carbon dioxide produced is $C^{16}O^{18}O$ (46 amu), lattice oxygen must be incorporated into the product. Unlabeled $C^{16}O_2$ (44 amu) is also formed from ^{16}O oxygen from dissociated CO; ^{16}O cannot be from the titania support since no $C^{16}O$ is observed for recombinant CO desorption, and therefore titania is not a source of ^{16}O. We propose that when the Re clusters are initially deposited, oxygen from the support diffuses onto the Re surface. After deposition of Pt on Re and exposure to CO, the oxygen on the Re surface facilitates oxidation of CO on Pt. However, when Re is deposited on Pt, diffusion of lattice oxygen onto Re does not occur due to lack of direct contact between Re and titania, and

consequently CO_2 production is not observed. When a lower coverage of Pt is deposited on the 1.7 ML Re clusters, the CO_2 yield decreases; similarly, the CO_2 yield decreases when the Re coverage is decreased from 1.7 ML to 0.85 ML. It appears that Re at the cluster-support interface is needed to promote oxygen diffusion from titania, and surface Pt is needed for CO adsorption and reaction. Therefore, decreasing either the Re or Pt concentrations will diminish CO_2 production. When a greater coverage of Pt (2.5 ML) is deposited onto 1.7 ML of Re, the CO_2 production remains the same because sufficient Pt sites are already available at the 2.0 ML Pt coverage.

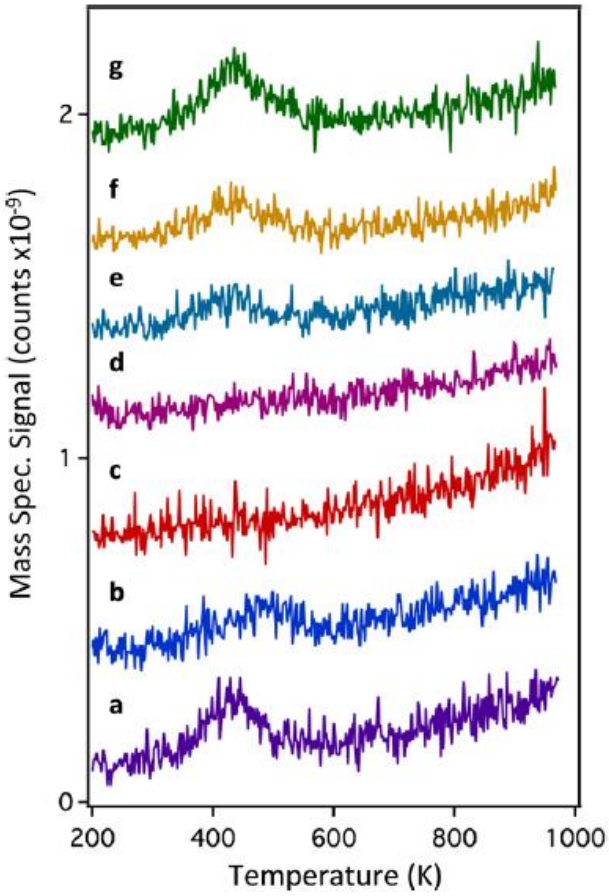

Figure 5.9: Temperature programmed desorption data (44 amu signal) for a saturation exposure of CO at room temperature on the following surfaces: a) 1.7 ML Re+2.0 ML Pt; b) 2.0 ML Pt; c) 1.7 ML Re; d) 2.0 ML Pt+1.7 ML Re; e) 1.7 ML Re+1.0 ML Pt; f) 0.88 ML Re+2.0 ML Pt; and g) 1.7 ML Re+2.5 ML Pt.

5.4 CONCLUSIONS

Bimetallic Pt-Re clusters are grown on a TiO_2 support via sequential deposition of Pt on Re at low coverages and through either order of deposition at high coverages. Only bimetallic clusters are formed when the diffusion lengths for the atoms of the second metal are shorter than the intercluster distance. Since Re atoms have lower mobilities and shorter diffusion lengths than Pt atoms on TiO_2, bimetallic clusters will always be formed when Pt is deposited on an equal coverage of Re clusters. CO TPD and LEIS experiments show that when Pt is deposited on Re for the higher coverage clusters (3.7 ML), the bimetallic surfaces are ~100% Pt, as expected based on the lower surface free energy of Pt compared to Re. However, the higher coverage bimetallic surfaces consist of both Pt and Re atoms when Re is deposited on Pt due to kinetic limitations for diffusion of atoms within the clusters. CO TPD experiments with different coverages of Re deposited on 2.0 ML Pt clusters demonstrate that Re completely diffuses subsurface for coverages <0.43 ML, and the fraction of deposited Re that diffuses into the clusters decreases with increasing Re coverage.

Re interacts strongly with the TiO_2 support upon deposition at room temperature. Specifically, the titania support is reduced, and the low coverage Re clusters appear to be partially oxidized. Furthermore, the Re clusters are covered by TiO_x even for high Re coverages (13 ML), and CO desorption studies show loss of Re activity due to site blocking by TiO_x or oxygen. Therefore, highly dispersed Re clusters are likely to be partially oxidized, and lattice oxygen is expected to play a role in reactions on these surfaces. For both Re and Pt-Re clusters, dissociation of CO and subsequent recombination of surface carbon and oxygen involves oxygen from the titania lattice. CO

is oxidized to CO2 by lattice oxygen on Pt-Re bimetallic clusters, which provide Pt sites for CO adsorption as well as Re sites that promote diffusion of oxygen from the titania lattice to the surface of the clusters. These studies demonstrate that Re and Re-containing catalysts should interact strongly with metal oxide supports such as titania. However, the high coverage Pt-Re bimetallic clusters have CO adsorption capacities that are similar to that of pure Pt clusters; this implies that although the bimetallic clusters may be decorated by lattice oxygen or TiO_x, the clusters are still have mainly metallic adsorption behavior.

5.5 Supporting Information

Histograms of cluster sizes, XPS data for low coverage clusters, LEIS peak fits for low coverage clusters, STM images of clusters heated to 800 K, and TPD data for CO on bimetallic clusters supported on ^{18}O-TiO_2.

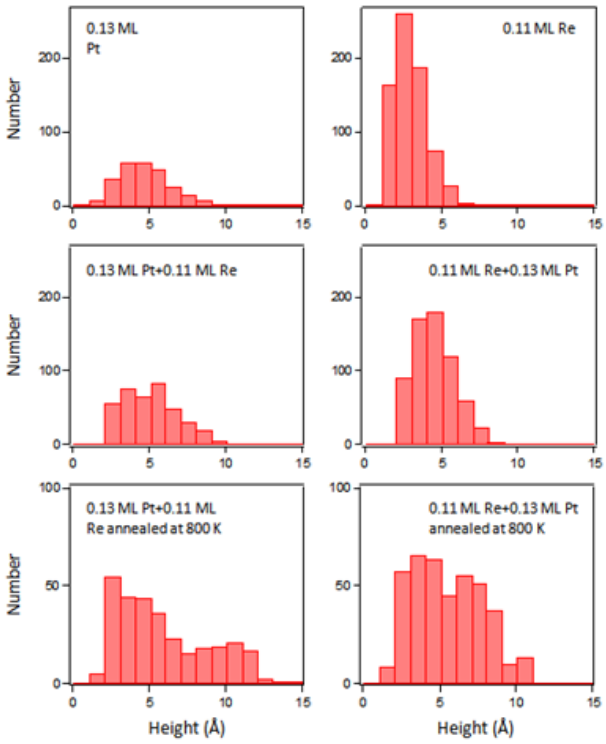

Figure 5.10: Histograms of cluster heights for surfaces with approximately 0.25 ML total metal coverage.

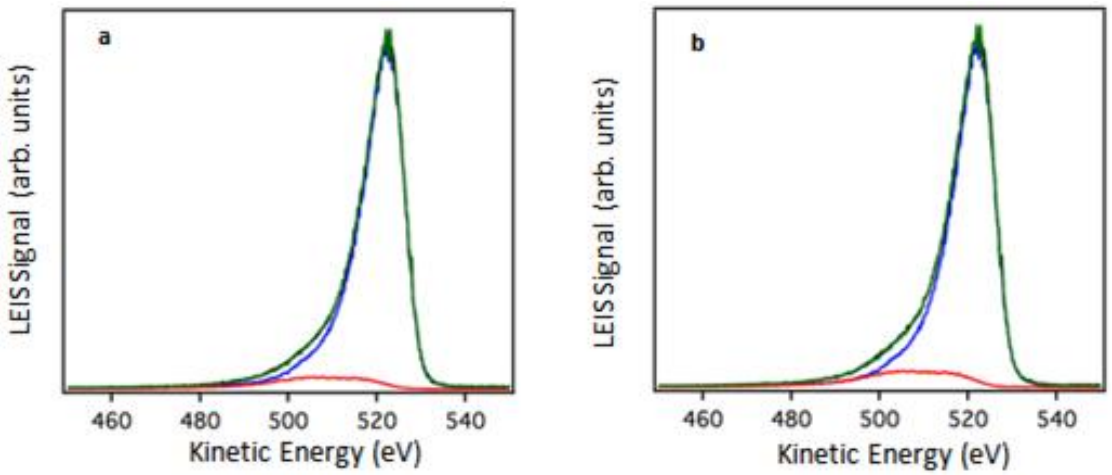

Figure 5.11: Peak fits for the low energy ion scattering spectra for a) 0.11 ML Re+0.13 ML Pt; and b) 0.13 ML Pt+0.11 ML Re on TiO_2(110). The red trace is the contribution from the pure Re spectrum, the blue trace is the contribution from the pure Pt spectrum, the raw data is shown in black and the fit spectrum is shown in green.

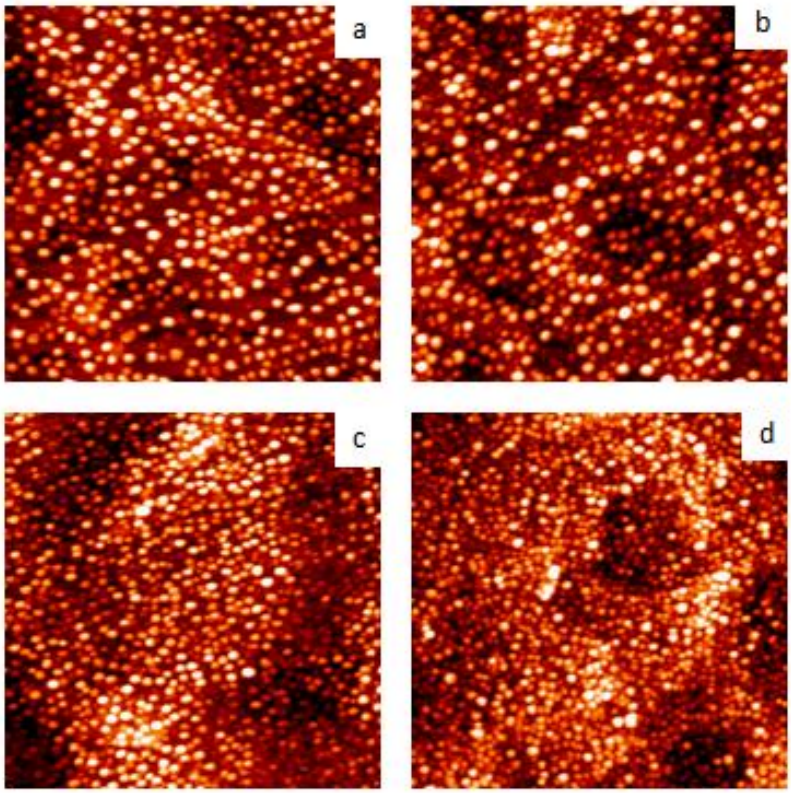

Figure 5.12: Scanning tunneling microscopy images for the following metals on TiO_2(110) after annealing to 800 K for 1 min: a) 0.25 ML Pt; b) 0.13 ML Pt+0.11 ML Re; c) 0.11 ML Re+0.13 ML Pt; and d) 0.22 ML Re. All images are 1000 Å x 1000 Å

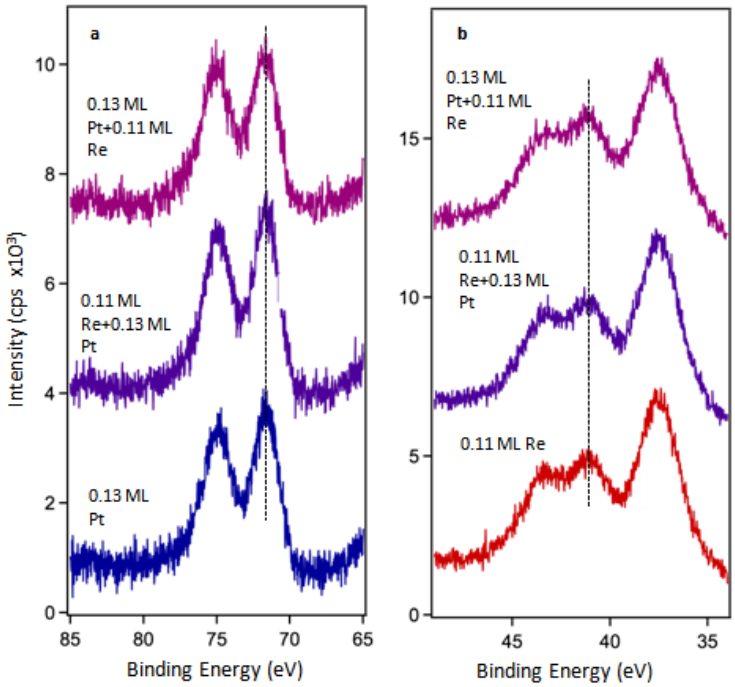

Figure 5.13: X-ray photoelectron spectroscopy data for the low coverage clusters on TiO_2(110): a) Pt(4f) and b) Re(4f) regions. The peak at 37 eV in the Re(4f) region is from Ti(3p).

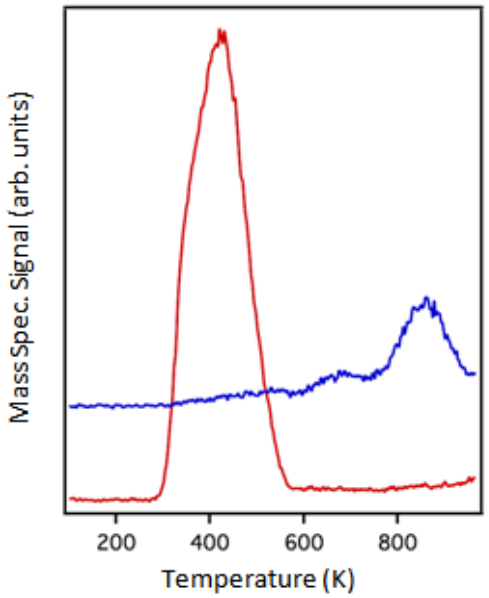

Figure 5.14: Temperature programmed desorption data for CO on 2.0 ML Pt+1.7 ML Re deposited on a TiO_2 surface that was preoxidized with $^{18}O_2$ for $C^{16}O$ (28 amu, red) and $C^{18}O$ (30 amu, blue).

ACKNOWLEDGEMENTS

Thanks very much to Dr. Randima Galhenage and Grant Seuser for the STM, LEIS and XPS characterizations of Pt, Re and Pt-Re bimetallic clusters supported on TiO_2.

Thanks a lot to Dr. Hui Yan for the TPD study of Pt-Re system (lower coverage)

5.6 REFERENCES

(1) Kluksdahl, H. E. Reforming a sulfur-free naphtha with a platinum-rhenium catalyst. US Patent 3415737, 1968.

(2) Sinfelt, J. H., *Bimetallic Catalysts. Discoveries, Concepts, and Applications*. John Wiley and Sons: New York, **1983**.

(3) Huang, Z.; Fryer, J. R.; Park, C.; Stirling, D.; Webb, G., Transmission Electron Microscopy and Energy Dispersive X-Ray Spectroscopy Studies of Pt-Re/γ-Al_2O_3 Catalysts. *Journal of Catalysis* **1994,** 148 (2), 478-492.

(4) Fung, A. S.; Kelley, M. J.; Koningsberger, D. C.; Gates, B. C., γ-Al_2O_3-Supported Re−Pt Cluster Catalyst Prepared from $[Re_2Pt(CO)_{12}]$: Characterization by Extended X-ray Absorption Fine Structure Spectroscopy and Catalysis of Methylcyclohexane Dehydrogenation. *Journal of the American Chemical Society* **1997,** 119 (25), 5877-5887.

(5) Macleod, N.; Fryer, J. R.; Stirling, D.; Webb, G., Deactivation of bi- and multimetallic reforming catalysts: influence of alloy formation on catalyst activity. *Catalysis Today* **1998,** 46 (1), 37-54.

(6) Johnson, M. F. L.; LeRoy, V. M., The state of rhenium in Pt/Re/alumina catalysts. *Journal of Catalysis* **1974,** 35 (3), 434-440.

(7) Carter, J. L.; McVinker, G. B.; Weissman, W.; Kmak, M. S.; Sinfelt, J. H., Bimetallic catalysts; application in catalytic reforming. *Applied Catalysis* **1982,** 3 (4), 327-346.

(8) Barbier, J., Deactivation of reforming catalysts by coking - a review. *Applied Catalysis* **1986,** 23 (2), 225-243.

(9) Parera, J. M.; Beltramini, J. N., Stability of bimetallic reforming catalysts. *Journal of Catalysis* **1988,** 112 (2), 357-365.

(10) Godbey, D. J.; Garin, F.; Somorjai, G. A., The hydrogenolysis of ethane over Re-Pt(111) and Pt-Re(0001) bimetallic crystal surfaces. *Journal of Catalysis* **1989,** 117 (1), 144-154.

(11) Querini, C. A.; Fung, S. C., Coke and Product Profiles Formed Along the Catalyst Bed During n-Heptane Reforming. *Journal of Catalysis* **1993,** 141 (2), 389-406.

(12) Sato, Y.; Terada, K.; Hasegawa, S.; Miyao, T.; Naito, S., Mechanistic study of water–gas-shift reaction over TiO_2 supported Pt–Re and Pd–Re catalysts. *Applied Catalysis A: General* **2005,** 296 (1), 80-89.

(13) Iida, H.; Igarashi, A., Structure characterization of Pt-Re/TiO_2 (rutile) and Pt-Re/ZrO_2 catalysts for water gas shift reaction at low-temperature. *Applied Catalysis A: General* **2006,** 303 (2), 192-198.

(14) Iida, H.; Igarashi, A., Difference in the reaction behavior between Pt–Re/TiO_2 (Rutile) and Pt–Re/ZrO_2 catalysts for low-temperature water gas shift reactions. *Applied Catalysis A: General* **2006,** 303 (1), 48-55.

(15) Azzam, K. G.; Babich, I. V.; Seshan, K.; Lefferts, L., A bifunctional catalyst for the single-stage water–gas shift reaction in fuel cell applications. Part 2. Roles of the support and promoter on catalyst activity and stability. *Journal of Catalysis* **2007,** 251 (1), 163-171.

(16) Azzam, K. G.; Babich, I. V.; Seshan, K.; Lefferts, L., Role of Re in Pt–Re/TiO_2 catalyst for water gas shift reaction: A mechanistic and kinetic study. *Applied Catalysis B: Environmental* **2008,** 80 (1–2), 129-140.

(17) Iida, H.; Yonezawa, K.; Kosaka, M.; Igarashi, A., Low-temperature water gas shift reaction over Pt–Re/TiO_2 catalysts prepared by a sub-critical drying method. *Catalysis Communications* **2009,** 10 (5), 627-630.

(18) Azzam, K. G.; Babich, I. V.; Seshan, K.; Mojet, B. L.; Lefferts, L., Stable and Efficient Pt–Re/TiO_2 catalysts for Water-Gas-Shift: On the Effect of Rhenium. *ChemCatChem* **2013,** 5 (2), 557-564.

(19) Ciftci, A.; Eren, S.; Ligthart, D. A. J. M.; Hensen, E. J. M., Platinum–Rhenium Synergy on Reducible Oxide Supports in Aqueous-Phase Glycerol Reforming. *ChemCatChem* **2014,** 6 (5), 1260-1269.

(20) Ciftci, A.; Ligthart, D. A. J. M.; Sen, A. O.; van Hoof, A. J. F.; Friedrich, H.; Hensen, E. J. M., Pt-Re synergy in aqueous-phase reforming of glycerol and the water–gas shift reaction. *Journal of Catalysis* **2014,** 311, 88-101.

(21) Ciftci, A.; Ligthart, D. A. J. M.; Hensen, E. J. M., Influence of Pt particle size and Re addition by catalytic reduction on aqueous phase reforming of glycerol for carbon-supported Pt(Re) catalysts. *Applied Catalysis B: Environmental* **2015,** 174–175, 126-135.

(22) Wei, Z.; Karim, A. M.; Li, Y.; King, D. L.; Wang, Y., Elucidation of the roles of Re in steam reforming of glycerol over Pt–Re/C catalysts. *Journal of Catalysis* **2015,** 322, 49-59.

(23) Kunkes, E. L.; Simonetti, D. A.; Dumesic, J. A.; Pyrz, W. D.; Murillo, L. E.; Chen, J. G.; Buttrey, D. J., The role of rhenium in the conversion of glycerol to synthesis gas over carbon supported platinum–rhenium catalysts. *Journal of Catalysis* **2008,** 260 (1), 164-177.

(24) Daniel, O. M.; DeLaRiva, A.; Kunkes, E. L.; Datye, A. K.; Dumesic, J. A.; Davis, R. J., X-ray Absorption Spectroscopy of Bimetallic Pt–Re Catalysts for Hydrogenolysis of Glycerol to Propanediols. *ChemCatChem* **2010,** 2 (9), 1107-1114.

(25) Zhang, L.; Karim, A. M.; Engelhard, M. H.; Wei, Z.; King, D. L.; Wang, Y., Correlation of Pt–Re surface properties with reaction pathways for the aqueous-phase reforming of glycerol. *Journal of Catalysis* **2012,** 287, 37-43.

(26) Ciftci, A.; Ligthart, D. A. J. M.; Hensen, E. J. M., Aqueous phase reforming of glycerol over Re-promoted Pt and Rh catalysts. *Green Chemistry* **2014,** 16 (2), 853-863.

(27) Kirilin, A. V.; Tokarev, A. V.; Manyar, H.; Hardacre, C.; Salmi, T.; Mikkola, J. P.; Murzin, D. Y., Aqueous phase reforming of xylitol over Pt-Re bimetallic catalyst: Effect of the Re addition. *Catalysis Today* **2014,** 223, 97-107.

(28) Huber, G. W.; Chheda, J. N.; Barrett, C. J.; Dumesic, J. A., Production of Liquid Alkanes by Aqueous-Phase Processing of Biomass-Derived Carbohydrates. *Science* **2005,** 308 (5727), 1446-1450.

(29) Falcone, D. D.; Hack, J. H.; Klyushin, A. Y.; Knop-Gericke, A.; Schlögl, R.; Davis, R. J., Evidence for the Bifunctional Nature of Pt–Re Catalysts for Selective Glycerol Hydrogenolysis. *ACS Catalysis* **2015,** 5 (10), 5679-5695.

(30) Manyar, H. G.; Paun, C.; Pilus, R.; Rooney, D. W.; Thompson, J. M.; Hardacre, C., Highly selective and efficient hydrogenation of carboxylic acids to alcohols using titania supported Pt catalysts. *Chemical Communications* **2010,** 46 (34), 6279-6281.

(31) Rozmysłowicz, B.; Kirilin, A.; Aho, A.; Manyar, H.; Hardacre, C.; Wärnå, J.; Salmi, T.; Murzin, D. Y., Selective hydrogenation of fatty acids to alcohols over highly dispersed ReO_x/TiO_2 catalyst. *Journal of Catalysis* **2015,** 328, 197-207.

(32) Chen, B.; Li, F.; Huang, Z.; Yuan, G., Tuning catalytic selectivity of liquid-phase hydrogenation of furfural via synergistic effects of supported bimetallic catalysts. *Applied Catalysis A: General* **2015,** 500, 23-29.

(33) Ramstad, A.; Strisland, F.; Raaen, S.; Borg, A.; Berg, C., CO and O_2 adsorption on the Re/Pt(111) surface studied by photoemission and thermal desorption. *Surface Science* **1999,** 440 (1–2), 290-300.

(34) Detwiler, M. D.; Majumdar, P.; Gu, X.-K.; Delgass, W. N.; Ribeiro, F. H.; Greeley, J.; Zemlyanov, D. Y., Characterization and theory of Re films on Pt(111) grown by UHV-CVD. *Surface Science* **2015,** 640, 2-9.

(35) Godbey, D. J.; Somorjai, G. A., The adsorption and desorption of hydrogen and carbon monoxide on bimetallic Re-Pt(111) surfaces. *Surface Science* **1988,** 204 (3), 301-318.

(36) Duke, A. S.; Galhenage, R. P.; Tenney, S. A.; Ammal, S. C.; Heyden, A.; Sutter, P.; Chen, D. A., In Situ Ambient Pressure X-ray Photoelectron Spectroscopy Studies of Methanol Oxidation on Pt(111) and Pt–Re Alloys. *The Journal of Physical Chemistry C* **2015,** 119 (40), 23082-23093.

(37) Dexpert, H.; Lagarde, P.; Bournonville, J. P., Exafs studies of bimetallic Pt-Re/Al_2O_3 catalysts. *Journal of Molecular Catalysis* **1984,** 25 (1–3), 347-355.

(38) Rezgui, S.; Jentoft, R.; Gates, B. C., Supported Pt and Re–Pt on Alumina Prepared by Sol-Gel Synthesis within SituWater Formation: Role of Rhenium. *Journal of Catalysis* **1996,** 163 (2), 496-500.

(39) Purnell, S. K.; Gates, B. C.; Chang, J. R., NaY zeolite-supported rhenium-platinum catalysts prepared from organometallic precursors: evidence of the Re-Pt interaction from infrared and x-ray absorption spectroscopies. *The Journal of Physical Chemistry* **1993,** 97 (16), 4196-4205.

(40) Choung, S. Y.; Ferrandon, M.; Krause, T., Pt-Re bimetallic supported on CeO_2-ZrO_2 mixed oxides as water–gas shift catalysts. *Catalysis Today* **2005,** 99 (3–4), 257-262.

(41) Charcosset, H.; Fr ètey, R.; Leclercq, G.; Mend ès, E.; Primet, M.; Tournayan, L., The state of Re in Pt-Re/γ-Al_2O_3 catalysts. *Journal of Catalysis* **1979,** 56 (3), 468-471.

(42) Bastein, A. G. T. M.; Toolenaar, F. J. C. M.; Ponec, V., Adsorption of carbon monoxide on platinum alloys: An infrared investigation. *Journal of Catalysis* **1984,** 90 (1), 88-95.

(43) Fung, A. S.; McDevitt, M. R.; Tooley, P. A.; Kelley, M. J.; Koningsberger, D. C.; Gates, B. C., A Model γ-Al_2O_3-Supported Re-Pt Catalyst Prepared from [$Re_2Pt(CO)_{12}$]: I. Synthesis and Spectroscopic Characterization. *Journal of Catalysis* **1993,** 140 (1), 190-208.

(44) Pieck, C. L.; Marecot, P.; Querini, C. A.; Parera, J. M.; Barbier, J., Influence of PtRe interaction on activity and selectivity of reforming catalysts. *Applied Catalysis A: General* **1995,** 133 (2), 281-292.

(45) Prestvik, R.; Moljord, K.; Grande, K.; Holmen, A., The Influence of Pretreatment on the Metal Function of a Commercial Pt–Re/Al_2O_3Catalyst. *Journal of Catalysis* **1998,** 174 (2), 119-129.

(46) Prestvik, R.; Tøtdal, B.; Lyman, C. E.; Holmen, A., Bimetallic Particle Formation in Pt–Re/Al_2O_3 Reforming Catalysts Revealed by Energy-Dispersive X-Ray Spectrometry in the Analytical Electron Microscope. *Journal of Catalysis* **1998,** 176 (1), 246-252.

(47) Rønning, M.; Gjervan, T.; Prestvik, R.; Nicholson, D. G.; Holmen, A., Influence of Pretreatment Temperature on the Bimetallic Interactions in Pt-Re/Al_2O_3 Reforming Catalysts Studied by X-Ray Absorption Spectroscopy. *Journal of Catalysis* **2001,** 204 (2), 292-304.

(48) Yuan, Y.; Shido, T.; Iwasawa, Y., The new catalytic property of supported rhenium oxides for selective oxidation of methanol to methylal. *Chemical Communications* **2000,** (15), 1421-1422.

(49) Yuan, Y.; Iwasawa, Y., Performance and Characterization of Supported Rhenium Oxide Catalysts for Selective Oxidation of Methanol to Methylal. *The Journal of Physical Chemistry B* **2002,** 106 (17), 4441-4449.

(50) Varazo, K.; Parsons, F. W.; Ma, S.; Chen, D. A., Methanol Chemistry on Cu and Oxygen-Covered Cu Nanoclusters Supported on TiO_2(110). *The Journal of Physical Chemistry B* **2004,** 108 (47), 18274-18283.

(51) Zhou, J.; Ma, S.; Kang, Y. C.; Chen, D. A., Dimethyl Methylphosphonate Decomposition on Titania-Supported Ni Clusters and Films: A Comparison of Chemical Activity on Different Ni Surfaces. *The Journal of Physical Chemistry B* **2004,** 108 (31), 11633-11644.

(52) Ozturk, O.; Park, J. B.; Ma, S.; Ratliff, J. S.; Zhou, J.; Mullins, D. R.; Chen, D. A., Probing the interactions of Pt, Rh and bimetallic Pt–Rh clusters with the TiO2(110) support. *Surface Science* **2007,** 601 (14), 3099-3113.

(53) Park, J. B.; Ratliff, J. S.; Ma, S.; Chen, D. A., Understanding the Reactivity of Oxide-Supported Bimetallic Clusters: Reaction of NO with CO on TiO_2(110)-Supported Pt−Rh Clusters. *The Journal of Physical Chemistry C* **2007,** 111 (5), 2165-2176.

(54) Park, J. B.; Conner, S. F.; Chen, D. A., Bimetallic Pt−Au Clusters on TiO_2(110): Growth, Surface Composition, and Metal−Support Interactions. *The Journal of Physical Chemistry C* **2008,** 112 (14), 5490-5500.

(55) Tenney, S. A.; Ratliff, J. S.; Roberts, C. C.; He, W.; Ammal, S. C.; Heyden, A.; Chen, D. A., Adsorbate-Induced Changes in the Surface Composition of Bimetallic Clusters: Pt−Au on TiO_2(110). *The Journal of Physical Chemistry C* **2010,** 114 (49), 21652-21663.

(56) Tenney, S. A.; He, W.; Roberts, C. C.; Ratliff, J. S.; Shah, S. I.; Shafai, G. S.; Turkowski, V.; Rahman, T. S.; Chen, D. A., CO-Induced Diffusion of Ni Atoms to the Surface of Ni–Au Clusters on TiO_2(110). *The Journal of Physical Chemistry C* **2011,** 115 (22), 11112-11123.

(57) Tenney, S. A.; Cagg, B. A.; Levine, M. S.; He, W.; Manandhar, K.; Chen, D. A., Enhanced activity for supported Au clusters: Methanol oxidation on Au/TiO_2(110). *Surface Science* **2012,** 606 (15–16), 1233-1243.

(58) Galhenage, R. P.; Ammal, S. C.; Yan, H.; Duke, A. S.; Tenney, S. A.; Heyden, A.; Chen, D. A., Nucleation, Growth, and Adsorbate-Induced Changes in Composition for Co–Au Bimetallic Clusters on TiO_2. *The Journal of Physical Chemistry C* **2012,** 116 (46), 24616-24629.

(59) J. S. Ratliff. *The Morphology and Catalytic Activity of Bimetallic Nanoclusters Supported on TiO_2(110) Ph.D. thesis, University of South Carolina.* **2009**.

(60) Stempel, S.; Bäumer, M.; Freund, H. J., STM studies of rhodium deposits on an ordered alumina film-resolution and tip effects. *Surface Science* **1998,** 402–404, 424-427.

(61) Chen, D. A.; Bartelt, M. C.; Hwang, R. Q.; McCarty, K. F., Self-limiting growth of copper islands on TiO_2(110)-(1×1). *Surface Science* **2000,** 450 (1–2), 78-97.

(62) Zhou, J.; Kang, Y. C.; Ma, S.; Chen, D. A., Adsorbate-induced dissociation of metal clusters: TiO_2(1 1 0)-supported Cu and Ni clusters exposed to oxygen gas. *Surface Science* **2004,** 562 (1–3), 113-127.

(63) Wagner, R.; Schlatterbeck, D.; Christmann, K., The interaction of copper with a rhenium(0001) surface: structure, energetics, and growth modes. *Surface Science* **1999,** 440 (1–2), 231-251.

(64) Galhenage, R. P.; Yan, H.; Tenney, S. A.; Park, N.; Henkelman, G.; Albrecht, P.; Mullins, D. R.; Chen, D. A., Understanding the Nucleation and Growth of Metals on TiO_2: Co Compared to Au, Ni, and Pt. *The Journal of Physical Chemistry C* **2013,** 117 (14), 7191-7201.

(65) Campbell, C. T., Ultrathin metal films and particles on oxide surfaces: structural, electronic and chemisorptive properties. *Surface Science Reports* **1997,** 27 (1–3), 1-111.

(66) Zhou, J.; Kang, Y. C.; Chen, D. A., Controlling island size distributions: a comparison of nickel and copper growth on TiO2(1 1 0). *Surface Science* **2003,** 537 (1–3), L429-L434.

(67) Galhenage, R. P.; Yan, H.; Ahsen, A. S.; Ozturk, O.; Chen, D. A., Understanding the Growth and Chemical Activity of Co–Pt Bimetallic Clusters on TiO2(110):

CO Adsorption and Methanol Reaction. *The Journal of Physical Chemistry C* **2014,** 118 (31), 17773-17786.

(68) Park, J. B.; Ratliff, J. S.; Ma, S.; Chen, D. A., In situ scanning tunneling microscopy studies of bimetallic cluster growth: Pt–Rh on TiO_2(1 1 0). *Surface Science* **2006,** 600 (14), 2913-2923.

(69) Pan, J.-M.; Maschhoff, B. L.; Diebold, U.; Madey, T. E., Structural study of ultrathin metal films on TiO2 using LEED, ARXPS and MEED. *Surface Science* **1993,** 291 (3), 381-394.

(70) Tenney, S.; He, W.; Ratliff, J.; Mullins, D.; Chen, D., Characterization of Pt–Au and Ni–Au Clusters on TiO_2 (110). *Topics in Catalysis* **2011,** 54 (1), 42-55.

(71) Ozturk, O.; Park, J. B.; Black, T. J.; Rodriguez, J. A.; Hrbek, J.; Chen, D. A., Methanethiol chemistry on TiO2-supported Ni clusters. *Surface Science* **2008,** 602 (19), 3077-3088.

(72) Yao, H. C.; Shelef, M., Surface interactions in the system Reγ-Al_2O_3. *Journal of Catalysis* **1976,** 44 (3), 392-403.

(73) Björneholm, O.; Nilsson, A.; Tillborg, H.; Bennich, P.; Sandell, A.; Hernnäs, B.; Puglia, C.; Mårtensson, N., Overlayer structure from adsorbate and substrate core level binding energy shifts: CO, CCH_3 and O on Pt(111). *Surface Science* **1994,** 315 (1–2), L983-L989.

(74) Ramstad, A.; Strisland, F.; Raaen, S.; Worren, T.; Borg, A.; Berg, C., Growth and alloy formation studied by photoelectron spectroscopy and STM. *Surface Science* **1999,** 425 (1), 57-67.

(75) Mason, M. G., Electronic structure of supported small metal clusters. *Physical Review B* **1983,** 27 (2), 748-762.

(76) Wertheim, G. K.; DiCenzo, S. B.; Youngquist, S. E., Unit Charge on Supported Gold Clusters in Photoemission Final State. *Physical Review Letters* **1983,** 51 (25), 2310-2313.

(77) Bäumer, M.; Freund, H.-J., Metal deposits on well-ordered oxide films. *Progress in Surface Science* **1999,** 61 (7–8), 127-198.

(78) Dalacu, D.; Klemberg-Sapieha, J. E.; Martinu, L., Substrate and morphology effects on photoemission from core-levels in gold clusters. *Surface Science* **2001,** 472 (1–2), 33-40.

(79) Howard, A.; Clark, D. N. S.; Mitchell, C. E. J.; Egdell, R. G.; Dhanak, V. R., Initial and final state effects in photoemission from Au nanoclusters on TiO2(1 1 0). *Surface Science* **2002,** 518 (3), 210-224.

(80) Santra, A. K.; Goodman, D. W., Oxide-supported metal clusters: models for heterogeneous catalysts. *Journal of Physics: Condensed Matter* **2003,** 15 (2), R31.

(81) Seuser, G. S.; Galhenage, R. P.; Chen, D. A., Oxidation of Re-Pt Surfaces: Supported Clusters and Thin Films. . **Manuscript in preparation.**

(82) Zaera, F.; Somorjai, G. A., The chemisorption of O_2, CO, D_2 and C_2H_4 over epitaxially grown rhenium crystalline films. *Surface Science* **1985,** 154 (1), 303-314.

(83) Morant, C.; Galán, L.; Sanz, J. M., X-ray photoelectron spectroscopic study of the oxidation of polycrystalline rhenium by exposure to O2 and low energy O2+ ions. *Analytica Chimica Acta* **1994,** 297 (1–2), 179-186.

(84) Liu, P.; Shuh, D. K., Adsorption of O_2 on polycrystalline rhenium metal at room temperature studied by synchrotron X-ray photoemission spectroscopy. *Journal of Electron Spectroscopy and Related Phenomena* **2001,** 114–116, 319-325.

(85) Chan, A. S. Y.; Chen, W.; Wang, H.; Rowe, J. E.; Madey, T. E., Methanol Reactions over Oxygen-Modified Re Surfaces: Influence of Surface Structure and Oxidation. *The Journal of Physical Chemistry B* **2004,** 108 (38), 14643-14651.

(86) Chan, A. S. Y.; Wertheim, G. K.; Wang, H.; Ulrich, M. D.; Rowe, J. E.; Madey, T. E., Surface atom core-level shifts of clean and oxygen-covered Re(123¯1). *Physical Review B* **2005,** 72 (3), 035442.

(87) Ducros, R.; Alnot, M.; Ehrhardt, J. J.; Housley, M.; Piquard, G.; Cassuto, A., A study of the adsorption of several oxygen-containing molecules (O_2, CO, NO, H_2O) on Re(0001) by XPS, UPS and temperature programmed desorption. *Surface Science* **1980,** 94 (1), 154-168.

(88) Ducros, R.; Fusy, J., Core level binding energy shifts of rhenium surface atoms for a clean and oxygenated surface. *Journal of Electron Spectroscopy and Related Phenomena* **1987,** 42 (4), 305-312.

(89) Wagner, C. D.; Muilenberg, G. E., *Handbook of x-ray photoelectron spectroscopy : a reference book of standard data for use in x-ray photoelectron spectroscopy*. Physical Electronics Division, Perkin-Elmer Corp.: Eden Prairie, Minn., **1979**.

(90) F.R. de Boer, R. B., W.C.M. Mattens, A.R. Miedema, A.K. Niessen, *Cohesion in Metals: Transition Metal Alloys*. North-Holland Physics Publishing: Amsterdam, **1998**.

(91) Tauster, S. J.; Fung, S. C.; Garten, R. L., Strong metal-support interactions. Group 8 noble metals supported on titanium dioxide. *Journal of the American Chemical Society* **1978,** 100 (1), 170-175.

(92) Tauster, S. J.; Fung, S. C.; Baker, R. T. K.; Horsley, J. A., Strong Interactions in Supported-Metal Catalysts. *Science* **1981,** 211 (4487), 1121-1125.

(93) Tauster, S. J., Strong metal-support interactions. *Accounts of Chemical Research* **1987,** 20 (11), 389-394.

(94) Diebold, U.; Pan, J.-M.; Madey, T. E., Ultrathin metal film growth on TiO_2(110): an overview. *Surface Science* **1995,** 331–333, Part B, 845-854.

(95) Luo, J. S.; Tobin, R. G.; Lambert, D. K.; Fisher, G. B.; DiMaggio, C. L., CO adsorption site occupation on Pt(335): a quantitative investigation using TPD and EELS. *Surface Science* **1992,** 274 (1), 53-62.

(96) Skelton, D. C.; Tobin, R. G.; Lambert, D. K.; DiMaggio, C. L.; Fisher, G. B., Oxidation of CO on Gold-Covered Pt(335). *The Journal of Physical Chemistry B* **1999,** 103 (6), 964-971.

(97) Shigeishi, R. A.; King, D. A., Chemisorption of carbon monoxide on platinum {111}: Reflection-absorption infrared spectroscopy. *Surface Science* **1976,** 58 (2), 379-396.

(98) Collins, D. M.; Spicer, W. E., The adsorption of CO, O_2, and H_2 on Pt: I. Thermal desorption spectroscopy studies. *Surface Science* **1977,** 69 (1), 85-113.

(99) Fair, J.; Madix, R. J., Low and high coverage determinations of the rate of carbon monoxide adsorption and desorption from Pt(110). *The Journal of Chemical Physics* **1980,** 73 (7), 3480-3485.

(100) Housley, M.; Ducros, R.; Piquard, G.; Cassuto, A., The adsorption of carbon monoxide on rhenium: Basal (0001) and stepped 14 (0001) × (10$\bar{1}$1) planes. *Surface Science* **1977,** 68, 277-284.

(101) Ducros, R.; Fusy, J.; Jupille, J.; Pareja, P.; Tatarenko, S., CO adsorption on rhenium single crystal surfaces: Characterization of molecular and dissociated states and influence of structural defects. *Applied Surface Science* **1987,** 29 (2), 179-193.

(102) Illingworth, A.; Zhou, J.; Ozturk, O.; Chen, D. A., Design of a heating-cooling stage for scanning tunneling microscopy and temperature programmed desorption experiments. *Journal of Vacuum Science & Technology B* **2004,** 22 (5), 2552-2554.

CHAPTER 6 REACTIONS OF METHANOL OXIDATION ON TITANIA SUPPORTED PT-RE CLUSTERS

6.1 INTRODUCTION

The activity, selectivity and lifetime of a monometallic catalyst in a specific reaction can be manipulated by the addition of another metal. Due to the wide use of platinum in catalysis, Pt-based bimetallic catalysts are extensively studied in industrial processes and have been playing a crucial role in the understanding of surface catalysis [1, 2]. There is growing interest in Pt-Re bimetallic system since the first commercial use of Pt-Re catalysts in naphtha reforming [3-8], which is a vital process in the petroleum refining. The addition of Re to Pt-based catalysts brings many benefits to reforming reactions. For naphtha reforming, Pt-Re/Al_2O_3 can reduce the deactivation rate and enhance hydrogen uptake and aromatic yields compared with pure Pt [9-11]. Another example is the aqueous phase reforming (APR) of xylitol, where the bimetallic Pt-Re/TiO_2 catalysts show a higher selectivity to alkanes compared to the monometallic catalysts which are more selective toward hydrogen formation [12].

Although much attention has been paid to study the attractive effects of the Re in Pt-Re catalyst for reforming and oxidation reactions, the explored results were inconclusive. For instance, in the aqueous-phase reforming of glycerol, Zhang et al. found that the acidity of Pt nanoparticles supported on carbon was increased with Re addition, which favors C–O over C–C cleavage [13]; the work by Dumesic group suggested the primary promotional effect of Re in Pt-Re/C is to weaken the interaction of CO with the surface, decreasing the CO coverage and allowing the catalyst to operate at high rates [14]. Ciftci et al. has reported that the overall APR catalytic performance correlates with the water–gas shift (WGS) reaction: the role of Re in the bimetallic Pt-Re/C catalysts is to facilitate water dissociation, lower steady-state CO coverage and increase the glycerol conversion

rates [15, 16]. In addition, studies of Pt-Re/TiO_2 or CeO_2 by Azzam proposed that Re can form ReO_x to provide an additional redox route for WGS reaction [17, 18]. So far, the effects of added Re in Pt-based system are still not fully understood, mainly due to the fact that catalyst preparation is not well controlled and the Re oxidation state is difficult to identify.

The model catalyst approach uses a simplified and well-controlled surface to gain fundamental understanding about more complicated catalytic systems. Recently, Galhenage and co-workers have studied the growth of vapor-deposited Pt-Re bimetallic clusters supported on TiO_2 (110) by STM, XPS, LEIS and TPD [19]. Based on this work, Pt-Re bimetallic clusters can be formed in either sequential deposition order on TiO_2, Pt-Re core-shell alloy can be formed when dose more than 0.75 ML Pt on top of 2 ML Re. Furthermore, the role that TiO_2 support plays during the evolution of CO_2 makes this bimetallic system more interesting towards oxidation reactions [19].

Methanol oxidation can serve as a model reaction for the oxidation of alcohols and provides valuable information for reforming reactions. Methanol itself is an abundant liquid fuel that can easily be transported and stored, while the partial oxidation products formaldehyde and formic acid are good synthesis reactants, and the hydrogen generated from methanol is such an attractive clean feed for proton exchange membrane (PEM) and direct-methanol fuel cells [20-23]. Potentially, the high atomic ratio of H/C makes oxidation of methanol more interesting in hydrogen energy related field. The reaction of methanol on Pt catalysts has been well studied in higher pressure reactors[24-26] and UHV chambers[27-29], while only few work in Pt-Re systems has been reported[30] in near reaction condition.

One of the biggest benefits to study methanol is the accessibility of gas-solid surface, so that a number of UHV surface analysis techniques can be employed for the careful characterization of Pt-Re bimetallic system. Meanwhile, the higher turnover frequency (TOF) of methanol oxidation allows the reactor to be operated at lower temperatures under continuous flow mode, where the concentrations of products are high enough for the analysis of regular gas chromatograph with thermal conductivity detector. In addition, the study of Pt-Re system could potentially provide valuable insights for steam reforming of methanol [31-33] and oxidative steam reforming of alcohols [34-36]. In this chapter, the methanol oxidation by oxygen is chosen as the probe reaction to study the bimetallic Pt-Re/TiO_2 system under oxidation conditions. The reactivity of Pt/TiO_2, Re/TiO_2 and Pt-Re/TiO_2 was evaluated in the reactor under single-pass mode at 80- 150 ℃. Post-reaction XPS analysis was conducted to understand the oxidation state of Re after reaction.

6.2 EXPERIMENTAL

The TiO_2 (110) supported Pt, Re, and Pt-Re bimetallic clusters for higher pressure activity studies were prepared in an UHV chamber to which the micro-reactor is coupled [37]. This chamber is also equipped with a mass spectrometer (Stanford Research Systems, RGA 300), a dual Al/Mg anode X-ray source (Leybold Heraeus, RQ 20/63), a hemispherical analyzer (SPECS, EA10) for X-ray photoelectron spectroscopy (XPS), a set of retractable optics with a retarding field analyzer (SPECS, ErLEED-4) for low energy electron diffraction (LEED) and Auger electron spectroscopy (AES), which has been described elsewhere [38]. The rutile TiO_2 (110) single crystal support (Princeton Scientific Corporation, 10 mm x 10 mm x 1 mm) was cleaned by a number of cycles of Ar^+ sputtering (1000 V, 3.0-3.2 μA, twenty minutes) and annealing (673 ℃, three

minutes). The surface structure of TiO_2 (110) was confirmed by LEED. The Pt, Re and Pt-Re clusters were prepared by sequential vapor deposition of Pt and Re onto the clean TiO_2 (110) surface. The coverages of Pt and Re were measured by an independently calibrated quartz crystal microbalance (QCM). For Pt, one monolayer (ML) is defined according to the packing density of Pt (111) (1.50×10^{15} atoms/cm^2); for Re, 1 ML is defined according to the packing density of Re (0001) (1.52×10^{15} atoms/cm^2).

After being prepared and characterized in the UHV chamber, the catalyst sample was transferred to the reactor under vacuum (pressure~ 2.5 x10^{-8} Torr). The detail of reactor and transfer have been illustrated elsewhere [37]. After loading the sample, the reactor cell was heated to the desired temperature (80 ℃ or 100 ℃) in a 50 sccm continuous flow of He (Airgas, 99.999%), at a heating rate of 1.5~2 ℃ /s; the rest of reactor loop and lines were heated to ~60 ℃. The temperature of the reactor cell was controlled externally by heating tapes (Briskheat, BWHD), which were regulated by a temperature controller (Auber SYL-4342P) for approximately linear heating. The temperature of sample surface was monitored by a type K thermocouple (Omega, KMQSS-040G-6), which was installed through the reactor cell and close to the surface of crystal. The temperature of the loop was maintained using two Valco Instruments temperature controllers. The pressure of reactor system is monitored by two manometer gauges (MKS Instruments Baratron 722A): one installed in the beginning of feed line (790 Torr ~ 800 Torr) and another located downstream of reactor loop (770 Torr ~ 780 Torr).

After maintaining the sample at a desired temperature in helium for one hour, the feed was switched to the reaction mixture (2% MeOH, 4% oxygen and 94% Helium). The single-pass mode was chosen for the activity test because of the concentration of each

product is high enough for GC analysis. Methanol (MeOH) vapor was introduced into the feed gas line by a home-made vapor-liquid equilibrator (VLE), which is filled with methanol (Fisher Chemical, 99.9%) and helium serves as the sweep gas. The temperature of VLE is controlled by a VWR refrigerated and heated circulating bath. The methanol concentration in out-let VLE is calculated from Antoine equation of pure methanol. Three mass flow controllers (Brooks 5850e and 5850i) are used to control the gas flow for those lines: sweep helium (Airgas 99.999%), oxygen (Airgas 99.5%) and balance helium (Airgas 99.999%), so that the feed concentration was maintained at 2% methanol, 4% oxygen and 94% Helium, with a total flow of 58 sccm. Every twenty minutes, the sampling loop (~1.096 cm^3) was injected to a HP 5890A gas chromatograph (GC), where a thermal conductivity detector (TCD) is equipped. The TCD is connected to a PoraPLOT Q capillary GC column for the quantitatively analysis of potential products: CO_2, H_2O, formaldehyde (HCHO), MeOH, formic acid (HCOOH), etc. For experiments held at one fixed temperature: activity tests at 80 ℃ were conducted for 10 hours, while tests at 100 ℃ were conducted for 6 hours. For activation energy experiments, the surfaces were firstly kept under 94 sccm of reaction mixture at 80 ℃ for 12 hours under single-pass mode, followed by 80 minutes' test for each higher temperature (100 ℃, 130 ℃ and 150 ℃) with the same flow rate at 94 sccm. The heating rate between reaction temperatures was 1.5 ℃ /s. The reaction rate and selectivity calculation is based on the formation rates of CO_2, HCHO and HCOOH. The sample was cooled down to ~30 ℃ at a rate of 1.5~2 ℃ /s in pure helium after each experiment. Then the reactor cell was pumped to vacuum and the post-reaction sample was transferred back into UHV chamber for further XPS analysis.

6.3 Result and Discussion

Before and after all methanol oxidation experiments on Pt-Re/TiO_2, the activity of clean TiO_2 support was shown to be zero at 60-150 ℃. Different from the studies that our group had done previously on a Pt foil and Re-Pt surface alloy [39], the activity of 2 ML Pt/TiO_2 in this work is zero at 60 ℃, even after exposing to reaction mixture for sufficient time period (~12 hours) under recirculation mode; however, significant activity can be observed on the Pt foil for CO_2 and HCOOH formation at 60 ℃ [39] after few hours. Figure 6.1 shows the total formation rate vs reaction time which measured on 2 ML Pt/TiO_2 at 80 ℃ for ten hours. Here carbon products CO_2, HCHO and HCOOH were detected, a total formation rate was calculated to be 210 μmol/hour (Selectivity: 11.5% for CO_2, 42% for HCHO and 46.5% for HCOOH). Previous studies of methanol oxidation did not report HCOOH as product [24-26] because the temperature range in those studies was much higher.

As can been seen from Figure 6.1, there is an onset time for the reaction: initially no carbon product can be detected, and the activity slowly increases with reaction time; hence several hours of reaction time is needed for the oxygen to dissociate on Pt surface. This behavior was also observed on a clean Pt foil at 60 ℃ [39] under same experimental conditions, but no HCHO product was observed on Pt foil at that temperature, and HCOOH was the dominant product. This result supports the fact that oxygen should dissociate on Pt first to initiate any reaction on Pt/TiO_2. Meanwhile, the dissociation of oxygen on supported Pt clusters is apparently difficult than that on Pt foil since a higher temperature is required.

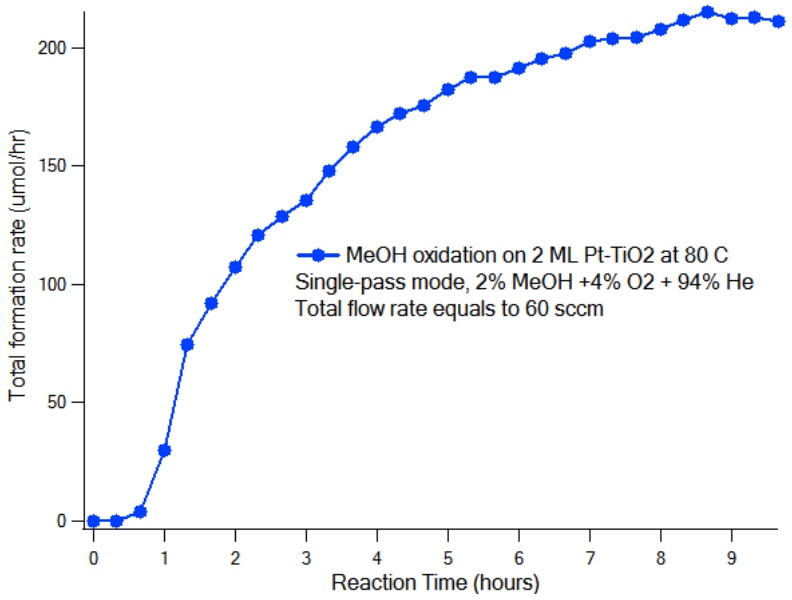

Figure 6.1: MeOH oxidation, total formation rate of CO2, HCHO and HOOCH on 2 ML Pt/TiO_2 at 80 ℃ for 10 hours, 2%MeOH +4%O_2+94% He single-pass mode at 58 sccm.

Figure 6.2 shows the total formation rates of CO_2, HCHO and HCOOH on 2 ML Pt/TiO_2, 2 ML Re/TiO_2, 2 ML Pt+2 ML Re/TiO_2, 2 ML Re+2 ML Pt/TiO_2 surfaces at 100 ℃ under single-pass mode for six hours. As expected, the 2 ML Re clusters supported on TiO_2 exhibit no activity for methanol oxidation, while the 2 ML Pt surface is the most active sample. Meanwhile, at 100 ℃ the onset time for 2 ML Pt/TiO_2 (less than one hour) is much less than that at 80 ℃ (~eight hours). Turnover frequency for the 2 ML Pt-TiO_2(110) catalyst at 100 ℃ for 6 hours was 70 $site^{-1}$ s^{-1}, which is calculated from the observed rate and the concentration of active sites ($1.5x10^{15}$ cm^{-2}). The active sites were estimated from the total Pt surface area that was calculated from a numerical integration of a STM image for 2 ML Pt on TiO_2 [37]. Compared with the TOF value 48.8 $site^{-1}$ s^{-1}estimated from Pt foil with same experimental configuration. Compared with Pt foil, 2 ML Pt/TiO_2 is much more active, and this much higher reaction rate is not due to a larger surface area. One possible reason could be Pt-interfacial sites promote reactions.

The activity of 2 ML Pt clusters is significantly diminished when adding 2 ML Re to 2 ML Pt/TiO_2 to form 2 ML Pt+2 ML Re. This indicates that surface Re on top of Pt has no contribution to the observed activity, though 2 ML Pt+2 ML Re should have more total surface sites than 2 ML Pt when equilibrium is reached, based on the CO temperature programmed desorption (TPD) studies from our group [19]. Meanwhile, at six hours the activity of 2 ML Re+2 ML Pt/TiO_2 surface (500 μmol//hr) is ~12% higher than 2 ML Pt+2 ML Re/TiO_2 (450 μmol/hr). This might be due to more Pt sites on the 2 ML Re+2 ML Pt in the six hours' time frame, since Pt atoms are initially present at the surface in this deposition order.

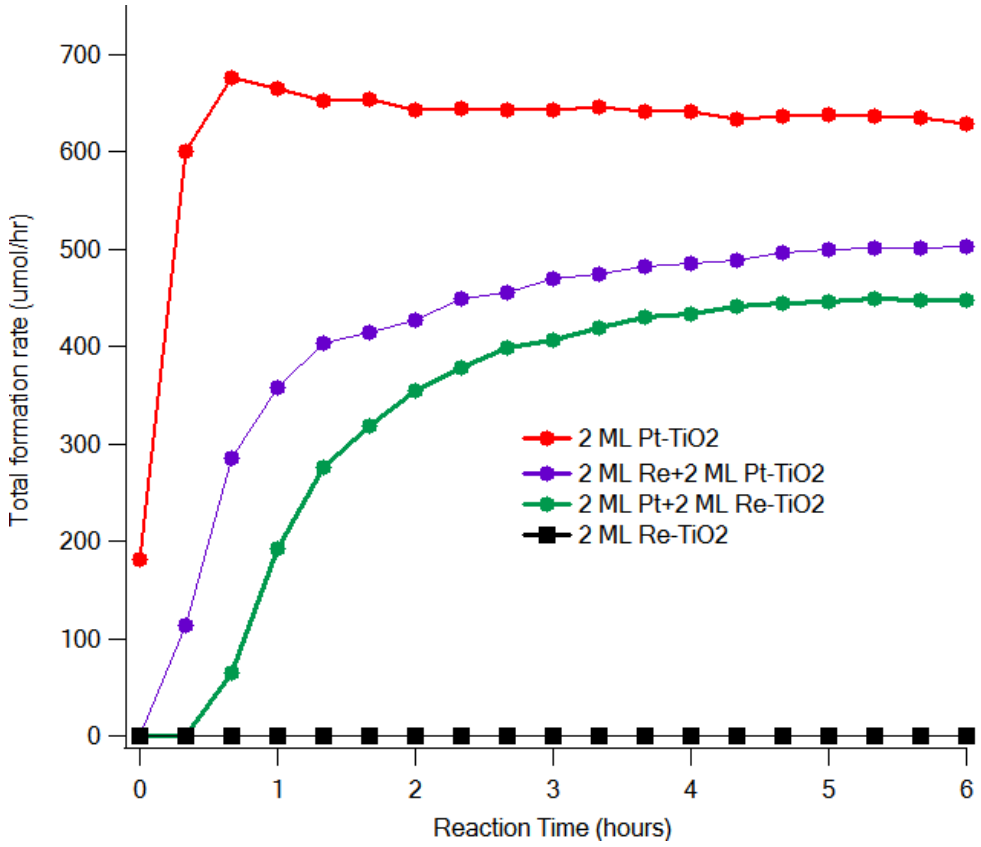

Figure 6.2: MeOH oxidation, total formation rate of CO2, HCHO and HOOCH on 2 ML Pt, 2 ML Re, 2 ML Pt+2 ML Re, 2 ML Re + 2 ML Pt on TiO_2 at 100 ℃ for 6 hours, 2%MeOH +4%O_2+94% He single-pass mode at 58 sccm.

Figure 6.3 shows XPS result of Re (4f) region on 2 ML Re+2 ML Pt/TiO_2, 2 ML Re/TiO_2, and 2 ML Pt+2ML Re/TiO_2 surface before and after the methanol oxidation at 100 ℃. For both Pt+Re and Re+Pt surfaces, the position of Re (4f) peak before reaction is un-shifted compared with 2 ML Re/TiO_2 (42.8 eV). After methanol oxidation, for all surfaces the Re signal diminished dramatically, while the residual Re signal shifts to much higher oxidation states such as +4, +6 and +7. It is well-known that Re_2O_7 is volatile and can easily leave the surface [39, 40]. Therefore at this reaction temperature surface Re is unstable under methanol oxidation condition. However, the post-reaction Re signal on 2 ML Re + 2 ML Pt/TiO_2 is much less than the case of 2 ML Re/TiO_2 after reaction, indicates that Re on top of Pt is more easily oxidized than Re on top of Re.

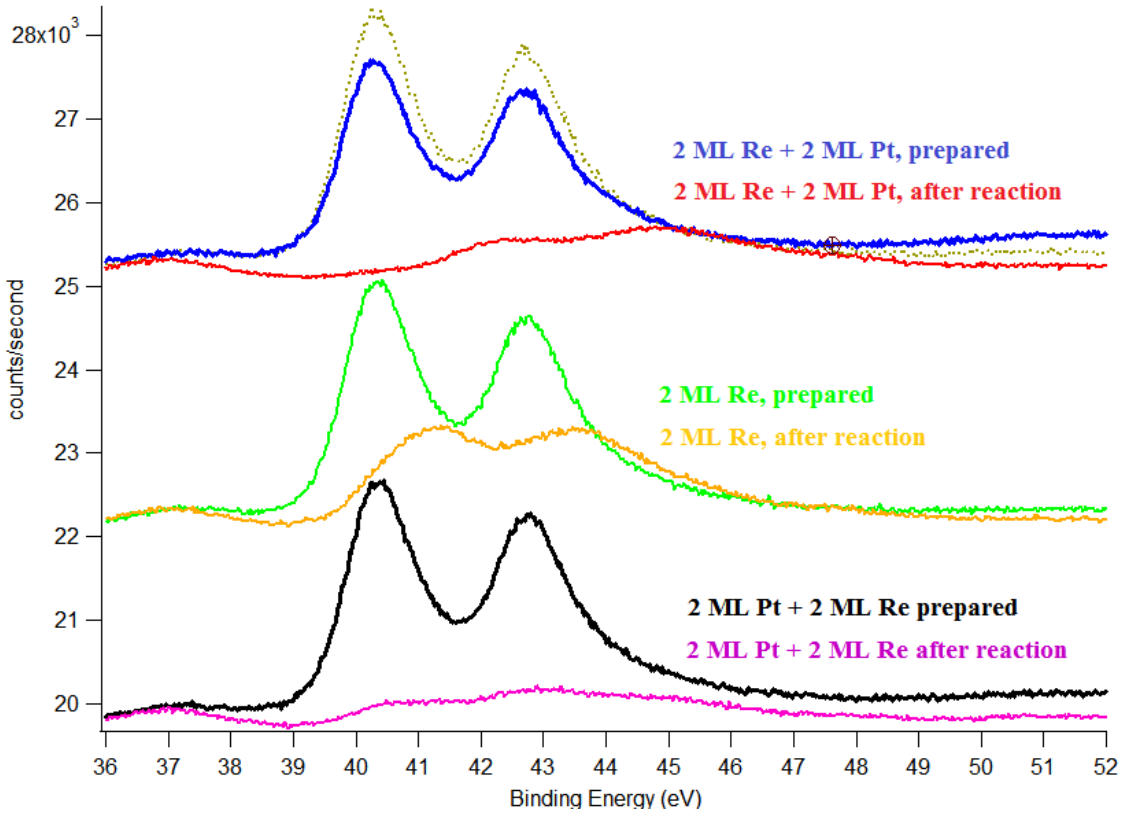

Figure 6.3: Post- vs pre- reaction XPS Re(4f) result on 2 ML Re, 2 ML Pt+2 ML Re, 2 ML Re + 2 ML Pt supported onTiO_2 after MeOH oxidation at 100 ℃ for 6 hours

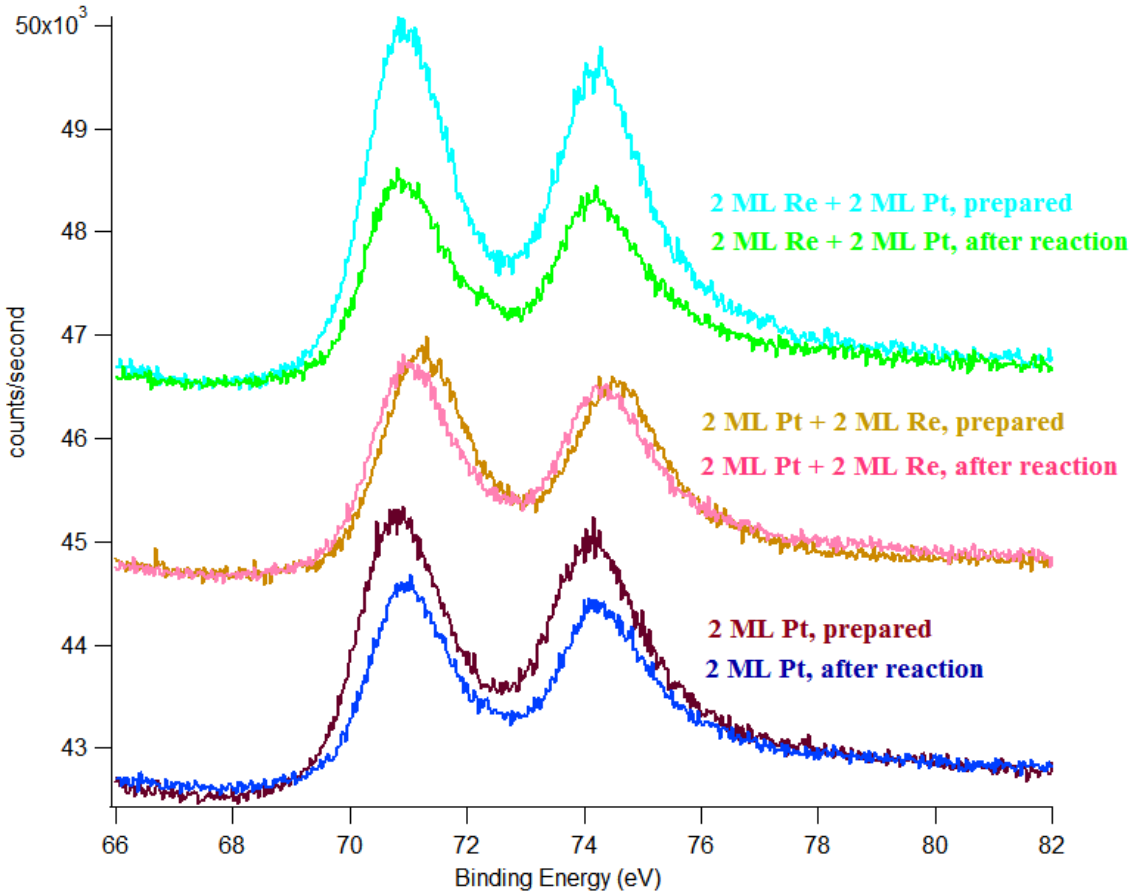

Figure 6.4: post- vs pre- reaction XPS Pt(4f) result on 2 ML Re, 2 ML Pt+2 ML Re, 2 ML Re + 2 ML Pt supported onTiO_2 after MeOH oxidation at 100 ℃ for 6 hours

Figure 6.4 presents the XPS result of Pt (4f) region on 2 ML Re+2 ML Pt/TiO_2, 2 ML Pt+2 ML Re/TiO_2, and 2 ML Pt/TiO_2 surface before and after methanol oxidation at 100 ℃ for six hours. As can be seen, the deposition of 2 ML Re on top of 2 ML Pt (2 ML Pt+2 ML Re) shifts the Pt (4f) peak to a higher binding energy, which is attributed to an effect known as core level shift (SCLS). This effect was seen on Pt when atoms or adsorbates are deposited on the surface[41, 42]. Based on the growth study of Pt-Re bimetallic clusters by STM, Pt-core and Re-shell bimetallic clusters will be formed by dosing 2 ML Re on top of 2 ML Pt/TiO_2 [19]. The Pt (4f) peak shifts back after exposing to reaction mixtures, which suggests that Re is lost from the surface.

Activity was monitored from 80-150 ℃ on 2 ML Pt/TiO_2 to study the distribution of products as a function of temperature as well as the activation energy. In contrast to the experiments at 80 ℃ or 100 ℃ alone, the total flow rate of reaction mixture is increased to 94 sccm instead of 58 sccm, to avoid any mass transfer limitation at high reaction temperatures. The feed concentration is maintained at 2% methanol, 4% oxygen and balance helium. Based on the activity trend at 80 ℃, the activity of 2 ML Pt surface was firstly stabilized at 80 ℃ for 12 hours before ramping to 100 ℃. For each temperature above 80 ℃, the temperature was maintained at that value for 1.5 hours, and the data was averaged from three consecutive injections.

Figure 6.5 shows the individual formation rate of CO_2, HCHO and HCOOH on 2 ML Pt/TiO_2 from 80-150 ℃ under single-pass mode. As can be seen, at 80 ℃ the formation rate of HCHO is almost the same as HCOOH, which is the main product at lower temperatures and also observed on clean Pt foil [39]. The formation rate of formic acid reaches its maximum at 100 ℃ and decreases substantially with increasing reaction temperature. CO_2 is a minor product at 80 ℃, and its formation rate increases significantly with reaction temperature. HCHO becomes the dominant product after heating the reactor to 100 ℃, and the exact formation rate is approximately twice that of the CO_2 formation rate. At 150 ℃, the formation rate of HCHO only increases by ~5% compared with that at 130 ℃. The selectivity of each product was calculated from the individual rate divided by the total formation rate (Figure 6.6). The selectivity of HCHO is 60% from 100-130 ℃ and remains at 55% at 150 ℃. This is different from the result obtained on Pt foil, where CO_2 has a slightly higher selectivity than HCHO at 150 ℃ [39].

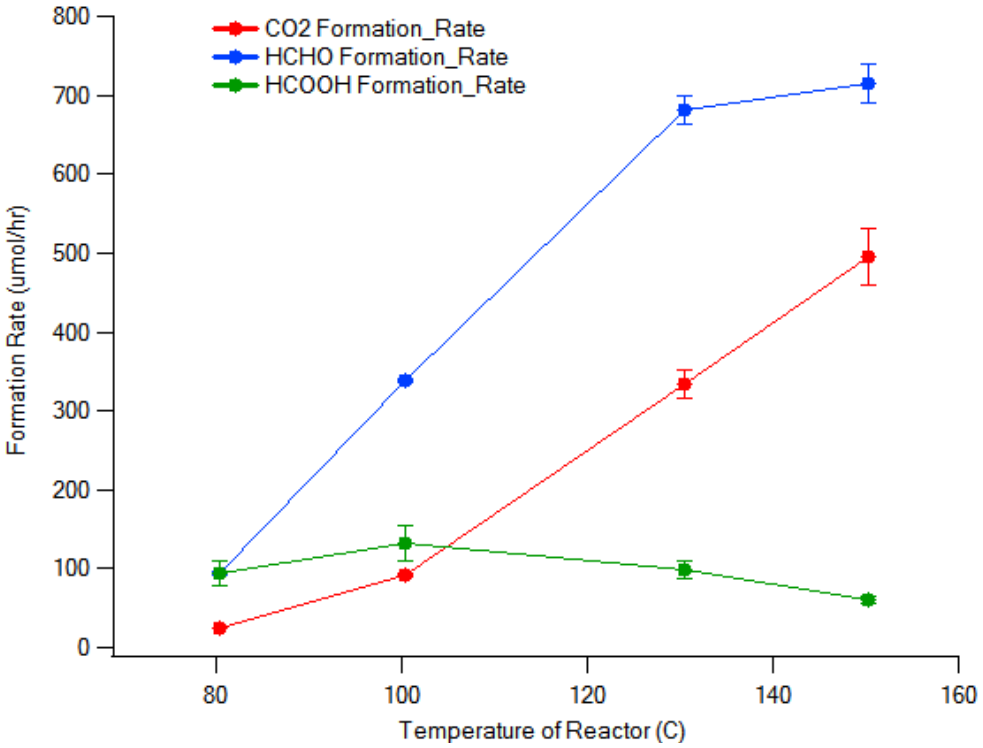

Figure 6.5: MeOH oxidation, formation rate for CO_2, HCHO and HCOOH on 2 ML Pt from 80-150 ℃, single-pass mode, 2%MeOH+4%O_2+He, 94 sccm

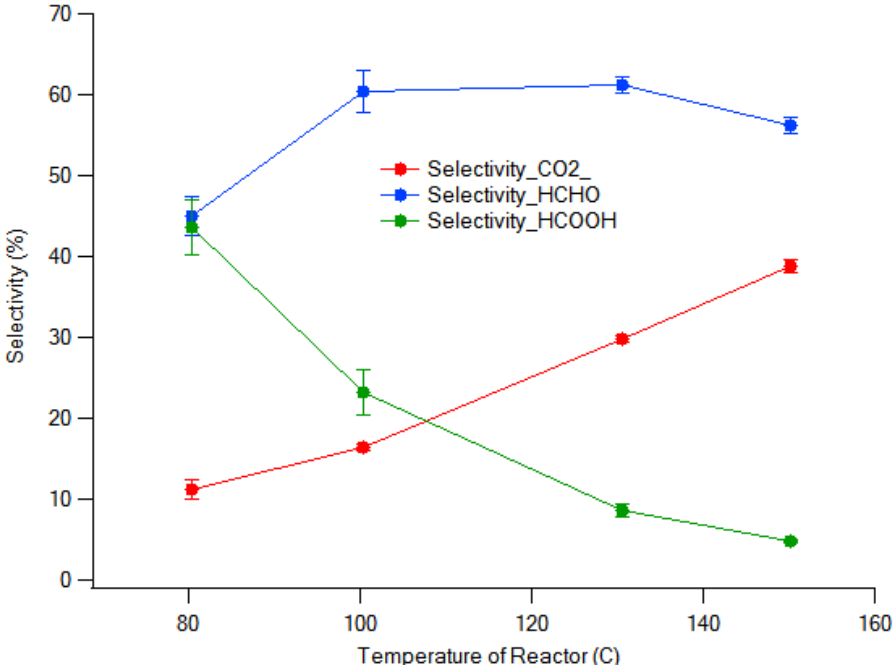

Figure 6.6: MeOH oxidation, selectivity of carbon products as a function of reactor temperature on 2 ML Pt from 80-150 ℃, single-pass mode, 2%MeOH+4%O_2+He, 94 sccm.

The total formation rate of the three carbon products from 80-150 ℃ is shown in Figure 6.7. As mentioned previously, on Pt clusters supported on TiO_2(110), no activity was found at at 60 ℃ , while on the Pt foil, HCOOH and CO_2 were observed at 60 ℃. This suggests the dissociation energy of oxygen on supported Pt clusters is higher than pure Pt foil. At 80 ℃, the total formation rate on 2 ML Pt/TiO_2 is also much lower than the Pt foil [39] (210 vs 420 umol/hr). At 100 ℃, the total formation rate observed on 2 ML Pt is ~10% higher than Pt foil (560 vs 500 umol/hr), owing to much more HCHO formation on Pt clusters supported on TiO_2, and the observed rate is much higher than Pt foil at 130 ℃ (1100 vs 600 umol/hr), and 150 ℃ (1270 vs 800 umol/hr). This suggests that the higher activity on 2 ML Pt is not due to a higher surface area, given that the surface sites on 2 ML Pt and Pt foil are comparable.

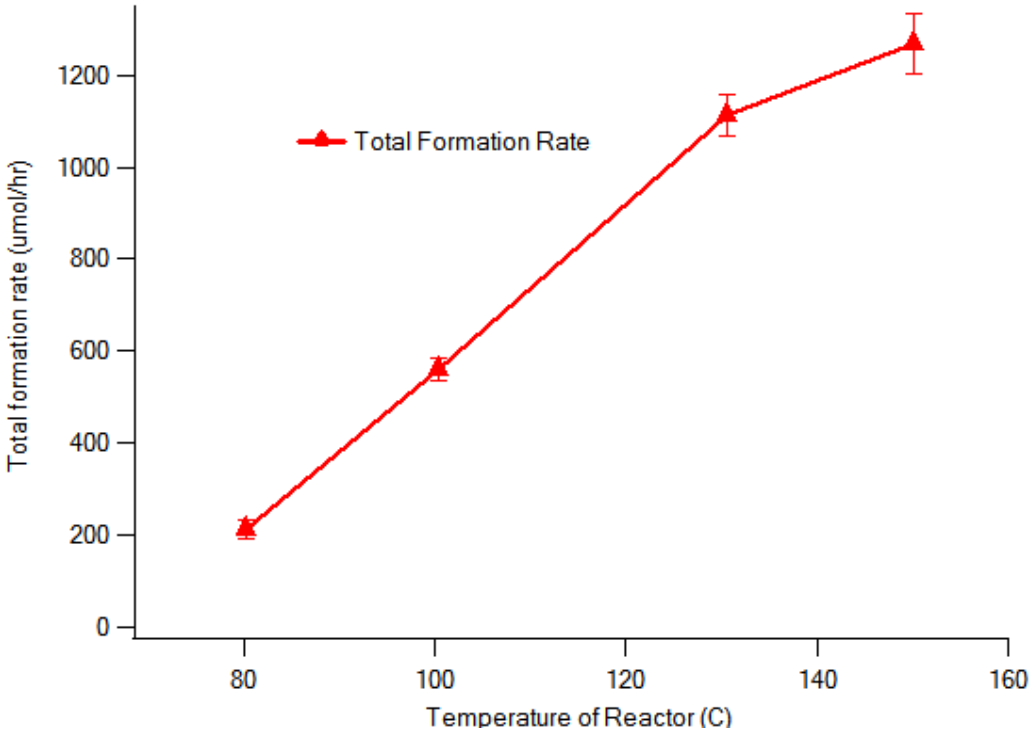

Figure 6.7: MeOH oxidation, total formation rate on 2 ML Pt from 80-150 ℃, single-pass mode, 2%MeOH+4%O_2+He, 94 sccm.

MeOH conversion on 2 ML Pt/TiO_2 as a function of reactor temperature (80-150 ℃) is shown in Figure 6.8. At 80 ℃, only ~5% of the methanol feed was converted to CO_2, HCHO and HCOOH. Over a temperature range of 100- 130 ℃, the calculated methanol conversion is increased from 11% to 22%, and at 150 ℃ the conversion reaches 26%, which is a relatively high value for a steady-state study. In order to check whether there is mass transfer limitation at 150 ℃, the total flow rate of was increased to 120 sccm for additional two injection periods following data collection at 94 sccm. The calculated total formation rate with the increased flow rate was the same as that with 94 sccm, which indicates that there was no mass transfer limitation for this activation energy experiment.

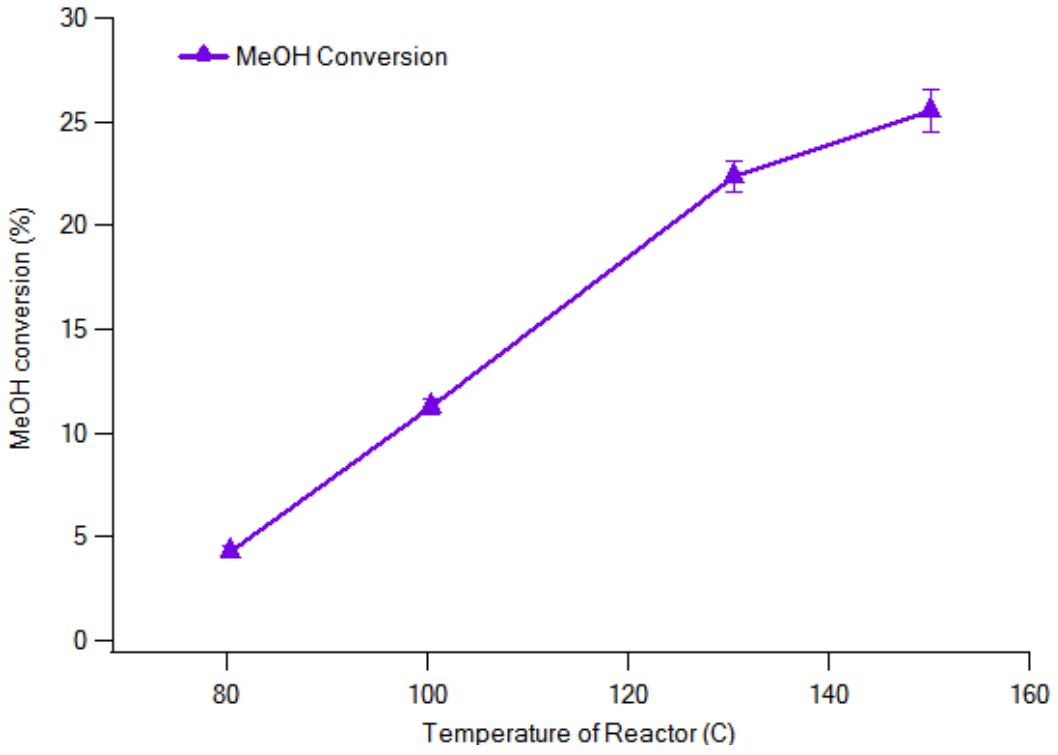

Figure 6.8: MeOH conversion as a function of temperature on 2 ML Pt from 80-150 ℃, single-pass mode, 2%MeOH+4%O_2+He, 94 sccm.

The total product formation rate vs temperature (Figure 6.7) does not follow Arrhenius behavior. Furthermore, the formation rate of HCOOH sharply decreases with reaction temperature, and it is suggested that under these experimental conditions there are multiple reaction pathways for the methanol oxidation process, and HCOOH is believed to be a reaction intermediate. In this work we estimate the activation energy for the formation of CO_2 only based on Arrhenius equation.

Figure 6.9 shows the Arrhenius plot for CO_2 product on 2 ML Pt/TiO_2 at 80-150 ℃. It is not suitable to do the linear fitting and get the activation energy for this wide temperature region because the formation rate of CO_2 appears too low at 80 ℃. The reason might be that there are two reaction pathways: first, CO_2 can be formed directly on Pt cluster supported on TiO_2; secondly, CO_2 production also occurs via oxidation of HCOOH. At 80 ℃ there is a significant amount of HCOOH in the reaction system, which yields a selectivity of ~45%; hence the CO_2 formation rate is lower at 80 ℃ compared to all higher temperatures. At 100 ℃ and higher temperatures, the reaction intermediate HCOOH is quickly consumed to form CO_2 and the residual HCOOH is at a very low concentration: in this reaction pathway, CO_2 formation is almost constant and the activation energy plot for this region should be linear. Therefore, by removing the data point at 80 ℃, a linear plot is obtained for CO_2 formation on 2 ML Pt (Figure 6.10), and the activation energy for CO_2 is calculated to be 47.6 kJ/mol. This value is much higher than the values we obtained on clean Pt foil at 100-150 [39] (27.9 kJ/mol, 100-150 ℃). It is also higher than Endo et al.'s work on Pt(111) [28](33 kJ.mol, 144-277 ℃), and slightly higher than what McCabe et al. reported on highly oxidized Pt wire [26] (42 kJ.mol, 130-260 ℃).

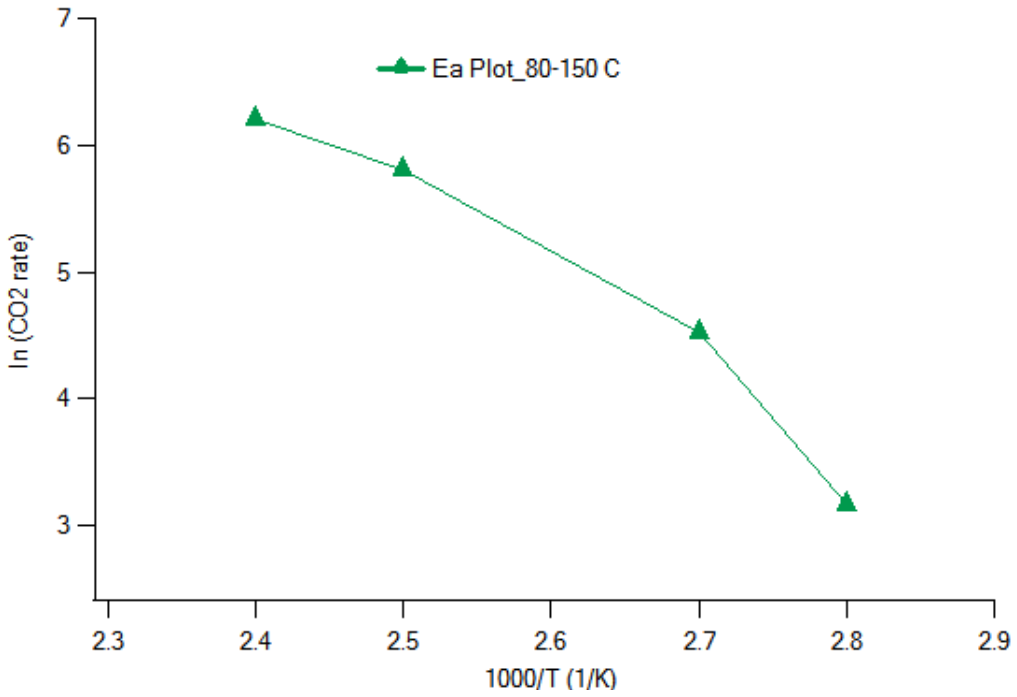

Figure 6.9: Activation energy calculation for CO_2 formation on 2 ML Pt from 80-150 ℃, single-pass mode, 94 sccm.

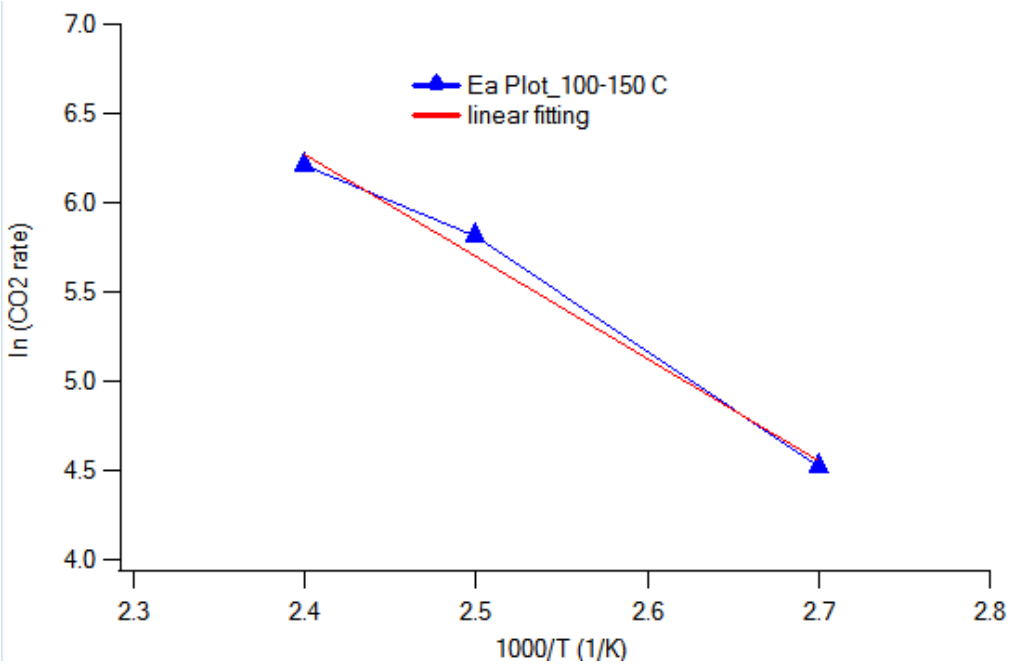

Figure 6.10: Activation energy calculation for CO_2 formation on 2 ML Pt from 100-150 ℃, single-pass mode, 94 sccm.

6.4 Conclusions

Onset time is required for methanol oxidation on Pt/TiO_2, which is attributed to the accumulation of atomic oxygen on surface for reaction. Pt sites are the active sites for methanol oxidation, while Re clusters on TiO_2 are inactive for methanol oxidation and can block the active sites for Pt. Under these experimental conditions, at 60-80 ℃ the 2 ML Pt/TiO_2 is less active than clean Pt foil, at 100 ℃ the total formation rate is comparable for both surfaces, but at 130-150 ℃ it is much more active than clean Pt foil. For CO_2 formation, the activation energy observed on 2 ML Pt/TiO_2 is much higher than Pt foil. Surface Re is unstable due to the formation and subsequent sublimation of Re_2O_7 during methanol oxidation conditions.

Acknowledgements

Thanks to Amy Brandt and Thathsara Maddumapatabandi for the preparation and XPS characterizations of the TiO_2 supported Pt and Pt-Re catalysts in ultrahigh vacuum.

6.5 References

(1) Yu, W.; Porosoff, M. D.; Chen, J. G., Review of Pt-Based Bimetallic Catalysis: From Model Surfaces to Supported Catalysts. *Chemical Reviews* **2012,** 112 (11), 5780-5817.

(2) Ananthan, S. A.; Narayanan, V.; Suresh, R.; Giribabu, K., Preparation and Characterization of Pt Based Mono and Bimetallic Nano Catalysis and Their Application of Citral Hydrogenation. *Asian Journal of Chemistry* **2012,** 24 (12), 5525-5529.

(3) Xiao, J.; Puddephatt, R. J., Pt-Re clusters and bimetallic catalysts. *Coordination Chemistry Reviews* **1995,** 143, 457-500.

(4) Kluksdahl, H. E. Reforming a sulfur-free naphtha with a platinum-rhenium catalyst. US Patent 3415737, 1968.

(5) Kelley, M. J.; Freed, R. L.; Swartzfager, D. G., Distribution of Pt and Re in Pt-Re:Al_2O_3 naphtha reforming catalysts. *Journal of Catalysis* **1982,** 78 (2), 445-453.

(6) Mon, E.; Baird, W. C., Reforming using a Pt/Re catalyst. Google Patents: 1996.

(7) D'Ippolito, S. A.; Vera, C. R.; Epron, F.; Samoila, P.; Especel, C.; Marécot, P.; Gutierrez, L. B.; Pieck, C. L., Catalytic Properties of Pt−Re/Al_2O_3 Naphtha-Reforming Catalysts Modified by Germanium Introduced by Redox Reaction at Different pH Values. *Industrial & Engineering Chemistry Research* **2009,** 48 (8), 3771-3778.

(8) Sánchez, M. A.; Mazzieri, V. A.; Grau, J. M.; Yori, J. C.; Pieck, C. L., Catalytic activity of Pt-Re-Pb/Al_2O_3 naphtha reforming catalysts. *Journal of Chemical Technology & Biotechnology* **2011,** 86 (9), 1198-1204.

(9) Viswanadham, N.; Kamble, R.; Sharma, A.; Kumar, M.; Saxena, A. K., Effect of Re on product yields and deactivation patterns of naphtha reforming catalyst. *Journal of Molecular Catalysis A: Chemical* **2008,** 282 (1–2), 74-79.

(10) Baghalha, M.; Mohammadi, M.; Ghorbanpour, A., Coke deposition mechanism on the pores of a commercial Pt–Re/γ-Al_2O_3 naphtha reforming catalyst. *Fuel Processing Technology* **2010,** 91 (7), 714-722.

(11) Turaga, U. T.; Ramanathan, R., Catalytic Naphtha Reforming: Revisiting its Importance in the modern Refinery. *Journal of Scientific & Industrial Research* **2003** 62, 963-978.

(12) Kirilin, A. V.; Tokarev, A. V.; Manyar, H.; Hardacre, C.; Salmi, T.; Mikkola, J. P.; Murzin, D. Y., Aqueous phase reforming of xylitol over Pt-Re bimetallic catalyst: Effect of the Re addition. *Catalysis Today* **2014,** 223, 97-107.

(13) Zhang, L.; Karim, A. M.; Engelhard, M. H.; Wei, Z.; King, D. L.; Wang, Y., Correlation of Pt–Re surface properties with reaction pathways for the aqueous-phase reforming of glycerol. *Journal of Catalysis* **2012,** 287, 37-43.

(14) Simonetti, D. A.; Kunkes, E. L.; Dumesic, J. A., Gas-phase conversion of glycerol to synthesis gas over carbon-supported platinum and platinum–rhenium catalysts. *Journal of Catalysis* **2007,** 247 (2), 298-306.

(15) Ciftci, A.; Ligthart, D. A. J. M.; Hensen, E. J. M., Aqueous phase reforming of glycerol over Re-promoted Pt and Rh catalysts. *Green Chemistry* **2014,** 16 (2), 853-863.

(16) Ciftci, A.; Ligthart, D. A. J. M.; Sen, A. O.; van Hoof, A. J. F.; Friedrich, H.; Hensen, E. J. M., Pt-Re synergy in aqueous-phase reforming of glycerol and the water–gas shift reaction. *Journal of Catalysis* **2014,** 311, 88-101.

(17) Azzam, K. G.; Babich, I. V.; Seshan, K.; Lefferts, L., Role of Re in Pt–Re/TiO_2 catalyst for water gas shift reaction: A mechanistic and kinetic study. *Applied Catalysis B: Environmental* **2008,** 80 (1–2), 129-140.

(18) Azzam, K. G.; Babich, I. V.; Seshan, K.; Mojet, B. L.; Lefferts, L., Stable and Efficient Pt–Re/TiO_2 catalysts for Water-Gas-Shift: On the Effect of Rhenium. *ChemCatChem* **2013,** 5 (2), 557-564.

(19) Galhenage, R. P.; Xie, K.; Yan, H.; Seuser, G. S.; Chen, D. A., Understanding the Growth, Chemical Activity, and Cluster–Support Interactions for Pt–Re Bimetallic Clusters on TiO_2(110). *The Journal of Physical Chemistry C* **2016,** 120 (20), 10866-10878.

(20) Park, E. D.; Lee, D.; Lee, H. C., Recent progress in selective CO removal in a H-2-rich stream. *Catalysis Today* **2009,** 139 (4), 280-290.

(21) Lin, Y.-C.; Hohn, K. L.; Stagg-Williams, S. M., Hydrogen generation from methanol oxidation on supported Cu and Pt catalysts: Effects of active phases and supports. *Applied Catalysis A: General* **2007,** 327 (2), 164-172.

(22) Huang, T.; Mao, S.; Zhou, G.; Zhang, Z.; Wen, Z.; Huang, X.; Ci, S.; Chen, J., A high-performance catalyst support for methanol oxidation with graphene and vanadium carbonitride. *Nanoscale* **2015,** 7 (4), 1301-1307.

(23) Yung, T.-Y.; Lee, J.-Y.; Liu, L.-K., Nanocomposite for methanol oxidation: synthesis and characterization of cubic Pt nanoparticles on graphene sheets. *Science and Technology of Advanced Materials* **2013,** 14 (3), 035001.

(24) Firth, J. G., Catalytic oxidation of methanol over platinum. *Transactions of the Faraday Society* **1971,** 67 (0), 212-215.

(25) Gentry, S. J.; Jones, A.; Walsh, P. T., Kinetics of methanol oxidation over platinum wire catalysts. *Journal of the Chemical Society, Faraday Transactions 1: Physical Chemistry in Condensed Phases* **1980,** 76 (0), 2084-2095.

(26) McCabe, R. W.; McCready, D. F., Kinetics and reaction pathways of methanol oxidation on platinum. *The Journal of Physical Chemistry* **1986,** 90 (7), 1428-1435.

(27) Sexton, B. A., Methanol decomposition on platinum (111). *Surface Science* **1981,** 102 (1), 271-281.

(28) Endo, M.; Matsumoto, T.; Kubota, J.; Domen, K.; Hirose, C., In Situ IRAS Observation of Catalytic Deep Oxidation of Methanol on Pt(111) under Ambient Pressure Conditions. *The Journal of Physical Chemistry B* **2001,** 105 (8), 1573-1577.

(29) Miller, A. V.; Kaichev, V. V.; Prosvirin, I. P.; Bukhtiyarov, V. I., Mechanistic Study of Methanol Decomposition and Oxidation on Pt(111). *The Journal of Physical Chemistry C* **2013,** 117 (16), 8189-8197.

(30) Duke, A. S.; Galhenage, R. P.; Tenney, S. A.; Ammal, S. C.; Heyden, A.; Sutter, P.; Chen, D. A., In Situ Ambient Pressure X-ray Photoelectron Spectroscopy Studies of Methanol Oxidation on Pt(111) and Pt–Re Alloys. *The Journal of Physical Chemistry C* **2015,** 119 (40), 23082-23093.

(31) Jiang, C. J.; Trimm, D. L.; Wainwright, M. S.; Cant, N. W., Kinetic study of steam reforming of methanol over copper-based catalysts. *Applied Catalysis A: General* **1993,** 93 (2), 245-255.

(32) Ito, S.-i.; Suwa, Y.; Kondo, S.; Kameoka, S.; Tomishige, K.; Kunimori, K., Steam reforming of methanol over Pt–Zn alloy catalyst supported on carbon black. *Catalysis Communications* **2003,** 4 (10), 499-503.

(33) Lee, J. K.; Ko, J. B.; Kim, D. H., Methanol steam reforming over $Cu/ZnO/Al_2O_3$ catalyst: kinetics and effectiveness factor. *Applied Catalysis A: General* **2004,** 278 (1), 25-35.

(34) Kulprathipanja, A.; Falconer, J. L., Partial oxidation of methanol for hydrogen production using ITO/Al_2O_3 nanoparticle catalysts. *Applied Catalysis A: General* **2004,** 261 (1), 77-86.

(35) Chang, C.-C.; Chang, C.-T.; Chiang, S.-J.; Liaw, B.-J.; Chen, Y.-Z., Oxidative steam reforming of methanol over $CuO/ZnO/CeO_2/ZrO_2/Al_2O_3$ catalysts. *International Journal of Hydrogen Energy* **2010,** 35 (15), 7675-7683.

(36) Chang, C.-C.; Hsu, C.-C.; Chang, C.-T.; Chen, Y.-P.; Liaw, B.-J.; Chen, Y.-Z., Effect of noble metal on oxidative steam reforming of methanol over $CuO/ZnO/Al_2O_3$ catalysts. *International Journal of Hydrogen Energy* **2012,** 37 (15), 11176-11184.

(37) Tenney, S. A.; Xie, K.; Monnier, J. R.; Rodriguez, A.; Galhenage, R. P.; Duke, A. S.; Chen, D. A., Novel recirculating loop reactor for studies on model catalysts: CO oxidation on $Pt/TiO_2(110)$. *Review of Scientific Instruments* **2013,** 84 (10), 104101.

(38) Duke, A. S. *From Model System to Real Catalysts: Bridging the Pressure and Materials Gaps (Doctoral dissertation).* University of South Carolina, Columbia, **2016**.

(39) Duke, A. S.; Xie, K.; Monnier, J. R.; Chen, D. A., Superior Long-Term Activity for a Pt-Re Alloy Compared to Pt in Methanol Oxidation Reactions. **submitted**

(40) Burch, R., The Oxidation State of Rhenium and Its Role in Platinum-Rhenium Reforming Catalysts. *Platinum Metals Review* **1978,** 22 (2), 57-60.

(41) Björneholm, O.; Nilsson, A.; Tillborg, H.; Bennich, P.; Sandell, A.; Hernnäs, B.; Puglia, C.; Mårtensson, N., Overlayer structure from adsorbate and substrate core

level binding energy shifts: CO, CCH_3 and O on Pt(111). *Surface Science* **1994,** 315 (1–2), L983-L989.

(42) Ramstad, A.; Strisland, F.; Raaen, S.; Worren, T.; Borg, A.; Berg, C., Growth and alloy formation studied by photoelectron spectroscopy and STM. *Surface Science* **1999,** 425 (1), 57-67.

APPENDIX A TEMPERATURE PROGRAMMED DESORPTION STUDY OF METHANOL ON PT-RE CLUSTERS SUPPORTED ON TiO_2

Summary

In this section, the temperature programmed desorption (TPD) study of methanol on Pt, Re and Pt-Re clusters supported on TiO_2 (110) was conducted in order to understand the sites of Pt-Re clusters and the role titania support might play. The representative mass fractions (CO, H_2, CH_4 and H_2O) were collected by a mass spectrometer during TPD. Post-TPD AES was also recorded and served as supplementary information to confirm metal coverage and probe surface composition.

Experimental setup

The preparation of Pt, Re and Pt-Re bimetallic clusters supported on TiO_2 were done in a UHV chamber (base pressure ~$1.0x10^{-10}$ Torr), which has been described elsewhere [1, 2]. This rutile TiO_2 (110) single crystal support was cleaned by a number of cycles of sputter (Ar^+, 1000 V, 3.0μA, twenty minutes) and anneal (960 K, three minutes). The surface structure of TiO_2 is confirmed by LEED; the cleanness was verified by AES.

For every experiment, after the last sputter and anneal cycle, the clean TiO_2 was cooled to ~100 K with liquid nitrogen, followed by flashing to 960 K to further remove adsorbates from chamber background. After this cool-flash –cool procedure, the surface was maintained at room temperature during vapor deposition of metal clusters, which was achieved by heating via a filament behind the crystal. Pt clusters were deposited from a homemade source consisting of Pt wire (ESPI, 0.25 mm diameter, 99.999%)

wrapped around a tungsten wire (0.50 mm) through which current was passed. The Pt flux (0.06-0.08 ML/min) was calibrated with a QCM before each deposition. The definition of ML is same as previously mentioned. Re clusters were deposited from a Re rod (ESPI, 1.6 mm diameter, 99.99%), with an Omicron electron beam evaporator (EFM3). The internal flux monitor of the evaporator was used to control Re flux (0.02 ML/min), which was initially calibrated with a QCM. After metal deposition, sample surface was exposed to methanol (Fisher Scientific, 99.9%) via a stainless steel directed dosing tube. The fresh methanol was purified by three freeze-pump-thaw cycles. During methanol dosing, the surface was held at ~100 K. Saturation exposures of methanol were determined from the appearance of the methanol multilayer peak in the TPD data.

For each TPD experiment, the surface of crystal was positioned ~3 mm in front of a 4 mm diameter hole cut in the shroud of the mass spectrometer in order to prevent detection of products desorbing from the sample holder. The sample was biased at -100 V during TPD experiments to prevent damage from the electrons emitted by the mass spectrometer filament. The sample was heated by the filament in the back and the ramping rate was kept at 2 K/s from 100 K to 950 K, controlled by programmable power supply. Nine masses were collected in a typical TPD experiment. Wide mass scan experiments (40 channels for 26-66 amu and 66-106 amu) were also conducted to check for additional products if possible. No significant amount of carbon was detected on the surface in post-TPD Auger experiments after methanol adsorption/reaction. The mass fractions of products (CO, H_2, CH_4 and H_2O) were collected. For isotope labeled experiment, the crystal was exposed to 1×10^{-7} Torr of $^{18}O_2$ at 800 K for 5 min via directed dosing, while ^{18}O related mass fractions were also monitored.

Result and Discussions

Methanol desorption on pure Pt/TiO_2

Figure A.1 shows the 28 amu (CO) desorption profile from different coverage (0.13-4.0 ML) of Pt clusters supported onTiO_2 (110) during methanol TPD from 100 K to 960 K. As expected, there is no CO peak from clean TiO_2 support after desorption of physically adsorbed methanol layers at ~100 K. For Pt on TiO_2, there is one major CO peak observed at ~480 K. The methanol desorption behavior on 2 ML Pt/TiO_2 surface was compared to that of CO on the same surface, as shown in Figure A.13. In CO-TPD experiments, the higher temperature peak at ~500 K was attributed to the CO molecules desorbed from step edge sites of Pt [2], while the major peak at ~400 K should correspond to normal terrace Pt sites. In MeOH-TPD experiment, only one peak (~ 500 K) was observed on pure Pt clusters. This can be explained by the coverage effect, and the step edge sites of Pt are preferred to be filled than terrace sites. The measured CO peak area from MeOH-TPD on 2 ML Pt/TiO_2 is less than half of that from CO-TPD, since CO is a much smaller molecule than methanol.

The integrated CO desorption peaks area from MeOH TPD on 0.13, 0.25, 0.50, 1.0, 2.0 and 4.0 ML Pt/TiO_2 are shown in Figure A.14. The integrated CO peak area does not increase much when the Pt coverage is increased from 0.25 ML to 0.50 ML, while it is greatly enhanced from 0.50 ML Pt to 1.0 ML Pt. For CO desorption on 1 ML Pt and 2 ML Pt, the CO area looks almost identical. Adding another 2 ML Pt cluster on top of 2 ML Pt (4 ML Pt in total) only increased the CO peak signal by ~10% compared to 2 ML Pt, suggesting that for methanol adsorption, Pt sites are nearly saturated on 2 ML Pt. This trend curve for MeOH TPD experiments is significantly different from that for CO TPD

ones, which are shown in Figure A.15. The Pt sites for CO adsorption still increased significantly from 2 ML Pt to 4 ML Pt on TiO_2.

Figure A.2 shows the 2 amu (H_2) desorption signal from methanol TPD on different coverage (0.13-4.0 ML) of Pt clusters on TiO_2. There is no hydrogen desorption peak from clean TiO_2 surface. On 0.13 ML Pt, we saw a primary peak located at ~480 K and another peak at ~280 K with much less intensity. This observation is consistent with the study by Wang et al. on the Pt(110)-(1x1) surface, although their reported second peak position is much lower (430~450 K) [3]. When the Pt coverage increases to 0.25 ML and above, the 280 K peak becomes the main peak; its intensity increases with Pt coverage, and can be regarded as a characteristic H_2 desorption peak on Pt. The intensity of the second peak is maximized on 0.25 ML Pt, and it does not increase when the Pt coverage ranges from 0.50 ML to 4.0 ML, suggesting those sites must be related to the interface of Pt and TiO_2 support.

The 16 amu (CH_4) desorption signal from methanol TPD on the Pt clusters is shown in Figure A.3. On clean TiO_2 there is a small and broad 16 amu signal. On pure Pt/TiO_2, the biggest CH_4 desorption peak is observed on 0.25 ML Pt, and 0.13 ML Pt surface also generates a large amount of methane. The CH_4 yield on 0.50 ML Pt is much less than 0.25 ML Pt. When the Pt coverage was increased from 0.50 ML to 4 ML, there is no significant change for methane product. Therefore it is also proposed that CH_4 is generated from interface of Pt and TiO_2. When a lower coverage of Pt (<0.25 ML) was dosed on TiO_2, smaller clusters are formed and more Pt-TiO_2 interface sites are present. When more Pt is dosed, the size of Pt clusters increases and there is less such interface sites available.

Methanol desorption on pure Re/TiO_2

Figure A.4 shows the 28 amu (CO) desorption profile from different coverages (0.11-3.5 ML) of Re clusters supported on same TiO_2 (110) support during methanol TPD experiments. Two peaks were observed on Re/TiO_2: the lower temperature peak (430 K) corresponds to the CO molecule desorption peak on Re, and the higher temperature figure (~900 K) is a recombinant peak from dissociated carbon and surface oxygen. It is a characteristic CO desorption peak from reaction on Re, since Pt is not able to dissociate C-O bond hence no such recombinant peak is observed on Pt. Re clusters can be covered by the TiO_2 support so for lower coverages of Re, the Re might exist as ReO_x on TiO_2 [2] and the CO molecule desorption peak looks similar for 0.11 ML Re and 0.22 ML Re. The position of CO molecule desorption peak shifts to lower temperature when the Re coverage increases from 0.11 ML to 3.5 ML, while the recombination peak shifts to higher temperature with increasing Re coverage. Therefore on higher Re coverages, the baseline for the higher temperature peak did not return to zero at the end of the temperature ramp to 960 K.

The integrated CO desorption peaks areas from MeOH TPD on 0.11, 0.22, 0.43, 0.87, 1.70 and 3.5 ML Re/TiO_2 are shown in Figure A.16. Re sites increased significantly from 0.11 ML to 1.7 ML, but there is only a 10% increase from 1.7 ML to 3.5 ML. As a comparison, the integrated CO peaks from CO TPD on 0.11-1.7 ML Re are shown in Figure A.17. The result: on same Re/TiO_2 surface, more CO adsorption can be achieved on Re than methanol adsorption, since CO is a much smaller molecule than methanol.

Figure A.5 shows the 2 amu (H_2) desorption profile from different coverage (0.11-3.5 ML) of Re clusters supported on TiO_2 (110) during methanol TPD. Re can be

covered by TiO_x [2], and therefore on 0.11 ML and 0.22 ML Re, the first hydrogen peak (220 K) might from surface ReO_x, and such peak is not observed on higher coverages. The peak at ~440 K gradually shifts to lower temperature when increasing the Re coverage. On 0.87-3.5 ML Re, a large desorption peak was observed at ~340 K, which is 60 K higher than methanol on Pt clusters (~280 K).

Figure A.6 presents the 16 amu (CH_4) desorption signal from 0.11 to 3.50 ML Re clusters on TiO_2. On pure Re/TiO_2, the biggest CH_4 desorption peak was observed on 0.25 ML Re and 0.13 ML Re, which is consistent with Pt's case. The CH_4 yield on 0.50 ML Re and higher coverages is much less than 0.25 ML Pt, and therefore it is believed that CH_4 is generated from interface of Re-TiO_2 interfacial sites.

Methanol desorption on 2 ML Pt +1.7 Re and 1.7 ML Re+2 ML Pt/TiO_2

The CO (28 amu) desorption profiles on 2 ML Pt, 1.7 ML Re, 2 ML Pt+1.7 ML Re and 1.7 ML Re+2 ML Pt/TiO_2 from methanol TPD are shown in Figure A.7. The dashed lines presented are the CO desorption profile from CO TPD on various surfaces. For 28 amu desorption signal on 2 ML Pt surface, the difference between CO TPD and MeOH TPD has been described in Figure A.13 previously. As for the molecule desorption peak (~500 K) on each surface, the total CO signal of methanol TPD experiment is much less than that of CO TPD case, and the peak onset is at a higher temperature. The recombinant CO peak is absent for the 1.7 ML Re+2 ML Pt surface, since the initially deposited Re is totally covered by deposited Pt, and the surface is 100% Pt. For recombinant peak on Re and Pt+Re bimetallic surfaces, the peak intensity is similar for MeOH TPD and CO TPD.

The normalized integrated CO areas on 2 ML Pt+1.7 ML Re, 2 ML Pt, 1.7 ML Re+2 ML Pt and 1.7 ML Re onTiO_2 from methanol experiments are shown in Figure A.17; values are normalized to that of 2 ML Pt. The results for CO TPD are shown in Figure A.18. For MeOH TPD, the total number of sites on 2 ML Re is similar to that on Pt; 1.7 ML Re+2 ML Pt surface has ~36% fewer sites than 2 ML Pt or 2 ML Re, and 2 ML Pt+1.7 ML Re has ~27% more sites than 2 ML Pt. These results are different from the CO TPD experiments, where the number of 2 ML Re sites is ~58% of that on 2 ML Pt, and the sites on 1.7 ML Re+2 ML Pt are ~19% less than 2 ML Pt. The 2 ML Pt+1.7 ML Re surface has the most CO sites: it is ~18% more than 2 ML Pt for CO TPD.

The H_2 (2 amu) desorption profiles for methanol TPD on 2 ML Pt, 1.7 ML Re, 2 ML Pt+1.7 ML Re and 1.7 ML Re+2 ML Pt on TiO_2 are shown in Figure A.8. On 1.7 ML Re+2 ML Pt, there is also less H_2 desorption compared to 2 ML Pt. A new peak at ~200 K was seen on 2 ML Pt + 1.7 ML Re, which is not observed on either 2 ML Pt or 2 ML Re surface, and it is also absent on 1.7 ML Re+2 ML Pt surface. This peak is attributed to reaction on Pt-Re bimetallic sites.

The CH_4 (16 amu) desorption profiles on those four surfaces are shown in Figure A.9. The peak position for 2 ML Pt is different from the other three, and appears at a higher temperature. There is no significant difference for the integrated areas of methane on all of the surfaces, indicating that similar metal-TiO_2 sites available.

Methanol desorption on 2 ML Pt +x ML ReTiO$_2$ set

For a more comprehensive coverage study, 2 ML Pt+x ML Re surfaces (x=0, 0.22, 0.43, 0.87 and 1.7 ML) were prepared and investigated by methanol TPD, and in Figure A.10, the CO (28 amu) desorption profiles are shown. The characteristic CO desorption

peak from Re was not observed on 2 ML Pt+0.22 ML Re, and there is only a trace of such a peak on 2 ML Pt+0.43 ML Re. When a significant amount of Re (> 0.5 ML) was dosed on 2 ML Pt, Re exists on the surface and the recombinant CO peak can be observed clearly. These results are consistent with our CO TPD experiments on the same 2 ML Pt+ x ML Re surfaces. As the Re coverage is increased from 0 to 1.7 ML, the molecular desorption peak gradually shifts from 450 K to 420 K.

The integrated CO areas from the MeOH TPD experiments are shown in Figure A.19. Adding 0.5 ML Re to 2 ML Pt increases the Pt sites that are available for CO adsorption by ~20%, and no further increase was seen when more Re is deposited. However, the situation is much difference for CO-TPD which is shown in Figure A.20.: there is no big difference for 2 ML Pt and 2 MLPt+0.87 ML Re, and a substantial increase in surface sites compared to 2 ML Pt is observed only when more than 1 ML Re is deposited on 2 ML Pt.

The H_2 (2 amu) desorption profiles for methanol TPD on 2 ML Pt+x ML Re/TiO_2 (x=0, 0.22, 0.43, 0.87 and 1.7 ML) are shown in Figure A.11. The most interesting peak is the one at 200 K. On the 2 ML Pt and 2 ML Pt+0.22 ML Re surfaces, which are nearly 100% Pt, this peak does not appear. The 200 K peak is first observed on 2 ML Pt +0.43 ML Re and the peak intensity is enhanced when more Re is dosed. This peak is attributed to reaction at Pt-Re sites since its intensity is highest when both Pt and Re atoms are at the surface.

The CH_4 (16 amu) desorption profiles for methanol TPD are shown in Figure A.12. On 2 ML Pt +x ML Re (x>=0.43) surfaces, an additional CH_4 peak is detected at ~240 K. Similar to the H_2 feature, this peak is only seen on Pt+Re, and is absent from

pure Pt, pure Re or the Re+Pt surfaces. Therefore it is believed that dosing substantial amounts of Re onto 2 ML Pt surface can form unique Pt-Re bimetallic sites which facilitate the formation of methane at a much lower temperature.

Conclusion

1. Methanol desorption behavior on Re is similar to CO desorption; the recombinant CO peak characteristic of CO dissociation on Re can be observed at ~900 K.
2. The interfacial sites of Pt-TiO_2 or Re-TiO_2 are proposed to lead the formation of methane and hydrogen at ~450 K.
3. For methanol adsorption, the 2 ML Pt +1.7 ML Re surface has more sites available for methanol adsorption than 2 ML Pt, 1.7 ML Re and 1.7 ML Re+2 ML Pt.
4. In contrast to CO TPD, the CO desorption signal from methanol TPD is similar for the 1.7 ML Re and 2 ML Pt surfaces.
5. Methanol TPD studies confirmed that the surface composition of 2 ML Pt + x ML Re/TiO_2 ($x<0.43$) is ~100% Pt.
6. When more than 0.43 ML Re is dosed on 2 ML Pt, new Pt-Re sites that facilitate hydrogen and methane production are created.

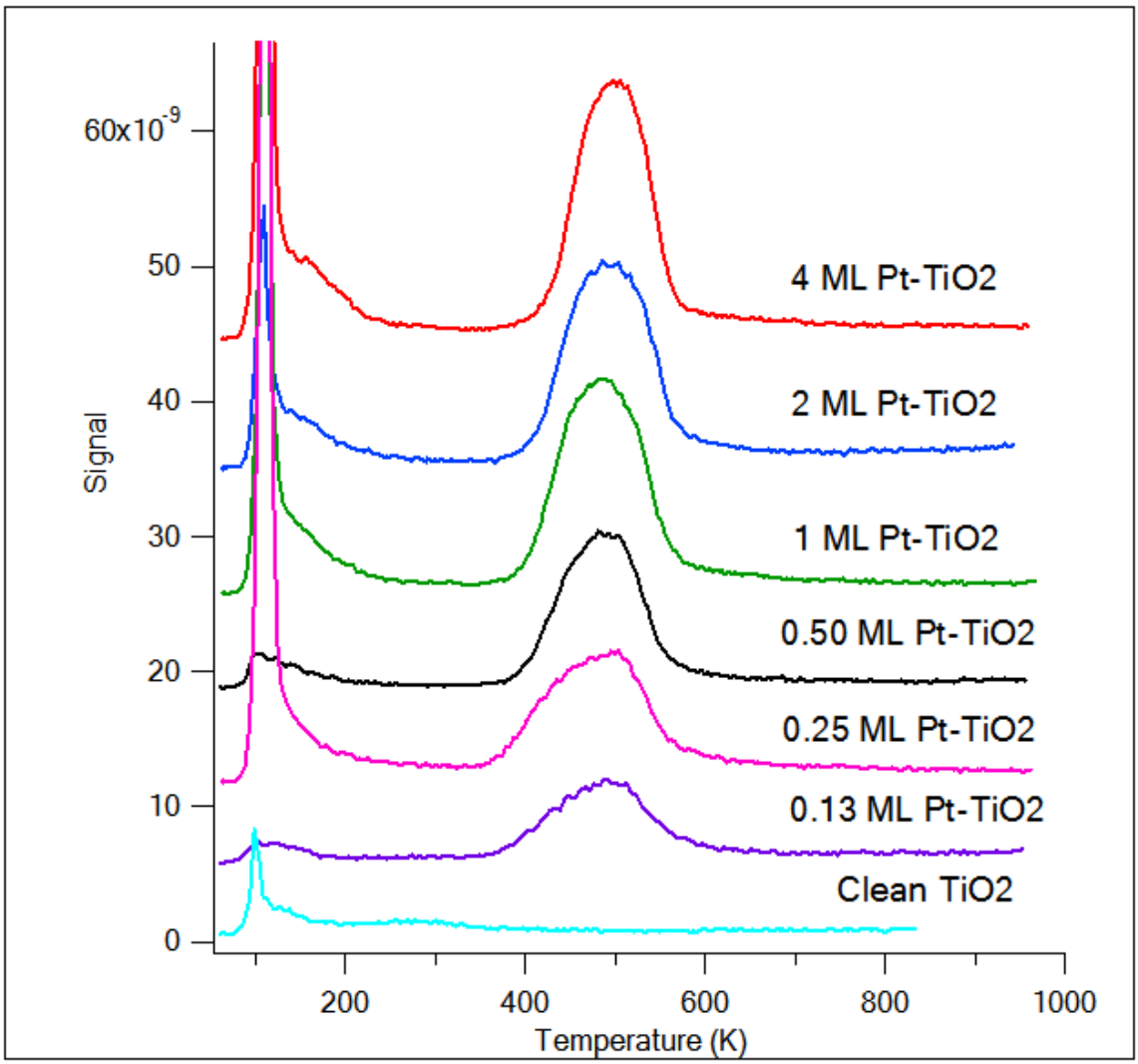

Figure A.1: MeOH TPD CO (28 amu) desorption profile on, 0.13, 0.25, 0.50, 1.0, 2.0, 4.0 ML Pt on TiO_2 and clean TiO_2

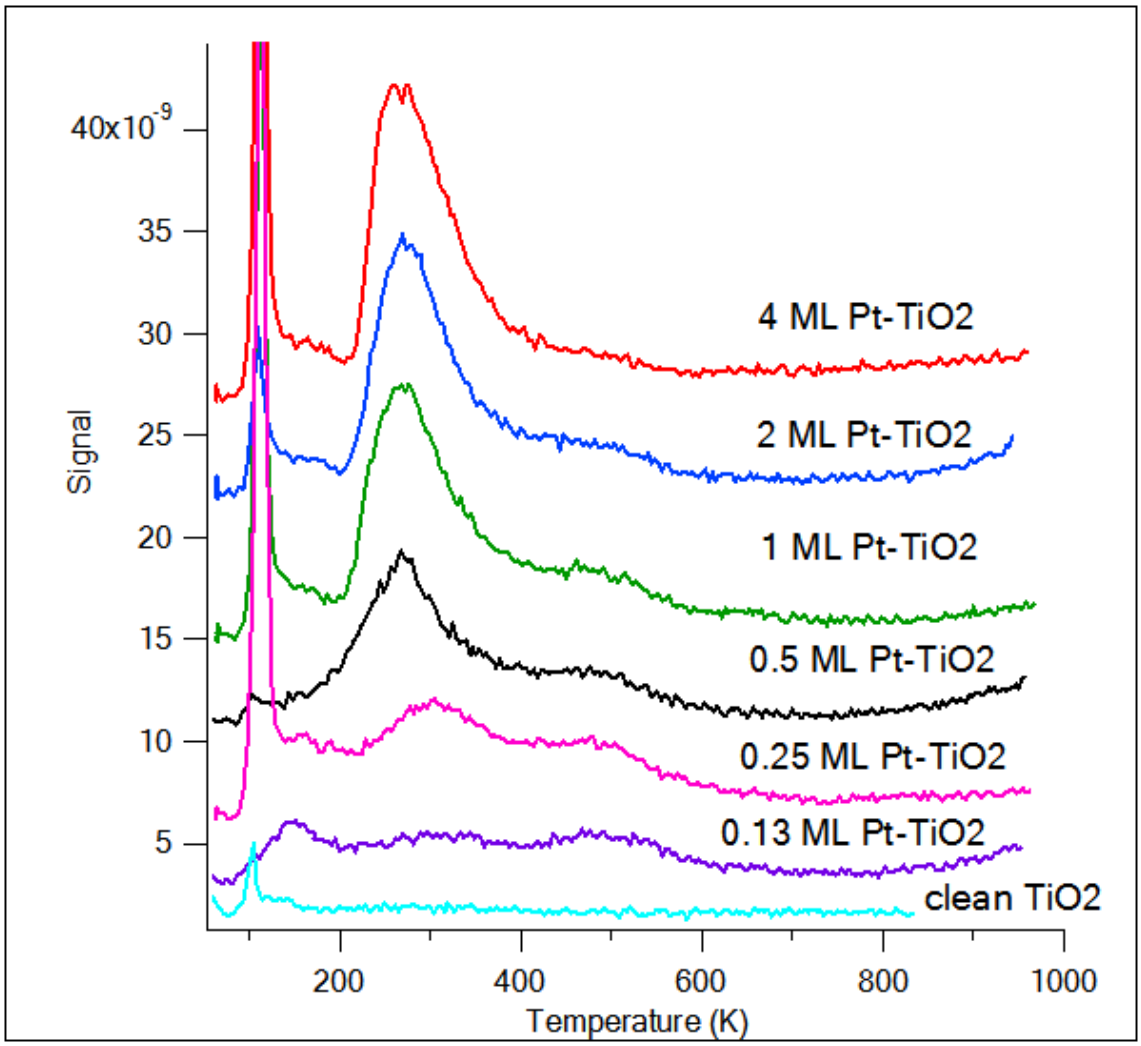

Figure A.2: MeOH TPD H_2 (2 amu) desorption profile on, 0.13, 0.25, 0.50, 1.0, 2.0, 4.0 ML Pt on TiO_2 and clean TiO_2

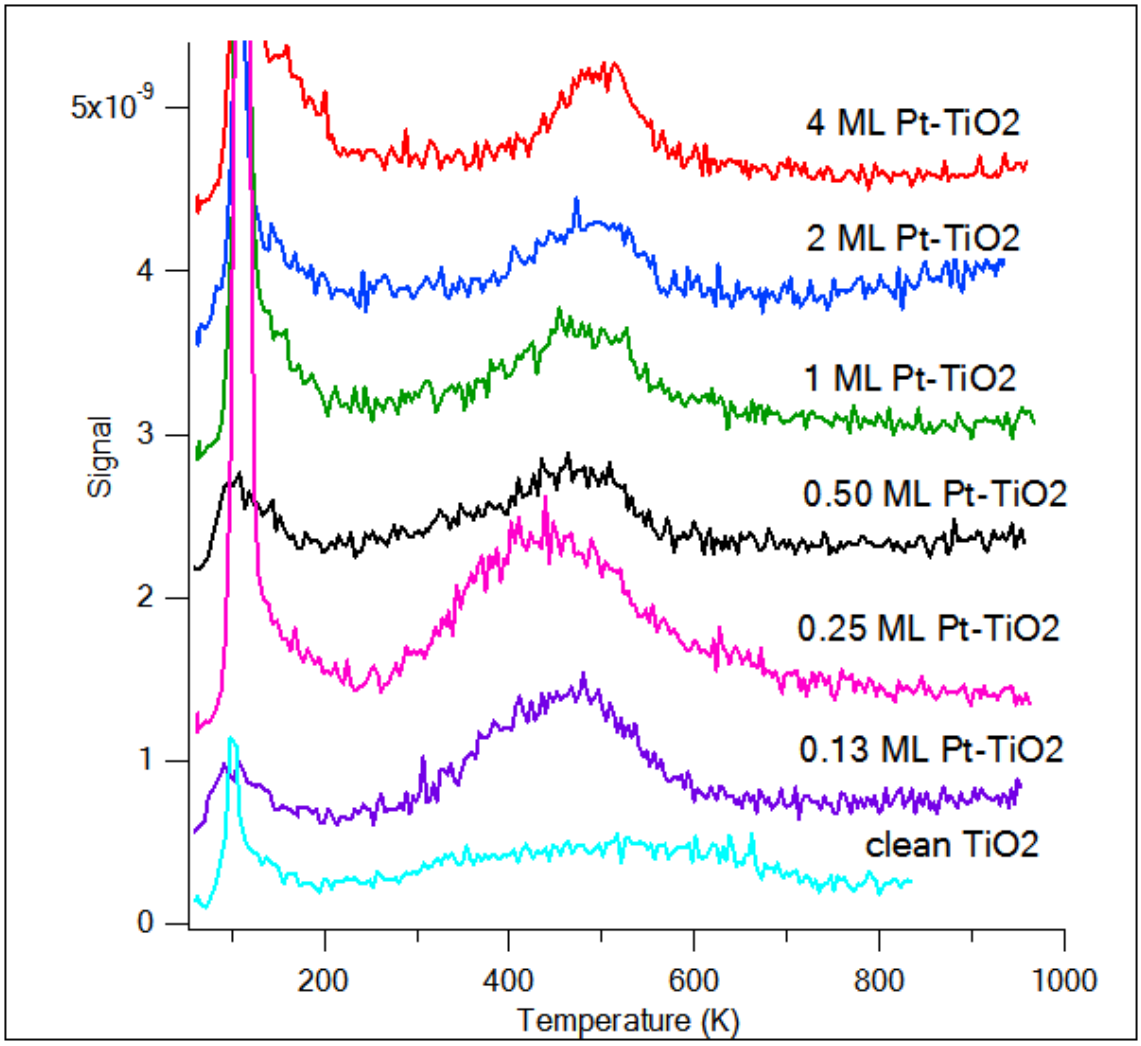

Figure A.3: MeOH TPD CH_4 (16 amu) desorption profile on, 0.13, 0.25, 0.50, 1.0, 2.0, 4.0 ML Pt on TiO_2 and clean TiO_2

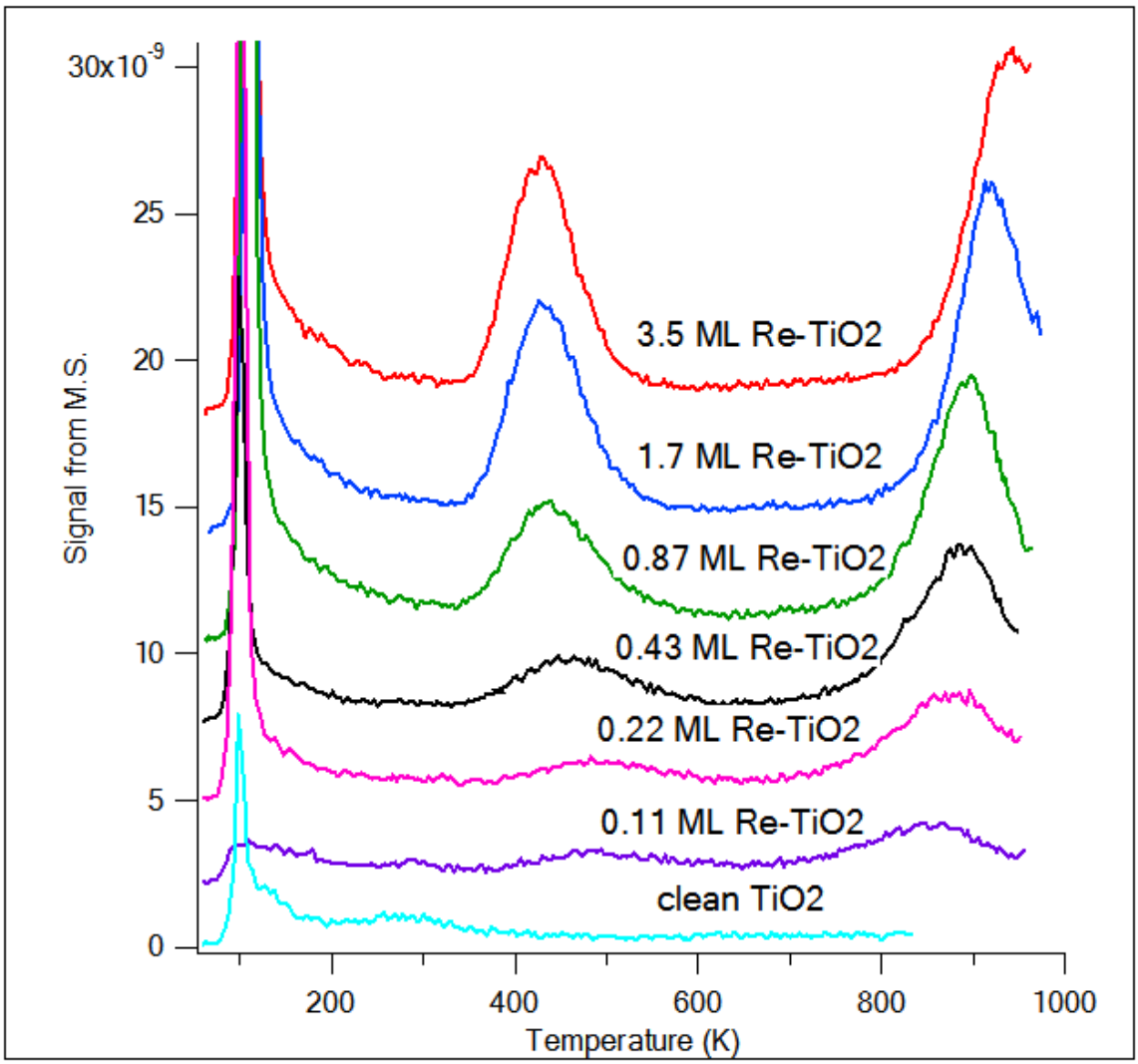

Figure A.4: MeOH TPD CO (28 amu) desorption profile on 0.11-3.5 ML Re on TiO_2

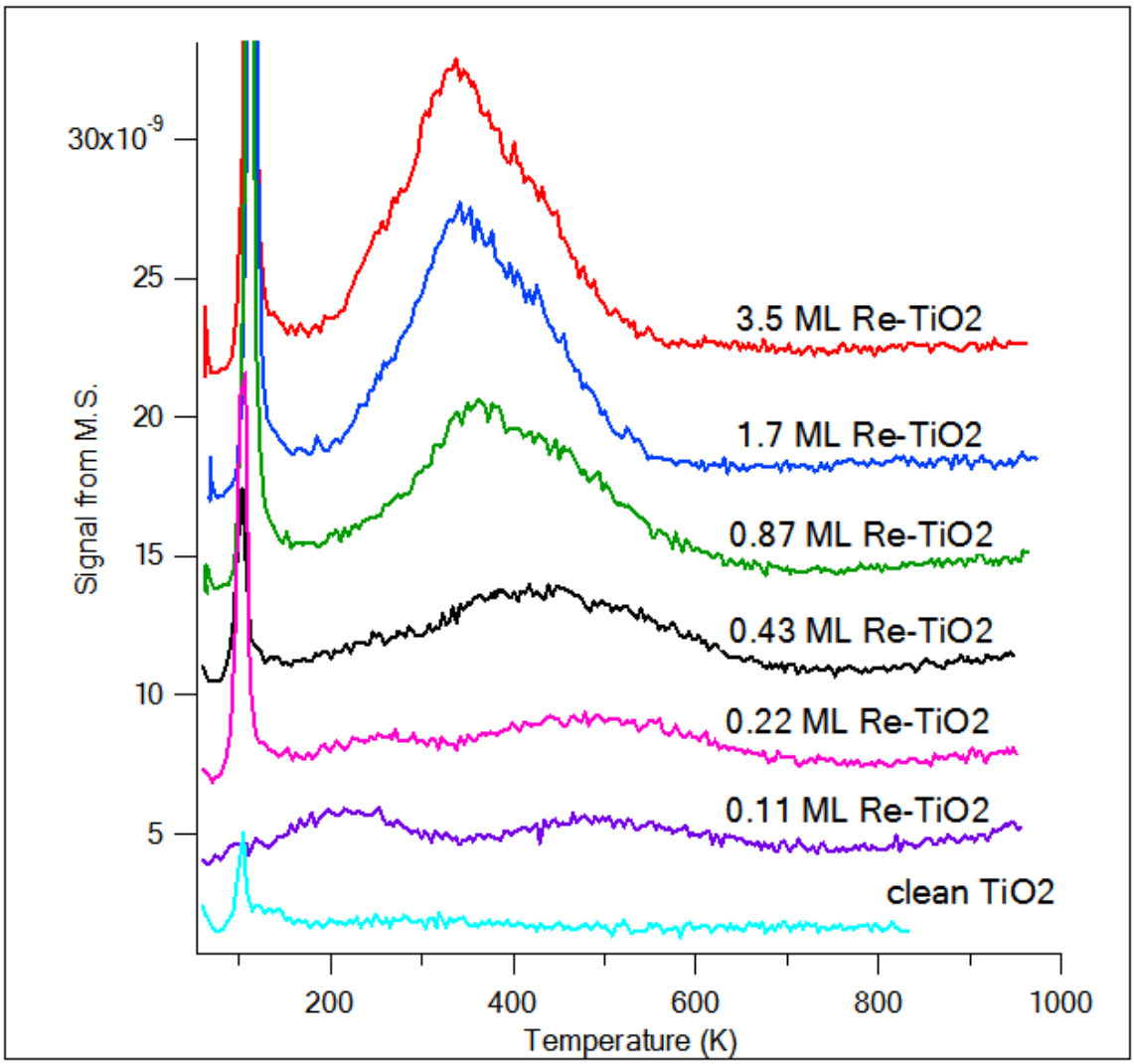

Figure A.5: MeOH TPD H_2 (2 amu) desorption profile on 0.11-3.5 ML Re on TiO_2

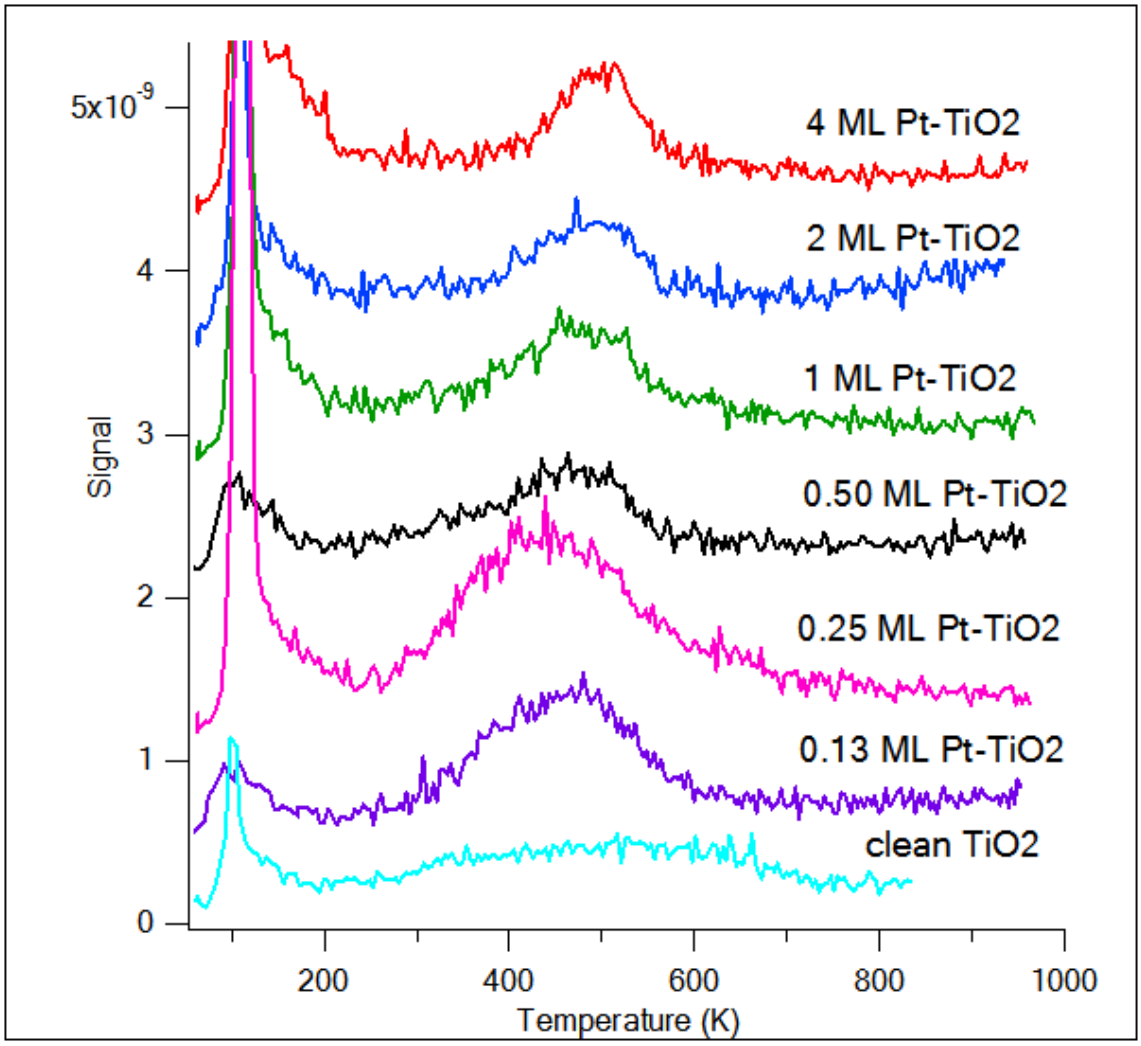

Figure A.6: MeOH TPD CH_4 (16 amu) desorption profile on 0.11-3.5 ML Re

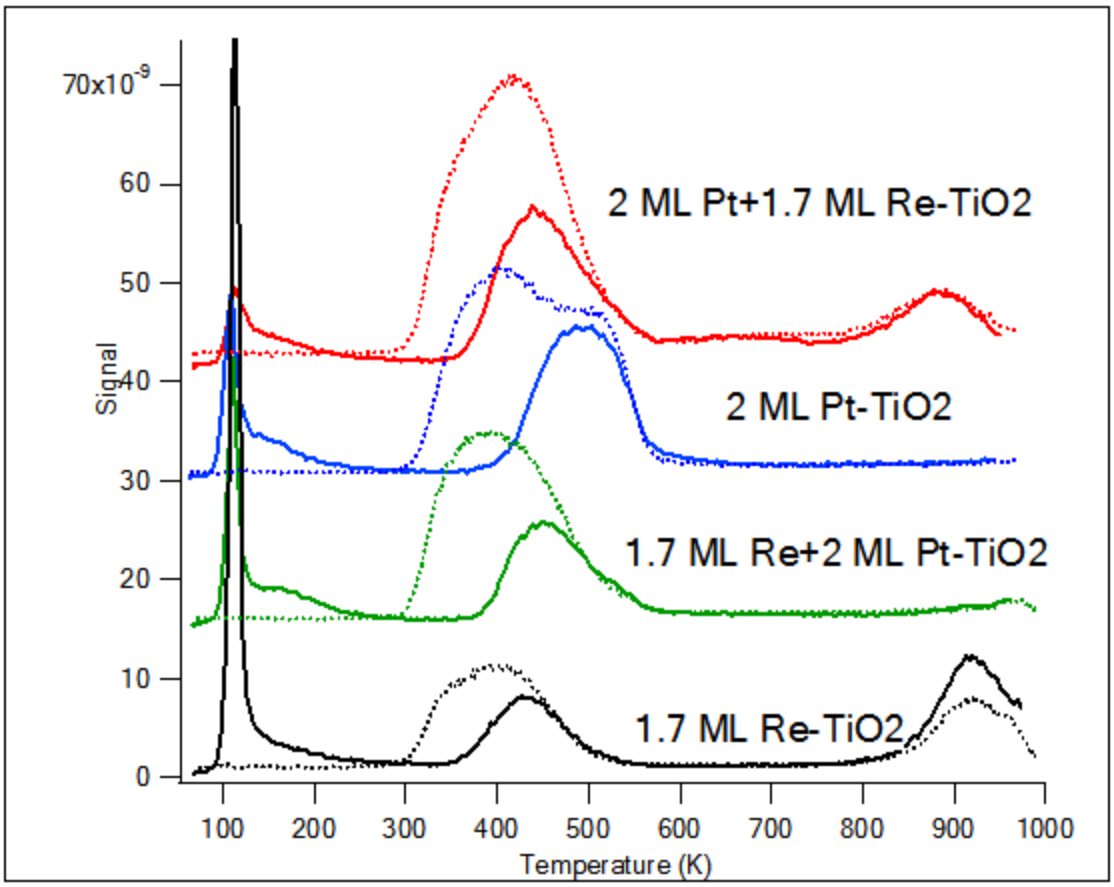

Figure A.7: MeOH TPD CO (28 amu) desorption on 2 ML Pt, 1.7 ML Re, 2 ML Pt+1.7 ML Re and 1.7 ML Re+2 ML Pt on TiO_2. The dashed line is the CO desorption profile that on same bimetallic surface.

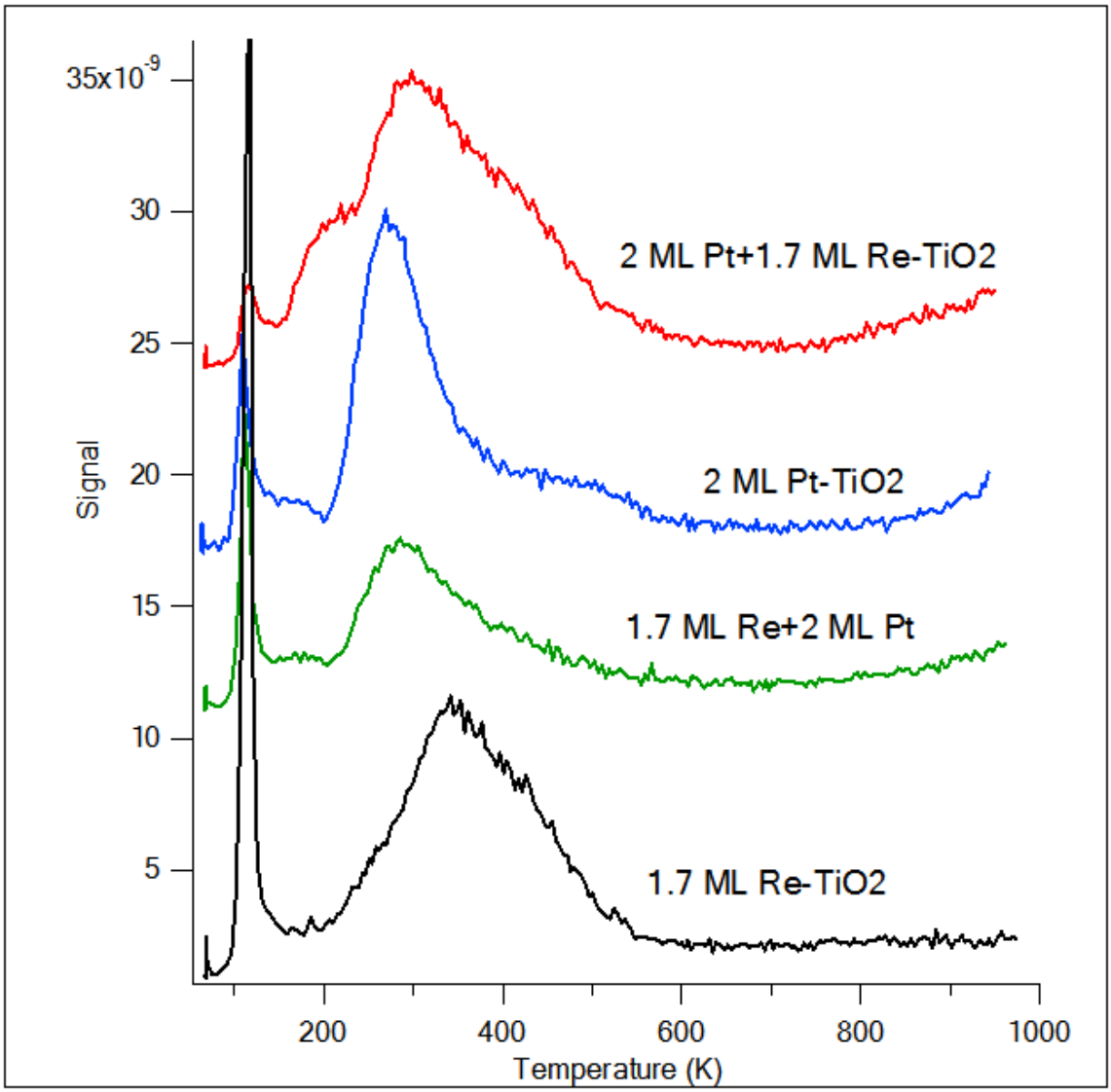

Figure A.8: MeOH TPD H_2 (2 amu) desorption on 2 ML Pt, 1.7 ML Re, 2 ML Pt+1.7 ML Re and 1.7 ML Re+2 ML Pt on TiO_2

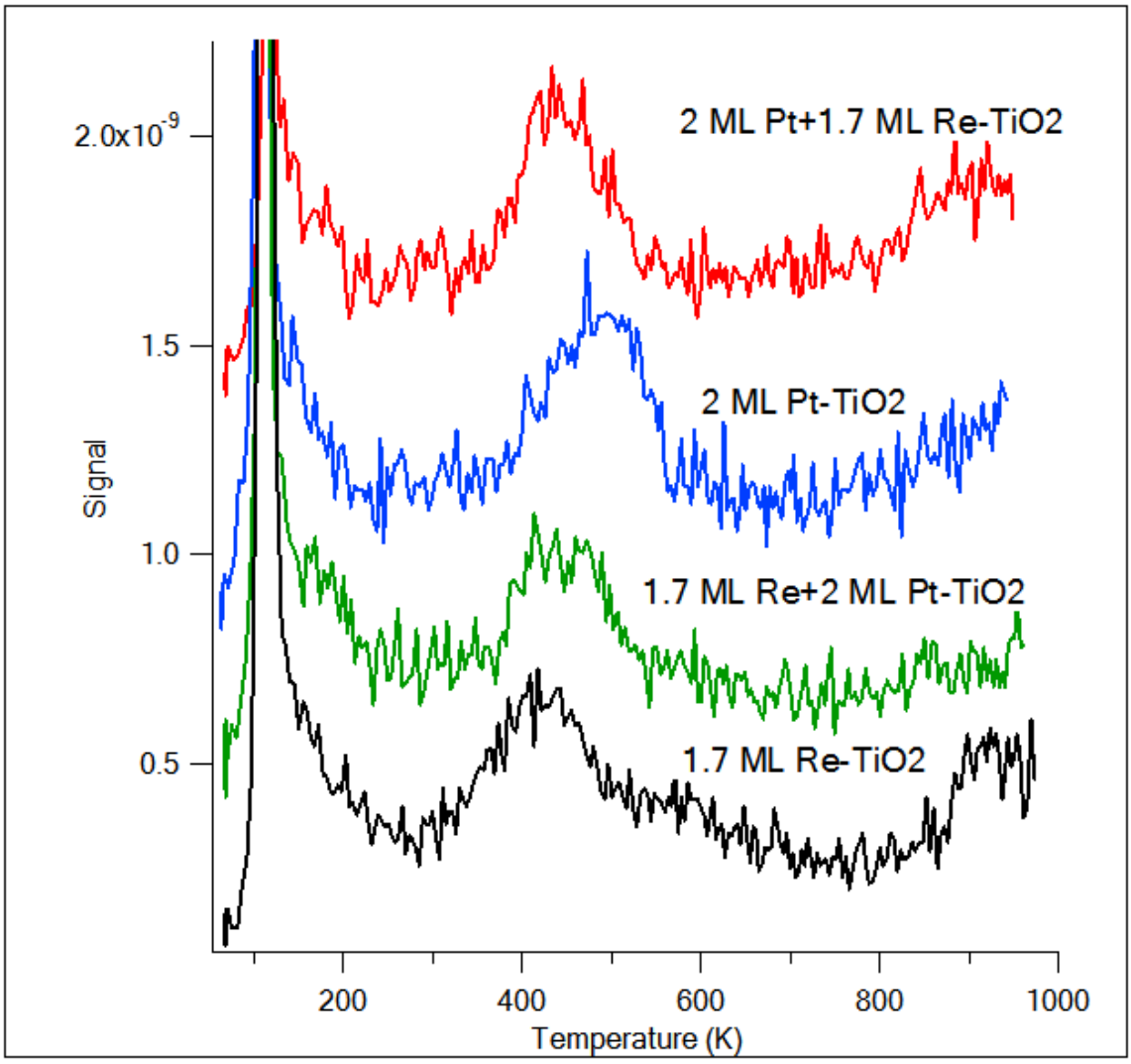

Figure A.9: MeOH TPD CH_4 (16 amu) desorption on 2 ML Pt, 1.7 ML Re, 2 ML Pt+1.7 ML Re and 1.7 ML Re+2 ML Pt on TiO_2

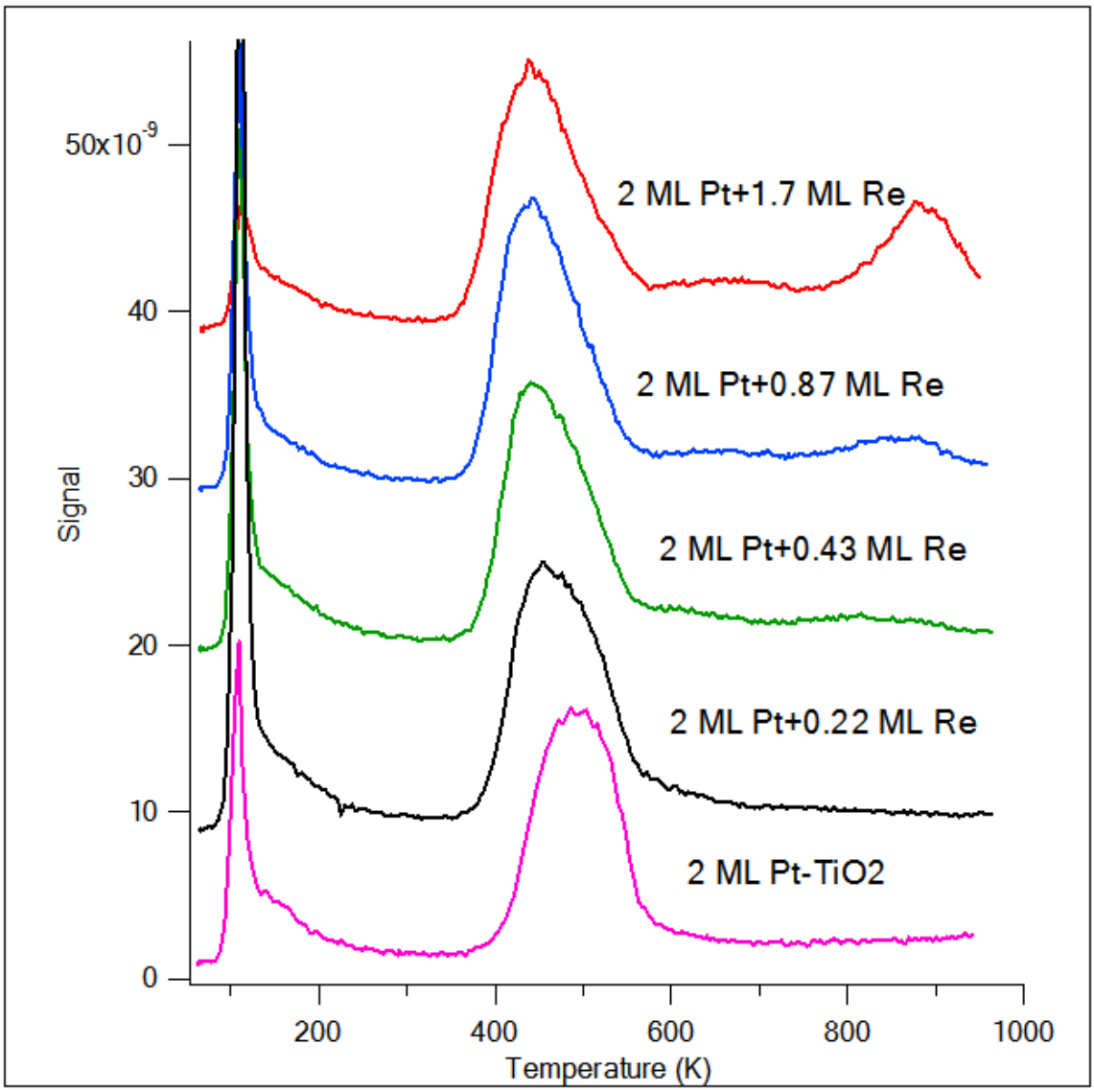

Figure A.10: MeOH TPD CO (28 amu) desorption on 2 ML Pt+x ML Re on TiO_2 where x=0, 0.22, 0.43, 0.87 and 1.7 ML.

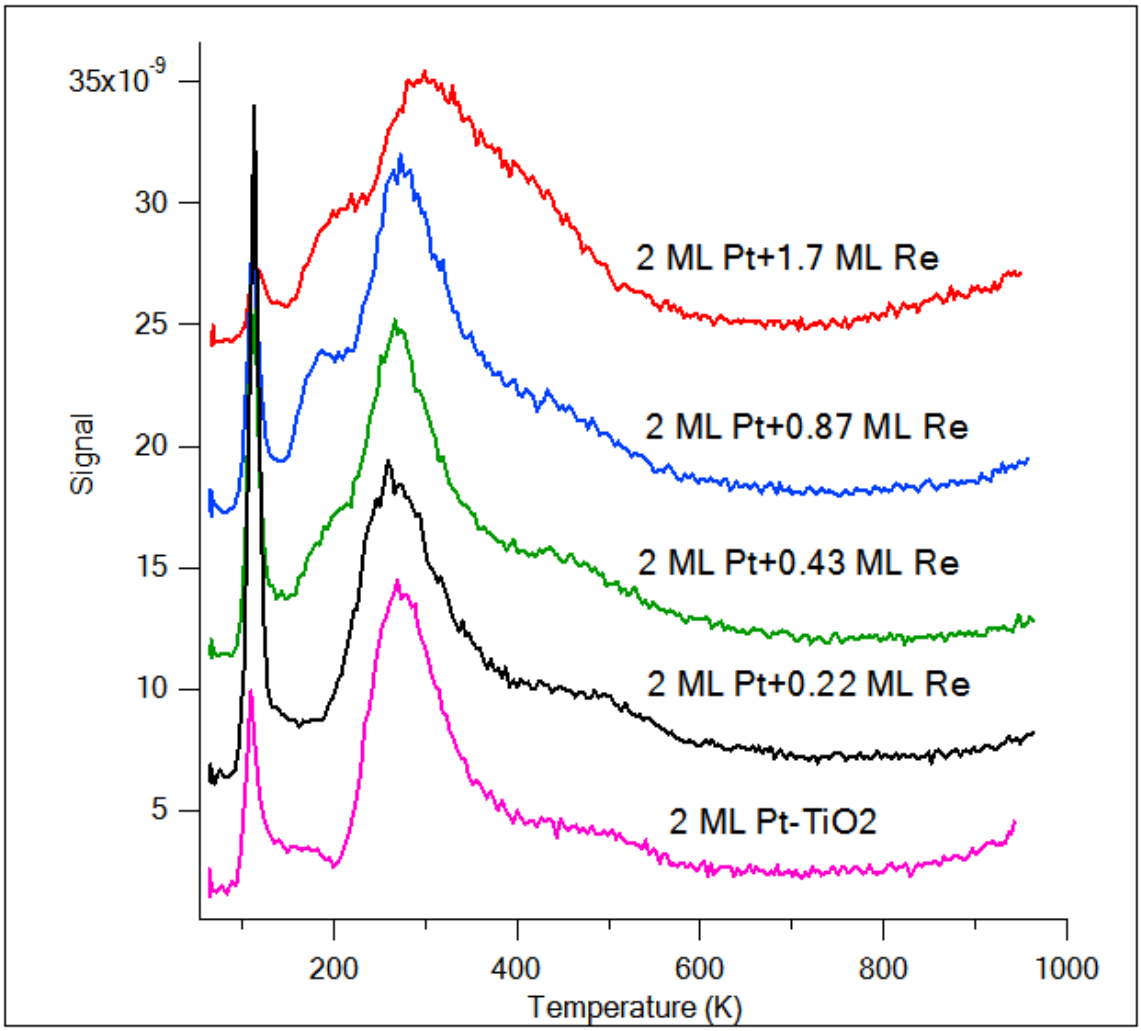

Figure A.11: MeOH TPD H_2 (2 amu) desorption on 2 ML Pt+x ML Re on TiO_2 where x=0, 0.22, 0.43, 0.87 and 1.7 ML.

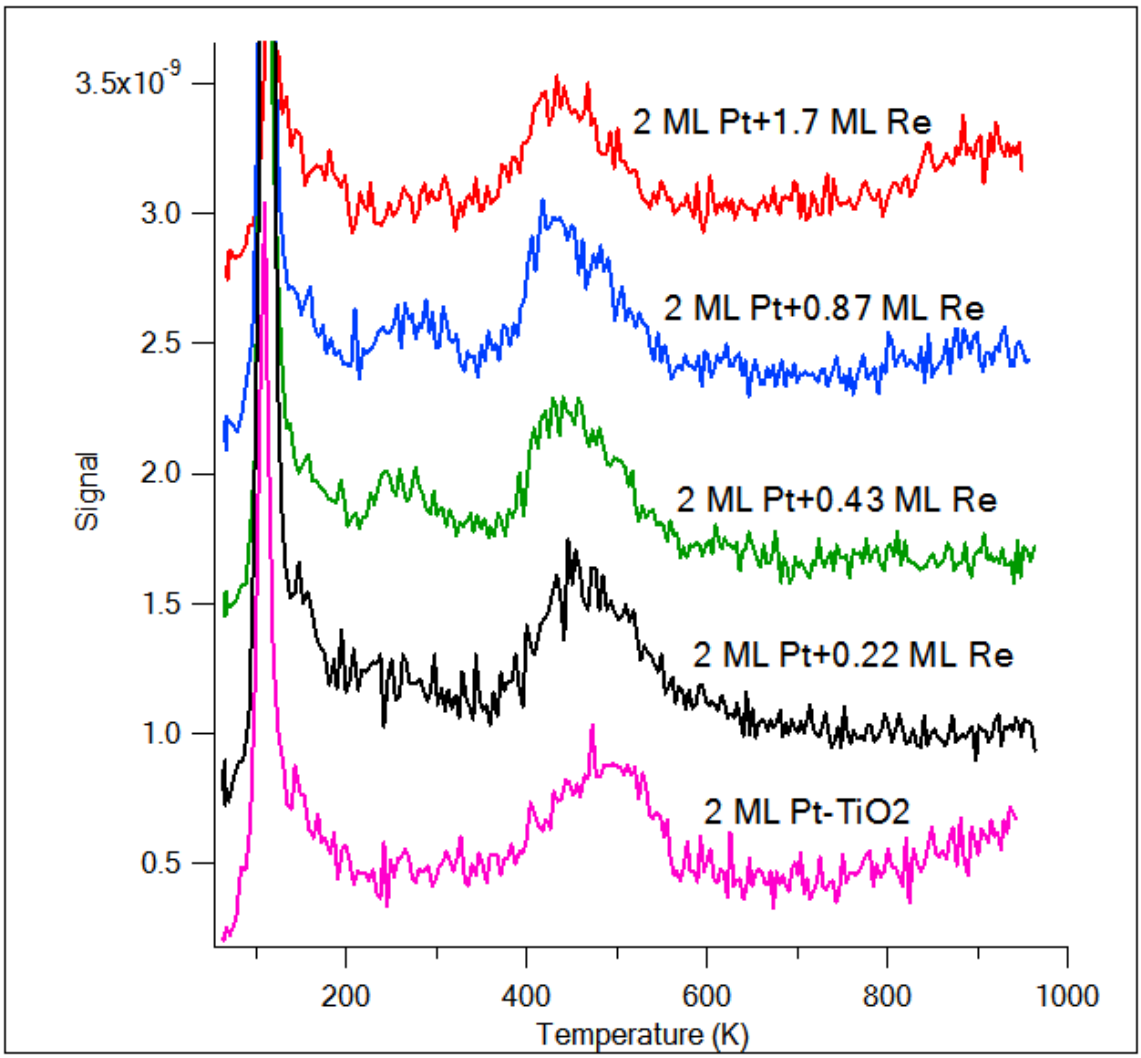

Figure A.12: MeOH TPD CH_4 (16 amu) desorption on 2 ML Pt+x ML Re on TiO_2 where x=0, 0.22, 0.43, 0.87 and 1.7 ML.

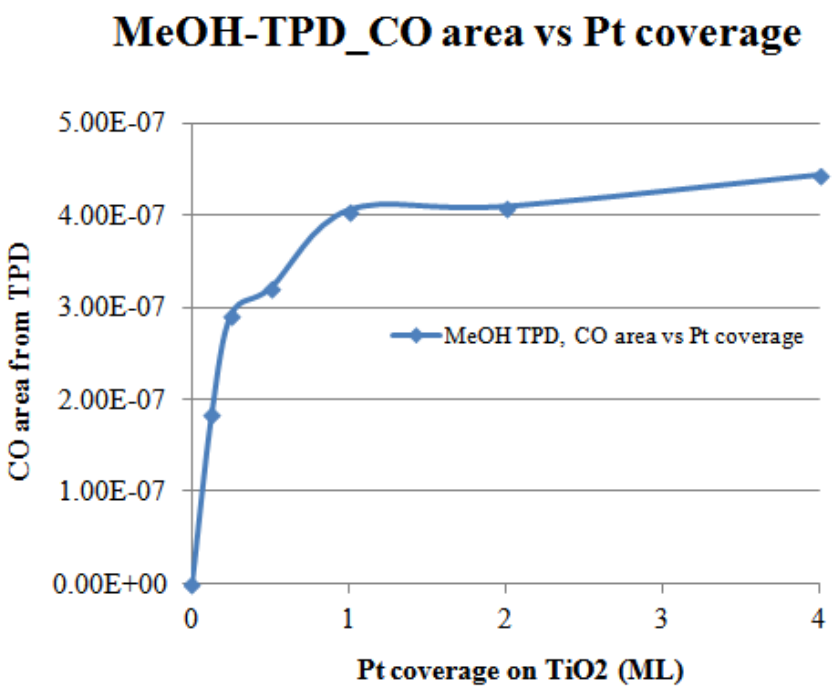

Figure A.13: MeOH TPD, integrated CO area as a result of Pt coverage on TiO_2

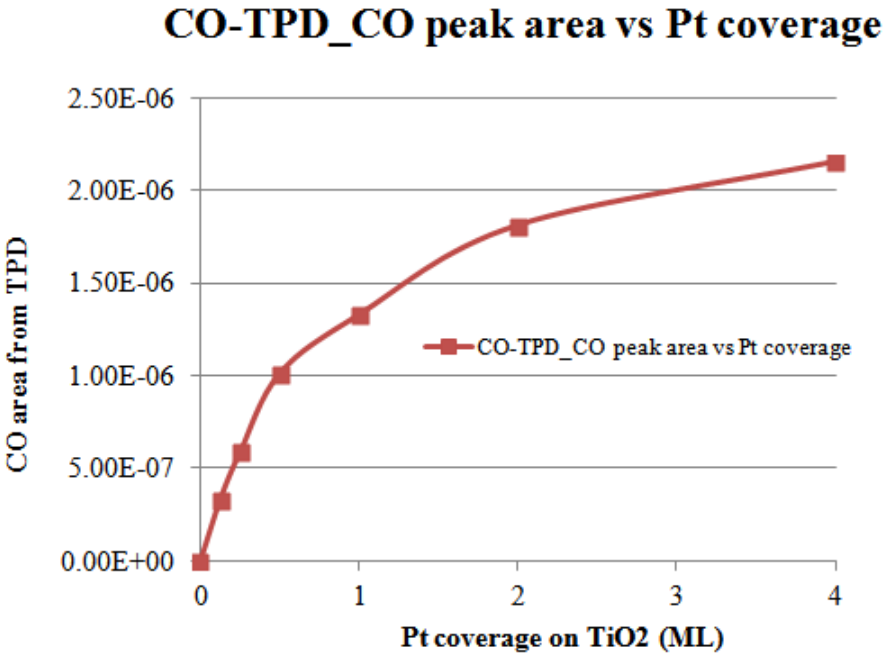

Figure A.14: CO TPD, integrated CO area as a result of Pt coverage on TiO_2

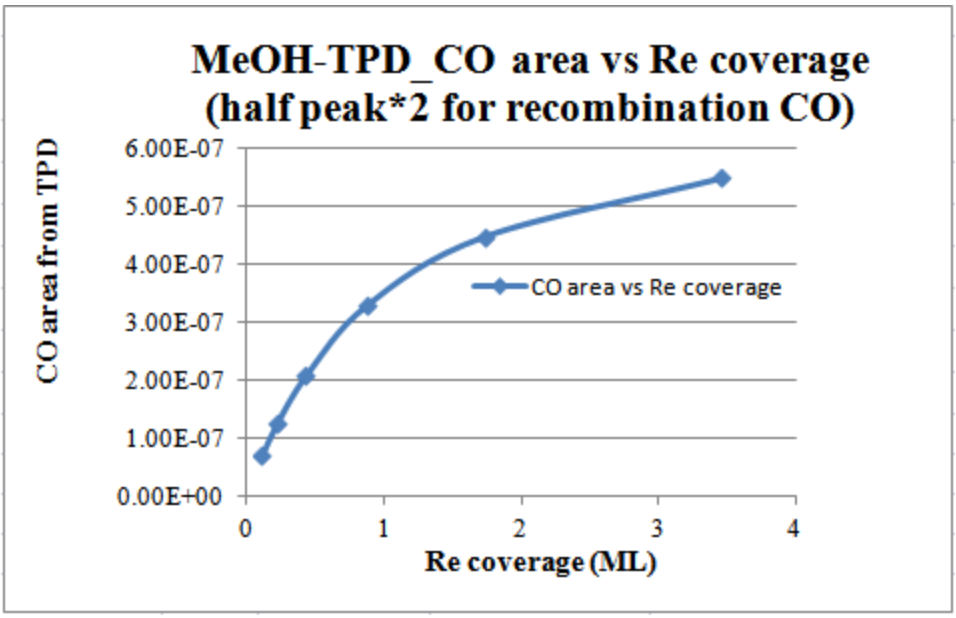

Figure A.15: MeOH TPD, integrated CO area as a result of Re coverage on TiO_2

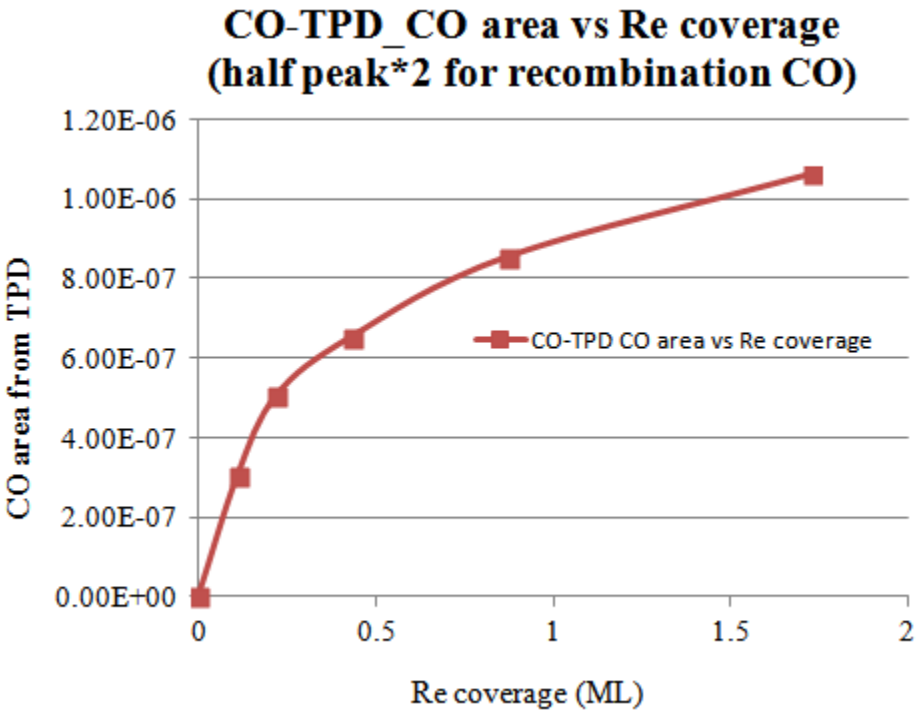

Figure A.16: CO TPD, integrated CO area as a result of Re coverage on TiO_2

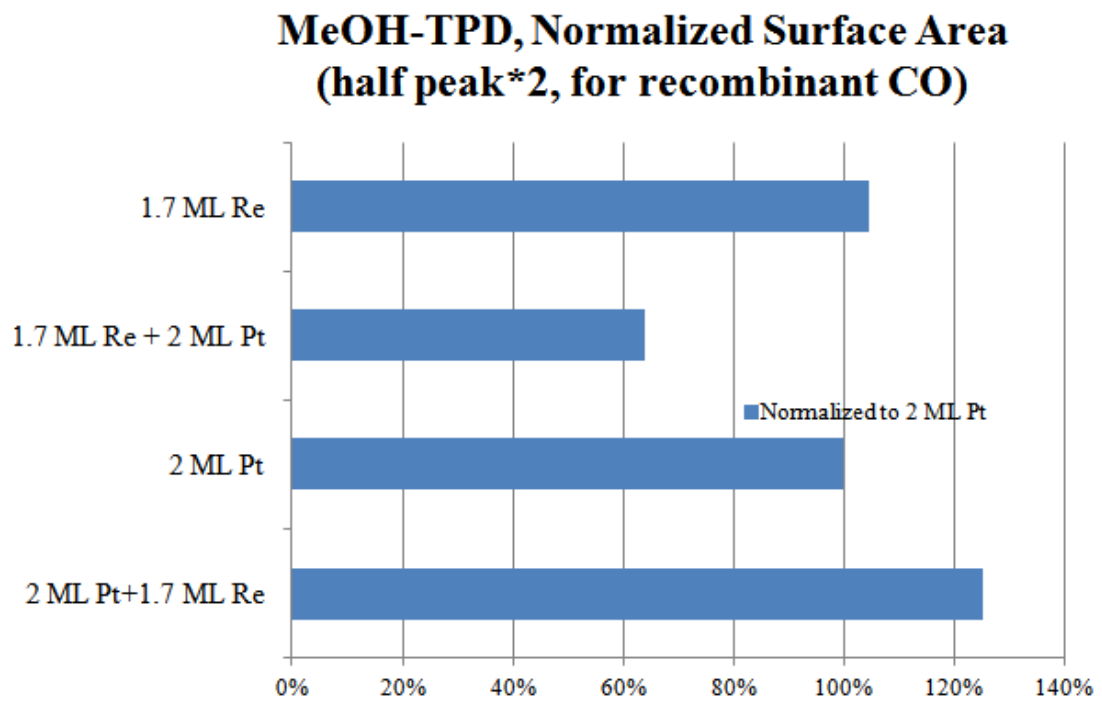

Figure A.17: MeOH TPD, integrated CO area on 2 ML Pt+1.7 ML Re, 2 ML Pt, 1.7 ML Re+2 ML Pt and 1.7 ML Re on TiO_2

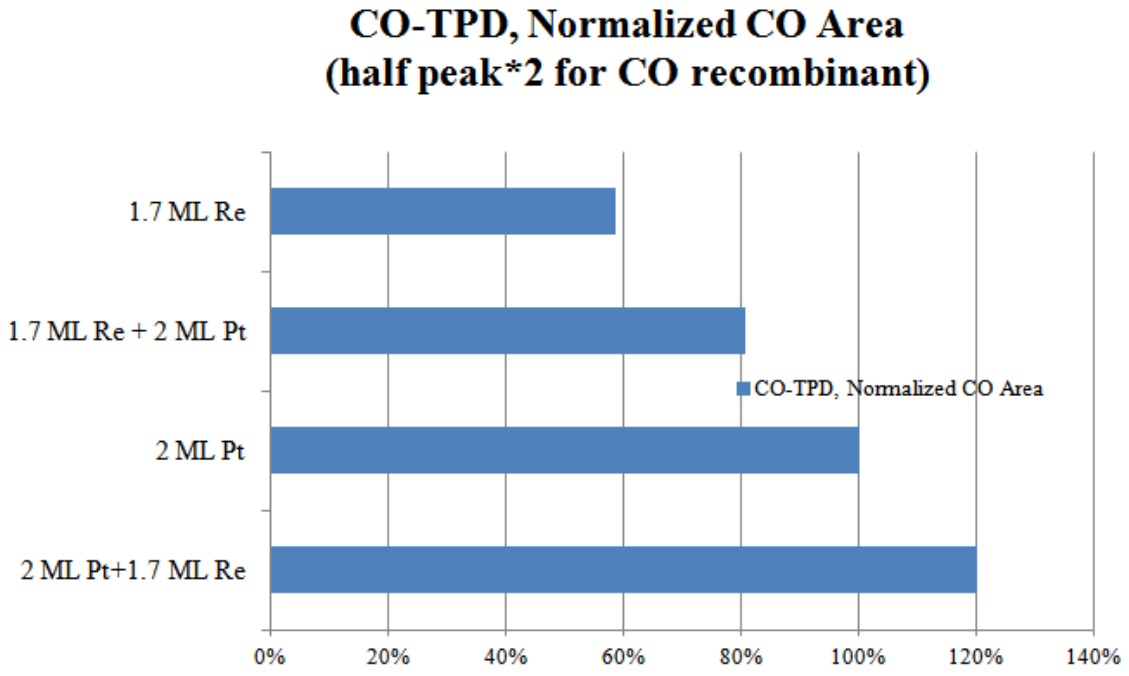

Figure A.18: CO-TPD, integrated CO area as a result of Re coverage on 2 ML Pt+1.7 ML Re, 2 ML Pt, 1.7 ML Re+2 ML Pt and 1.7 ML Re on TiO_2

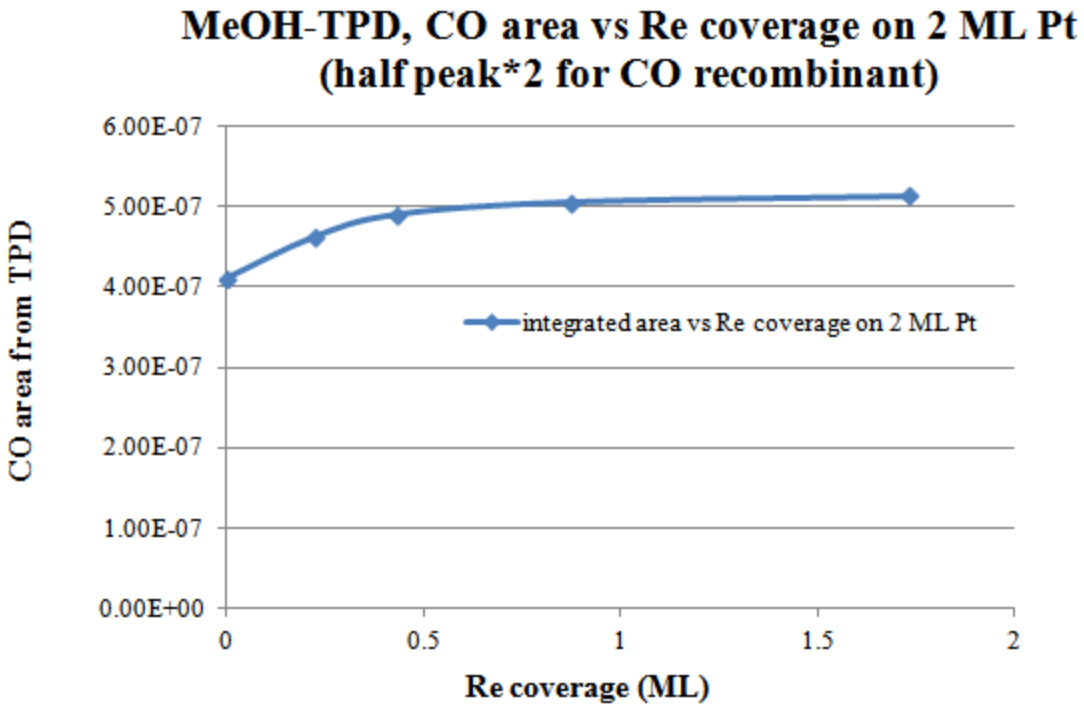

Figure.A.19: MeOH TPD, integrated CO area as a function of Re coverage on top of 2 ML Pt supported on TiO_2

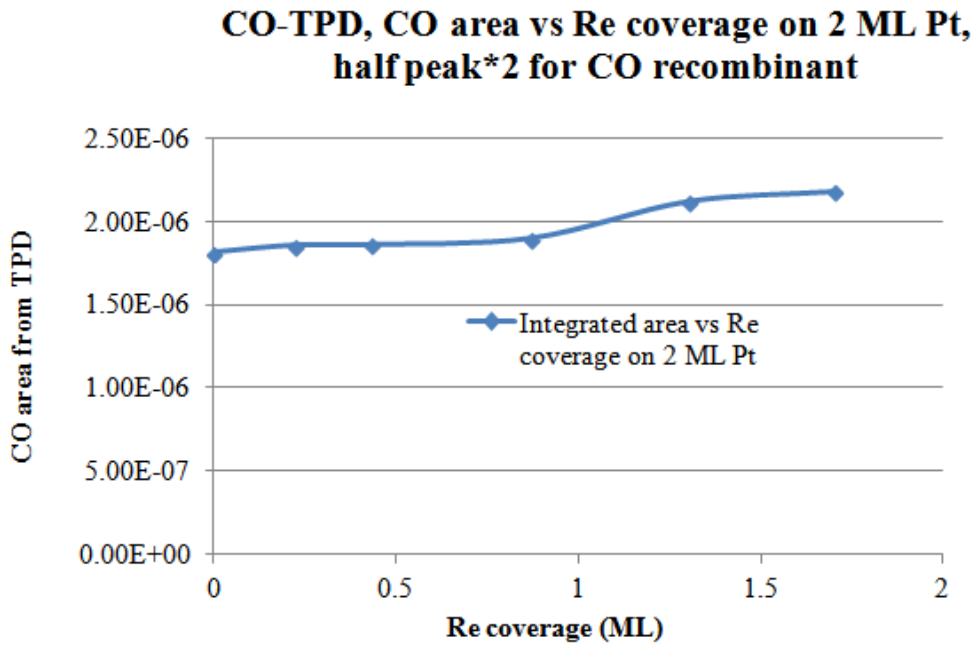

Figure A.20: CO-TPD, integrated CO area as a function of Re coverage on top of 2 ML Pt supported on TiO_2

Reference for Appendix A

(1) Galhenage, R. P.; Yan, H.; Tenney, S. A.; Park, N.; Henkelman, G.; Albrecht, P.; Mullins, D. R.; Chen, D. A., Understanding the Nucleation and Growth of Metals on TiO_2: Co Compared to Au, Ni, and Pt. *The Journal of Physical Chemistry C* **2013,** 117 (14), 7191-7201.

(2) Galhenage, R. P.; Xie, K.; Yan, H.; Seuser, G. S.; Chen, D. A., Understanding the Growth, Chemical Activity, and Cluster–Support Interactions for Pt–Re Bimetallic Clusters on TiO_2(110). *The Journal of Physical Chemistry C* **2016,** 120 (20), 10866-10878.

(3) Wang, J.; Masel, R. I., Structure sensitivity of methanol decomposition on (1×1) and (2×1) Pt(110). *Journal of Vacuum Science & Technology A* **1991,** 9 (3), 1879-1884.

APPENDIX B SOME STUDIES OF STRONG ELECTROSTATIC ADSORPTION AND ELECTROLESS DEPOSITION

1. Strong electrostatic adsorption (SEA)

1.1 SEA study of Pt on TiO_2-P25 powder

1.1.1 Summary:

The precursor salt of Pt here is $PtCl_2$ $(NH_3)_4$ H_2O (PTA). The pH of solution was adjusted by NaOH and HCl. 0.400g TiO_2 powder was added to 20ml Pt solution and shake for 60 minutes. All PTA solutions were diluted form 1ml to 10ml. Adsorption Atomic Absorption Spectroscopy (AAS) were conducted for initial and post adsorbed Pt solution for each pH. Also, the quantitatives of Pt adsorbed on the TiO_2 had been calculated by wt%.

1.1.2 Conclusion:

1. Pt^+ cation can be easily deposited on the surface of TiO_2 P25 Powder;
2. The highest deposition happened at a initial pH 11.5~12.0;
3. The maximum uptake for this experiment is determined to be 0.78 wt%, which is less than expected 2wt%.

1.1.3 Experiment detail:

(1) Precursor salts: $PtCl_2$ $4(NH_3)$ H_2O, 10%HCl, 1%La.

Solutions for pH adjustment: DI water; 0.1N, 1N and 10N NaOH; 0.1N, 1N and 12.5N HCI.

Equipments and instruments: pH meter, beakers, burette/droppers.

Initial Pt solution- PTA has already been prepared.

Concentration of [Pt] is about 200 ppm.

The pH of initial [Pt] solution is 11.24.

TiO_2-P25 powder: surface area= 50 m^2/gram, not porous, the PZC is about 4.4.

(2) pH Adjustment

i) Base pH range: 8, 8.5, 9, 10, 10.5, 11, 11.5… 13.5, totally 11 sample solution;

ii) Acid pH range: 6-7, 5.0, totally 2 pH sample solutions.

iii) Adjusted with 0.1N, 1N and 10N NaOH and 0.1N, 1N and 12.5N HCI.

We collected a little more than 5 ml solution for each pH to do AA for the concentration of initial solutions (Ci); in the same time, collected 20 ml solution for each pH to do adsorption on TiO_2 P25 powder.

(3) Absorption for Pt on TiO_2 powder.

i) Weighed 13 set of 0.4000 gram powder.

ii) Put the powder into the bottle with base pH range.

iii) Shake for 1 hour.

(4) Final pH test and dilution

After adsorption, using filter to take another 5ml from the after-adsorption solutions do AA for (Cf). Test the final pH for each after-adsorption solutions. Dilute all the solutions by 10 times. From 1 ml to 10ml (~200 ppm to 20 ppm)

(5) AAS test for each pH condition,

Use [C(i) - C(f)] to estimate the Pt adsorbed on the TiO_2 surface.

For AAS tests, the original samples can be diluted to meet the best probe region of instruments. Results are shown in Table B.1 and Figure B.1 below:

Table B.1 Pt uptake on TiO_2 data with different initial pH

Set pH	initial pH	Final pH	Initial Conc.	final Conc.	Ci-Cf=ΔC(uptake)
5	5.02	4.33	20.52	19.81	0.71
6-7	6.62	4.71	20.09	19.02	1.07
8	7.99	5.08	20.16	18.65	1.08
9	8.99	5.17	19.71	18.00	1.71
9.5	9.51	5.43	19.74	17.43	2.31
10	10.00	5.63	19.47	16.69	2.78
10.5	10.49	6.16	19.12	15.53	3.59
11	11.00	8.23	18.73	8.751	9.979
11.5	11.50	10.16	18.81	3.876	14.934
12	**12.01**	**11.68**	**18.55**	**3.006**	**15.544**
12.5	12.50	12.35	18.30	6.96	11.34
13	13.01	12.92	18.18	12.64	5.54
13.5	13.46	13.36	19.80	16.23	3.57

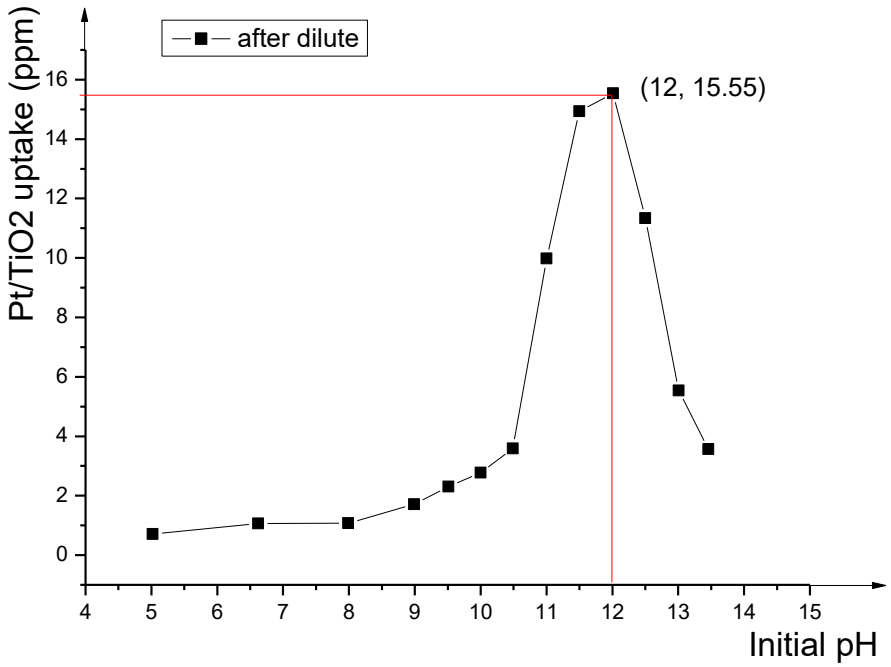

Figure B.1: The Graph of Pt uptake on TiO_2 VS initial pH.

If choose the condition with initial concentration of Pt salt at195 ppm and adjust it to pH=12, the estimation wt% of Pt uptake on TiO_2 power should be 0.78%, the detail is: 15.544ppm*(10ml/1ml)*20ml*(≈1.0g/ml)/0.4g = 0.007772 ≈ 0.78%. This wt% value is lower than what we expected before this experiment.

Figure B.2 shows the plot of Pt uptake on TiO_2 power (P-25) in terms of the final pH. As can be seen, the plot is much different since the pH of system could substantially changed by Pt deposition. The maximum uptake happened at pH value ~11.5. Therefore, in next part of following experiment we would select an initial pH between 11.5 and 12 to make the ≈0.80 wt% Pt/TiO_2 catalyst. The purpose is to get as much as deposition of Pt, providing more Pt sites on surface.

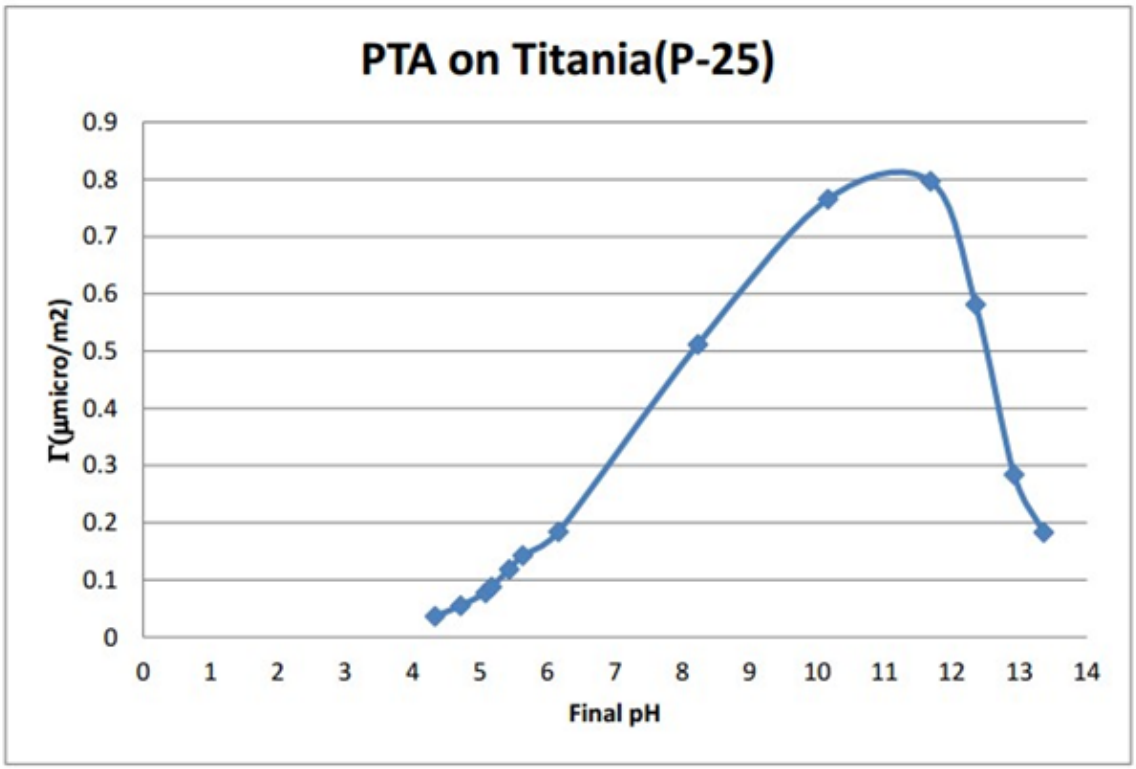

Figure B.2: The Graph of Pt uptake on TiO_2 as a function of final pH

1.2 Preparation of 0.82 wt% Pt on TiO_2 – P25

1.2.1 Summary:

Here the precursor salt of Pt is PTA, $PtCl_2 \cdot (NH_3)_4 \cdot H_2O$. In the sample container, the initial pH was adjusted to 11.76. A weight of 4.000g TiO_2 (P-25) powder was added to the 200 ml Pt solution and was moderately shake for 60 minutes. The final pH was measured at 11.22. Both initial and after-absorption solutions were diluted form 1ml to 10ml for Adsorption Atomic Absorption Spectroscopy (AAS) test. Finally, the amount of Pt deposited on the TiO_2 was calculated in terms of wt%.

1.2.2 Conclusion:

1. The uptake under this condition is higher than last time (0.78 wt%), the maximum uptake in this experiment is 0.82 wt%;
2. The obtained value is still less than 0.94 wt%, the reported maximum for Pt on TiO_2;
3. We used 4.0 g TiO_2 powder for adsorption and finally we obtained 3.2g Pt/TiO_2.

1.2.3 Experiment detail:

(1) Precursor salts: $PtCl_2 \cdot 4(NH_3) \cdot H_2O$, 10%HCl, 1%La

Solutions for pH adjustment: 10N NaOH.

Equipment and instruments: pH meter, beakers, burette/dropper

Initial concentration of [Pt] is about 200 ppm

TiO_2 P-25 powder: surface area= 50 m^2/g, not porous, PZC is about 4.4;

(2) pH Adjustment

Adjusted with 3 drops 10N NaOH then pH went to 11.76. Collect a little more than 5 ml solution to do AA for the concentration of initial solutions (Ci); in the same time, the rest 200 ml solution for each pH to do adsorption on TiO_2 P-25 powder.

(3) Absorption for Pt on TiO_2 powder.

4.00 gram powder was weighted. The powder was added into the bottle with base pH range. After that, the mixtures were shaking for 1 hour.

(4) Final pH test and dilution

After adsorption, we used filters to take about 2ml from the after-adsorption solutions do AA for (Cf). Test the final pH for each after-adsorption solutions. Final pH=11.22 Dilute all the solutions by 10 times. From 1 ml to 10ml (~200 ppm to 20 ppm)

(5) For AAs test of these solutions, [C(i) - C(f)] was used to estimate the Pt adsorbed on the TiO_2 surface. Results are shown below:

Set pH	Actual pH	Final pH	Ci	Cf	Ci-Cf
11.8	11.76	11.22	20.26 ppm	3.898 ppm	16.362 ppm

Therefore the estimated wt% of $Pt/TiO_2 \approx 0.82\%$

16.362ppm*(10ml/1ml)*200ml*(≈1.0g/ml)/0.4g = 0.008181 ≈ 0.82%

(6) Catalyst collection: the operator obtained 3.2g Pt/TiO_2.

(7) Temperature programmed reduction (TPR) test was also done by Hye-Ran,

The condition is 10% hydrogen in Ar, heated from room temperature to 800C with a constant ramping rate at 3 C/min.

The reduced PTA on P-25 was held at 200 C.

(8) Chemical absorption test result of Pt/TiO_2:

Wt. % (Coverage) = 0.8%;

% dispersion of Pt on TiO_2 =60.6%;

Number of metal atoms per gram=$2.47*10^{19}$;

Number of metal atoms per gram=$1.50*10^{19}$;

2. Electroless Deposition (ED)

2.1 TiO_2 as the support

The experiments on TiO_2 (110) were based on the successful deposition of metal salts on TiO_2 P-25 powder. The material gap could be bridged if the ED deposition of Ag on Pt-TiO_2 (110) or HOPG can be established.

2.1.1 Typical experimental parameters for Ag on Pt/TiO_2

ED bath main components and conditions:

Ag salt: $KAg(CN)_2$, 10 ppm;

Reducing Agent (RA): hydrazine, N_2H_4,

Ratio of RA to Ag= 10/1;

RA will be added at t=0, 1, 1.5 hour.

Temperature=0-5 C; (ice- water bath control)

ED bath pH=10; (adjusted with HCl and NaOH)

ED bath volume=100ml;

Deposition time=2 hours in total, including the stability check at 0-0.5 hour.

Under this ED conditions, it has been verified that there is no deposition of Ag on TiO_2 P-25 powder support so Ag can selectively adsorb on Pt sites to form bimetallic catalysts.

2.2 HOPG as the support

The experiments on HOPG are based on the successful deposition on XC-72 powder.

2.2.1 Typical experimental parameters for Pt on Ru/HOPG

Sample: HOPG-3 (10mm*10mm);

0.50 ML Ru on lm-HOPG

Conditions: Volume of ED bath: ~120 ml;

The Pt source is H_2PtCl_6, initial concentration=2 ppm

Temperature of surrounding: 70 C;

pH=11.1 +/- 0.2; (adjusted with HCl and NaOH)

Reducing agent: DMAB, 5/1=[RA]/[Pt] , added in t=0 and 0.5h.

After ED, clean the HOPG surface with DI water, standard wash

2.2.2 Typical experimental parameters for Ru on Pt/HOPG:

Sample: HOPG-3 (10mm*10mm);

0.50ML Pt on highly modified surface. (hm-HOPG)

Ru source: $Ru(NH_3)_6Cl_3$, ~50 ppm;

Conditions: Volume of ED bath: 120 ml;

Temperature of surrounding: 100 C;

pH=4 -5 ; (adjusted with HCl and NaOH)

Reducing agent: formic acid, 10/1=[RA]/[Ru] , added in t=0, 1h and 1.5h.

After ED, clean the HOPG surface with DI water, standard wash

2.2.3 Typical experimental parameters for Ag on Pt/HOPG:

ED bath main components and conditions:

Ag salt: $KAg(CN)_2$, ~10 ppm;

Reducing Agent (RA): hydrazine, N2H4,

Ratio of RA to Ag= 10/1;

RA will be added at t=0, 1, 1.5 hr.

Temperature=0-5 C; (ice- water bath control)

ED bath pH=10; (adjust with HCl and NaOH)

ED bath volume=100 ml;

Deposition time=2 hours in total, including the stability check at 0-0.5 hour.

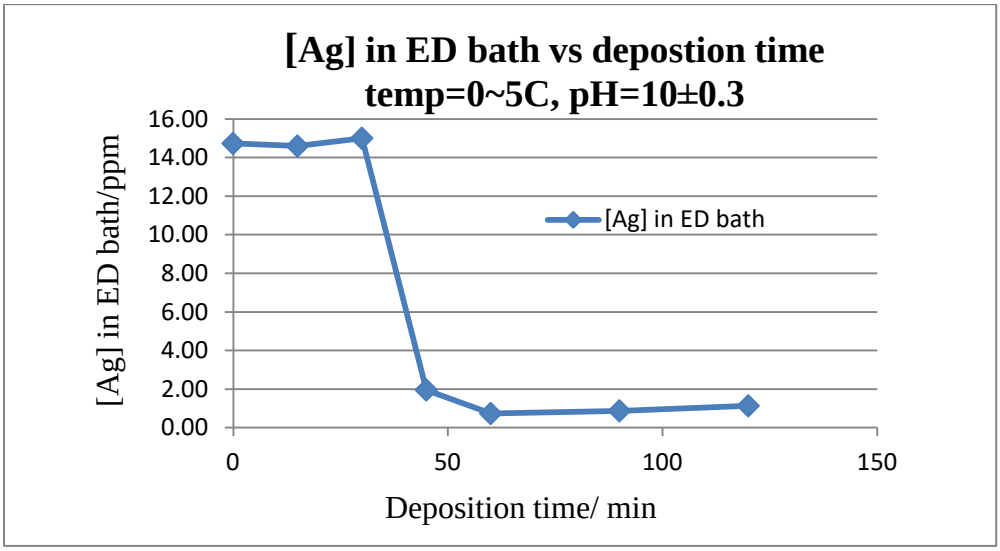

Figure B.3: The ED of Ag on Pt/XC-72 under conditions of temperature=0-5C and pH=10

Preliminary result on activated carbon was shown in Figure B.3. The exact parameters are shown below: Under this ED conditions, it has been verified that there is no deposition of Ag on HOPG support so Ag can selectively adsorb on Pt sites to form bimetallic catalysts. Exact parameters are shown below:

Sample: 0.50 ML Pt on XC-72.

Conditions: Volume of ED bath: ~100 ml;

The Ag source is $KAg(CN)_2$, initial conc.=15 ppm

Temperature of surrounding: 0-5 C; (ice- water bath control)

pH=10 +/- 0.3; (adjusted with HCl and NaOH)

Reducing agent: hydrazine (N_2H_4), 10/1=[RA]/[Ag] , added in t=0 h and 1h.

Deposition time=2 hours in total including the stability check

APPENDIX C DESCRIPTION OF REACTOR GENERATION II

The purpose of creating reactor generation II is to broaden the temperature range that reactor sample can be operated, which is the major limitation of generation I, and to increase the heating efficiency, so as to minimize the required time for sample heating.

As described in chapter 2, the current maximum operating temperature of reactor generation I is 200 ℃ (sample surface). The heating tapes were wrapped from outside of the flange, thus even though we can heat the outer-flange to 250 ℃, the temperature of the reactor (monitored by the TC in the middle of reactor housing) could not go beyond 200 ℃. Meanwhile, significant background activity was observed when the empty reactor (without sample or catalyst) was heated to ~170 ℃ for CO oxidation reaction and 190 ℃ for water gas shift reaction under recirculating mode, with our standard feed gas concentration. Therefore, the design of reactor generation II mainly focuses on two parts (a) heating the sample from inside of flange, to increase the upper temperature limit; (b) coating the reactor housing surface to minimize the activity from background when the reactor is kept at higher temperature.

1. Diagram and measurements

In general, the body frame of generation II is a copy of generation I, since the transfer mechanism of sample surfaces between micor-reactor and UHV chamber should be the same. The measurements-based diagrams for both generations are shown below (Figure A1-A6). Some of the details are explained below each figure if possible.

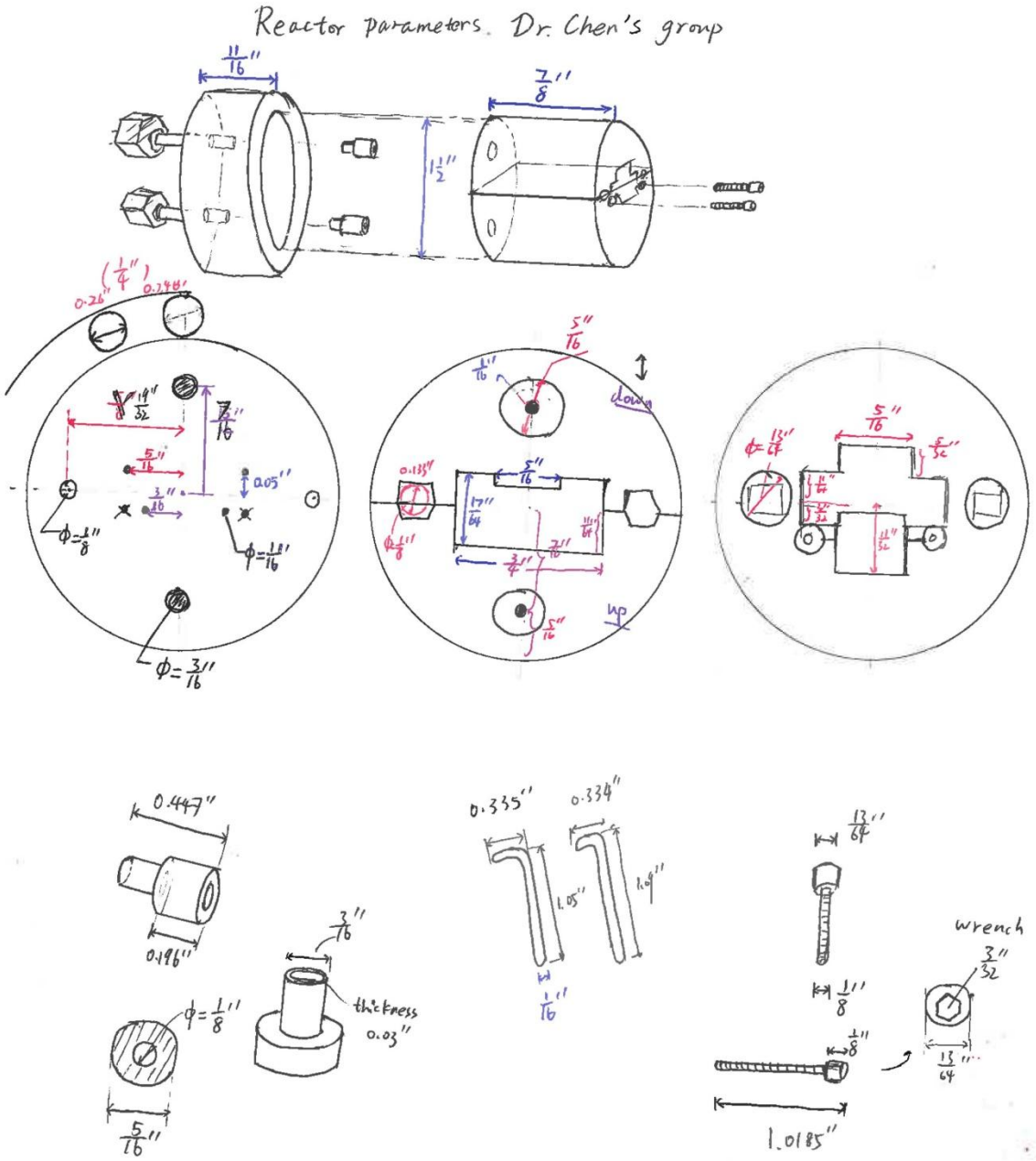

Figure C.1: Measurements of reactor generation I, view-1

Figure C.1 describes the parameters of current reactor, with upper and down pieces assembled. Figure C.2 and C.3 describes the parameters of current reactor, with upper and down pieces disassembled.

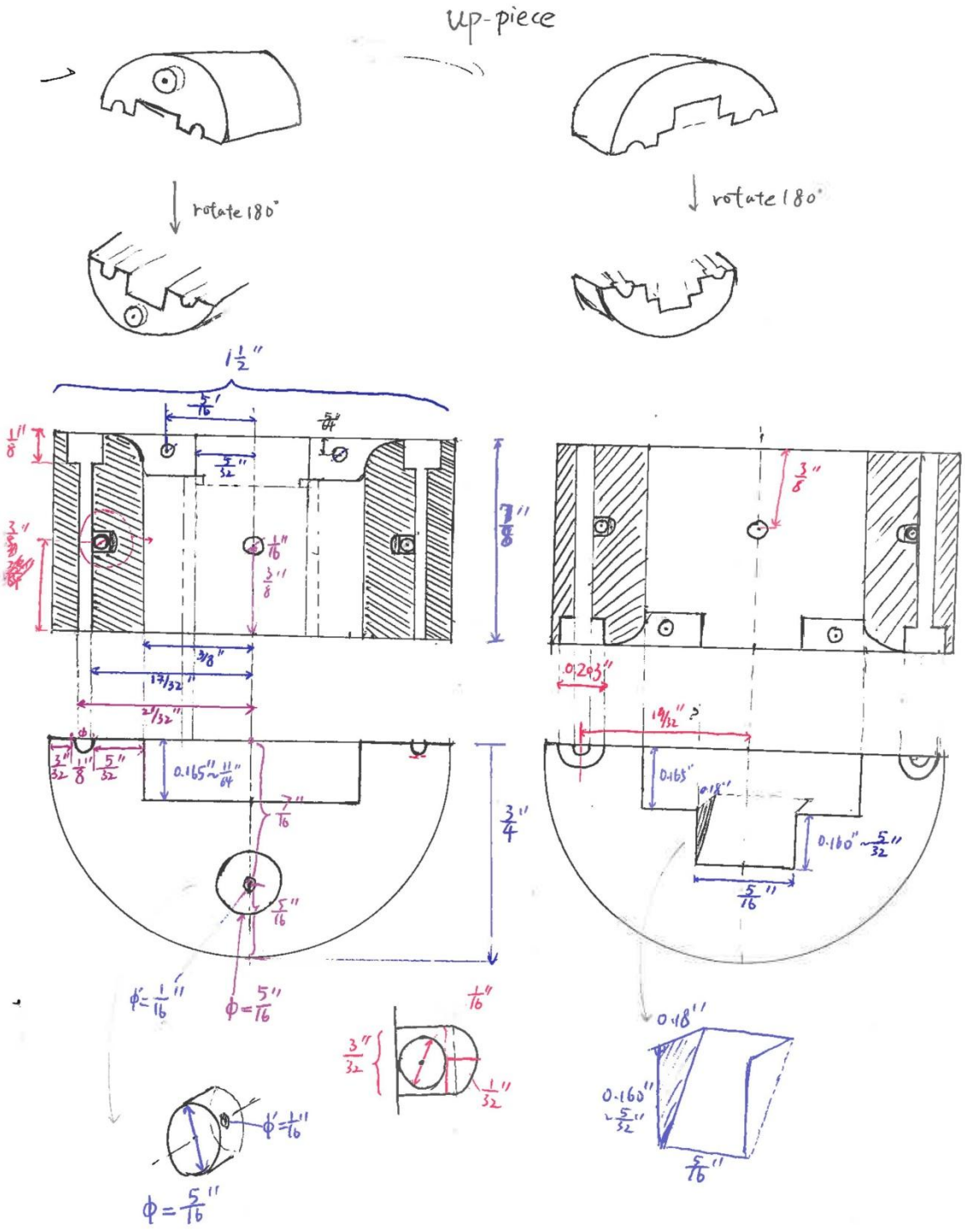

Figure C.2: Measurements of reactor generation I, view-2

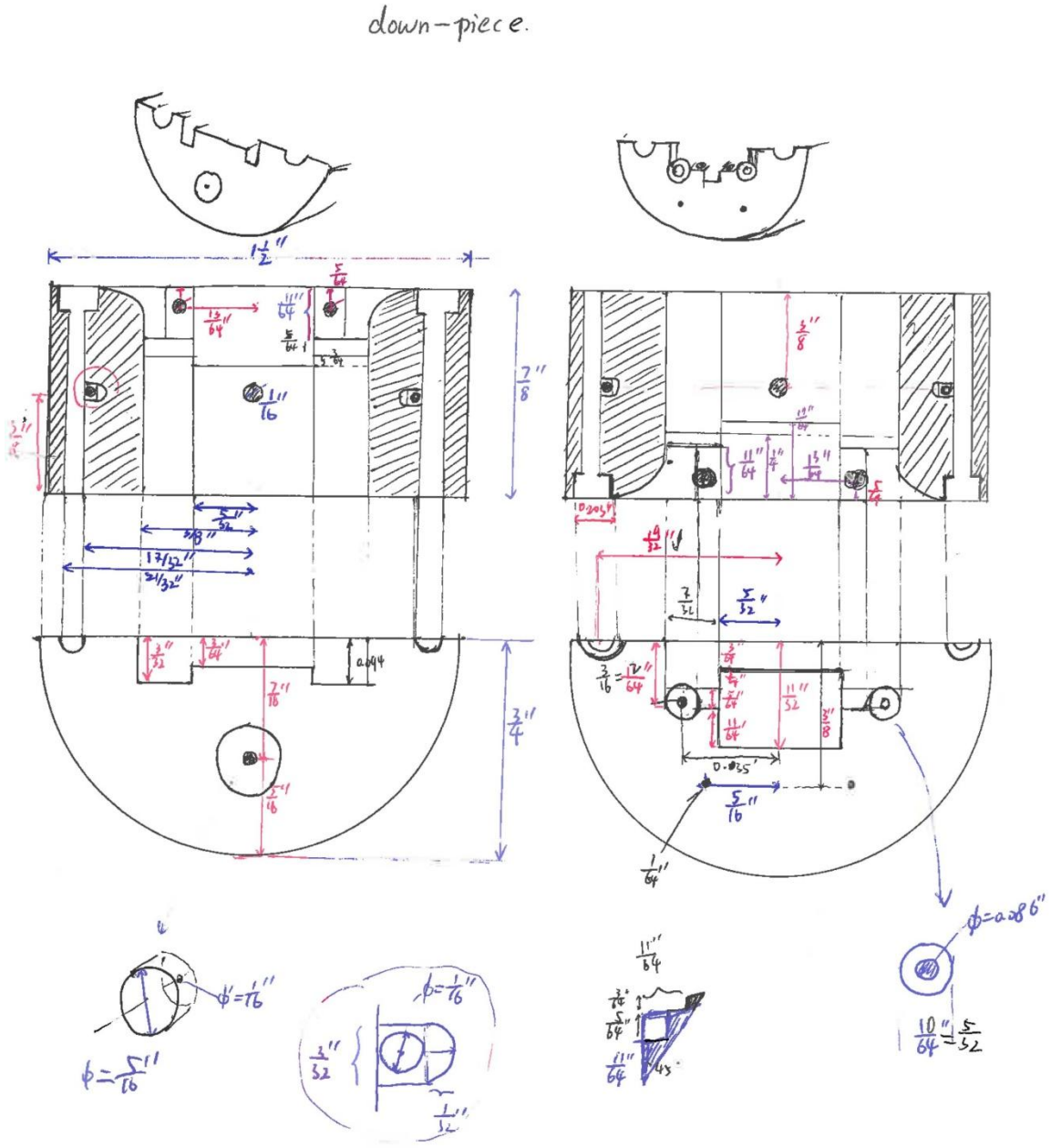

Figure C.3: Measurements of reactor generation I, view-3

Figure C.4 describes the parameters of reactor generation II, with upper and down pieces assembled. Figure C.5 and C.6 describes the parameters of current reactor, with upper and down pieces disassembled.

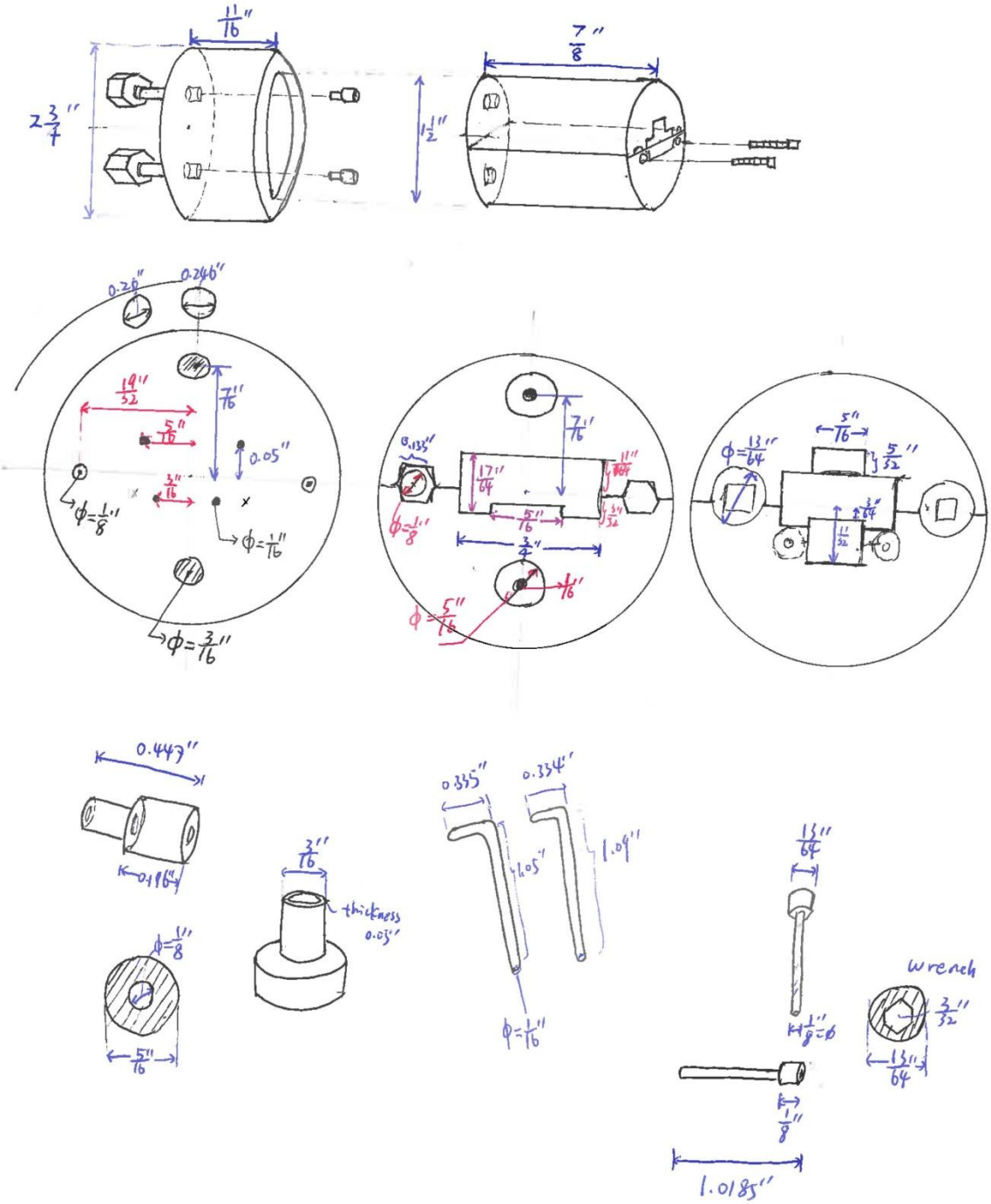

Figure C.4: Measurements of reactor generation II, view-1

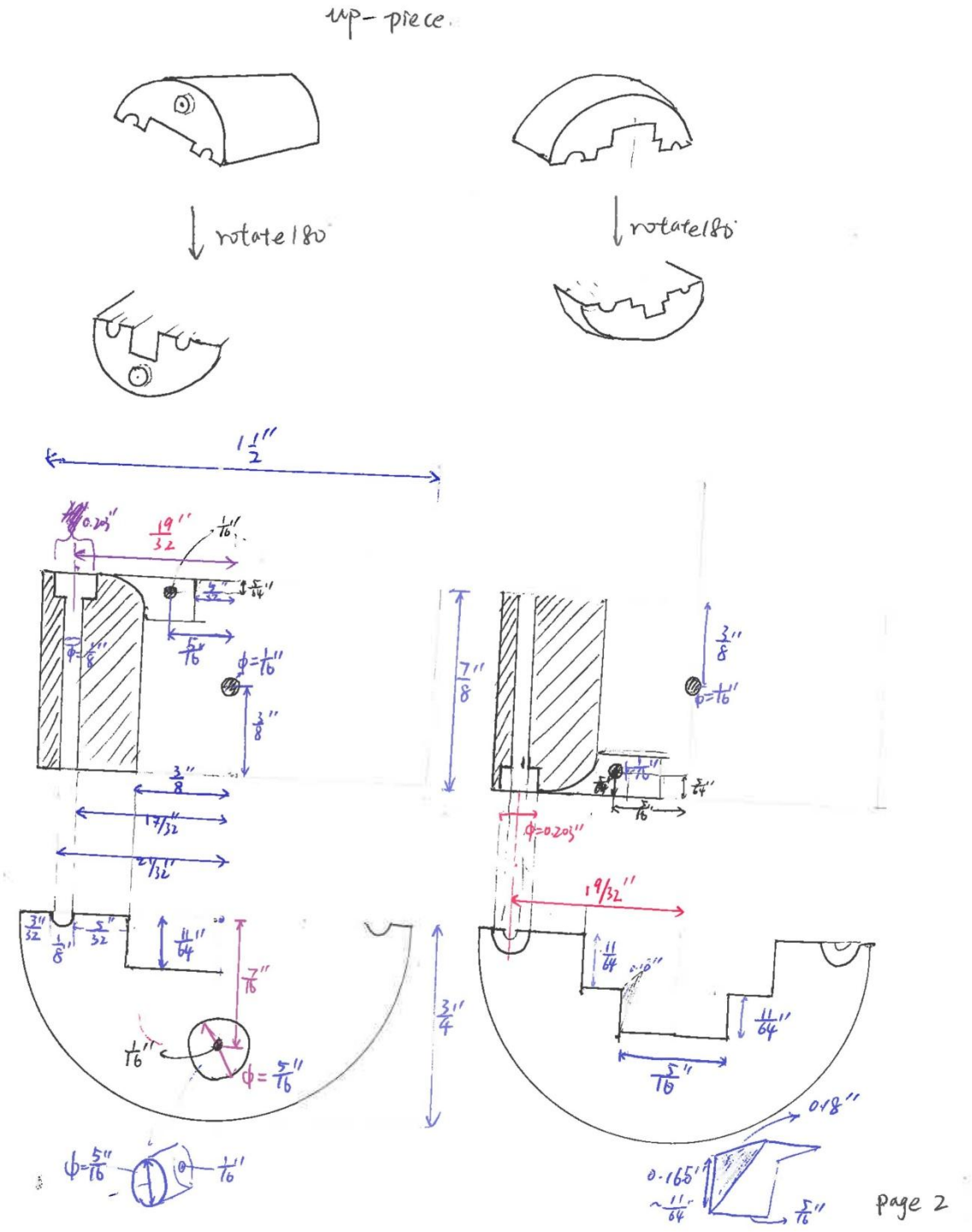

Figure C.5: Measurements of reactor generation II, view-2

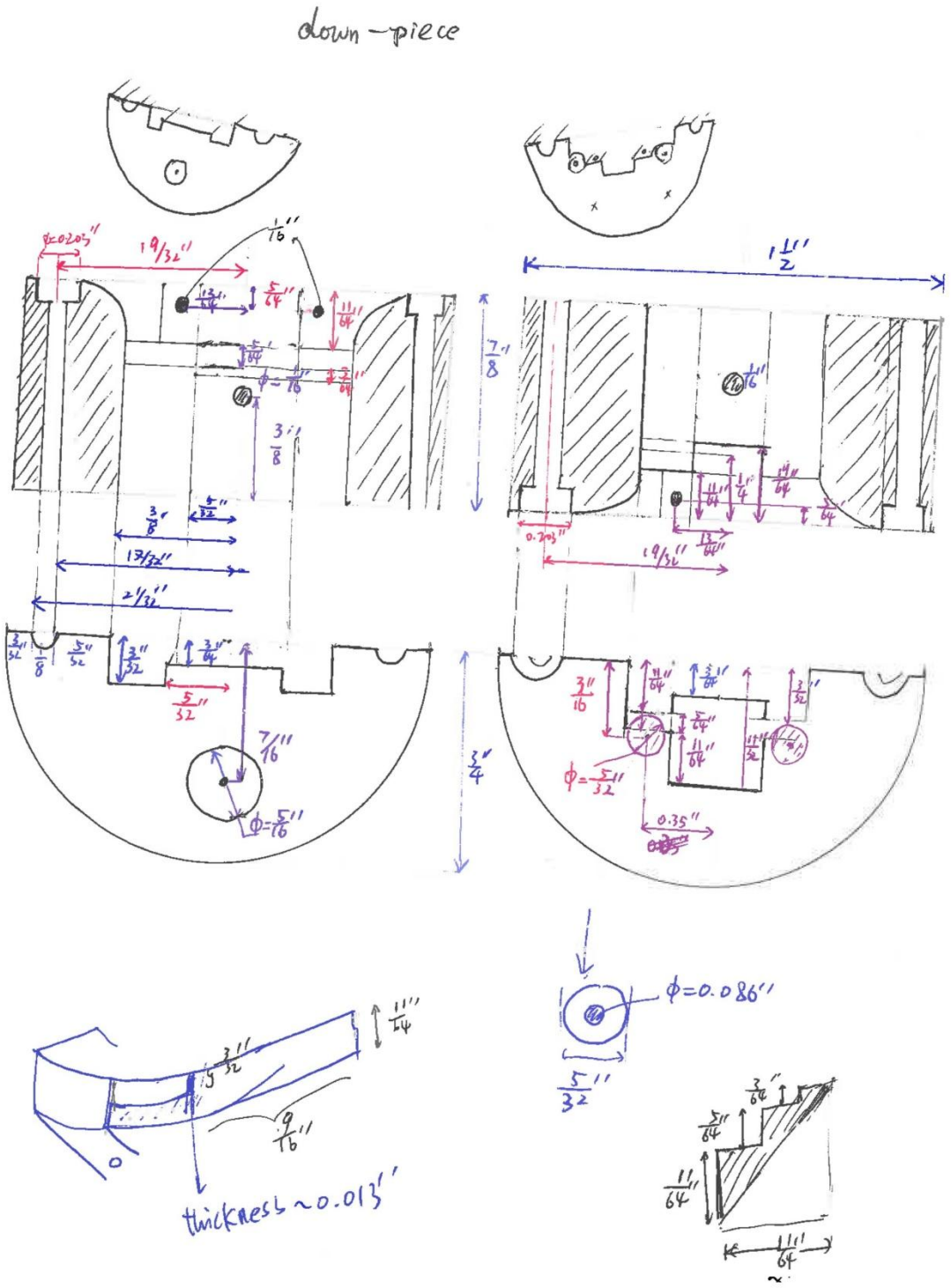

Figure C.6: Measurements of reactor generation II, view-3

2. Heating rods configuration

To achieve our goal that heating from inside of the flange, the as-received flange was modified by Art and Allen from the machine shop. It is found suitable for us to install four cartridge rods based on the allowable space. As can be seen from Figure C7, this drawing overlapped the front and back side of reactor. The circles with blue color are the locations for the reactor heater. The heating efficiency test has been done without attaching this reactor flange to the UHV chamber and our goal was achieved: the reactor can be heated to 150 ℃ in twenty minutes, and the outside temperature is lower than the temperature probe near reactor sample.

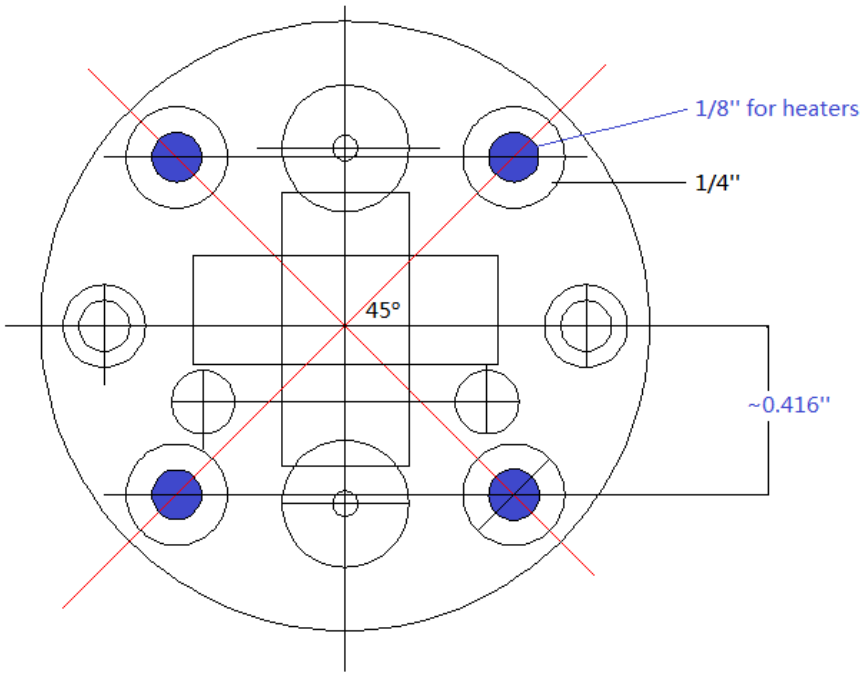

Figure C.7: The locations for the four heating rods

Ordering information for the heating rods of generation II: Company: McMaster-Carr;Part number: 8376T22, (P=50W each, U=120V, I=0.42A) diameter=1/8"; Description: Miniature High-Temperature Cartridge Heater 1-1/4" Length, 50 Watts, 120 VAC. Website link*: http://www.mcmaster.com/#die-cartridge-heaters/=l8db08*

3. Information of surface coating

This part of work was primarily done by Joe Swanstrom from Dr. Michael Myrick's group and the lab that locates on the first floor of Sumwalt College. To begin with, a reactor dummy was tested for proof of principle, later the true reactor generation II was coated with SiO_2. The reactor dummy pieces were initially cleaned with acetone and methanol, and were heated in a clean oven at 220 ℃ for 12 hours to passivate the surface. Then the dummy was placed in the drum (Figure C.8), during the coating process, the drum was evenly rotated to make sure the exposed surface get approximately same SiO_2 coverage. Based on Joe's calculation, approximately one micron layer of SiO_2 is estimated to be on the surface.

Figure C.8: Drum in the coating chamber in Dr.Myrick lab

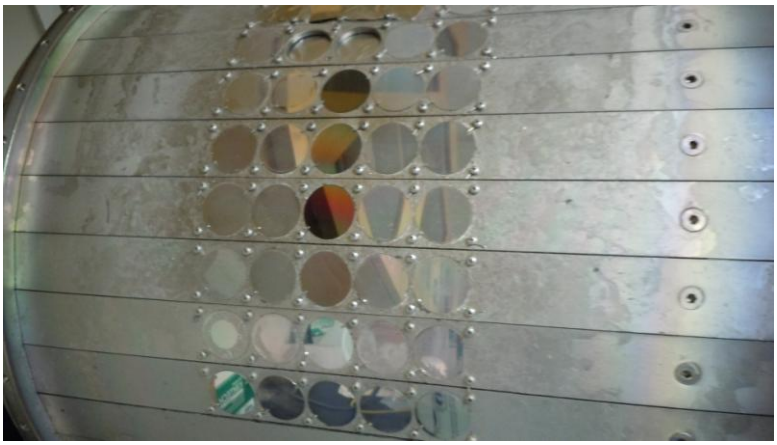

Figure C.9: Drum surface looking from outside

Figure C.9 shows the surface view of the drum mentioned before. There were many round plates fixed by stainless steel wires held by screws. Several of those plates were removed during coating, to provide locations for reactor dummy pieces and reactor generation II. The coating of dummy piece was successful, as can be seen in Figure C.10.

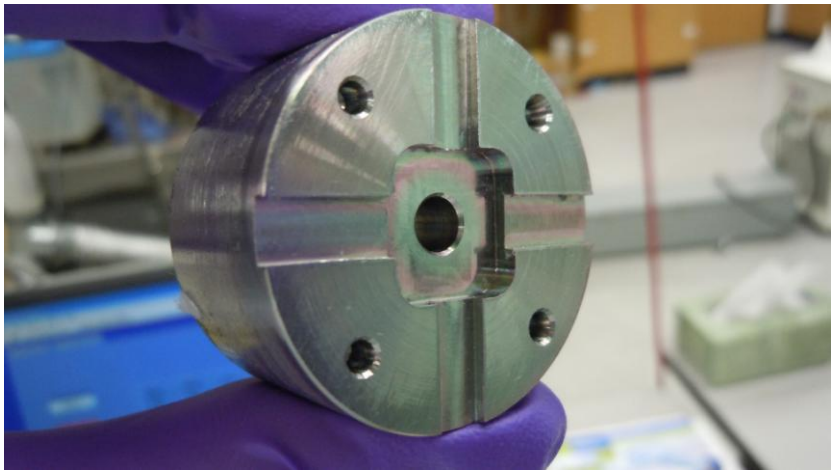

Figure C.10: SiO_2 coated reactor dummy

After that the real reactor generation II was put into the chamber and was coated with the same parameters as dummy piece.

APPENDIX D DEAD VOLUME MEASUREMENT OF REACTOR

This measurement was done by the author on July 3rd 2013 with reactor generation I. Before this measurement, a tube which has certain volume must be ready. For the test here the tube was borrowed from Dr. John Monnier. The fixed volume is 16.54 cm^3 when fully open; 0.45 $cm^3$when fully closed. The steps are follower below:

Step 1: connect this tube to the reactor loop, the needle there valve should be open; (If necessary, attach the auxiliary bridge also)

Step 2: under single pass mode, fill the whole loop with pure helium;

Step 3: Switch the V4 valve to the CCW position, result the recirculation mode, record the pressure of gauge 1 (P0), then close the needle to the added tube;

Step 3: pump down the whole reactor loop with the desired mode in page 2;

Step 4, open the needle to the added tube and record the pressure of gauge 1 (Pi).

Repeat the step 2 to step 4 for all needed modes.

Some definitions: $V_{Total} = V_{SL} + V_{1\text{-}3} + V_R + V_{RL\text{-}R}$

V_{SL}~ *Volume of sampling loop (red)*

$V_{1\text{-}3}$~ *Volume of tubing between V1 and V3 (blue)*

V_R ~ *Volume of reactor cell part (orange)*

$V_{RL\text{-}R}$ ~ *Volume of whole reactor loop minus the (V_R , V_{sl} and $V_{1\text{-}3}$) (green)*

V_B ~ *Volume of the assistant bridge (pink)*

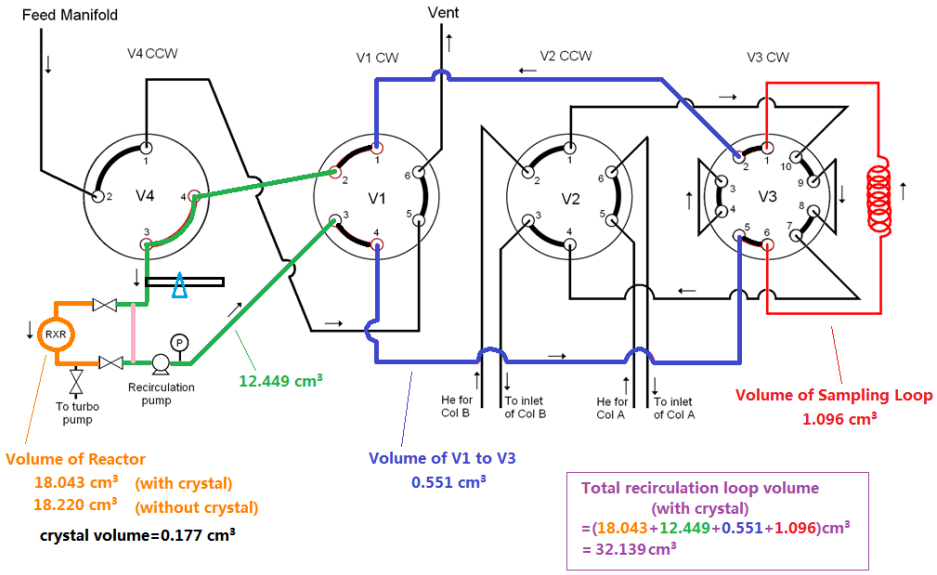

Figure D.1: Measurement result of dead volume of reactor generation I.

(1) Make-up mode

V4	V1	V3
CCW	CCW	CW

$$P_0*16.54=P_1*(16.54+0.45+V_R+V_{RL-R})$$
$$V_R+V_{RL-R}=16.54\ *P_0/P_1-16.99 \qquad \textit{Equation\#1}$$

(2) Make-up mode plus the bridge

V4	V1	V3
CCW	CCW	CW

$$P_0*16.54=P_2*(16.54+0.45+V_R+V_{RL-R}+V_B)$$
$$V_R+V_{RL-R}+V_B=16.54\ *P_0/P_2-16.99 \qquad \textit{Equation\#2}$$

(3) Make-up mode plus the bridge minus the reactor part

V4	V1	V3
CCW	CCW	CW

$$P_0*16.54=P_3*(16.54+0.45+V_B+V_{RL-R})$$
$$V_{RL-R}+V_B=16.54\ *P_0/P_3-16.99 \qquad \textit{Equation\#3}$$

(4) Sampling mode

V4	V1	V3
CCW	CW	CCW

$$P_0*16.54=P_4*(16.54+0.45+V_R+V_{RL-R}+V_{1-3})$$

$$V_R+V_{RL-R}+V_{1-3}=16.54*P_0/P_4-16.99 \qquad \text{Equation\#4}$$

(5) Recirculation mode

V4	V1	V3
CCW	CW	CW

$$P_0*16.54=P_5*(16.54+0.45+V_R+V_{RL-R}+V_{1-3}+V_{SL})$$

$$V_R+V_{RL-R}+V_{1-3}+V_{SL}=16.54*P_0/P_5-16.99 \qquad \text{Equation\#5}$$

Calculation details for the dead volume of each section:

Equation#1 combines with Equation#2, to get V_B,

Equation#2 combines with Equation#3, to get V_R,

then put it back to Equation#1 to get V_{RL-R}

Equation#4 combines with Equation#5, to get V_{SL},

Equation#1 combines with Equation#4, to get V_{1-3},

or, Equation#1 combines with Equation#5, to get (V_{SL} plus V_{1-3}).

Attention: *Record the temperature, better to keep the reactor at the same temperature as the loop (no heating is provided). After that all the measured volumes need to be normalized to those at standard temperature or 298 K. For future experiments all result s are based on standard conditions

APPENDIX E PERMISSION TO PRINT: CHAPTER 2 AND 5

Copyright Clearance Center RightsLink®

Home | Account Info | Help | Live Chat

Title:	Novel recirculating loop reactor for studies on model catalysts: CO oxidation on Pt/TiO2(110)
Author:	Samuel A. Tenney,Kangmin Xie,John R. Monnier, et al.
Publication:	Review of Scientific Instruments
Volume/Issue	84/10
Publisher:	AIP Publishing LLC
Date:	Oct 18, 2013
Page Count:	8

Rights managed by AIP Publishing LLC.

Logged in as:
Kangmin Xie
LOGOUT

Order Completed

Thank you for your order.

This Agreement between Kangmin Xie ("You") and AIP Publishing LLC ("AIP Publishing LLC") consists of your license details and the terms and conditions provided by AIP Publishing LLC and Copyright Clearance Center.

Your confirmation email will contain your order number for future reference.

Get the printable license.

License Number	3966220413887
License date	Oct 11, 2016
Licensed Content Publisher	AIP Publishing LLC
Licensed Content Publication	Review of Scientific Instruments
Licensed Content Title	Novel recirculating loop reactor for studies on model catalysts: CO oxidation on Pt/TiO2(110)
Licensed Content Author	Samuel A. Tenney,Kangmin Xie,John R. Monnier, et al.
Licensed Content Date	Oct 18, 2013
Licensed Content Volume	84
Licensed Content Issue	10
Requestor type	Author (original article)
Format	Print and electronic
Portion	Excerpt (> 800 words)
Requestor Location	Kangmin Xie [redacted] [redacted] United States Attn: Kangmin Xie
Billing Type	Invoice
Billing address	Kangmin Xie [redacted] [redacted] United States Attn: Kangmin Xie
Total	0.00 USD

ORDER MORE CLOSE WINDOW

https://s100.copyright.com/AppDispatchServlet 1/2

AIP PUBLISHING LLC LICENSE TERMS AND CONDITIONS

Oct 11, 2016

This Agreement between Kangmin Xie ("You") and AIP Publishing LLC ("AIP Publishing LLC") consists of your license details and the terms and conditions provided by AIP Publishing LLC and Copyright Clearance Center.

License Number	3966220413887
License date	Oct 11, 2016
Licensed Content Publisher	AIP Publishing LLC
Licensed Content Publication	Review of Scientific Instruments
Licensed Content Title	Novel recirculating loop reactor for studies on model catalysts: CO oxidation on Pt/TiO2(110)
Licensed Content Author	Samuel A. Tenney,Kangmin Xie,John R. Monnier, et al.
Licensed Content Date	Oct 18, 2013
Licensed Content Volume Number	84
Licensed Content Issue Number	10
Type of Use	Thesis/Dissertation
Requestor type	Author (original article)
Format	Print and electronic
Portion	Excerpt (> 800 words)
Will you be translating?	No
Title of your thesis / dissertation	UNDERSTANDING THE KINETICS OF REAL CATALYTIC REACTIONS VIA MODEL CATALYSTS
Expected completion date	Nov 2016
Estimated size (number of pages)	230
Requestor Location	Kangmin Xie [redacted] [redacted] United States Attn: Kangmin Xie
Billing Type	Invoice
Billing Address	Kangmin Xie [redacted] [redacted] United States Attn: Kangmin Xie
Total	0.00 USD
Terms and Conditions	

AIP Publishing LLC -- Terms and Conditions: Permissions Uses

AIP Publishing hereby grants to you the non-exclusive right and license to use and/or distribute the Material according to the use specified in your order, on a one-time basis, for the specified term, with a maximum distribution equal to the number that you have ordered. Any links or other content accompanying the Material are not the subject of this license.

1. You agree to include the following copyright and permission notice with the reproduction of the Material:"Reprinted from [FULL CITATION], with the permission of AIP Publishing." For an article, the credit line and permission notice must be printed on the first page of the article or book chapter. For photographs, covers, or tables, the notice may appear with the Material, in a footnote, or in the reference list.
2. If you have licensed reuse of a figure, photograph, cover, or table, it is your responsibility to ensure that the material is original to AIP Publishing and does not contain the copyright of another entity, and that the copyright notice of the figure, photograph, cover, or table does not indicate that it was reprinted by AIP Publishing, with permission, from another source. Under no circumstances does AIP Publishing purport or intend to grant permission to reuse material to which it does not hold appropriate rights.
   You may not alter or modify the Material in any manner. You may translate the Material into another language only if you have licensed translation rights. You may not use the Material for promotional purposes.
3. The foregoing license shall not take effect unless and until AIP Publishing or its agent, Copyright Clearance Center, receives the Payment in accordance with Copyright Clearance Center Billing and Payment Terms and Conditions, which are incorporated herein by reference.
4. AIP Publishing or Copyright Clearance Center may, within two business days of granting this license, revoke the license for any reason whatsoever, with a full refund payable to you. Should you violate the terms of this license at any time, AIP Publishing, or Copyright Clearance Center may revoke the license with no refund to you. Notice of such revocation will be made using the contact information provided by you. Failure to receive such notice will not nullify the revocation.
5. AIP Publishing makes no representations or warranties with respect to the Material. You agree to indemnify and hold harmless AIP Publishing, and their officers, directors, employees or agents from and against any and all claims arising out of your use of the Material other than as specifically authorized herein.
6. The permission granted herein is personal to you and is not transferable or assignable without the prior written permission of AIP Publishing. This license may not be amended except in a writing signed by the party to be charged.
7. If purchase orders, acknowledgments or check endorsements are issued on any forms containing terms and conditions which are inconsistent with these provisions, such inconsistent terms and conditions shall be of no force and effect. This document, including the CCC Billing and Payment Terms and Conditions, shall be the entire agreement between the parties relating to the subject matter hereof.

This Agreement shall be governed by and construed in accordance with the laws of the State of New York. Both parties hereby submit to the jurisdiction of the courts of New York County for purposes of resolving any disputes that may arise hereunder.

V1.1

Questions? customercare@copyright.com or +1-855-239-3415 (toll free in the US) or +1-978-646-2777.